

**Synthesis, Characterization of Novel Porous Carbon Materials and Their Application
in CO₂ Capture**

by

Xiaotian Zhang

A thesis submitted in partial fulfillment of the requirements for the degree of

Doctor of Philosophy

in

Materials Engineering

Department of Chemical and Materials Engineering
University of Alberta

© Xiaotian Zhang, 2015

Abstract

This research is aimed at developing novel, porous activated carbon materials that are used for CO₂ capture. The research is mainly composed of two parts: synthesis, characterization of novel porous carbons produced via KOH activation; and evaluation of their preliminary CO₂ capture performances.

Various kinds of porous carbons were synthesized via KOH activation method. Through activation of multi-wall carbon nanotubes, the mechanism of pore formation was proposed. This understanding of the pore-forming mechanism also provides a good platform to investigate the effect of absorbent's pore structures on its CO₂ capture behavior. This study demonstrated the significant role of pore sizes less than 1 nm in the physisorption of CO₂ molecules. Furthermore, activated carbons with ultrahigh surface area were synthesized by KOH activation of polyaniline. By studying the effect of the preheating stage, it was determined that formation of network-like nanostructure at preheating stage of the activation process is beneficial to the pore development and can lead to activated carbons with exceptionally high surface area. It is believed that this mechanism could be applied to the activation of other carbon precursors in order to achieve improved specific surface area (SSA) and micropore volume.

The evaluation of the CO₂ capture performances were conducted for two novel activated carbons: porous carbons derived from a liquid carbon precursor (polyethylenimine), and LiCl-incorporated activated carbons. For the porous carbons derived from polyethylenimine, they possess microporosity and rich nitrogen content. At 1 bar the CO₂ uptake of the carbons was 4.9-5.7 mmol g⁻¹ at 0 °C. These carbons also demonstrated a selectivity of 33 for CO₂ over N₂ at 25 °C and less than 1% decrease of the performance after 30 cycles. For

LiCl-incorporated porous carbons, the CO₂ adsorption capacity decreased after LiCl incorporation, mainly because of blocking of the small micropores. However, the increase of initial Q_{st} after LiCl incorporation indicated a positive role of LiCl in terms of CO₂ interaction with sorbent surfaces.

Preface

This thesis is an original work by Xiaotian Zhang. The research conducted for this thesis was supervised by Professor Weixing Chen at University of Alberta.

Chapter 2 of the thesis has been published as Xiaotian Zhang, Weixing Chen, Mechanisms of pore formation on multi-wall carbon nanotubes by KOH activation, *Microporous and Mesoporous Materials*, 2015,**206**, 194–201. I was responsible for the experiments, data collection and analysis as well as the manuscript composition. Dr. Weixing Chen was the supervisory author and was involved with the concept formation and manuscript edits.

Chapter 3 of the thesis has been published as Xiaotian Zhang, Xinwei Cui and Weixing Chen, A comprehensive study of polyaniline-derived porous carbons via KOH activation, *RSC Adv.*, 2015,**5**, 77629-77636. I was responsible for the experiments, data collection and analysis as well as the manuscript composition. Dr. Xinwei Cui collected transmission electron microscopic images and contributed to concept formation and manuscript edits. Dr. Weixing Chen was the supervisory author and was involved with manuscript edits.

Chapter 4 of the thesis has been published as Xiaotian Zhang, Donghai Lin and Weixing Chen, Nitrogen-doped porous carbon prepared from a liquid carbon precursor for CO₂ adsorption, *RSC Adv.*, 2015,**5**, 45136-45143. I was responsible for the experiments, data collection and analysis as well as the manuscript composition. Dr. Donghai Lin conducted part of the CO₂ capture experiments and contributed to manuscript edits. Dr. Weixing Chen was the supervisory author and was involved with the concept formation and manuscript edits.

Acknowledgements

I would like to thank my supervisor Professor Weixing Chen, for his direction, patience and encouragement during my pursuit of doctoral degree. He always inspires me to explore and endeavor, to be precise and authentic, and to finally contribute to scientific research. Without his help and support, this thesis would not have been possible.

I appreciate all the help I received from Dr. Chen's group. Specifically, I wish to thank Dr. Xinwei Cui for his valuable suggestions to my research as well as his patient review and critical suggestions of my publications. I also wish to thank Dr. Donghai Lin and Mr. Mingwen Gao for their cooperation and assistance in various ways. I would like to extend my appreciation to my other colleagues, Dr. Tianfei Wang, Dr. Hao Li, Dr. Ziqiang Dong, Mr. Devin Engel and many others for their kind helps in the lab.

Dr. Nancy Zhang trained me to use the Autosorb machine and deal with the data analysis. Dr. Arunkumar Samanta and Dr. Moshfiqur Rahman unselfishly offered advices on TGA tests. Dr. James Sawada kindly helped me with many adsorption tests and data analysis. Many thanks to them, Dr. Shihong Xu, Dr. Weizhu An, Dr. Deepak Pudasainee and other people who helped me complete the research,.

Carbon Management Canada is acknowledged for financial support.

Last but not the least, my thanks would go to my beloved parents, who love me and care about me all the time.

Table of Contents

Chapter 1	Introduction.....	1
1.1	CO₂ emission and carbon capture.....	1
1.1.1	Fossil fuel, CO ₂ emission and global warming	1
1.1.2	CO ₂ emission from point sources	5
1.1.3	Carbon capture and storage (CCS).....	7
1.2	CO₂ capture technologies and materials.....	9
1.2.1	Options for CO ₂ capture	9
1.2.2	State-of-the-art materials for CO ₂ capture.....	10
1.2.2.1	Aqueous amine-based solutions.....	11
1.2.2.2	Physical solvents	13
1.2.2.3	Membranes	15
1.3	Solid sorbents (adsorbents).....	16
1.3.1	Zeolites	19
1.3.2	Activated carbons (ACs)	22
1.3.3	Metal organic frameworks (MOFs).....	25
1.3.4	Amine functionalized materials.....	29
1.3.5	Others	34
1.4	Activated carbons (ACs)	35
1.4.1	Production of ACs	36
1.4.1.1	Raw materials.....	36
1.4.1.2	AC preparation	37
1.4.2	CO ₂ adsorption in ACs	42
1.4.2.1	Surface energy for adsorption	42
1.4.2.2	Surface modification of ACs for CO ₂ capture	45

1.4.2.3	Pore development of ACs for CO ₂ capture	47
1.5	Objectives of the thesis	49
1.6	Thesis organization	50
1.7	References	51
Chapter 2	Mechanisms of Pore Formation on Multi-wall Carbon Nanotubes by	
	KOH Activation	76
2.1	Introduction.....	76
2.2	Experimental	77
2.3	Results and discussion	80
2.3.1	Influence of temperature.....	80
2.3.2	Influence of time.....	84
2.3.3	Pore-forming mechanism	87
2.3.3.1	Micropores	87
2.3.3.2	Mesopores	89
2.3.3.3	Over-activation.....	93
2.3.4	CO ₂ adsorption	95
2.4	Conclusions.....	96
2.5	References	97
Chapter 3	A Comprehensive Study of Polyaniline-derived Porous Carbons via	
	KOH Activation	102
3.1	Introduction.....	102
3.2	Experimental	104
3.3	Results and discussion	107

3.3.1	Study of pore structure	107
3.3.2	Study of the preheating stage	111
3.4	Conclusion	120
3.5	References	120
Chapter 4	Nitrogen-doped porous carbon prepared from liquid carbon precursor for CO₂ adsorption	127
4.1	Introduction.....	127
4.2	Experimental	129
4.2.1	Preparation of PEI-derived carbon	129
4.2.2	Characterization.....	130
4.2.3	CO ₂ adsorption	131
4.3	Results and Discussion.....	132
4.3.1	Porous structure	132
4.3.2	Chemical characterization	135
4.3.3	CO ₂ adsorption performance	139
4.4	Conclusion	143
4.5	References.....	144
Chapter 5	Preparation of LiCl-incorporated Activated carbons for CO₂ adsorption	152
5.1	Introduction.....	152
5.2	Experimental	154
5.2.1	Synthesis of porous ACs	154

5.2.2	Synthesis of LiCl-incorporated ACs	155
5.2.3	Characterization.....	155
5.2.4	CO ₂ adsorption	156
5.3	Results and discussion	157
5.3.1	Chemical properties.....	157
5.3.2	Porous structure	158
5.3.3	CO ₂ adsorption	162
5.4	Conclusions.....	166
5.5	References.....	167
Chapter 6	Conclusions and Recommendations.....	171
6.1	Summarized conclusions	171
6.1.1	Mechanism of pore formation on multi-wall carbon nanotubes by KOH activation.....	171
6.1.2	A comprehensive study of polyaniline-derived porous carbons via KOH activation.....	172
6.1.3	Nitrogen-doped porous carbon prepared from a liquid carbon precursor for CO ₂ adsorption	173
6.1.4	Preparation of LiCl-incorporated Activated carbons for CO ₂ adsorption ..	173
6.2	Research contributions.....	174
6.3	Recommendations for future work	174
6.4	References.....	175
References	176

List of Tables

Table 1.1	Data for major greenhouse gases (Water vapor excluded).....	4
Table 1.2	CO ₂ adsorption capacities of some commercialized zeolites.....	21
Table 1.3	CO ₂ adsorption capacity of selected ACs.....	23
Table 1.4	CO ₂ adsorption capacities of selected MOFs.....	26
Table 1.5	Structure of Amines for adsorbent functionalization [109].....	30
Table 1.6	CO ₂ adsorption capacity of some amine-functionalized mesoporous silica.....	32
Table 2.1	XPS elemental analysis of as-received MWCNTs.....	78
Table 2.2	ICP-MS analysis of metal composition of as-received MWCNTs.....	78
Table 2.3	Statistical pore structure information and CO ₂ uptake of activated CNTs under different temperature.	82
Table 2.4	Statistical pore structure information and CO ₂ uptake of activated CNTs with different time.	85
Table 2.5	XPS elemental analysis of activated CNTs.	88
Table 3.1	Porous structure data of PANI-derived carbons under various activation conditions.....	110
Table 3.2	Porous structure data of PANI after different preheating condition.....	114
Table 4.1	Porous structure of PEI-derived carbon and their CO ₂ capture performance..	134
Table 4.2	XPS element content and the contribution of nitrogen species.	139
Table 4.3	CO ₂ adsorption capacity of PEI-derived carbons at different temperatures....	140
Table 5.1	XPS elemental analysis of original and modified ACs.	157
Table 5.2	Porous structure parameters and CO ₂ adsorption capacity of all prepared ACs.	162

List of Figures

Figure 1.1	Natural carbon cycle (Reprint with permission from [2], copyright 2011 American Chemical Society).....	2
Figure 1.2	Atmospheric CO ₂ level at Mauna Loa Observatory [3].	3
Figure 1.3	Atmospheric CO ₂ and Global Temperature Anomaly (data from NASA [8]) from 1964 to 2008.	5
Figure 1.4	Global anthropogenic CO ₂ emission contributions by sector in 2008. (Adapted from data in the Emission Database for Global Atmospheric Research version 4.2 [10])	6
Figure 1.5	Diagrammatic representation of carbon capture and storage chain (From [21], reprinted with permission from AAAS).	8
Figure 1.6	Processes capture condition and advantages/disadvantages of post-combustion, pre-combustion and oxy-combustion systems. (Adapted from [22], copyright 2008, with permission from Elsevier)	10
Figure 1.7	General reaction schemes between CO ₂ and a) primary/secondary and b) tertiary amine-containing solvents [24].	11
Figure 1.8	An improved amine-scrubbing system using 8M piperazine (PZ) for post-combustion CO ₂ capture (From [16], copyright 2013, with permission from Royal Society of Chemistry).	12
Figure 1.9	Selexol scrubbing process (With removal of sulfur, source from [31]).	14
Figure 1.10	(a) Temperature swing adsorption (TSA); (b) pressure swing adsorption (PSA); (c) vacuum swing adsorption (VSA). (Adapted with permission from [44], copyright 2008 American Chemical Society)	17

Figure 1.11 Pure component CO ₂ isotherms of different zeolites at 295K (From [52], copyright 2004, with permission from Elsevier).	20
Figure 1.12 CO ₂ adsorption isotherms on activated carbon, zeolite 13X and zeolite 4A at 298 K (Reprinted with permission from [75], copyright 2001 American Chemical Society).	24
Figure 1.13 CO ₂ adsorption isotherms at ambient temperature for different MOFs (Reprinted with permission from [88], copyright 2005 American Chemical Society).	27
Figure 1.14 General flow sheet for the production of thermal ACs.	38
Figure 1.15 Schematics of different sized pore and their example microscopic images. (Adapted from [193-195])	48
Figure 2.1 N ₂ adsorption isotherms of pristine CNTs and activated CNTs obtained at different temperatures	81
Figure 2.2 Pore size distribution of pristine and activated CNTs at different temperature. (a) micropore size distribution; (b) mesopore size distribution.	84
Figure 2.3 Pore structure of activated MWCNTs with different activation time. (a) isotherm; (b) micropore size distribution; (c) mesopore size distribution.	86
Figure 2.4 High resolution TEM images. (a) Pristine MWCNTs; (b) activated MWCNTs (sample: ACNT-800-2h, with white arrows pointing to developed micropores)	88
Figure 2.5 Frequency histogram of pristine CNTs inner diameter distribution. (Overlay: PSD of ACNT-600-2h).	90
Figure 2.6 High resolution SEM images of MWCNTs. a) pristine CNTs; b) activated CNTs (ACNT-600-2h).	90

Figure 2.7 a) XRD analysis of activated MWCNTs at different temperature, with corresponding SEM images and EDX Mappings; b) XRD analysis of activated MWCNTs at 500°C with different activation time.	92
Figure 2.8 High resolution TEM image of ACNT-900-2h. (Black dashes denote the edges of graphene layers; white arrows denote carbon particles.)	93
Figure 2.9 Schematic diagram of pore forming mechanisms for KOH activated MWCNTs.	94
Figure 2.10(a) CO ₂ uptake vs. pore (<15nm) volume; (b) CO ₂ uptake vs. pore (<1nm) volume.	96
Figure 3.1 Schematic of temperature program for KOH activation process.....	106
Figure 3.2 Morphologies of PANI and PANI-derived carbons (C-2-200-800): (a) SEM image of PANI; (b) TEM image of PANI; (c) SEM image of C-2-200-800; (d) High-resolution TEM image of C-2-200-800.....	108
Figure 3.3 Isotherms (a, c, e) and pore size distributions (b, d, f) of PANI-derived carbons under various activation conditions. (a) (b): different activation temperature; (c) (d): different KOH ratio; (e) (f): different preheating temperature. (C-2-800 represents the sample without preheating stage)	109
Figure 3.4 Morphologies of PANI after preheating stage of different temperatures.	112
Figure 3.5 (a) Isotherms and (b) pore size distributions (based on BJH desorption model) of samples after preheating stage of different temperatures.....	114
Figure 3.6 (a) FTIR spectra of PANI and samples after preheating stage of different temperatures; (b) schematic for thermal crosslinking of PANI.(remake from [36])	117

Figure 3.7 (a) DSC curves of original PANI and (b) TGA and its derivative curves of the original PANI.....	119
Figure 4.1 Schematic diagram for branched Polyethylenimine (PEI).	129
Figure 4.2 SEM and TEM images of PEI-derived carbon (C-600): a) surface; b) cross-section; c) TEM image; d) HR-TEM image.	132
Figure 4.3 Nitrogen adsorption/desorption isotherms (a) and pore size distribution (b) of PEI-derived carbon samples under different temperature.	134
Figure 4.4 (a) FT-IR spectrums of PEI-derived carbons at different activation temperatures (Curves were displaced vertically in order to be differentiated.) ; (b) hypothesized carbonization of PEI.	136
Figure 4.5 XPS N 1s spectra of PEI-derived carbons. (a) Schematics of different nitrogen groups on PEI-derived carbons; (b) resolved peaks XPS N 1s spectra of PEI-derived carbons with different conditions.	137
Figure 4.6 CO ₂ adsorption isotherms of PEI-derived carbons at different temperatures. (a) 0 °C; (b) 25 °C; (c) 50 °C; (d) 75 °C.	141
Figure 4.7 Isosteric heat of adsorption for PEI-derived carbons.	142
Figure 4.8 Stability test (30 cycles) for PEI-derived carbon (C-600) at 25 °C. 1st cycle: 3.18 mmol/g, 2nd cycle: 3.35 mmol/g; 30th cycle: 3.32 mmol/g.....	143
Figure 4.9 (a) CO ₂ and N ₂ isotherms of PEI-derived carbon (C-600) at 25 °C and (b) initial slope for CO ₂ /N ₂ selectivity calculation.....	143
Figure 5.1 Li 1s XPS spectra of LiCl-incorporated ACs.	158
Figure 5.2 SEM images of ACs and LiCl-incorporated ACs (black arrows indicate small pieces of LiCl).	159

Figure 5.3	N ₂ adsorption/desorption isotherms of ACs and LiCl-incorporated ACs.	161
Figure 5.4	CO ₂ adsorption isotherms of ACs and LiCl-incorporated ACs at 0 °C.	163
Figure 5.5	CO ₂ adsorption isotherms of ACs and LiCl-incorporated ACs at various elevated temperatures (25/30 °C, 50 °C, and 75 °C).	165
Figure 5.6	Heat of adsorption (Q _{st}) of ACs and LiCl-incorporated ACs.	166

Chapter 1 Introduction

1.1 CO₂ emission and carbon capture

Since industrial revolution, the total amount of CO₂ emission caused by utilizing fossil fuel has been increasing. The subsequent results put a warning to human beings that mitigation of excessive CO₂ in the atmosphere has to be done in order to supplement the natural carbon cycle.

1.1.1 Fossil fuel, CO₂ emission and global warming

Even before the industrial age, humans have been relying on biomass such as woods, vegetation for heating, cooking etc. But not until the advent of the industrial revolution had fossil fuels (mainly coals at the time) become the main energy source and been massively exploited. With prosperity and booming population comes the increasing demand of fossil fuels. Putting aside the irreversibility of these natural resources and the fact that they are currently being depleted, a major problem caused by significant use of fossil fuels and related products is carbon dioxide, one of the several common greenhouse gases.

In natural carbon cycle (Figure 1.1), most atmospheric CO₂ is recycled via photosynthesis process. Plants use photosynthesis to convert CO₂ and H₂O into carbohydrates such as sugars. The energy stored in these carbohydrates could supply lives of the plants, and subsequently lives of herbivores' and carnivores'. Under some conditions, bodies of these plants and animals not consumed by bacteria are buried, preserved and fossilized. The fossilization process is slow and could take millions of years. Therefore most of the fossil fuels we use today contain carbon content accumulated through millions of years.

Eventually these carbons are released into the environment mainly in form of CO₂. Based on estimation from Carbon Dioxide Information Analysis Center (CDIAC) [1], global fossil fuel emission was 9.6 billion metric tons of carbon in 2012.

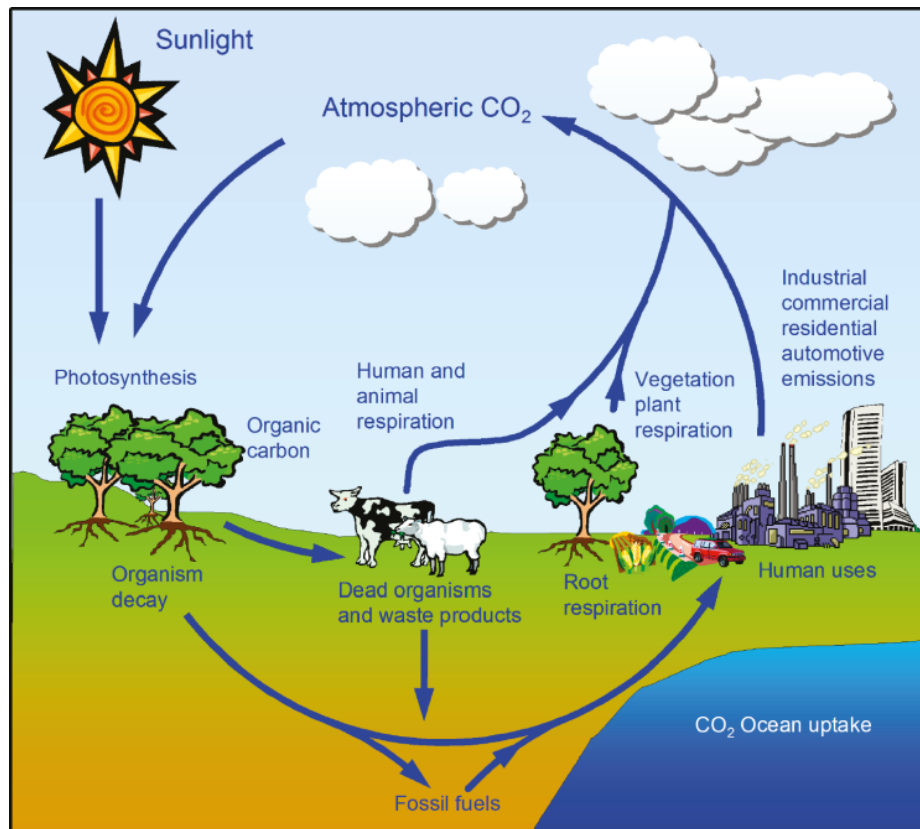


Figure 1.1 Natural carbon cycle (Reprint with permission from [2], copyright 2011 American Chemical Society).

The excessive emission of CO₂ has placed great influences on global atmospheric carbon balance. Figure 1.2 from National Oceanic and Atmospheric Administration (NOAA) shows a direct measurement of CO₂ from the atmosphere at Mauna Loa Observatory. It is clearly observed that the CO₂ concentration has been having a constant increasing trend since 1960. It was also reported that the CO₂ concentration has reached 400 ppm in 2015.

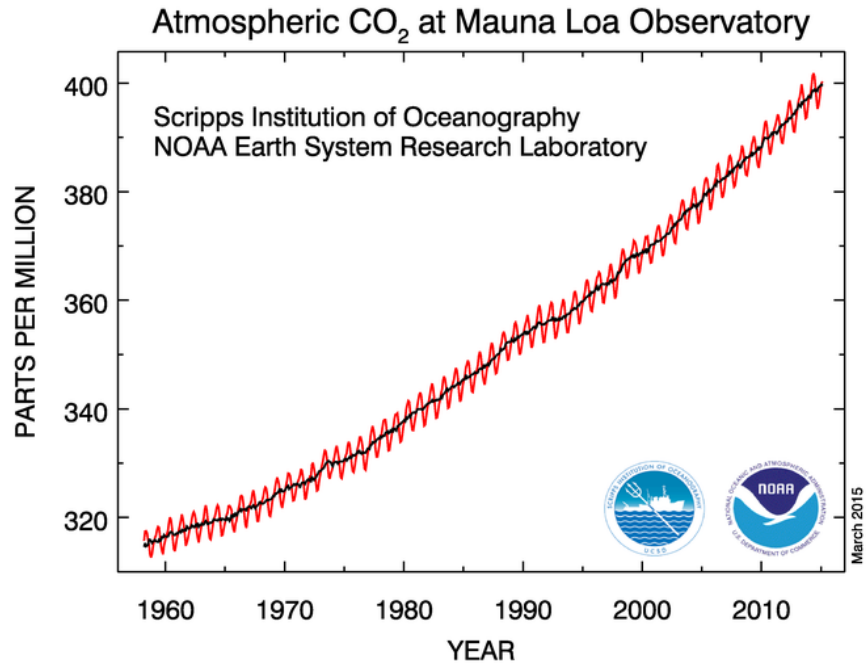


Figure 1.2 Atmospheric CO₂ level at Mauna Loa Observatory [3].

Global warming refers to the observed long-time rise in the average temperature of the Earth's system. Major effects of global warming include sea level rise, decrease in snow/ice extent and climate change. A severe global-warming effect could lead to increasing occurrence of extreme weather and species extinction [4]. The cause of temperature change is debatable, but it is well-acknowledged that change in atmospheric composition of the greenhouse gases is an important factor [5]. As could be seen in Table 1.1, although CO₂ has low global-warming potential (GWP), its concentration is significantly higher than any other gas. Therefore CO₂ is one of the main greenhouse gases in the atmosphere. Figure 1.3 also indicates that the recent trend of temperature change coincides with the drastically increasing CO₂ concentration in atmosphere, implying a critical role of CO₂ in global warming.

Table 1.1 Data for major greenhouse gases (Water vapor excluded).

	Recent tropospheric concentrations [1]	Lifetime [4] (years)	Global-warming potential (GWP) for 20-year period [4]
Carbon dioxide (CO ₂)	395 ppm ^a	30-95	1
Methane (CH ₄)	1893 ppb ^b	12	72
Nitrous oxide (N ₂ O)	326 ppb	114	289
Tropospheric ozone (O ₃)	337 ppb	-	-
CFC-12 (CCl ₂ F ₂)	527 ppt ^c	100	11,000

^appm: parts per million; ^bppb: parts per billion; ^cppt: parts per trillion.

In this context, international agreements such as Kyoto Protocol [6] have been reached to enforce reduction of greenhouse gases (mainly carbon dioxide) emission. Other policies [7] such as emission tax and renewable energy subsidies will soon be implemented. In this case, carbon emission reduction is not only for a sustainable future, but mandatory economically.

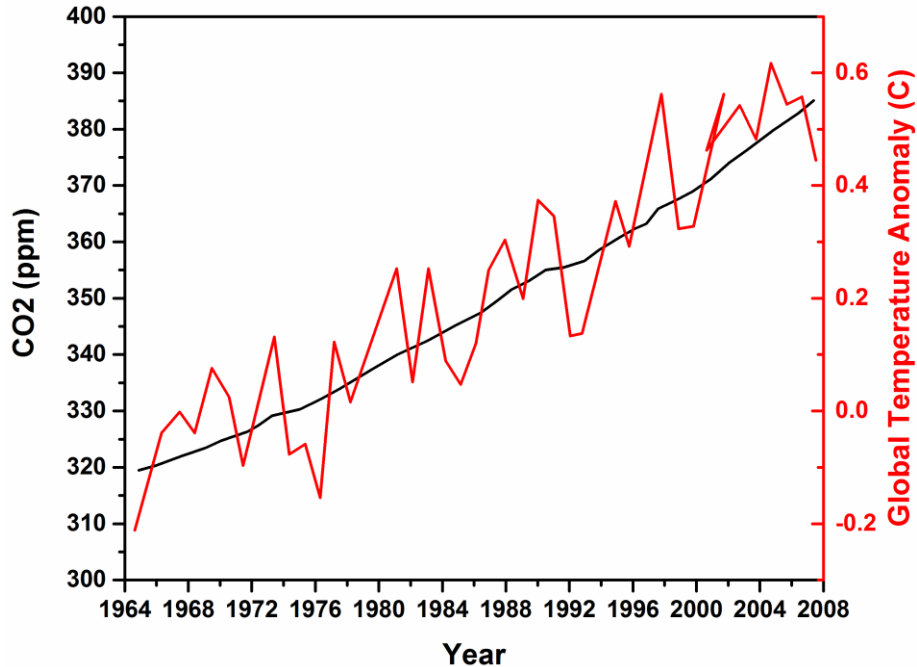


Figure 1.3 Atmospheric CO₂ and Global Temperature Anomaly (data from NASA [8]) from 1964 to 2008.

1.1.2 CO₂ emission from point sources

Before we move to CO₂ mitigation, a detailed analysis of CO₂ emission sources is necessary. Use of fossil fuel such as coal, oil and gas is the dominant source for anthropogenic CO₂ emission, with the remainders including land use change (primarily deforestation) and chemical processing (cement production etc.). According to a recent review [9] from CDIAC, the total CO₂ emission from fossil fuel burning in 2013 alone was ~36.3 Gigatons, 2.3% above the emission amount in 2012, sustaining a growth trend in the last several decades. Figure 1.4 shows the relative fraction of anthropogenic CO₂ emission from 6 categories of sources, which obviously indicates a significant role of contribution from power station.

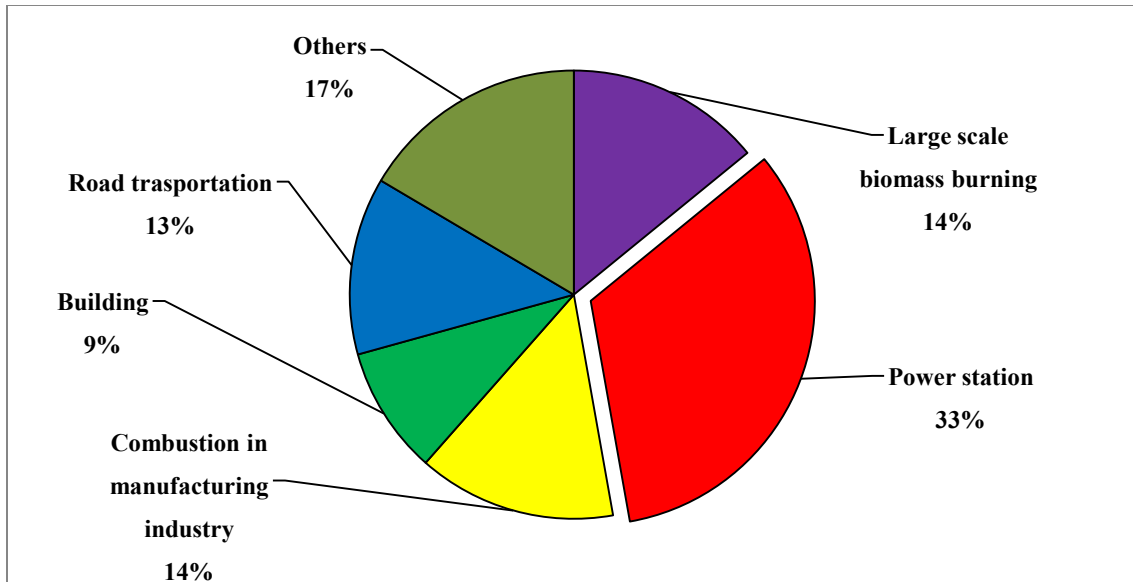


Figure 1.4 Global anthropogenic CO₂ emission contributions by sector in 2008.
(Adapted from data in the Emission Database for Global Atmospheric Research
version 4.2 [10])

Specifically for the U.S. which contributes the largest CO₂ emission amount, a report [11] from Energy Information Administration also shows that in 2012 CO₂ emission from electric power was 2039 million metric tons, taking up 38% of the total emission budget. As the world's second largest country of CO₂ emission, China has power generation which accounts for 73% of the total carbon emission [12]. What's more, fossil-fuelled power stations are still going to be in demand in the future to satisfy the increasing electricity use and to compensate for intermittent renewable energy source such as wind and solar plants. It is fair to say that these large point sources are the first and the most urgent part to start with when it comes to CO₂ mitigation.

1.1.3 Carbon capture and storage (CCS)

Currently existing options [13] for reducing CO₂ emission include demand-side conservation, supply-side efficiency improvement, increasing reliance on nuclear and renewable energy, and carbon capture and storage (CCS). However, CCS is considered to be the most practical approach for long term CO₂ mitigation. For a conventional 1000 MW coal-pulverized power plant, CO₂ waste per year is 6~8 Megatons [14]. With CCS application this value could be reduced by approximately 80~90% [15].

Generally, CCS (Figure 1.5) is comprised of three main processes: (1) CO₂ capture at point sources (such as coal-fired power plants); (2) CO₂ compression, transportation (through e.g. pipelines); (3) CO₂ injection to suitable storage sites (such as depleted oil fields, saline aquifers, etc.).

Parts of the CCS chain have been demonstrated to be at or close to industrial scale, while their integration into a single process is still a significant challenge [16]. The concept of CCS was proposed in 1989 and strategically confirmed by the U.S. Department of Energy in 2003 [17], the first integrated pilot-scale CCS power plant began operating in 2008 [15]. However, till the end of 2014 there were only 13 large-scale CCS projects in operation globally [18]. Some of the projects were abandoned during construction or after short-term operation due to unviable technology [19, 20].

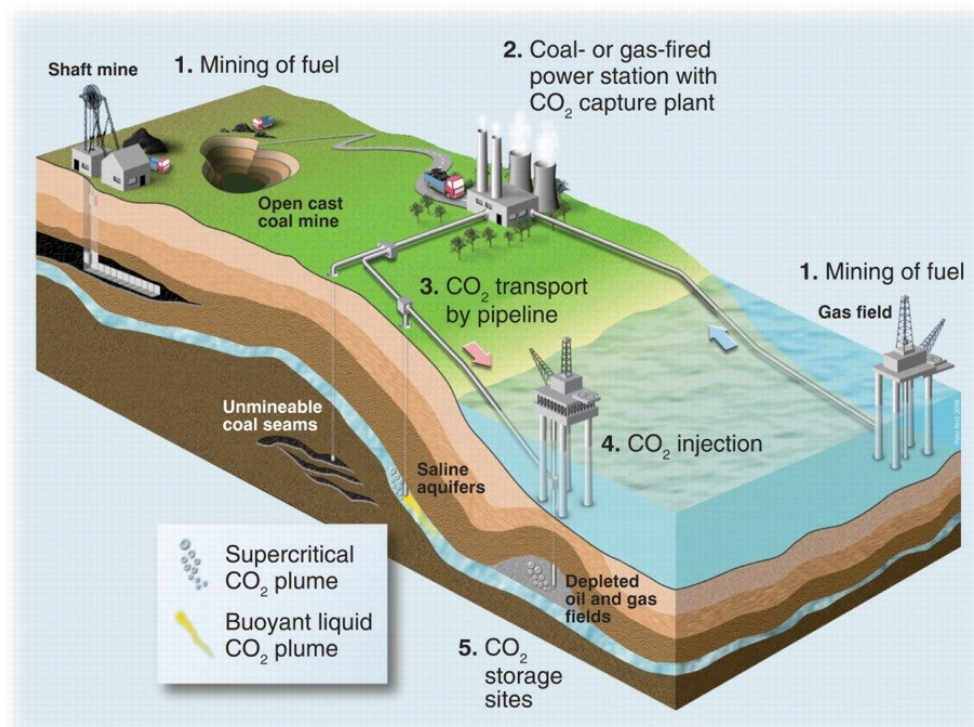


Figure 1.5 Diagrammatic representation of carbon capture and storage chain (From [21], reprinted with permission from AAAS).

Under current technological conditions, it is estimated that the capture stage accounts for 70~90% of the total cost of CCS system [14]. For a common coal-burning power plant, installation and operation of a state-of-the-art CO₂ capture system (e.g. amine scrubbing system) would decrease the net output by ~33% [22]. Therefore, in order to implement more practical CCS systems, it is imperative that new CO₂ capture technologies and materials be explored. In the following paragraphs, discussion will be focused on CO₂ capture technologies for large point sources.

1.2 CO₂ capture technologies and materials

Generally, current CO₂ capture from large point sources present several challenges: (1) how to improve CO₂ adsorption performance; (2) how to handle impurities (H₂O, SO_x and NO_x); (3) how to handle large quantities of continuous gas flow. Each of these challenges is connected to each other and has to be tackled without ignoring the others. Depending on applications, there are several technological systems for CO₂ capture. Most of the current technologies present cost-inefficiency, urging us to look for new and better technologies and materials.

1.2.1 Options for CO₂ capture

Main technological pathways for CO₂ capture include: post-combustion capture, pre-combustion capture and oxy-combustion capture. Figure 1.6 illustrates processes, CO₂ capture conditions and advantages/disadvantages of different approaches. It is of great importance to understand each approach, because different CO₂ waste condition leads to different capture technologies and materials. Post-combustion capture is to sequester CO₂ from flue gas produced by direct combustion of primary fuels. In pre-combustion capture, carbon content is converted to CO₂ (e.g. through gasification) before the combustion. The separation process occurs at very high pressure. Oxy-combustion uses pure oxygen instead of air to mix with fuels, to produce high concentration of CO₂ stream. Post-combustion capture usually applies to most air-fired, coal-fueled power plants. Pre-combustion capture can be applied to gasification plants and natural gas processing. Oxy-combustion can be applied to newer generation plants in future [22]. Among the three approaches, post-combustion capture is the most economically favored for existing power plants because retrofitting existing plants with post-combustion capture is expected to have the least cost

[15]. Oxy-combustion capture is still in demonstration phase [23]. Therefore in the following discussion only post-combustion and pre-combustion capture will be included.

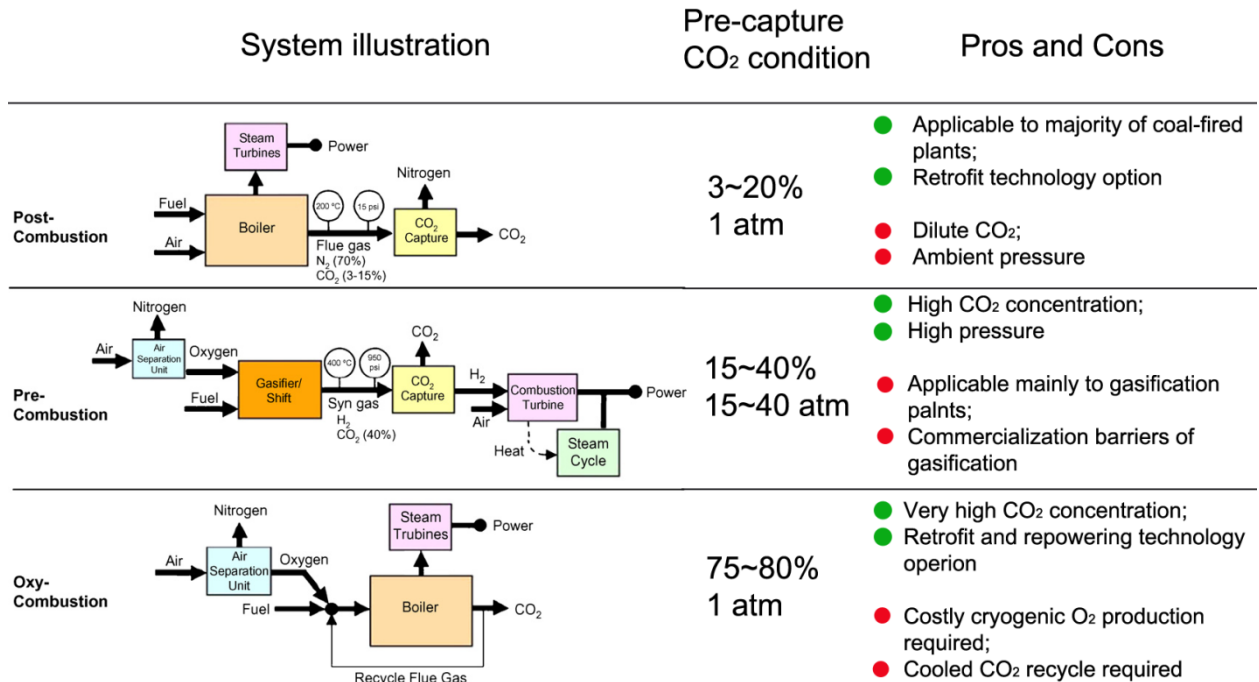


Figure 1.6 Processes capture condition and advantages/disadvantages of post-combustion, pre-combustion and oxy-combustion systems. (Adapted from [22], copyright 2008, with permission from Elsevier)

1.2.2 State-of-the-art materials for CO₂ capture

A key factor for separating CO₂ from mixed gas is to fully utilize the small differences between CO₂ and other gases, either physically or chemically. Depending on specific condition, evaluation of the best material for CO₂ capture is different. In this part the reviewed materials are mainly state-of-the-art materials for CO₂ capture.

1.2.2.1 Aqueous amine-based solutions

State-of-the-art aqueous amine absorption system or “wet scrubbing” technique has been employed industrially for over half a century and now is very mature in post-combustion capture. The basic principle of this technique is reaction between CO₂ molecule and chemicals containing amine groups (see Figure 1.7). Industrially monoethanolamine (MEA) is one of the most commonly used chemicals for absorption.

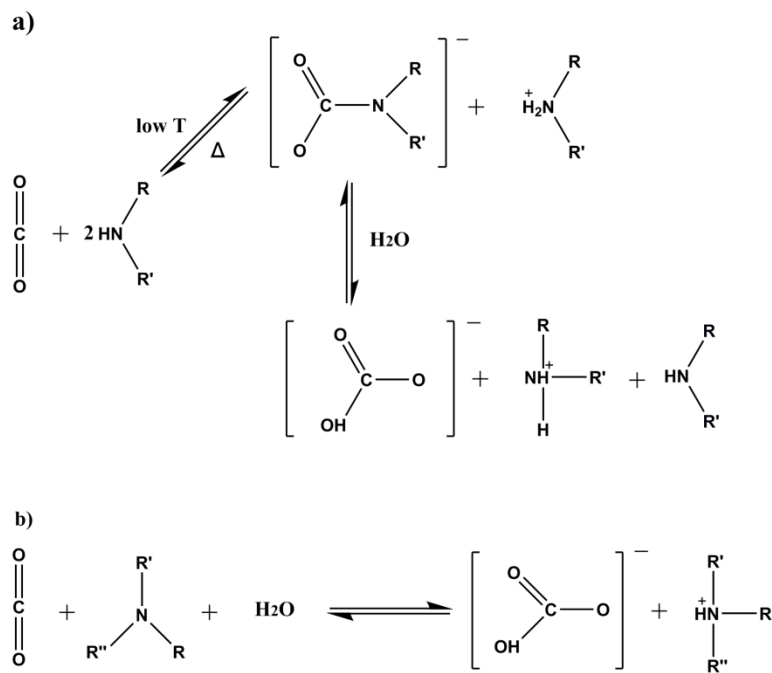


Figure 1.7 General reaction schemes between CO₂ and a) primary/secondary and b) tertiary amine-containing solvents [24].

As illustrated in Figure 1.8, the process involves the passage of a cold amine solution from the top of an absorption tower, while a gaseous stream of flue gas containing CO₂ is pumped at bottom. Upon completion of absorption, the CO₂-rich solution is sent to a

stripping tower (scrubber) where the solution will be heated to 100~150°C to liberate CO₂. Then the amine solution is cycled back to the previous tower for absorption again.

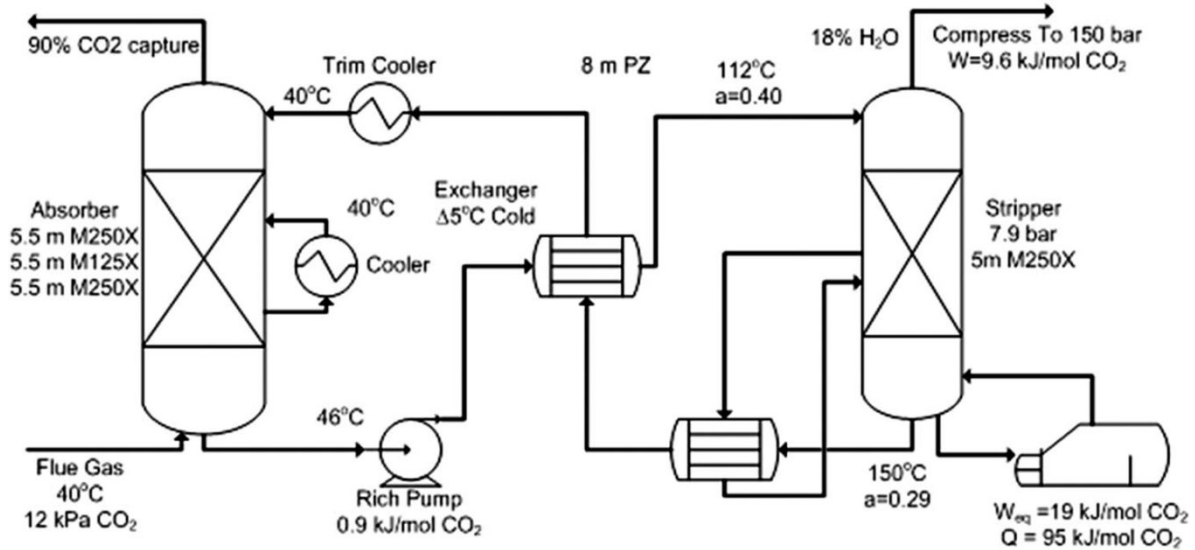


Figure 1.8 An improved amine-scrubbing system using 8M piperazine (PZ) for post-combustion CO₂ capture (From [16], copyright 2013, with permission from Royal Society of Chemistry).

This technology is end-of-pipe, easy for retrofitting to existing facilities without unduly affecting the flexibility of operation. Additionally, amine-based system is good at handling low CO₂ partial pressures. However, major drawbacks are obvious: (1) It has very high energy penalty during regeneration, which could account for 30% of the total power generated by plants. This penalty is primarily from heating large quantities of water in the solvent. (2) The absorption capacity is 0.85~2.11 mol CO₂ per kg H₂O [25], the improvement of the capacity is limited due to issues such like amine evaporation, degradation and corrosion.

Recently, several new amine-typed solvents (e.g. piperazine (PZ) [26, 27] and N-methyl-diethanolamine (MDEA) [28]) and mixed amines [29] have been explored and showed improved thermal/chemical stability and better performances. However, except the inherent limitations mentioned above, scale-up is also an issue for coal-fired power plants. Current technologies have an adsorption capacity of 320~800 tons/day CO₂ while a typical 500 MW power plant emits ~8000 tons/day CO₂. Much larger capture facilities need to be constructed for full-loaded operation.

1.2.2.2 Physical solvents

Physical solvents capture CO₂ from gas mixture by dissolving CO₂ in the solution instead of by chemical reaction. Based on Henry's Law, a high-efficiency capture requires conditions of high CO₂ partial pressure and low temperature [22]. Therefore, physical solvents absorption is more suitable for pre-combustion capture. There are currently four commercialized physical solvents: Selexol, Rectisol, Fluor and Purisol. In a typical process (see Figure 1.9), the primary fuel (coal, natural gas, etc.) is first gasified to produce syngas (CO & H₂). The CO is then converted to CO₂ in a shift converter, followed by contact with physical solvents. After absorption, the CO₂-rich solvent is regenerated by flash desorption (step depressurization).

Physical solvents have been proved in industrial-scale plants such like refineries. This technology also generates CO₂ under pressure thus less energy is required for compression. Regeneration is less energy-costly using pressure reduction. However, prior to CO₂ capture, the gas feed (syngas) must be pretreated to eliminate moisture and sulfur content. In addition, scale up is still required for integrated gasification combined cycle (IGCC) power plants and retrofit to existing plants is costly and difficult [30].

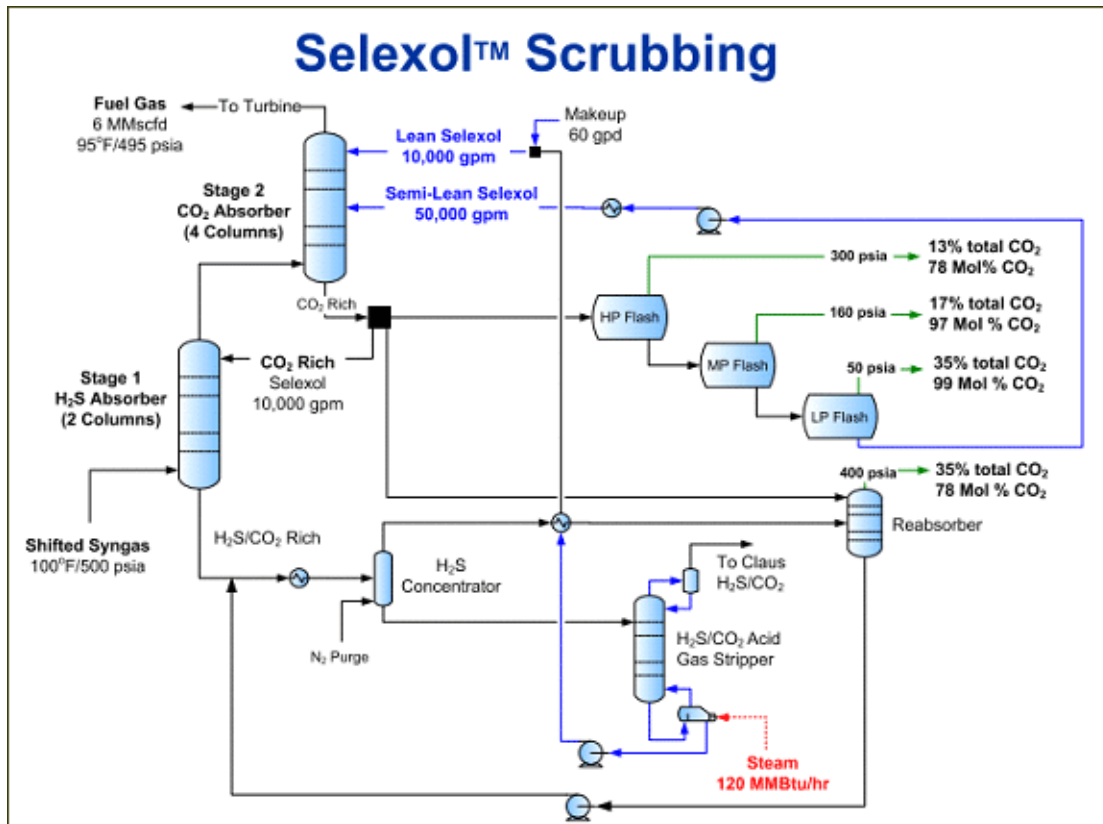


Figure 1.9 Selexol scrubbing process (With removal of sulfur, source from [31]).

Recently emerging ionic liquids (ILs) could also be considered as a type of physical solvent. The general area of IL use for CCS has been reviewed [32-35]. ILs could also be applied in post-combustion capture [36]. Compared with other physical solvents, ILs present lower energy demand for regeneration, lower volatility and higher thermal stability. The disadvantages of this material include high viscosity, unknown toxicity and production cost. The most suitable ILs for CO₂ capture have only been synthesized in small quantities in academic laboratories [22]. Time to commercialization of this material is considerable.

1.2.2.3 Membranes

The membrane acts as a filter to remove one or more gas components from the mixed gas (flue gas or syngas). The driving force behind this act is the pressure difference between both sides of the membrane, as seen by Fick's Law in Eq. (1.1).

$$J_i = \frac{P_{i^*}}{\delta} A_m \Delta p \quad (1.1)$$

Where J_i is the flux of component I across the membrane ($\text{cm}^3 \text{ s}^{-1}$), P_{i^*} is the permeability of the membrane in terms of component i ($10^{-10} \text{ cm}^3 \text{ (STP) cm s}^{-1} \text{ cm}^2 \text{ cm Hg}$), δ is the membrane thickness (cm), A_m is the membrane area (cm^2), and Δp is the pressure difference (cm Hg) across the membrane.

Permeability and selectivity are two characteristics that describe the performance of a membrane. These two factors vary depending on the gas stream component and intrinsic property of the membrane. In order to increase CO_2 selectivity, amine groups were incorporated into silica membranes [37, 38]. These inorganic membranes are more thermally and chemically stable. Organic membranes [39] (such as polyaniline [40], poly(arylene ether) [41], poly(ethylene oxide) [42], etc.), on the other hand, demonstrated better permeability. There are also mixed matrix membranes reported, but with high cost [43].

Currently, membrane technology has already been commercially used in CO_2 removal from natural gas [15]. When it comes to post-combustion capture, membranes present more energy consumption than amine absorption due to low CO_2 content and ambient pressure. For pre-combustion capture, a lab-scaled polybenzimidazole (PBI) membrane [22] has been reported to present H_2/CO_2 selectivity versus permeability that exceeded current standards

and long-term hydrothermal stability up to 400 °C. However, cost efficiency needs to be evaluated.

1.3 Solid sorbents (adsorbents)

Solid sorbents adsorption is considered as one of the most promising technologies in CCS [22]. Adsorbents use gas adsorption (physisorption or chemisorption) to capture CO₂ from the mixed gas. In post-combustion, capturing CO₂ by adsorption requires much less regeneration energy than solvent absorption, which is a major advantage for adsorbents. Adsorbents are usually loaded in packed bed. After adsorption, the material must go through a desorption stage, during which adsorbed CO₂ is driven off the adsorbent and the adsorbent is consequently regenerated for the next adsorption process. By regeneration method the processes could be divided into temperature swing adsorption (TSA), pressure swing adsorption (PSA), vacuum swing adsorption (VSA) and vacuum-pressure swing adsorption (VPSA) etc. Figure 1.10 illustrates some of the processes schematically. In TSA process CO₂ is desorbed by increasing temperature, while in PSA process the bed is pressurized for adsorption and depressurized for desorption. VSA process is similar to PSA, except that it uses vacuum for desorption. VPSA process is a combination of PSA and VSA processes. Temperature swing method could maintain a high CO₂ partial pressure during regeneration, which is beneficial to the subsequent CO₂ compression process. On the other hand, the process is time-consuming. In pressure swing methods (PSA, VSA, PVSA), regeneration could be finished in seconds while the purified CO₂ needs to be re-compressed [24].

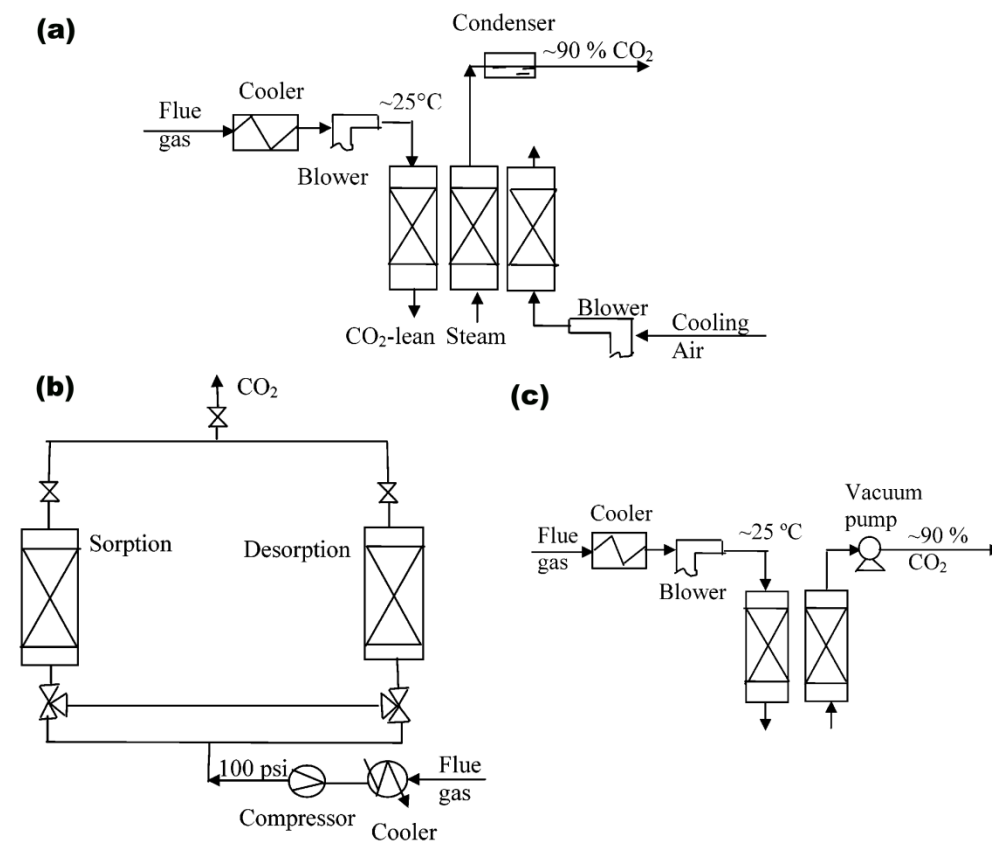


Figure 1.10 (a) Temperature swing adsorption (TSA); (b) pressure swing adsorption (PSA); (c) vacuum swing adsorption (VSA). (Adapted with permission from [44], copyright 2008 American Chemical Society)

When evaluating adsorbents for CO₂ capture, several merits need to be considered:

1. High CO₂ adsorption capacity: good CO₂ adsorption capacity of the adsorbent helps reduce the size of the facility when scale-up is needed. Care must be taken here that although equilibrium CO₂ adsorption capacity is important, working capacity is more preferred for practical material evaluation. Working capacity depends on adsorption time, gas component etc. It is suggested that in order to economically surmount the current

amine-based system, an adsorbent should possess a working capacity of 2~4 mol CO₂ per kg adsorbent, which is a criterion based on zeolite 13X in a PSA process [45].

2. Fast kinetics: the kinetics of the adsorbent determines adsorption/desorption rate, which is of paramount importance to the working capacity. For example, fast kinetics shortens adsorption time, thus reducing the single cycle period.

3. High CO₂ selectivity: the adsorbent must preferentially adsorb CO₂ over the other gas components (such as N₂ in flue gas, H₂ in syngas). A high selectivity produces high purity CO₂ during regeneration.

4. Mild regeneration condition: less energy is required under a mild regeneration condition, which is basically related to a weak binding force between CO₂ molecules and the adsorbent surface. The detailed interaction between CO₂ molecule and the surface will be discussed in 1.4.2.1.

5. Good stability during the adsorption/desorption cycle: an enduring adsorbent should not present significant performance decrement during a long period of operation time. This also helps reduce the cost by reducing the frequency of adsorbent replacement.

6. Tolerance of impurities: a good adsorbent must be tolerant to various impurities (SO_x, NO_x, H₂O for flue gas and H₂S, H₂O for syngas). Sometimes the impurities could significantly reduce the CO₂ adsorption capacity and even degrade the adsorbent.

7. Low cost: with similar performance, adsorbents with low synthesis cost would be preferred.

It should be noted that in reality no single ideal adsorbent is possible to possess all merits described above. Rather, it is only meaningful to evaluate each adsorbent within a specific CO₂ capture practice. According to Department of Energy of the U.S., a specific overall criterion is to capture over 90% CO₂ at the cost of electricity of less than 20% for large-scale power plants post-combustion applications. In the following, several widely studied adsorbents are reviewed in terms of their CO₂ capture performance. (If not mentioned, the CO₂ capture condition is post-combustion capture.)

1.3.1 Zeolites

Zeolites are highly ordered porous crystalline aluminosilicates. The presence of aluminum atoms in these silicate-based materials induces a negative charged framework that is compensated with exchangeable cations (often alkali ions) in the pore space. Zeolites are amongst the most widely reported adsorbents for CO₂ capture in the patent and journal literature [46].

Early CO₂ adsorption studies using zeolites have shown the primary mechanism of adsorption to be physisorption [47]. It was reported that the electric field created by the charge-balancing cations in the pores and by hydrogen bonding with surface silanol groups significantly influenced the physisorption process [47-49]. Therefore, extraframework cations largely affect the CO₂ performance of zeolites. Some studies [50, 51] showed that a low Si/Al ratio (or an ideally high content of cations) is desired for CO₂ adsorption. In a comparison study [52] of zeolites with various Si/Al ratios, including 5A, 13X, NaY, ZSM-5(MFI) and HiSiv-3000 (see Figure 1.11), the isotherms of these zeolites revealed an increasing adsorption capacity with Si/Al ratio in a following order: 13X (Si/Al=2.2) > NaY (Si/Al=5.1) > HZSM-5-30 (Si/Al=30) > HiSiv-3000 (Si/Al>1000). Additionally,

LeVan's group [51] tested the performances of zeolites exchanged with different alkali metal cations. It was found the CO₂ adsorption capacities increased as the cation radii decreased, in the order of Cs⁺ < Rb⁺ < K⁺ < Na⁺ < Li⁺.

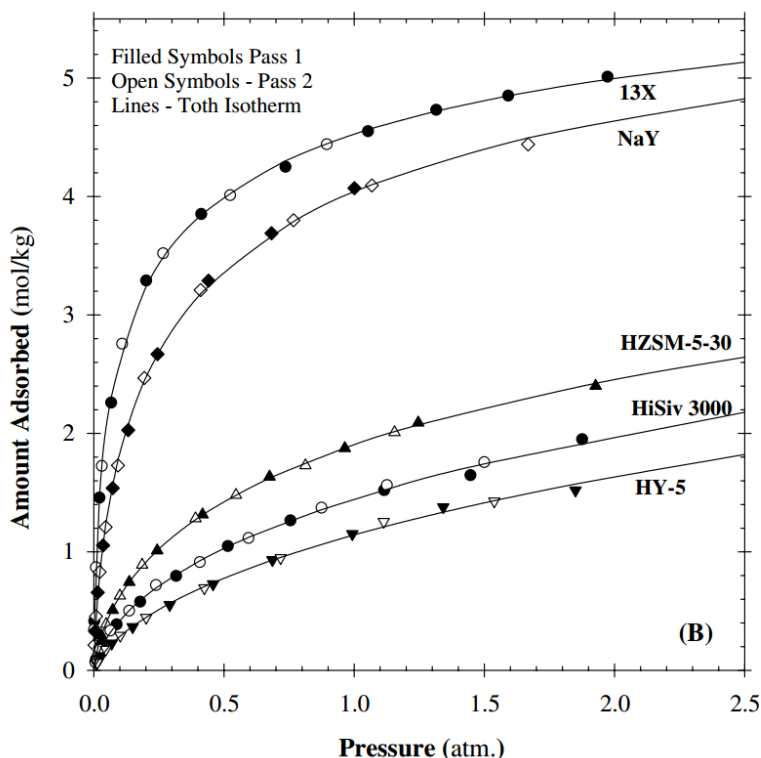


Figure 1.11 Pure component CO₂ isotherms of different zeolites at 295K (From [52], copyright 2004, with permission from Elsevier).

It was also found that the CO₂ adsorption properties were influenced by the porous structure of the framework. Among several commercially available zeolites, Siriwardane [53] reported a highest adsorption capacity of 13X, which had the largest pore diameter and volume. In Table 1.2 listed the CO₂ adsorption capacity of some zeolites, indicating favorable CO₂ adsorption capacity of these zeolites at ambient temperature and 1atm. In

post-combustion CO₂ condition where $p_{CO_2} \approx 0.15$ atm, the capacities shown in Table 1.2 are still far from satisfactory.

Table 1.2 CO₂ adsorption capacities of some commercialized zeolites.

Zeolites	Adsorption temperature (K)	Adsorption pressure p_{CO_2} (atm)	Adsorption capacity (mol kg ⁻¹)	Reference
Natural	298	0.15	1.25	[54]
13X	298	1	6.50	[55]
13X	393	0.15	0.70	[53]
4A	393	0.15	0.5	[53]
NaX	323	1	2.70	[56]
NaY	303	1	5.5	[57]
ZSM-5	313	0.1	0.32	[58]

In terms of kinetics, Barrer [59] proposed a diffusion model assuming an isothermal, constant-volume condition, which was employed by many later studies. A non-isothermal uptake model [60] came up to justify those zeolites which did not match the isothermal model. Whatever the model is, zeolites can be recognized as the fastest adsorbent for CO₂ adsorption, reaching their equilibrium capacity within a few minutes. Sometimes elevated temperature or pressure further accelerates the adsorption rate [59].

Zeolites usually have long-term regenerability by PSA. However, it was reported by some study [61] that a small amount of irreversible adsorption during PSA was due to

chemisorbed CO₂, which could be desorbed at elevated temperature [54]. Meanwhile, zeolite-based TSA process usually requires relatively high desorption temperature (~135 °C) [62].

More importantly, many investigations conducted experimentally and computationally [63-66] showed a high selectivity of CO₂ over other gases. For example, the high working capacity and selectivity made zeolite 13X one of the best choice for CO₂ capture from flue gas [52, 55, 67] and a benchmark material in many cases.

However, preferential adsorption of H₂O over CO₂ is the most detrimental problem for zeolites application in CO₂ capture. A good affinity between zeolites and H₂O makes dehydration during regeneration merely impossible. It was reported the dehydration of H₂O-containing NaX requires over 60 h [68]. And the CO₂ adsorption capacity would be significantly compromised [69]. Currently, costly multi-stage impurity removal system must be added for zeolite-based adsorbents. What's more, scale-up has not been reported in spite of many efforts [70, 71] that were made to optimize zeolite-based PSA process industrially.

1.3.2 Activated carbons (ACs)

Activated carbons (ACs) are well-known adsorbents and competitive because of their low price. This type of carbons is typically micro- and mesoporous, with a high Brunauer-Emmett-Teller (BET) surface area and a broad pore size distribution. ACs could be produced from various resources, which in turn brings about materials with various porous structures and surface properties. These different textural properties of ACs make their adsorption behavior highly variable.

In terms of CO₂ capture, adsorption on ACs is mostly physisorption, similar with that on zeolites. Generally, it is recognized that ACs have a lower capacity than zeolites at ambient conditions. Table 1.3 lists some results of CO₂ uptakes on ACs. Early studies [72, 73] showed that a typical CO₂ adsorption capacity of ACs was 2~2.5 mmol g⁻¹ at 298 K and 1 bar, while that of zeolite 13X could reach 6.5 mmol g⁻¹ under the same condition. On the other hand, at high pressures ACs perform better than zeolites.

Table 1.3 CO₂ adsorption capacity of selected ACs.

ACs	Adsorption temperature (K)	Adsorption pressure p_{CO_2} (bar)	Adsorption capacity (mol kg ⁻¹)	Reference
AC	298	1	3.3	[74]
AC	298	1	2.5	[75]
AC-Norit RB1	294.1	1	2.46	[76]
Peat-based AC	298	1	2.07	[77]
C35N000	309	1	1.73	[78]
Anthracite-based AC	303	1	1.38	[79]

In Figure 1.12, it can be observed that the capacity of activated carbon exceeds that of zeolite at ~2 bar (30 psia). As the pressure increases, CO₂ uptake on AC keeps increasing to ~9 mmol g⁻¹, while those on zeolites remain at the same level. Some other study [80] also

reported similarly high values for different ACs. This is attributed to the high BET surface area of the AC. For this reason, ACs are attractive in pre-combustion capture.

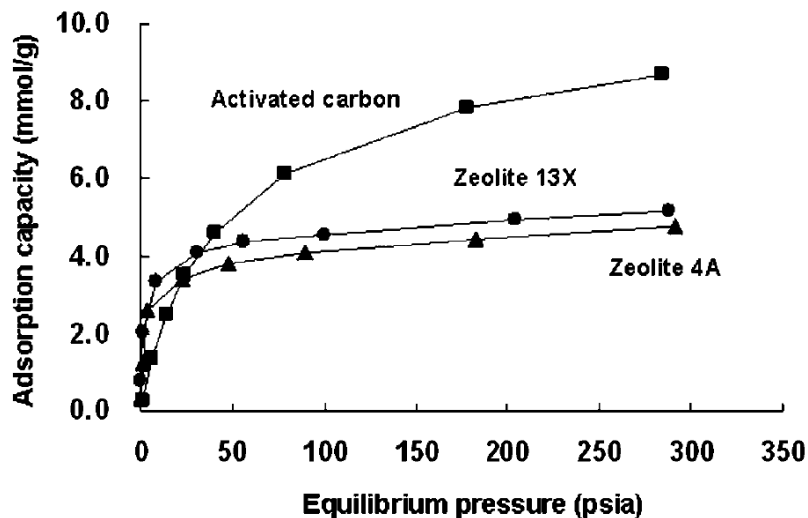


Figure 1.12 CO₂ adsorption isotherms on activated carbon, zeolite 13X and zeolite 4A at 298 K (Reprinted with permission from [75], copyright 2001 American Chemical Society).

The selectivity of CO₂ on ACs is generally lower than zeolites, for that ACs have relatively uniform surface electric field. This leads to a lower interaction, thus a lower heat of adsorption for CO₂. Specifically, a study [73] showed that for zeolite 13X the average value of heat of adsorption was $\sim 36 \text{ kJ mol}^{-1}$, while for AC it was $\sim 30 \text{ kJ mol}^{-1}$. CO₂ adsorption capacity at low pressures was partly influenced due to the same reason.

On the other hand, low heat of adsorption is beneficial to the regeneration condition, meaning that CO₂ could desorb at mild condition with less energy penalty. At the same time, ACs was proven to be one of the best CO₂ capture materials in terms of regenerability: it showed high reproducible results within many cycles [75].

Kinetics of ACs is also comparable to that of zeolites. This benign property was attributed to a typical bimodal distribution of pore size, which included diffusional transport mechanism in both micropores and macropores [81, 82]. However, due to variable carbon sources of different ACs, careful examination of pore structure is required. With optimized pore structure, AC adsorbents could achieve equilibrium on a time scale of minutes.

Impurities could be a major issue for ACs application in CO₂ capture. H₂O was reported to impair CO₂ adsorption capacity in spite of AC's hydrophobic property [46]. The reason for this is complex. In some research it was considered to be a synergic effect of CO₂ and H₂O for CO₂ chemical fixation [83]. Others [84] believed this was due to a simply adsorptive competition between CO₂ and H₂O molecules. However, the impact is not as severe as for zeolites. NO_x and SO_x have also been shown to compete with CO₂ for adsorption sites [13].

ACs will remain competitive in future CO₂ capture application because of their low raw material price and merits on regeneration and adsorption capacity at high pressures.

1.3.3 Metal organic frameworks (MOFs)

Metal organic frameworks are an emerging class of materials, composed of metal-based nodes (single ions or clusters) bridged by organic linking groups to form multi-dimensional coordination network. A recent trend of increasing popularity in MOFs-based CO₂ adsorbents has been observed. MOFs are particularly interesting because of their extremely high BET surface area and ability to easily tune pore parameters such as pore size and pore shape. For example, Yaghi's group [85] reported a type of MOF, MOF-210 with a BET surface area of ~6200 m² g⁻¹, which is much higher than reported values from zeolites (up to ~1000 m² g⁻¹) and ACs (up to ~3500 m² g⁻¹).

MOFs have made some excellent results for CO₂ adsorption at both low and high pressures. Table 1.4 listed some exceptional results of CO₂ uptakes on MOFs. As could be seen, at high pressures the CO₂ adsorption capacities of some MOFs have even surpassed those of ACs, suggesting that they are more applicable for pre-combustion capture. Most MOFs present satisfactory adsorption capacities at 1 bar. However in post-combustion condition where CO₂ partial pressure is 0.15 bar, only a few MOFs are competitive with zeolites in terms of capacity.

Table 1.4 CO₂ adsorption capacities of selected MOFs.

MOFs names	Adsorption temperature (K)	Adsorption pressure p_{CO_2} (bar)	Adsorption capacity (mol kg ⁻¹)	Reference
Mg-MOF-74	278	36	15.56	[86]
MOF-5	298	40	18.70	[87]
MOF-177	298	42	33.5	[88]
MIL-101c(Cr)	304	50	40	[89]
MOF-210	298	50	54.54	[85]
Mg-MOF-74	298	1	6.25	[90]
Co-MOF-74	298	1	5.66	[91]
HKUST-1	293	1	4.50	[92]
MOF-5	296	1	1.93	[93]
Mg-MOF-74	303	0.15	4.68*	[94]
Co-MOF-74	298	0.15	3.22*	[91]

HKUST-1	293	0.15	2.63*	[92]
MOF-5	298	0.15	0.11*	[91]

*: these values are estimated based on the data obtained from corresponding reference.

In a study carried out by Yaghi [88], isotherms of many MOFs conformed to a Langmuir-like shape, where at lower CO₂ partial pressures small changes in pressure resulted in large changes in capacity (see Figure 1.13). This property potentially obstructs MOFs' application in post-combustion CO₂ capture.

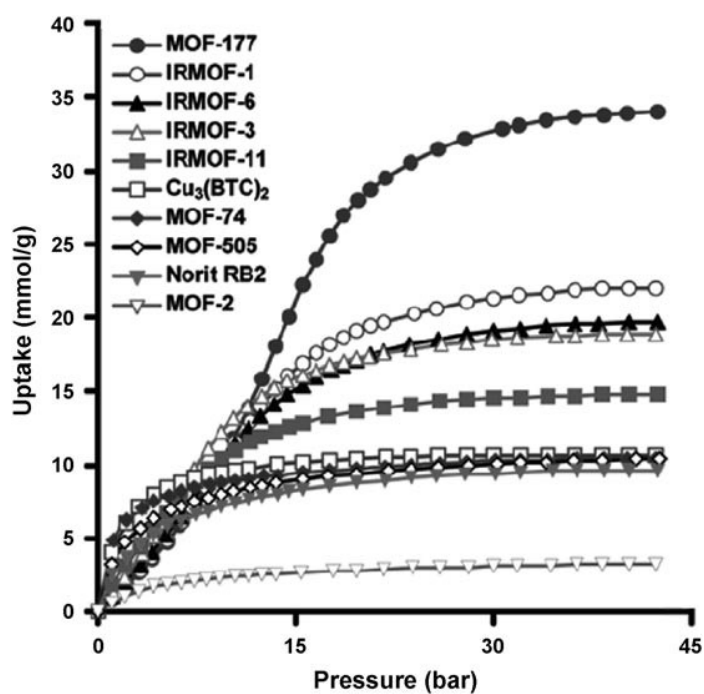


Figure 1.13 CO₂ adsorption isotherms at ambient temperature for different MOFs (Reprinted with permission from [88], copyright 2005 American Chemical Society).

Variable selectivity values of CO₂ on MOFs have been reported [92, 94, 95]. Based on simulation results, the high selectivity was caused by a high density of open metal sites or extra framework ions [96]. Other approaches to high selectivity include modification of the

solvent molecules with highly polar ligands [97] and modification of organic linkers [98], etc.

The regeneration of MOFs has not been comprehensively studied. Some studies suggested a hysteresis in adsorption/desorption tests for certain MOFs [99], while Ni-MOF-74 was found to retain its capacity over 10 runs under moisture condition [100]. In terms of heat of adsorption, the values of different MOFs varied a lot. The MOFs with highest value of heat of adsorption was reported to be amine-functionalized Cu-BTTri-mmen, with a Q_{st} value of 96 kJ mol^{-1} [95]. This value was relatively high even in regime of chemisorption. Q_{st} of some MOFs with exposed metal sites could also reach 60 kJ mol^{-1} [89]. However, some MOFs had a relatively low Q_{st} value of $15\sim 35 \text{ kJ mol}^{-1}$ [101-103].

While a high heat of adsorption would favor CO_2 uptake at lower pressures, this alone would not necessarily translate to good capture performance in CO_2 capture condition, where competing gas molecules exist. Moisture is always a critical problem for post-combustion capture. In the case of MOFs-based adsorbents, H_2O was able to displace the ligands and create structural defects in the crystal lattice of the MOF [104]. After many efforts, there have been several types of MOFs reported to be water-stable [105-108], although further investigation is still needed. Particularly, LeVan *et al.* examined Ni-MOF-74 at humid flue gas condition. The material presented a CO_2 capacity of 3.28 mmol g^{-1} , higher than the value of benchmark zeolites (5A and NaX) under the same condition [109].

Given that the field of MOFs is still emerging, most of the studies are focusing on CO_2 capture capacity and selectivity, more work need to be done for evaluation of MOFs-based sorbents in more practical CO_2 capture condition (e.g. post-combustion, pre-combustion).

1.3.4 Amine functionalized materials


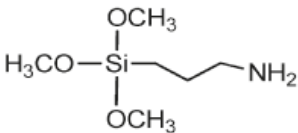
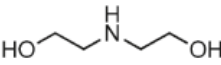
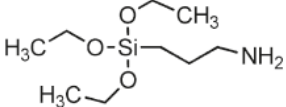
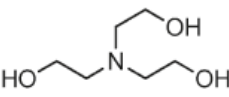
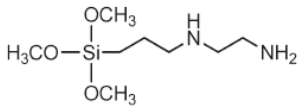
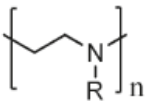
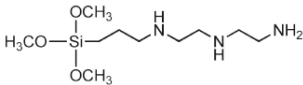
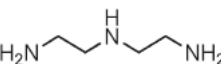
Most of the materials described above are physical adsorbents. These adsorbents usually display inadequate CO₂ adsorption capacity at low pressures and insufficient CO₂ selectivity. In contrast, amine-based absorption is more CO₂ selective. This is because of the chemical bond built between CO₂ and amine groups during the capture (Figure 1.7). Therefore a variety of microporous/mesoporous materials loaded with basic nitrogen functionality, more specifically, organic amine functionality have been synthesized and characterized to chemisorb CO₂ [109]. Supported amine adsorbents have been classified into three classes:

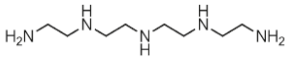

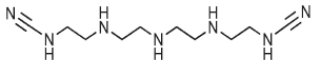
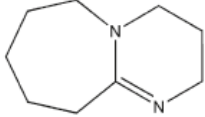
- Class 1: This class of adsorbents is prepared by physically loading monomeric or polymeric amine species into or onto the porous support (typically, the porous silica by impregnation technique).
- Class 2: This class of adsorbents is that in which the amine, mainly amine-containing silane, is covalently tethered to a solid support, such as porous silica. This is accomplished by binding amines to oxides via the use of silane chemistry or via preparation of polymeric supports with amine-containing side chains. This provides adsorbents with the potential to be completely regenerable through multicycle adsorption/desorption uses.
- Class 3: These adsorbents are based on porous support upon which amino-polymers are polymerized *in situ*. This category of support adsorbents can be considered a hybrid of the other two classes.

There have been a number of amines investigated for functionalization, with the guiding principle of maximizing the weight percentage of nitrogen. The intent of this principle is to

maximize the capture capacity per weight of adsorbent. However, other parameters are of great importance when determining the total CO₂ adsorption performance. From Figure 1.7, it is also important to be noted that tertiary amine binds with CO₂ more efficiently than primary and secondary amines. The structure of some widely used amines for functionalization is given in Table 1.5.

Table 1.5 Structure of Amines for adsorbent functionalization [109].

Name	Structure	Name	Structure
Amine		Silane	
Monoethanolamine (MEA)		3-aminopropyl-trimethoxysilane (APTS)	
Diethanolamine (DEA)		3-aminopropyl-triethoxysilane (APTES)	
Triethanolamine (TEA)		N-[3-(trimethoxysilyl)propyl]- ethylenediamine (AEAPTS)	
Polyethyleneimine (PEI)		N-[3-(trimethoxysilyl)propyl]- diethylenetriamine (DAEAPTS)	
Diethylenetriamine (DETA)		Cyclic	

Tetraethylenepent-amine(TEPA)		Aziridine	
Tetraethylenepent-amineacrylonitrile (TEPAN)		1,8-diazabicyclo[5.4.0]undec-7-ene (DBU)	

As for the support materials, amine functionalization usually blocks access to the original pores, leading to a decrease of the surface area of the porous support materials, thus a decrease of physisorption. Therefore, a trade off exists for amine functionalization of microporous materials. However, a relatively larger-sized pore would make room for more amine groups, at the same time it allows reasonable diffusion of CO₂. Therefore mesoporous materials are more popular when it comes to amine functionalization. In the following we will be focusing on amine-functionalized mesoporous materials.

For the discussion on CO₂ adsorption of mesoporous materials, the first type of materials that has to be mentioned is ordered mesoporous silica. They have many advantages: easy to synthesize, reproduce and characterize. The first amine-impregnated ordered mesoporous silica used for CO₂ capture was reported by Song *et al.* [110] in 2002. In the following work MCM-41 was loaded with 75 wt% PEI and presented a CO₂ uptake of 3.02 mmol g⁻¹ at 75 °C, 1 atm [111]. This kind of materials was termed as “molecular baskets” [111, 112]. The majority of CO₂ adsorption capacity was considered to come from chemisorption of PEI loaded, since the unmodified MCM-41 showed negligible adsorption. Additionally, it was hypothesized that there is a synergetic effect of MCM-41 on the PEI for the adsorption of CO₂ [111]. Another mesoporous silica with relatively larger pore, SBA-15 was

developed and modified with PEI [113]. Subsequently, several groups have reported the use of amine-functionalized silica as CO₂ adsorbents with various results. Table 1.6 shows some CO₂ adsorption results of these materials. It could be observed that in some cases the reported performances of the amine-functionalized silica were rather satisfactory, although the grafted silica showed relatively lower capacities than the impregnated ones. More importantly, most test conditions were under 75 °C and 0.15 atm, which is more practical for post-combustion CO₂ capture (even though heating of the flue gas is needed for best performance in some conditions). Another worth nothing point is that there was a critical value of amine loading, passing which the capacity and amine efficiency would start to decrease [114]. The silica pore structure also plays an important role. The CO₂ adsorption capacities of different pore-size support materials with same PEI loading were in the following order [115]:

KIT-6 (d=6.5 nm) > SBA-15 (d=5.5 nm) ≈ SBA-16 (d=4.1nm) > MCM-48 (d=3.1 nm) > MCM-41 (d=2.1 nm)

d represents average pore diameter.

Table 1.6 CO₂ adsorption capacity of some amine-functionalized mesoporous silica.

Support	amine	Adsorption temperature (°C)	Adsorption pressure p_{CO_2} (bar)	Adsorption capacity* (mol kg ⁻¹)	Reference
MCM-41	PEI	75	1	3.02	[110]

MCM-41	TEPA	75	0.05	4.54	[116]
SBA-15	PEI	75	0.15	3.18	[113]
KIT-6	PEI	75	0.05	1.95	[115]
SBA-15	DAEAPTS (grafted)	60	0.15	1.1	[117]
SBA-15	APTES (grafted)	25	0.1	1.53	[118]
SBA-15	Aziridine polymer (grafted)	25	0.1	(5.55)	[119]
MCM-41	DAEAPTS (grafted)	70	0.05	2.28	[120]

*: values in brackets are in humid condition.

The adsorption/desorption rate of amine-functionalized silica is as good as, if not better than, that of zeolites. However, the adsorption curves usually present a quick adsorption phase followed by a slow approach to equilibrium. Generally, the factors influencing the rate of CO₂ adsorption include amine loading, pore size and amine type [46]. Xu *et al.* [111] also pointed out that the overall adsorption capacity could be kinetically limited by adsorption rate.

Amine-functionalized silica shows a very high CO₂ selectivity, which is mainly attributed to their chemisorption nature. In a simulated study carried out by Xu *et al.* [121], PEI modified MCM-41 showed a separation selectivity of >1000 for CO₂/N₂ at a temperature range of 25~100 °C. This result is much better than that of any physisorption adsorbent.

However, heat of adsorption for amine-functionalized silica is also one of the highest among the materials, in the range of 60~90 kJ mol⁻¹ [109]. This results in a high regeneration energy penalty, leading to a high desorption temperature (>100 °C) during TSA process. But this is still more cost-efficient than amine-based absorption. The major defect lies in the poor regenerability of amine-impregnated silica, because of amine leaching or adsorbent degradation [122] problem at high regeneration temperatures. Amine grafting was reported to be more stable than amine impregnation [114], but with lower CO₂ adsorption capacity. For alternative approach, lower temperature [123, 124] or PSA [125] were suggested.

In contrast to other adsorbents, amine-functionalized silica is theoretically advantageous in humid CO₂ capture condition. Most studies [126-129] reported improved CO₂ adsorption capacities with addition of H₂O. Except for formation of carbamates (Figure 1.7), formation of carbonates and bicarbonates was assumed to be the mechanism for CO₂ capacity increase [126, 130].

1.3.5 Others

Carbon molecular sieves (CMSs) represent a class of microporous carbon materials whose characteristics permits kinetic separation of the gas mixture. For CO₂ capture CMSs must possess a narrow pore size distribution, consisting of pore mouths of molecular sizes and a relatively high micropore volume. These features resulted in high selectivity and capacity, respectively [131]. On the other hand, CMSs demonstrate slow kinetics due to their microporous property.

Carbon-based nanomaterials, represented by carbon nanotubes (CNTs) [132, 133], hydrothermal carbons [134] and graphene [135], show a great potential in many aspects of applications including CO₂ capture. Their unique nano-scale structures endow them with high BET surface area and exclusive properties. Su *et al.* [132] reported an APTES-modified CNT with CO₂ adsorption capacity of ~2.59 mmol g⁻¹ at 20 °C. Recently many graphene-based adsorbents [135] also have been designed for CO₂ capture. However, these emerging new materials lack results under practical conditions.

Apart from amine-functionalized silica, some other amine-functionalized materials demonstrate competitive CO₂ capture performances. A commercially available Y-type zeolite (Si/Al = 60) impregnated with TEPA presented a CO₂ capacity of 4.27 mmol g⁻¹ at 60 °C in the presence of 15% CO₂ and 7% water vapor in gas stream [136]. Another PMMA-supported TEPAN exhibited cyclic capacity as high as 10.21 mmol g⁻¹ at 40 °C [137]. Although displaying high CO₂ capture capacities, these adsorbents lack regeneration data during multi-cycle tests.

In conclusion, amine-based absorption system and physical solvent are still the most mature technologies for post-combustion capture and pre-combustion capture, respectively. The emerging technologies and materials are promising, but still need implementation of pilot study before they could practically replace the state-of-art technologies.

1.4 Activated carbons (ACs)

Activated carbon (AC) is the collective name for a group of highly porous carbons obtained through activation process. Various carbon-based materials could be used as precursors for activation, which allows us to produce ACs at low cost. Other AC's advantages include

high BET surface area (up to $3500 \text{ m}^2 \text{ g}^{-1}$), well-developed porosity (especially microporosity), variable surface chemistry characteristics and a high degree of surface reactivity [138]. Therefore, it is considered as a very effective adsorbent for water treatment [139, 140] and gas adsorption/separation [141]. The use of ACs could date back to 1500 BC, when ancient Egyptians used them for medical purpose. At World War I, ACs were found to be effective mask materials against chlorine gas, and thus the AC-related development was stimulated. It was estimated that in 2018 global demand of ACs is projected to rise 8.1% per year to reach 2.1 million tons [142].

1.4.1 Production of ACs

ACs are produced from carbon-containing materials (carbon precursors). The precursor is transformed or activated by means of thermal treatments, during which solid mass is removed to create pores.

1.4.1.1 Raw materials

Conventional ACs refer to ACs derived from carbon precursors such like coal, wood and coconut shells etc. These materials are inexpensive and possess high carbon content, and therefore widely used. However, recently different types of materials have been explored as carbon precursors. This is due to the fact that the physical/chemical characteristics of the obtained ACs are to some extent determined by the texture/chemical content of the precursors. An exploration of new precursors offers an opportunity to create novel ACs.

(1) Renewable biomass precursors: this type of precursors has renewable features and wide availability. Except coconut shells, some of the newly developed precursors include: soy

beans [143], yeast [144], fungi [145], bean dreg [146], celtuce leaves [147] and bamboo [148], etc.

(2) Polymer-based precursors: the use of synthetic polymers as carbon precursors enable better chemical composition control, easy-to-achieve precise morphology, tunable pore system and targeted surface chemistry [149]. By controlling the synthesis process, polymers with desired properties could be obtained, which provides a promising opportunity to understand the physical and chemical properties of the subsequent ACs from molecular level. Some of the polymer-based precursors include: polyaniline [150], polyuria [151], polyimide [152], phenol-formaldehyde resin [153], etc..

(3) Templated carbon materials as precursors: This type of precursors contains porous carbons templated from other materials including zeolites [154], MOFs [155], ordered mesoporous silica [156], polymers (soft template) [157], metal carbides [158], etc.

(4) Nano-structured carbon materials as precursors: This type of precursors usually contains relatively high carbon content and unique microscopic structure. Typical materials of this type include: 2-dimensional carbons (graphene nanosheets [159] / films [160]), 1-dimensional carbons (carbon nanotubes [161] / fibres [162] / ribbons / scrolls), zero-dimensional carbons (graphenes [163] / graphene oxides [164]).

1.4.1.2 AC preparation

As shown in Figure 1.14, thermal activation process is generally divided into two thermally dependant steps: carbonization and the following activation. However, industrially additional treatments are often applied.

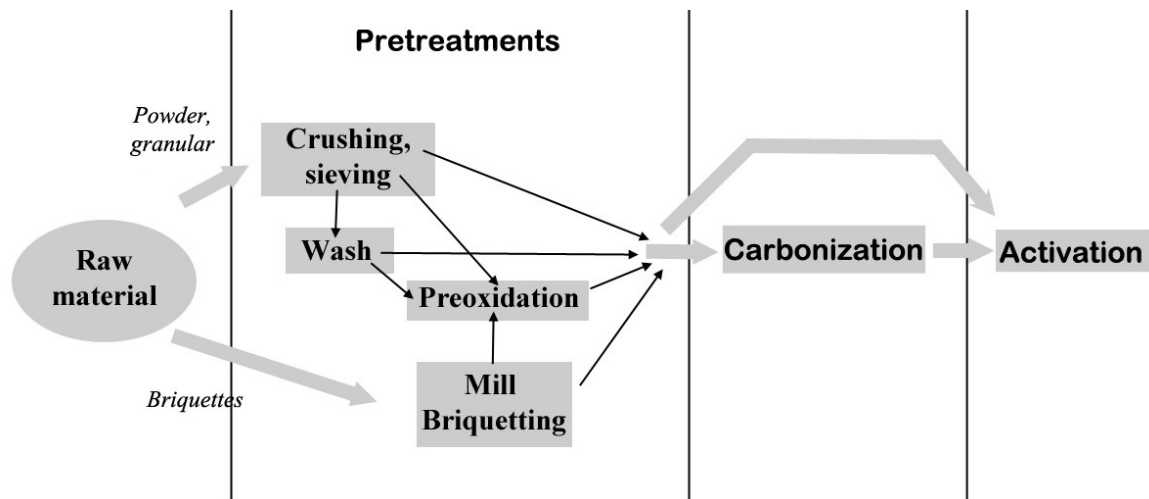


Figure 1.14 General flow sheet for the production of thermal ACs.

(1) Pre-treatments

The objective of pre-treatments is to prepare the raw materials for the next thermal activation preparation. The purpose of crushing, sieving and mill briquetting are to break raw materials into required particle size so porosity can be better developed in the following process. Washing is to remove some of the unnecessary content. If the raw material is a coking coal or liquid polymer, peroxidation treatment is required: a long period of peroxidation at moderate temperature (453~573 K) stabilized the materials by creating crosslinkage within the structure, which prevents the fluid phase from occurring during the following carbonization [165].

(2) Carbonization

In the carbonization process the precursor loses a lot of mass, which transforms into gas and volatile species. At the same time the precursor becomes more enriched in carbon content and aromaticity. The heating rate and temperature also play important roles in the

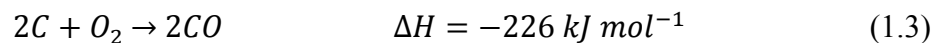
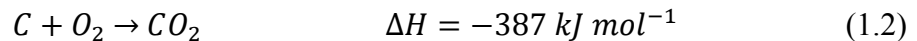
final porous structure of the ACs. A high heating rate produces a very quick devolatilization, giving rise to a solid with a well-developed mesopore and macropore network, a low density and a low abrasion and hardness index. On the other hand, low heating rate chars experience a slow release of volatiles during the devolatilization stage. This situation does not favor the formation of a large meso/macro network. The microporosity is supposed to be developed mainly in the following activation process.

(3) Activation

After carbonization, the product still has an incipient porous structure and a low BET surface area. Carbonization alone is not adequate to develop large porosity, hence activation is needed. Based on the activating agent, activation method can be generally divided into physical activation and chemical activation.

For physical activation, the product is usually activated by oxidizing gases, O₂, H₂O (steam), CO₂, in the order of their reactivity from high to low. The main scheme of activation is to partly remove the carbon atoms by oxidization or other reactions.

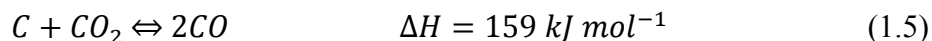
With O₂, the reactions are:



With steam, the reaction (gasification) is:

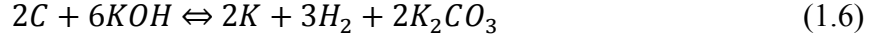


With CO₂, the reaction is:



Except with O₂, the reactions with H₂O and CO₂ are both endothermic and need energy input to be sustained. On the other hand, it is exactly the exothermic property of O₂ reaction that makes it difficult to control. Therefore, O₂ activation is scarcely applied. Steam activation is most widely used method due to the cost-efficiency of steam compared to other activating agent (CO₂, other chemicals). Although CO₂ and steam have similar pore development ability, CO₂ activation requires more stringent activation condition (e.g. temperature). However, CO₂ activation usually produces ACs with narrower pores than steam activation. At the same time, both of the methods need heating to keep the high activation temperature (973~1173 K).

In chemical activation, the carbon precursors are mixed with a chemical agent and thermal-processed at high temperatures. Some of the commonly-known agents include ZnCl₂, H₃PO₄ and KOH/NaOH. In terms of pore forming mechanism, early studies proposed that ZnCl₂ [166, 167] and H₃PO₄ [168, 169] have an effect of catalytically accelerating dehydration process and/or crosslinkage at low temperatures. The activation temperature using these two agents is usually 623~873 K, lower than those of physical activation. The later-developed KOH activation is more facile and reported to be able to produce ACs with extremely high surface area (> 3000 m² g⁻¹). The required temperature for KOH activation is 873~1073 K, higher than ZnCl₂ and H₃PO₄, but a little lower than physical activation. KOH activation is different from ZnCl₂ and H₃PO₄. In 2003 Lillo-Ródenas *et al.* proposed a global reaction for KOH activation based on experimental data and thermodynamic calculation (Eq. 1.6) [170].



However, recent studies [171-174] showed the mechanism of pore formation was much more than this. There are several other simultaneous/consecutive reactions including:



and Eq. 1.4, Eq. 1.5. It was concluded that there were three main activation mechanisms [175]: (a) Etching the carbon framework by the redox reactions (such as Eq. 1.6) between various potassium compounds as chemical activation reagents with carbon; (b) the formation of H₂O (Eq. 1.7) and CO₂ (Eq. 1.8 and Eq. 1.9) in the activation system, positively contributing to the further development of the porosity through the gasification of carbon, namely physical activation (Eq. 1.4 and Eq. 1.5); (c) the as-prepared metallic K (Eq. 1.6, 1.10 and 1.11), efficiently intercalating into the carbon lattices of the carbon matrix during the activation, resulting in the expansion of the carbon lattices. After the removal of the intercalated metallic K and other K compounds by washing, the expanded carbon lattices cannot return to their previous non-porous structure and thus the high microporosity that is necessary for large surface area and pore volume is created. Some recent study [172] showed that NaOH had similar activating effect with KOH. Since KOH

activation produces ACs with higher surface area and better porous structure than $ZnCl_2$ and H_3PO_4 , most of the recent chemical activation studies [176, 177] used KOH as activating agent.

1.4.2 CO₂ adsorption in ACs

In CO₂ adsorption in ACs, adsorption involves adhesion of CO₂ molecule to the surface of the AC. Before discussion of any development in this field, some of the basics need to be understood.

1.4.2.1 Surface energy for adsorption

Basically, adsorption happens at a critical condition where the potential energy ϕ is equal to the work done to bring a gas molecule to the adsorbed state. In other words, adsorption only happens when the work one has to do is smaller than the potential energy ϕ . As a first approximation, the adsorbed state is assumed to be at the saturated vapor pressure.

$$-\phi = -\Delta G = \int_P^{P_0} V dP = RT \ln \frac{P_0}{P} \quad (1.12)$$

In Eq. 1.12 ΔG is the free energy change and P_0 is the saturated vapor pressure. Hence P is the pressure when adsorption occurs for the given ϕ (ϕ is the sorbate-sorbate interaction energy on the liquid surface). If $P_{present} \geq P = P_0 e^{\frac{\phi}{RT}}$, adsorption will occur. At different adsorption site, ϕ is different for the specific adsorbate molecule (such as CO₂). The total potential between the adsorbate molecules and the adsorbent is the sum of the total adsorbate-adsorbate and the adsorbate-adsorbent interaction potentials:

$$\phi_{total} = \phi_{adsorbate-adsorbate} + \phi_{adsorbate-adsorbent} \quad (1.13)$$

In most cases, the second term is dominant, so we will refer to it as ϕ . Generally, a larger ϕ means stronger interaction.

There are three basic types of contributions to the adsorbate-adsorbent interactions: dispersion (or van der Waals interaction), electrostatic and chemical bond. The functional forms of individual contributors to the total potential have also been discussed in many literatures [178-182]. For a typical physical adsorption (such as adsorption on ACs), the first two items are the main contributors and thereby explained.

Van der Waals interaction includes attractive and repulsive forces. A common expression of this interaction is termed as Lennard-Jones potential:

$$\phi_V = \phi_D + \phi_R = \left(-\frac{A}{r^6}\right) + \left(\frac{B}{r^{12}}\right) \quad (1.14)$$

where ϕ_D = dispersion energy, ϕ_R = close-range repulsion energy, A and B are constant; A can be calculated with $A = \frac{6mc^2\alpha_i\alpha_j}{(\alpha_i/\chi_i)+(\alpha_j/\chi_j)}$ (Kirkwood–Muller formula) where α = polarizability, m = mass of electron, c = speed of light. Lennard-Jones equation is an approximation model especially for interaction of neutral atoms/molecules.

If an electrical field exists, there will be electrostatic interactions. Some of these interactions [183] include:

For induced dipole:

$$\phi_{Ind} = -\frac{1}{2}\alpha F^2 = -\frac{\alpha q^2}{2r^4(4\pi\epsilon_0)^2} \quad (1.15)$$

For point dipole:

$$\phi_{F\mu} = -F\mu \cos \theta = -\frac{q\mu \cos \theta}{r^2(4\pi\epsilon_0)} \quad (1.16)$$

For linear quadrupole:

$$\phi_{\dot{F}Q} = \frac{1}{2}Q\dot{F} = -\frac{Qq(3\cos^2\theta-1)}{4r^3(4\pi\epsilon_0)} \quad (1.17)$$

ϕ_{Ind} = induction energy, $\phi_{F\mu}$ = interaction between electric field (F) and a permanent dipole (μ), $\phi_{\dot{F}Q}$ = interaction between field gradient (\dot{F}) and a quadrupole (with quadrupole moment Q). F = electric field, q = electronic charge of ion on surface, ϵ_0 = permittivity of a vacuum, μ = permanent dipole moment, θ = angle between the direction of the field or field gradient and the axis of the dipole or linear quadrupole, Q = linear quadrupole moment (+ or -).

To conclude, the overall potential is

$$\phi = \phi_D + \phi_R + \phi_{Ind} + \phi_{F\mu} + \phi_{\dot{F}Q} \quad (1.18)$$

In the general expression Eq. 1.18, the first two items ($\phi_D + \phi_R$) are “nonspecific” [179], meaning that they exist in all sorbate-sorbent systems. The last three items are dependent of electric fields, which rise from charges on solid surface. For example, nonspecific interactions often dominate for activated. For adsorbate with a quadrupole (N_2 , CO_2), $\phi_{\dot{F}Q}$ will be considerably large. Also polarizability (α) plays a very important role for the first 3 contributors, ϕ_D , ϕ_R and ϕ_{Ind} . The polarizability increases with atomic weight for elements in the same family, and decreases with increasing atomic weight for elements in the same row of the periodic table as the outer-shell orbitals are being increasingly filled. Generally the alkali and alkaline earth metal atoms have very high polarizabilities. It is also

considered that bigger molecules have higher polarizabilities [183]. For example, CO₂ (2.91 Å³ per molecule) has a larger polarizability than N₂ (1.74 Å³ per molecule).

However, the situation is always more complicated in practice. Adsorption behavior rarely happens between a gas molecule and a single solid surface atom (as discussed above). Instead, a layer or several layers of surface atoms should be considered. Therefore, Eq. 1.18 should be

$$\phi_{Total} = \sum_i^n \phi_i = \sum_i^n (\phi_{D_i} + \phi_{R_i} + \phi_{Ind_i} + \phi_{F_{\mu_i}} + \phi_{F_{Q_i}} + \phi_{Other_i}) \quad (1.19)$$

Based on Eq. 1.19, there are two main approaches for improvement of CO₂ adsorption on ACs: increase ϕ_i and increase n . This corresponds to two main approaches for practical CO₂ adsorption: surface modification and pore development.

1.4.2.2 Surface modification of ACs for CO₂ capture

Due to the acidic role of CO₂ (weak Lewis acid), it is expected that the basic surfaces of ACs may favor the CO₂ capture performance. Basicity of ACs can be associated with: (1) resonating π -electrons of carbon aromatic rings that attract protons [184]; (2) basic functionalities (e.g. nitrogen containing groups) that are capable of binding with protons [185, 186]. It is obvious that the second method is more controllable. In terms of basic functionalities, most of the studies were focused on nitrogen containing groups. These nitrogen functionalities can be introduced either by reactions with nitrogen containing agents such as NH₃, HNO₃ and amines (post-synthesis modification) or by activation of nitrogen containing precursors (pre-synthesis modification).

A typical post-synthesis modification method is ammonia treatment at high temperatures. The increased CO₂ adsorption capacity [77, 78, 187] led to a conclusion that ammonia treatment was an effective method for improving CO₂ adsorption. However, the optimum treatment temperature seems to differ among different ACs [78, 187]. Maroto-Valer *et al.* [79] compared ammonia treatment with PEI impregnation of ACs and showed a better CO₂ performance of the latter method. Further, different amines (DEA, MEA, DETA and PEI) were compared and the results showed that different amine-impregnated ACs presented different optimal temperatures in terms of CO₂ uptake [188]. Due to a pore-blocking effect of amines, some anthracite-derived ACs presented decreased CO₂ performances after amine impregnation [189]. Compared with amine-modified silica (4~6 mmol g⁻¹), ACs produced by post-modification method usually have lower adsorption capacities (2~3 mmol g⁻¹) due to comparatively smaller pore sizes and subsequent lower amine impregnation ratio. Additionally, the regenerability needs to be improved.

Activation of N-containing precursors has been intensively investigated since recently. As previewed in 1.4.1.1, high nitrogen content, low cost, sustainable/chemically synthesized precursors were explored. At the same time, more works are focused on explaining interaction of nitrogen-containing groups with CO₂ molecules. In 2010, Hao *et al.* [153] attributed the positive effect of nitrogen to acid-base interaction. In 2011 Sevilla *et al.* [190] reported ACs by KOH activation of polypyrrole (PPy), with a high nitrogen content (~10 wt%) and promising CO₂ adsorption capacity (3.9 mmol g⁻¹, ambient pressure, 298 K). It was proposed that pyrodonic nitrogen is more effective than other types of nitrogen groups for CO₂ adsorption. Lately, through computational and experimental data Xing *et al.* [146] believed that nitrogen facilitates the hydrogen bonding interactions between the carbon

surface and CO₂ molecules. Till now, no conclusive point has been made for a general mechanism.

Apart from nitrogen, other heteroatoms introduced into ACs are also reported to benefit CO₂ adsorption. Plaza *et al.* [191] found significantly increased capacity of CO₂ adsorption after oxidation treatment and therefore proposed a positive effect of some oxygen groups. Seema *et al.* [192] reported an S-doped AC and studied the effect of sulfur content by experiments and density functional theory-modeled (DFT-modeled) calculation.

1.4.2.3 Pore development of ACs for CO₂ capture

As can be seen in Figure 1.15, there are macropores (pores with sizes > 50 nm), mesopores (pores with sizes between 2 nm and 50 nm) and micropores (pores with sizes < 2nm). For ACs, micropores and macropores are commonly observed. Micropores are developed through activation process, while macropores are usually the original structure of precursors (e.g. lignocellulosic materials). Mesopores are mostly merged pores from small micropores, or structure of the precursors (e.g. mesoporous carbons).

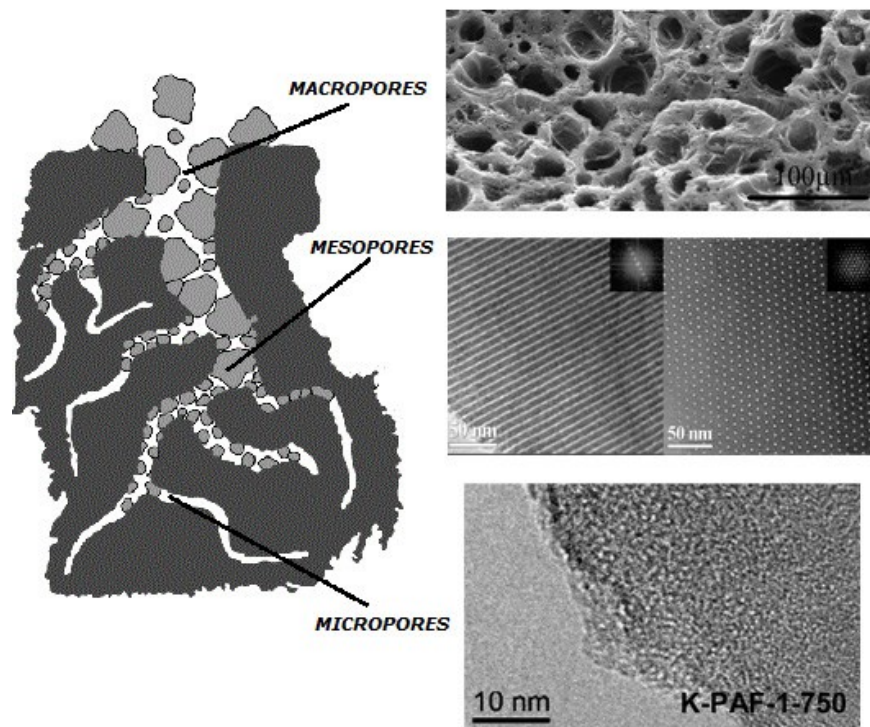


Figure 1.15 Schematics of different sized pore and their example microscopic images. (Adapted from [193-195])

It is widely agreed that the pore structure and pore size of carbon-based materials can influence their CO₂ capture. For ACs, materials produced by KOH activation are of most interests. A porous carbon produced from KOH activation of sawdust material [196] exhibited a very high CO₂ adsorption capacity of 4.8 mmol g⁻¹ at 298 K and 1 bar. In this study it was demonstrated how severe (KOH four times the precursor) and mild activation conditions (KOH two times the precursor) at various temperatures affected the texture of the porous carbons and their CO₂ adsorption ability. Lee *et al.*[197] and Wickramaratne *et al.* [198] also presented the significance of narrow micropores. Marco-Lozar *et al.* [199] found that for low CO₂ pressure, ACs should have maximum possible volume of micropores smaller than 0.7 nm. Other studies [158, 200, 201] argued that the critical pore

size for adsorption should be in the range of 0.5~1.0 nm and closely dependent of the adsorption pressure.

Mesopores and macropores are also of great importance. At low pressures, they are responsible for better diffusion of gas molecules; at high pressure, they are able to directly adsorb adsorbate. Some of the ACs [202] demonstrated a hierarchical porous structure by activation of mesoporous carbon and presented desirable CO₂ capacity and fast kinetics. Wahby *et al.* [203], Sevilla *et al.* [190] and Wang *et al.* [204] produced meso/microporous ACs with very high BET surface area (3100~3400 m² g⁻¹) and their CO₂ adsorption capacities were competitive (3.1~4.5 mmol g⁻¹, 25 °C, 1atm).

1.5 Objectives of the thesis

As the most popular activation method, KOH activation produces activated carbons with high specific surface areas and well-defined micro/mesoporous structures. These features usually favor adsorption of CO₂. Furthermore, the variety of carbon precursors also provide activated carbons with different textures and chemical compositions, granting opportunities to synthesize better carbon materials for CO₂ capture. Additionally, by post-synthesis modification, the interaction between CO₂ and the AC surfaces could be reinforced and thus the CO₂ capacity at ambient pressures and temperatures could be improved. However, there are problems in the related fields that have not been comprehensively studied or explained with convincing reasons. Some of them are,

- 1) How to engineer the porous structures of activated carbons to benefit CO₂ capture.
- 2) How to modify the surfaces of activated carbons with functional groups to benefit CO₂ capture.

Therefore, the objectives of the thesis are,

- 1) Trying to understand the detailed mechanisms of KOH activation, the pore forming mechanisms of the KOH-activated carbons, and their relationship between each other.
- 2) Exploring activated carbons produced from novel carbon precursors and their applications on CO₂ capture.
- 3) Modifying the surfaces of activated carbons with emerging CO₂-philic chemical/functional groups for CO₂ capture.

1.6 Thesis organization

Chapter 2 will study the KOH activation of multi-wall carbon nanotubes. In this chapter by studying KOH-activated multi-wall carbon nanotubes over a wide range of activation condition, the pore-forming mechanisms are revealed.

Chapter 3 will comprehensively discuss KOH activation of polyaniline-derived porous carbons. By tuning preheating temperature during the activation process, high surface area activated carbons could be obtained. The reason for the well-developed porous structure is also discussed.

Chapter 4 will explore KOH activation of a liquid carbon precursor, polyethylenimine (PEI). The activated carbon derived from polyethylenimine is carefully examined and its performance for CO₂ adsorption is presented.

Chapter 5 will explore LiCl incorporation of polyaniline-derived activated carbons. The activated carbons are successfully incorporated with LiCl via both melting diffusion

method and freeze drying method. The influence of the incorporated LiCl on the porous structures and the CO₂ adsorption capacities of the activated carbons are investigated.

1.7 References

- [1] Available from: http://cdiac.ornl.gov/trends/emis/meth_reg.html
- [2] Olah G.A., Prakash G.K.S., Goepfert A. Anthropogenic Chemical Carbon Cycle for a Sustainable Future. *Journal of the American Chemical Society*. 2011;**133**(33):12881-12898.
- [3] Available from: <http://www.esrl.noaa.gov/gmd/ccgg/trends/index.html>
- [4] Forster P., Ramaswamy V. Changes in Atmospheric Constituents and in Radiative Forcing. *Climate Change 2007: The Physical Science Basis*. 2007:129-234.
- [5] Kaufman D.S., Schneider D.P., McKay N.P., Ammann C.M., Bradley R.S., Briffa K.R., et al. Recent Warming Reverses Long-Term Arctic Cooling. *Science*. 2009;**325**(5945):1236-1239.
- [6] Change U.N.F.C.o.C. Kyoto Protocol. 1997.
- [7] Metz B., Davidson O.R., Bosch P.R., Dave R., Meyer L.A. Contribution of working group III to the fourth assessment report of the intergovernmental panel on climate change. Cambridge, United Kingdom and New York, NY, USA: Cambridge University Press 2007.
- [8] Available from: http://data.giss.nasa.gov/gistemp/taledata_v3/GLB.Ts+dSST.txt
- [9] Le Quéré C., Moriarty R., Andrew R.M., Peters G.P., Ciais P., Friedlingstein P., et al. Global carbon budget 2014. *Earth System Science Data Discussions*. 2014;**7**(2):521-610.
- [10] Available from: <http://edgar.jrc.ec.europa.eu/overview.php?v=42>
- [11] E.I.A. U.S. Annual energy outlook 2014; 2014.

- [12] Li L., Zhao N., Wei W., Sun Y.H. A review of research progress on CO₂ capture, storage, and utilization in Chinese Academy of Sciences. *Fuel*. 2013;**108**:112-130.
- [13] Spigarelli B.P., Kawatra S.K. Opportunities and challenges in carbon dioxide capture. *Journal of CO₂ Utilization*. 2013;**1**:69-87.
- [14] Herzog H., Golomb D. Carbon capture and storage from fossil fuel use. *Encyclopedia of energy*. 2004;**1**:1-11.
- [15] Bert Metz O.D., Heleen de Coninck, Manuela Loos, Leo Meyer. The IPCC special report on carbon dioxide capture and storage. United Kingdom and New York, NY, USA; 2005.
- [16] Boot-Handford M.E., Abanades J.C., Anthony E.J., Blunt M.J., Brandani S., Mac Dowell N., et al. Carbon capture and storage update. *Energy & Environmental Science*. 2014;**7**(1):130-189.
- [17] Klara S.M., Srivastava R.D., McIlvried H.G. Integrated collaborative technology development program for CO₂ sequestration in geologic formations—United States Department of Energy R&D. *Energy Conversion and Management*. 2003;**44**(17):2699-2712
- [18] Available from: <http://www.globalccsinstitute.com/projects/large-scale-ccs-projects>
- [19] Available from: <http://www.zeroco2.no/projects/countries/the-netherlands>
- [20] Available from: <http://www.thelocal.se/20140507/vattenfall-abandons-research-on-co2-storage>
- [21] Haszeldine R.S. Carbon Capture and Storage: How Green Can Black Be? *Science*. 2009;**325**(5948):1647-1652.

- [22] Figueroa J.D., Fout T., Plasynski S., McIlvried H., Srivastava R.D. Advances in CO₂ capture technology—The US Department of Energy's Carbon Sequestration Program. *International Journal of Greenhouse Gas Control*. 2008;**2**(1):9-20
- [23] Tan Y.Q., Thambimuthu K.V., Douglas M.A., Mortazavi R. Oxy-fuel combustion research at the CANMET Energy Technology Centre. *Coal Combustion Facing the 21st Century*. 2003:550-554.
- [24] D'Alessandro D.M., Smit B., Long J.R. Carbon dioxide capture: prospects for new materials. *Angewandte Chemie International Edition*. 2010;**49**(35):6058-6082.
- [25] Oyenekan B.A., Rochelle G.T. Alternative stripper configurations for CO₂ capture by aqueous amines. *Aiche Journal*. 2007;**53**(12):3144-3154.
- [26] Frailie P.T., Madan T., Sherman B.J., Rochelle G.T. Energy performance of advanced stripper configurations. *Greenhouse Gas Control Technology-11*. 2013;**37**:1696-1705.
- [27] Rochelle G., Chen E., Freeman S., Van Wagener D., Xu Q., Voice A. Aqueous piperazine as the new standard for CO₂ capture technology. *Chemical Engineering Journal*. 2011;**171**(3):725-733.
- [28] Voice A.K., Closmann F., Rochelle G.T. Oxidative degradation of amines with high-temperature cycling. *Greenhouse Gase Control Technology-11*. 2013;**37**:2118-2132.
- [29] Idem R., Wilson M., Tontiwachwuthikul P., Chakma A., Veawab A., Aroonwilas A., et al. Pilot plant studies of the CO₂ capture performance of aqueous MEA and mixed MEA/MDEA solvents at the University of Regina CO₂ capture technology development plant and the Boundary Dam CO₂ capture demonstration. *Industrial & Engineering Chemistry Research*. 2006;**45**(8):2414-2420.

- [30] Blomen E., Hendriks C., Neele F. Capture technologies: Improvements and Promising Developments. *Greenhouse Gas Control Technologies-9*. 2009;**1**(1):1505-1512.
- [31] Available from: http://www.spc.jst.go.jp/hottopics/1003biomass/r1003_danxing.html
- [32] Bara J.E., Carlisle T.K., Gabriel C.J., Camper D., Finotello A., Gin D.L., et al. Guide to CO₂ Separations in Imidazolium-Based Room-Temperature Ionic Liquids. *Industrial & Engineering Chemistry Research*. 2009;**48**(6):2739-2751.
- [33] Karadas F., Atilhan M., Aparicio S. Review on the Use of Ionic Liquids (ILs) as Alternative Fluids for CO₂ Capture and Natural Gas Sweetening. *Energy & Fuels*. 2010;**24**:5817-5828.
- [34] Zhang X.P., Zhang X.C., Dong H.F., Zhao Z.J., Zhang S.J., Huang Y. Carbon capture with ionic liquids: overview and progress. *Energy & Environmental Science*. 2012;**5**(5):6668-6681.
- [35] Ramdin M., de Loos T.W., Vlugt T.J.H. State-of-the-Art of CO₂ Capture with Ionic Liquids. *Industrial & Engineering Chemistry Research*. 2012;**51**(24):8149-8177.
- [36] Wappel D., Gronald G., Kalb R., Draxler J. Ionic liquids for post-combustion CO₂ absorption. *International Journal of Greenhouse Gas Control*. 2010;**4**(3):486-494.
- [37] Xomeritakis G., Tsai C.Y., Brinker C.J. Microporous sol-gel derived aminosilicate membrane for enhanced carbon dioxide separation. *Separation and Purification Technology*. 2005;**42**(3):249-257.
- [38] McCool B.A., DeSisto W.J. Amino-functionalized silica membranes for enhanced carbon dioxide permeation. *Advanced Functional Materials*. 2005;**15**(10):1635-1640.

- [39] Powell C.E., Qiao G.G. Polymeric CO₂/N₂ gas separation membranes for the capture of carbon dioxide from power plant flue gases. *Journal of Membrane Science*. 2006;**279**(1-2):1-49.
- [40] Illing G., Hellgardt K., Wakeman R.J., Jungbauer A. Preparation and characterisation of polyaniline based membranes for gas separation. *Journal of Membrane Science*. 2001;**184**(1):69-78.
- [41] Xu Z.K., Dannenberg C., Springer J., Banerjee S., Maier G. Novel poly(arylene ether) as membranes for gas separation. *Journal of Membrane Science*. 2002;**205**(1-2):23-31.
- [42] Lin H., Freeman B.D. Gas solubility, diffusivity and permeability in poly(ethylene oxide). *Journal of Membrane Science*. 2004;**239**(1):105-117.
- [43] Yang H.Q., Xu Z.H., Fan M.H., Gupta R., Slimane R.B., Bland A.E., et al. Progress in carbon dioxide separation and capture: A review. *Journal of Environmental Sciences-China*. 2008;**20**(1):14-27.
- [44] Radosz M., Hu X.D., Krutkramelis K., Shen Y.Q. Flue-gas carbon capture on carbonaceous sorbents: Toward a low-cost multifunctional Carbon Filter for "Green" energy producers. *Industrial & Engineering Chemistry Research*. 2008;**47**(10):3783-3794.
- [45] Ho M.T., Allinson G.W., Wiley D.E. Reducing the cost of CO₂ capture from flue gases using pressure swing adsorption. *Industrial & Engineering Chemistry Research*. 2008;**47**(14):4883-4890.
- [46] Choi S., Drese J.H., Jones C.W. Adsorbent Materials for Carbon Dioxide Capture from Large Anthropogenic Point Sources. *Chemsuschem*. 2009;**2**(9):796-854.

- [47] Ward J.W., Habgood H.W. The infrared spectra of carbon dioxide adsorbed on zeolite X. *The Journal of Physical Chemistry*. 1966;**70**(4):1178-1182.
- [48] Gallei E., Stumpf G. Infrared spectroscopic studies of the adsorption of carbon dioxide and the coadsorption of carbon dioxide and water on CaY and NiY zeolites. *Journal of Colloid and Interface Science*. 1976;**55**(2):415-420
- [49] Coriani S., Halkier A., Rizzo A., Ruud K. On the molecular electric quadrupole moment and the electric-field-gradient-induced birefringence of CO₂ and CS₂. *Chemical Physics Letters*. 2000;**326**(3-4):269-276.
- [50] Maurin G., Llewellyn P.L., Bell R.G. Adsorption mechanism of carbon dioxide in faujasites: Grand canonical Monte Carlo simulations and microcalorimetry measurements. *Journal of Physical Chemistry B*. 2005;**109**(33):16084-16091.
- [51] Walton K.S., Abney M.B., LeVan M.D. CO₂ adsorption in Y and X zeolites modified by alkali metal cation exchange. *Microporous and Mesoporous Materials*. 2006;**91**(1-3):78-84.
- [52] Harlick P.J.E., Tezel F.H. An experimental adsorbent screening study for CO₂ removal from N₂. *Microporous and Mesoporous Materials*. 2004;**76**(1-3):71-79.
- [53] Siriwardane R.V., Shen M.S., Fisher E.P. Adsorption of CO₂ on zeolites at moderate temperatures. *Energy & Fuels*. 2005;**19**(3):1153-1159.
- [54] Siriwardane R.V., Shen M.S., Fisher E.P. Adsorption of CO₂, N₂, and O₂ on natural zeolites. *Energy & Fuels*. 2003;**17**(3):571-576.
- [55] Cavenati S., Grande C.A., Rodrigues A.E. Adsorption equilibrium of methane, carbon dioxide, and nitrogen on zeolite 13X at high pressures. *Journal of Chemical and Engineering Data*. 2004;**49**(4):1095-1101.

- [56] Diaz E., Munoz E., Vega A., Ordonez S. Enhancement of the CO₂ retention capacity of Y zeolites by Na and Cs treatments: Effect of adsorption temperature and water treatment. *Industrial & Engineering Chemistry Research*. 2008;**47**(2):412-418.
- [57] Choudhary V.R., Mayadevi S., Singh A.P. Sorption Isotherms of Methane, Ethane, Ethene and Carbon-Dioxide on NaX, NaY and Na-Mordenite Zeolites. *Journal of the Chemical Society-Faraday Transactions*. 1995;**91**(17):2935-2944.
- [58] Harlick P.J.E., Tezel F.H. Adsorption of carbon dioxide, methane and nitrogen: pure and binary mixture adsorption for ZSM-5 with SiO₂/Al₂O₃ ratio of 280. *Separation and Purification Technology*. 2003;**33**(2):199-210.
- [59] Khodakov A.Y., Rees L.V.C. Effect of Propane on the Kinetics of Carbon-Dioxide Adsorption in NaA Zeolites. *Gas Separation & Purification*. 1995;**9**(4):253-257.
- [60] Yucel H., Ruthven D.M. Diffusion of CO₂ in 4A and 5A Zeolite Crystals. *Journal of Colloid and Interface Science*. 1980;**74**(1):186-195.
- [61] R. V. Siriwardane M.S.S., E. P. Fisher, J. A. Poston, A. Shamsi. Adsorption and Desorption of CO₂ on Solid Sorbents. *Journal of Energy Environment Research*. 2001;**1**:19-31.
- [62] Konduru N., Lindner P., Assaf-Anad N.M. Curbing the greenhouse effect by carbon dioxide adsorption with zeolite 13X. *Aiche Journal*. 2007;**53**(12):3137-3143.
- [63] Ghoufi A., Gaberova L., Rouquerol J., Vincent D., Llewellyn P.L., Maurin G. Adsorption of CO₂, CH₄ and their binary mixture in Faujasite NaY: A combination of molecular simulations with gravimetry-manometry and microcalorimetry measurements. *Microporous and Mesoporous Materials*. 2009;**119**(1-3):117-128.

- [64] Akten E.D., Siriwardane R., Sholl D.S. Monte Carlo simulation of single- and binary-component adsorption of CO₂, N₂, and H₂ in zeolite Na-4A. *Energy & Fuels*. 2003;**17**(4):977-983.
- [65] Krishna R., van Baten J.M. Segregation effects in adsorption of CO₂-containing mixtures and their consequences for separation selectivities in cage-type zeolites. *Separation and Purification Technology*. 2008;**61**(3):414-423.
- [66] Liu Q.L., Mace A., Bacsik Z., Sun J.L., Laaksonen A., Hedin N. NaKA sorbents with high CO₂-over-N₂ selectivity and high capacity to adsorb CO₂. *Chemical Communications*. 2010;**46**(25):4502-4504.
- [67] Dasgupta S., Biswas N., Aarti, Gode N.G., Divekar S., Nanoti A., et al. CO₂ recovery from mixtures with nitrogen in a vacuum swing adsorber using metal organic framework adsorbent: A comparative study. *International Journal of Greenhouse Gas Control*. 2012;**7**:225-229.
- [68] Bertsch L., Habgood H.W. An infrared spectroscopic study of the adsorption of water and carbon dioxide by Linde molecular sieve X1. *The Journal of Physical Chemistry*. 1963;**67**(8):1621-1628.
- [69] Brandani F., Ruthven D.M. The effect of water on the adsorption of CO₂ and C₃H₈ on type X zeolites. *Industrial & Engineering Chemistry Research*. 2004;**43**(26):8339-8344.
- [70] Ko D., Siriwardane R., Biegler L.T. Optimization of a pressure-swing adsorption process using zeolite 13X for CO₂ sequestration. *Industrial & Engineering Chemistry Research*. 2003;**42**(2):339-348.
- [71] Zhang J., Webley P.A. Cycle development and design for CO₂ capture from flue gas by vacuum swing adsorption. *Environmental Science & Technology*. 2008;**42**(2):563-569.

- [72] Kikkinides E.S., Yang R.T., Cho S.H. Concentration and Recovery of CO₂ from Flue-Gas by Pressure Swing Adsorption. *Industrial & Engineering Chemistry Research*. 1993;**32**(11):2714-2720.
- [73] Chue K.T., Kim J.N., Yoo Y.J., Cho S.H., Yang R.T. Comparison of Activated Carbon and Zeolite 13X for CO₂ Recovery from Flue-Gas by Pressure Swing Adsorption. *Industrial & Engineering Chemistry Research*. 1995;**34**(2):591-598.
- [74] Na B.K., Koo K.K., Eum H.M., Lee H., Song H.K. CO₂ recovery from flue gas by PSA process using activated carbon. *Korean Journal of Chemical Engineering*. 2001;**18**(2):220-227.
- [75] Siriwardane R.V., Shen M.S., Fisher E.P., Poston J.A. Adsorption of CO₂ on molecular sieves and activated carbon. *Energy & Fuels*. 2001;**15**(2):279-284.
- [76] Van der Vaart R., Huiskes C., Bosch H., Reith T. Single and mixed gas adsorption equilibria of carbon dioxide/methane on activated carbon. *Adsorption-Journal of the International Adsorption Society*. 2000;**6**(4):311-323.
- [77] Pevida C., Plaza M.G., Arias B., Feroso J., Rubiera F., Pis J.J. Surface modification of activated carbons for CO₂ capture. *Applied Surface Science*. 2008;**254**(22):7165-7172.
- [78] Przepiorski J., Skrodzewicz M., Morawski A.W. High temperature ammonia treatment of activated carbon for enhancement of CO₂ adsorption. *Applied Surface Science*. 2004;**225**(1-4):235-242.
- [79] Maroto-Valer M.M., Tang Z., Zhang Y.Z. CO₂ capture by activated and impregnated anthracites. *Fuel Processing Technology*. 2005;**86**(14-15):1487-1502.

- [80] Dreisbach F., Staudt R., Keller J.U. High pressure adsorption data of methane, nitrogen, carbon dioxide and their binary and ternary mixtures on activated carbon. *Adsorption-Journal of the International Adsorption Society*. 1999;**5**(3):215-227.
- [81] Andrieu J., Smith J.M. Rate Parameters for Adsorption of CO₂ in Beds of Carbon Particles. *Aiche Journal*. 1980;**26**(6):944-948.
- [82] Doong S.J., Yang R.T. Bulk Separation of Multicomponent Gas-Mixtures by Pressure Swing Adsorption - Pore Surface-Diffusion and Equilibrium-Models. *Aiche Journal*. 1986;**32**(3):397-410.
- [83] Wang Y.X., Zhou Y.P., Liu C.M., Zhou L. Comparative studies of CO₂ and CH₄ sorption on activated carbon in presence of water. *Colloids and Surfaces a-Physicochemical and Engineering Aspects*. 2008;**322**(1-3):14-18.
- [84] Adams L.B., Hall C.R., Holmes R.J., Newton R.A. An Examination of How Exposure to Humid Air Can Result in Changes in the Adsorption Properties of Activated Carbons. *Carbon*. 1988;**26**(4):451-459.
- [85] Furukawa H., Ko N., Go Y.B., Aratani N., Choi S.B., Choi E., et al. Ultrahigh Porosity in Metal-Organic Frameworks. *Science*. 2010;**329**(5990):424-428.
- [86] Dietzel P.D.C., Besikiotis V., Blom R. Application of metal-organic frameworks with coordinatively unsaturated metal sites in storage and separation of methane and carbon dioxide. *Journal of Materials Chemistry*. 2009;**19**(39):7362-7370.
- [87] Choi J.S., Son W.J., Kim J., Ahn W.S. Metal-organic framework MOF-5 prepared by microwave heating: Factors to be considered. *Microporous and Mesoporous Materials*. 2008;**116**(1-3):727-731.

- [88] Millward A.R., Yaghi O.M. Metal-organic frameworks with exceptionally high capacity for storage of carbon dioxide at room temperature. *Journal of the American Chemical Society*. 2005;**127**(51):17998-17999.
- [89] Llewellyn P.L., Bourrelly S., Serre C., Vimont A., Daturi M., Hamon L., et al. High uptakes of CO₂ and CH₄ in mesoporous metal-organic frameworks MIL-100 and MIL-101. *Langmuir*. 2008;**24**(14):7245-7250.
- [90] Bao Z.B., Yu L.A., Ren Q.L., Lu X.Y., Deng S.G. Adsorption of CO₂ and CH₄ on a magnesium-based metal organic framework. *Journal of Colloid and Interface Science*. 2011;**353**(2):549-556.
- [91] Yazaydin A.O., Snurr R.Q., Park T.H., Koh K., Liu J., LeVan M.D., et al. Screening of Metal-Organic Frameworks for Carbon Dioxide Capture from Flue Gas Using a Combined Experimental and Modeling Approach. *Journal of the American Chemical Society*. 2009;**131**(51):18198-18199.
- [92] Aprea P., Caputo D., Gargiulo N., Iucolano F., Pepe F. Modeling Carbon Dioxide Adsorption on Microporous Substrates: Comparison between Cu-BTC Metal-Organic Framework and 13X Zeolitic Molecular Sieve. *Journal of Chemical and Engineering Data*. 2010;**55**(9):3655-3661.
- [93] Zhao Z.X., Li Z., Lin Y.S. Adsorption and Diffusion of Carbon Dioxide on Metal-Organic Framework (MOF-5). *Industrial & Engineering Chemistry Research*. 2009;**48**(22):10015-10020.
- [94] Mason J.A., Sumida K., Herm Z.R., Krishna R., Long J.R. Evaluating metal-organic frameworks for post-combustion carbon dioxide capture via temperature swing adsorption. *Energy & Environmental Science*. 2011;**4**(8):3030-3040.

- [95] McDonald T.M., D'Alessandro D.M., Krishna R., Long J.R. Enhanced carbon dioxide capture upon incorporation of N,N'-dimethylethylenediamine in the metal-organic framework CuBTTri. *Chemical Science*. 2011;**2**(10):2022-2028.
- [96] Babarao R., Jiang J.W., Sandler S.I. Molecular Simulations for Adsorptive Separation of CO₂/CH₄ Mixture in Metal-Exposed, Catenated, and Charged Metal-Organic Frameworks. *Langmuir*. 2009;**25**(9):5239-5247.
- [97] Couck S., Denayer J.F.M., Baron G.V., Remy T., Gascon J., Kapteijn F. An Amine-Functionalized MIL-53 Metal-Organic Framework with Large Separation Power for CO₂ and CH₄. *Journal of the American Chemical Society*. 2009;**131**(18):6326-6327.
- [98] Bae Y.S., Farha O.K., Spokoyny A.M., Mirkin C.A., Hupp J.T., Snurr R.Q. Carborane-based metal-organic frameworks as highly selective sorbents for CO₂ over methane. *Chemical Communications*. 2008;**13**(35):4135-4137.
- [99] Pan L., Adams K.M., Hernandez H.E., Wang X.T., Zheng C., Hattori Y., et al. Porous lanthanide-organic frameworks: Synthesis, characterization, and unprecedented gas adsorption properties. *Journal of the American Chemical Society*. 2003;**125**(10):3062-3067.
- [100] Liu J., Wang Y., Benin A.I., Jakubczak P., Willis R.R., LeVan M.D. CO₂/H₂O Adsorption Equilibrium and Rates on Metal-Organic Frameworks: HKUST-1 and Ni/DOBDC. *Langmuir*. 2010;**26**(17):14301-14307.
- [101] Liang Z.J., Marshall M., Chaffee A.L. Comparison of Cu-BTC and zeolite 13X for adsorbent based CO₂ separation. *Greenhouse Gas Control Technologies* 2009;**1**(1):1265-1271.
- [102] Liang Z.J., Marshall M., Chaffee A.L. CO₂ Adsorption-Based Separation by Metal Organic Framework (Cu-BTC) versus Zeolite (13X). *Energy & Fuels*. 2009;**23**:2785-2789.

- [103] Wang Q.M., Shen D.M., Bulow M., Lau M.L., Deng S.G., Fitch F.R., et al. Metallo-organic molecular sieve for gas separation and purification. *Microporous and Mesoporous Materials*. 2002;**55**(2):217-230.
- [104] Low J.J., Benin A.I., Jakubczak P., Abrahamian J.F., Faheem S.A., Willis R.R. Virtual High Throughput Screening Confirmed Experimentally: Porous Coordination Polymer Hydration. *Journal of the American Chemical Society*. 2009;**131**(43):15834-15842.
- [105] Cavka J.H., Jakobsen S., Olsbye U., Guillou N., Lamberti C., Bordiga S., et al. A new zirconium inorganic building brick forming metal organic frameworks with exceptional stability. *Journal of the American Chemical Society*. 2008;**130**(42):13850-13851.
- [106] Ferey G., Serre C., Mellot-Draznieks C., Millange F., Surble S., Dutour J., et al. A hybrid solid with giant pores prepared by a combination of targeted chemistry, simulation, and powder diffraction. *Angewandte Chemie-International Edition*. 2004;**43**(46):6296-6301.
- [107] Ferey G., Mellot-Draznieks C., Serre C., Millange F., Dutour J., Surble S., et al. A chromium terephthalate-based solid with unusually large pore volumes and surface area. *Science*. 2005;**309**(5743):2040-2042.
- [108] Volkringer C., Popov D., Loiseau T., Guillou N., Ferey G., Haouas M., et al. A microdiffraction set-up for nanoporous metal-organic-framework-type solids. *Nature Materials*. 2007;**6**(10):760-764.
- [109] Samanta A., Zhao A., Shimizu G.K.H., Sarkar P., Gupta R. Post-Combustion CO₂ Capture Using Solid Sorbents: A Review. *Industrial & Engineering Chemistry Research*. 2012;**51**(4):1438-1463.

- [110] Xu X.C., Song C.S., Andresen J.M., Miller B.G., Scaroni A.W. Novel polyethylenimine-modified mesoporous molecular sieve of MCM-41 type as high-capacity adsorbent for CO₂ capture. *Energy & Fuels*. 2002;**16**(6):1463-1469.
- [111] Xu X.C., Song C.S., Andresen J.M., Miller B.G., Scaroni A.W. Preparation and characterization of novel CO₂ "molecular basket" adsorbents based on polymer-modified mesoporous molecular sieve MCM-41. *Microporous and Mesoporous Materials*. 2003;**62**(1-2):29-45.
- [112] Xu X.C., Song C.S., Miller B.G., Scaroni A.W. Influence of moisture on CO₂ separation from gas mixture by a nanoporous adsorbent based on polyethylenimine-modified molecular sieve MCM-41. *Industrial & Engineering Chemistry Research*. 2005;**44**(21):8113-8119.
- [113] Ma X.L., Wang X.X., Song C.S. "Molecular Basket" Sorbents for Separation of CO₂ and H₂S from Various Gas Streams. *Journal of the American Chemical Society*. 2009;**131**(16):5777-5783.
- [114] Zheng F., Tran D.N., Busche B., Fryxell G.E., Addleman R.S., Zemanian T.S., et al. Ethylenediamine-modified SBA-15 as regenerable CO₂ sorbents. *Abstracts of Papers of the American Chemical Society*. 2004;**227**:1086-1087.
- [115] Son W.J., Choi J.S., Ahn W.S. Adsorptive removal of carbon dioxide using polyethyleneimine-loaded mesoporous silica materials. *Microporous and Mesoporous Materials*. 2008;**113**(1-3):31-40.
- [116] Yue M.B., Sun L.B., Cao Y., Wang Y., Wang Z.J., Zhu J.H. Efficient CO₂ capturer derived from as-synthesized MCM-41 modified with amine. *Chemistry-a European Journal*. 2008;**14**(11):3442-3451.

- [117] Hiyoshi N., Yogo K., Yashima T. Adsorption of carbon dioxide on amine modified SBA-15 in the presence of water vapor. *Chemistry Letters*. 2004;**33**(5):510-511.
- [118] Zelenak V., Badanicova M., Halamova D., Cejka J., Zukal A., Murafa N., et al. Amine-modified ordered mesoporous silica: Effect of pore size on carbon dioxide capture. *Chemical Engineering Journal*. 2008;**144**(2):336-342.
- [119] Drese J.H., Choi S., Lively R.P., Koros W.J., Fauth D.J., Gray M.L., et al. Synthesis-Structure-Property Relationships for Hyperbranched Aminosilica CO₂ Adsorbents. *Advanced Functional Materials*. 2009;**19**(23):3821-3832.
- [120] Kim S.N., Son W.J., Choi J.S., Ahn W.S. CO₂ adsorption using amine-functionalized mesoporous silica prepared via anionic surfactant-mediated synthesis. *Microporous and Mesoporous Materials*. 2008;**115**(3):497-503.
- [121] Xu X., Song C., Andresen J.M., Miller B.G. Adsorption separation of CO₂ from simulated flue gas mixtures by novel CO₂ molecular basket adsorbents. *International journal of environmental technology and management*. 2004;**4**(1):32-52.
- [122] Drage T.C., Arenillas A., Smith K.M., Snape C.E. Thermal stability of polyethylenimine based carbon dioxide adsorbents and its influence on selection of regeneration strategies. *Microporous and Mesoporous Materials*. 2008;**116**(1-3):504-512.
- [123] Qi G.G., Wang Y.B., Estevez L., Duan X.N., Anako N., Park A.H.A., et al. High efficiency nanocomposite sorbents for CO₂ capture based on amine-functionalized mesoporous capsules. *Energy & Environmental Science*. 2011;**4**(2):444-452.
- [124] Sayari A., Belmabkhout Y. Stabilization of Amine-Containing CO₂ Adsorbents: Dramatic Effect of Water Vapor. *Journal of the American Chemical Society*. 2010;**132**(18):6312-6314.

- [125] Dasgupta S., Nanoti A., Gupta P., Jena D., Goswami A.N., Garg M.O. Carbon Dioxide Removal with Mesoporous Adsorbents in a Single Column Pressure Swing Adsorber. *Separation Science and Technology*. 2009;**44**(16):3973-3983.
- [126] Hiyoshi N., Yogo K., Yashima T. Adsorption characteristics of carbon dioxide on organically functionalized SBA-15. *Microporous and Mesoporous Materials*. 2005;**84**(1-3):357-365.
- [127] Huang H.Y., Yang R.T., Chinn D., Munson C.L. Amine-grafted MCM-48 and silica xerogel as superior sorbents for acidic gas removal from natural gas. *Industrial & Engineering Chemistry Research*. 2003;**42**(12):2427-2433.
- [128] Chang A.C.C., Chuang S.S.C., Gray M., Soong Y. In-situ infrared study of CO₂ adsorption on SBA-15 grafted with gamma-(aminopropyl)triethoxysilane. *Energy & Fuels*. 2003;**17**(2):468-473.
- [129] Khatri R.A., Chuang S.S.C., Soong Y., Gray M. Thermal and chemical stability of regenerable solid amine sorbent for CO₂ capture. *Energy & Fuels*. 2006;**20**(4):1514-1520.
- [130] Knowles G.P., Graham J.V., Delaney S.W., Chaffee A.L. Aminopropyl-functionalized mesoporous silicas as CO₂ adsorbents. *Fuel Processing Technology*. 2005;**86**(14-15):1435-1448.
- [131] Foley H.C. Carbogenic Molecular-Sieves - Synthesis, Properties and Applications. *Microporous Materials*. 1995;**4**(6):407-433.
- [132] Su F.S., Lu C.S., Cnen W.F., Bai H.L., Hwang J.F. Capture of CO₂ from flue gas via multiwalled carbon nanotubes. *Science of the Total Environment*. 2009;**407**(8):3017-3023.

- [133] Hsu S.C., Lu C., Su F., Zeng W., Chen W. Thermodynamics and regeneration studies of CO₂ adsorption on multiwalled carbon nanotubes. *Chemical Engineering Science*. 2010;**65**(4):1354-1361
- [134] Titirici M.M., White R.J., Falco C., Sevilla M. Black perspectives for a green future: hydrothermal carbons for environment protection and energy storage. *Energy & Environmental Science*. 2012;**5**(5):6796-6822.
- [135] Lee S.Y., Park S.J. Comprehensive review on synthesis and adsorption behaviors of graphene-based materials. *Carbon Letters*. 2012;**13**(2):73-87.
- [136] Su F.S., Lu C.Y., Kuo S.C., Zeng W.T. Adsorption of CO₂ on Amine-Functionalized Y-Type Zeolites. *Energy & Fuels*. 2010;**24**:1441-1448.
- [137] Lee S., Filburn T.P., Gray M., Park J.W., Song H.J. Screening test of solid amine sorbents for CO₂ capture. *Industrial & Engineering Chemistry Research*. 2008;**47**(19):7419-7423.
- [138] Alslaibi T.M., Abustan I., Ahmad M.A., Abu Foul A. A review: production of activated carbon from agricultural byproducts via conventional and microwave heating. *Journal of Chemical Technology and Biotechnology*. 2013;**88**(7):1183-1190.
- [139] Mukherjee S., Kumar S., Misra A.K., Acharya P.C. Removal of aqueous nickel (II) using laterite as a low-cost adsorbent. *Water Environment Research*. 2006;**78**(11):2268-2275.
- [140] Dias J.M., Alvim-Ferraz M.C.M., Almeida M.F., Rivera-Utrilla J., Sanchez-Polo M. Waste materials for activated carbon preparation and its use in aqueous-phase treatment: A review. *Journal of Environmental Management*. 2007;**85**(4):833-846.

- [141] Himeno S., Komatsu T., Fujita S. High-pressure adsorption equilibria of methane and carbon dioxide on several activated carbons. *Journal of Chemical and Engineering Data*. 2005;**50**(2):369-376.
- [142] Available from: <http://www.wwdmag.com/activated-carbon/global-demand-activated-carbon-rise-report-says>
- [143] Thote J.A., Iyer K.S., Chatti R., Labhsetwar N.K., Biniwale R.B., Rayalu S.S. In situ nitrogen enriched carbon for carbon dioxide capture. *Carbon*. 2010;**48**(2):396-402.
- [144] Shen W.Z., He Y., Zhang S.C., Li J.F., Fan W.B. Yeast-Based Microporous Carbon Materials for Carbon Dioxide Capture. *Chemsuschem*. 2012;**5**(7):1274-1279.
- [145] Wang J.C., Heerwig A., Lohe M.R., Oschatz M., Borchardt L., Kaskel S. Fungi-based porous carbons for CO₂ adsorption and separation. *Journal of Materials Chemistry*. 2012;**22**(28):13911-13913.
- [146] Xing W., Liu C., Zhou Z.Y., Zhang L., Zhou J., Zhuo S.P., et al. Superior CO₂ uptake of N-doped activated carbon through hydrogen-bonding interaction. *Energy & Environmental Science*. 2012;**5**(6):7323-7327.
- [147] Wang R.T., Wang P.Y., Yan X.B., Lang J.W., Peng C., Xue Q.J. Promising Porous Carbon Derived from Celtuce Leaves with Outstanding Supercapacitance and CO₂ Capture Performance. *Acs Applied Materials & Interfaces*. 2012;**4**(11):5800-5806.
- [148] Wei H.R., Deng S.B., Hu B.Y., Chen Z.H., Wang B., Huang J., et al. Granular Bamboo-Derived Activated Carbon for High CO₂ Adsorption: The Dominant Role of Narrow Micropores. *Chemsuschem*. 2012;**5**(12):2354-2360.
- [149] Lu A.-H.D., Sheng. *Porous Materials for Carbon Dioxide Capture*. Springer, 2014.

- [150] Lin D.H., Zhang X.T., Cui X.W., Chen W.X. Highly porous carbons with superior performance for CO₂ capture through hydrogen-bonding interactions. *Rsc Advances*. 2014;**4**(52):27414-27421.
- [151] Leventis N., Sotiriou-Leventis C., Chandrasekaran N., Mulik S., Larimore Z.J., Lu H.B., et al. Multifunctional Polyurea Aerogels from Isocyanates and Water. A Structure-Property Case Study. *Chemistry of Materials*. 2010;**22**(24):6692-6710.
- [152] Chidambareswarapattar C., Larimore Z., Sotiriou-Leventis C., Mang J.T., Leventis N. One-step room-temperature synthesis of fibrous polyimide aerogels from anhydrides and isocyanates and conversion to isomorphic carbons. *Journal of Materials Chemistry*. 2010;**20**(43):9666-9678.
- [153] Hao G.P., Li W.C., Qian D., Lu A.H. Rapid Synthesis of Nitrogen-Doped Porous Carbon Monolith for CO₂ Capture. *Advanced Materials*. 2010;**22**(7):853-857.
- [154] Matsuoka K., Yamagishi Y., Yamazaki T., Setoyama N., Tomita A., Kyotani T. Extremely high microporosity and sharp pore size distribution of a large surface area carbon prepared in the nanochannels of zeolite Y. *Carbon*. 2005;**43**(4):876-879.
- [155] Hu M., Reboul J., Furukawa S., Torad N.L., Ji Q.M., Srinivasu P., et al. Direct Carbonization of Al-Based Porous Coordination Polymer for Synthesis of Nanoporous Carbon. *Journal of the American Chemical Society*. 2012;**134**(6):2864-2867.
- [156] Liu N.N., Yin L.W., Wang C.X., Zhang L.Y., Lun N., Xiang D., et al. Adjusting the texture and nitrogen content of ordered mesoporous nitrogen-doped carbon materials prepared using SBA-15 silica as a template. *Carbon*. 2010;**48**(12):3579-3591.
- [157] Liang C.D., Li Z.J., Dai S. Mesoporous carbon materials: Synthesis and modification. *Angewandte Chemie-International Edition*. 2008;**47**(20):3696-3717.

- [158] Presser V., McDonough J., Yeon S.H., Gogotsi Y. Effect of pore size on carbon dioxide sorption by carbide derived carbon. *Energy & Environmental Science*. 2011;**4**(8):3059-3066.
- [159] Chandra V., Yu S.U., Kim S.H., Yoon Y.S., Kim D.Y., Kwon A.H., et al. Highly selective CO₂ capture on N-doped carbon produced by chemical activation of polypyrrole functionalized graphene sheets. *Chemical Communications*. 2012;**48**(5):735-737.
- [160] Shan M.X., Xue Q.Z., Jing N.N., Ling C.C., Zhang T., Yan Z.F., et al. Influence of chemical functionalization on the CO₂/N₂ separation performance of porous graphene membranes. *Nanoscale*. 2012;**4**(17):5477-5482.
- [161] Iijima S. Helical Microtubules of Graphitic Carbon. *Nature*. 1991;**354**(6348):56-58.
- [162] Yang K.S., Edie D.D., Lim D.Y., Kim Y.M., Choi Y.O. Preparation of carbon fiber web from electrostatic spinning of PMDA-ODA poly(amic acid) solution. *Carbon*. 2003;**41**(11):2039-2046.
- [163] Ghosh A., Subrahmanyam K.S., Krishna K.S., Datta S., Govindaraj A., Pati S.K., et al. Uptake of H₂ and CO₂ by graphene. *The Journal of Physical Chemistry C*. 2008;**112**(40):15704-15707.
- [164] Srinivas G., Burrell J., Yildirim T. Graphene oxide derived carbons (GODCs): synthesis and gas adsorption properties. *Energy & Environmental Science*. 2012;**5**(4):6453-6459.
- [165] Bandosz T.J. Activated Carbon Surfaces in Environmental Remediation. *Activated Carbon Surfaces in Environmental Remediation*. 2006;**7**:1-571.
- [166] Mazumdar B.K., Banerjee D.D., Ghosh G. Coal Zinc-Chloride Reaction - an Interpretation. *Energy & Fuels*. 1988;**2**(2):224-230.

- [167] Caturla F., Molinasabio M., Rodriguezreinoso F. Preparation of Activated Carbon by Chemical Activation with $ZnCl_2$. *Carbon*. 1991;**29**(7):999-1007.
- [168] Jagtoyen M., Derbyshire F. Some Considerations of the Origins of Porosity in Carbons from Chemically Activated Wood. *Carbon*. 1993;**31**(7):1185-1192.
- [169] Solum M.S., Pugmire R.J., Jagtoyen M., Derbyshire F. Evolution of Carbon Structure in Chemically Activated Wood. *Carbon*. 1995;**33**(9):1247-1254.
- [170] Lillo-Rodenas M.A., Cazorla-Amoros D., Linares-Solano A. Understanding chemical reactions between carbons and NaOH and KOH - An insight into the chemical activation mechanism. *Carbon*. 2003;**41**(2):267-275.
- [171] Lozano-Castello D., Calo J.M., Cazorla-Amoros D., Linares-Solano A. Carbon activation with KOH as explored by temperature programmed techniques, and the effects of hydrogen. *Carbon*. 2007;**45**(13):2529-2536.
- [172] Raymundo-Piñero E., Azais P., Cacciaguerra T., Cazorla-Amorós D., Linares-Solano A., Béguin F. KOH and NaOH activation mechanisms of multiwalled carbon nanotubes with different structural organisation. *Carbon*. 2005;**43**(4):786-795.
- [173] Qiao W.M., Yoon S.H., Mochida I. KOH activation of needle coke to develop activated carbons for high-performance EDLC. *Energy & Fuels*. 2006;**20**(4):1680-1684.
- [174] Wang H.L., Gao Q.M., Hu J. High Hydrogen Storage Capacity of Porous Carbons Prepared by Using Activated Carbon. *Journal of the American Chemical Society*. 2009;**131**(20):7016-7022.
- [175] Wang J.C., Kaskel S. KOH activation of carbon-based materials for energy storage. *Journal of Materials Chemistry*. 2012;**22**(45):23710-23725.

- [176] Yu Q.F., Li M., Ning P., Yi H.H., Tang X.L. Preparation and Phosphine Adsorption of Activated Carbon Prepared from Walnut Shells by KOH Chemical Activation. *Separation Science and Technology*. 2014;**49**(15):2366-2375.
- [177] Zhang X.T., Chen W.X. Mechanisms of pore formation on multi-wall carbon nanotubes by KOH activation. *Microporous and Mesoporous Materials*. 2015;**206**:194-201.
- [178] Ross S., Olivier J.P., de Boer J.H. On physical adsorption. New York: Interscience; 1964.
- [179] Barrer R.M. Zeolites and clay minerals as sorbents and molecular sieves. London - New York: Academic Press; 1978.
- [180] Horvath G., Kawazoe K. Method for the calculation of effective pore size distribution in molecular sieve carbon. *Journal of Chemical Engineering of Japan*. 1983;**16**(6):470-475
- [181] Israelachvili J.N. Intermolecular and surface forces. 3rd ed. University of California Santa Barbara, California, U.S.: Elsevier; 2011.
- [182] Cracknell R.F., Gubbins K.E., Maddox M., Nicholson D. Modeling fluid behavior in well-characterized porous materials. *Accounts of chemical research*. 1995;**28**(7):281-288
- [183] Yang R.T. Adsorbents: fundamentals and applications. Hoboken, New Jersey, U.S.: John Wiley & Sons; 2003.
- [184] Pereira M.F.R., Soares S.F., Orfao J.J.M., Figueiredo J.L. Adsorption of dyes on activated carbons: influence of surface chemical groups. *Carbon*. 2003;**41**(4):811-821.
- [185] El-Sayed Y., Bandosz T.J. Acetaldehyde adsorption on nitrogen-containing activated carbons. *Langmuir*. 2002;**18**(8):3213-3218.

- [186] Jia Y.F., Xiao B., Thomas K.M. Adsorption of metal ions on nitrogen surface functional groups in activated carbons. *Langmuir*. 2002;**18**(2):470-478.
- [187] Plaza M.G., Pevida C., Arias B., Feroso J., Casal M.D., Martin C.F., et al. Development of low-cost biomass-based adsorbents for postcombustion CO₂ capture. *Fuel*. 2009;**88**(12):2442-2447.
- [188] Maroto-Valer M.M., Lu Z., Zhang Y.Z., Tang Z. Sorbents for CO₂ capture from high carbon fly ashes. *Waste Management*. 2008;**28**(11):2320-2328.
- [189] Plaza M.G., Pevida C., Arenillas A., Rubiera F., Pis J.J. CO₂ capture by adsorption with nitrogen enriched carbons. *Fuel*. 2007;**86**(14):2204-2212.
- [190] Sevilla M., Valle-Vigon P., Fuertes A.B. N-Doped Polypyrrole-Based Porous Carbons for CO₂ Capture. *Advanced Functional Materials*. 2011;**21**(14):2781-2787.
- [191] Plaza M.G., Thurecht K.J., Pevida C., Rubiera F., Pis J.J., Snape C.E., et al. Influence of oxidation upon the CO₂ capture performance of a phenolic-resin-derived carbon. *Fuel Processing Technology*. 2013;**110**:53-60.
- [192] Seema H., Kemp K.C., Le N.H., Park S.W., Chandra V., Lee J.W., et al. Highly selective CO₂ capture by S-doped microporous carbon materials. *Carbon*. 2014;**66**:320-326.
- [193] Song C.W., Wu S.H., Cheng M.R., Tao P., Shao M.H., Gao G.R. Adsorption Studies of Coconut Shell Carbons Prepared by KOH Activation for Removal of Lead(II) From Aqueous Solutions. *Sustainability*. 2014;**6**(1):86-98.
- [194] Pei S.P., Qu S., Zhang Y.M. Direct Electrochemistry and Electrocatalysis of Hemoglobin at Mesoporous Carbon Modified Electrode. *Sensors*. 2010;**10**(2):1279-1290.

- [195] Li Y.Q., Ben T., Zhang B.Y., Fu Y., Qiu S.L. Ultrahigh Gas Storage both at Low and High Pressures in KOH-Activated Carbonized Porous Aromatic Frameworks. *Scientific Reports*. 2013, Doi 10.1038/Srep02420.
- [196] Sevilla M., Fuertes A.B. Sustainable porous carbons with a superior performance for CO₂ capture. *Energy & Environmental Science*. 2011;**4**(5):1765-1771.
- [197] Lee S.Y., Park S.J. Determination of the optimal pore size for improved CO₂ adsorption in activated carbon fibers. *Journal of Colloid and Interface Science*. 2013;**389**:230-235.
- [198] Wickramaratne N.P., Jaroniec M. Importance of small micropores in CO₂ capture by phenolic resin-based activated carbon spheres. *Journal of Materials Chemistry A*. 2013;**1**(1):112-116.
- [199] Marco-Lozar J.P., Kunowsky M., Suarez-Garcia F., Linares-Solano A. Sorbent design for CO₂ capture under different flue gas conditions. *Carbon*. 2014;**72**:125-134.
- [200] Zhang Z., Zhou J., Xing W., Xue Q., Yan Z., Zhuo S., et al. Critical role of small micropores in high CO₂ uptake. *Physical Chemistry Chemical Physics*. 2013;**15**(7):2523-2529.
- [201] Casco M.E., Martínez-Escandell M., Silvestre-Albero J., Rodríguez-Reinoso F. Effect of the porous structure in carbon materials for CO₂ capture at atmospheric and high-pressure. *Carbon*. 2014;**67**:230-235.
- [202] Yu J.Y., Guo M.Y., Muhammad F., Wang A.F., Zhang F., Li Q., et al. One-pot synthesis of highly ordered nitrogen-containing mesoporous carbon with resorcinol-urea-formaldehyde resin for CO₂ capture. *Carbon*. 2014;**69**:502-514.

[203] Wahby A., Ramos-Fernandez J.M., Martinez-Escandell M., Sepulveda-Escribano A., Silvestre-Albero J., Rodriguez-Reinoso F. High-Surface-Area Carbon Molecular Sieves for Selective CO₂ Adsorption. *Chemsuschem*. 2010;**3**(8):974-981.

[204] Wang J.C., Senkowska I., Oschatz M., Lohe M.R., Borchardt L., Heerwig A., et al. Highly porous nitrogen-doped polyimine-based carbons with adjustable microstructures for CO₂ capture. *Journal of Materials Chemistry A*. 2013;**1**(36):10951-10961.

Chapter 2 Mechanisms of Pore Formation on Multi-wall Carbon Nanotubes by KOH Activation¹

In this chapter, we are focusing on KOH activation of multi-wall carbon nanotubes and their CO₂ adsorption. This study contributes to the understanding of pore forming mechanisms of KOH activated materials.

2.1 Introduction

Activation by alkaline compounds such as KOH is a commonly used method for carbonaceous materials [1-6]. It has been reported that high-surface-area carbon with well-developed microporous structure can be obtained [1, 7]. However, the activation by KOH is rather complicated and its activation mechanism has been argued for a long time [8-11]. In 2003, Lillo-Ródenas *et al.* [12] proposed a global reaction for KOH activation based on experimental data and thermodynamic calculation. The global reaction suggested the chemical reaction between KOH and carbon atoms at high temperatures to form K₂CO₃, H₂ and metallic K. Since metallic K is very active, it was also found that the produced metallic K intercalated into layered graphitic structures, which provided additional amount of micropores [7, 13].

Although this global reaction has been widely adopted [1, 14-17], it is still difficult to generalize the pore structures of activated carbon materials because of various carbon sources used for the activation. For example, carbon sources like petroleum coke [18, 19], wood [14] and nutshells [2, 10] have been attempted due to economic considerations;

¹ Reproduced from X. Zhang, W. Chen, *Microporous and Mesoporous Materials*, **206** (2015), 194-201, with permission from the Royal Society of Chemistry.

however, the resulted specific surface areas are inconsistent varying from ~ 100 m²/g up to ~ 1600 m²/g, and carbon source materials with fixed chemical structure [20, 21] are preferred in order for an easier method to study the activation process.

Carbon nanotubes (CNTs) are an important type of carbon nanomaterials and have been extensively studied as the carbon source for the activation [7, 21], since activated CNTs were reported to have a great potential for the applications in energy storage [22] and gas storage [23, 24]. Previous studies have investigated the influence of activation temperature [21] and carbon/activation agent ratio [25] for different types of CNTs grown under different conditions [7, 26], but were still vague about the mechanism of pore formation on CNTs during the activation process. Therefore, it's critical that the pore structure and pore-forming mechanism be clearly elucidated for the activated CNTs.

In the present work, high-quality CVD grown multi-walled CNTs (MWCNTs) were used as the carbon source for the activation. The pore structures of activated MWCNTs under different activation temperatures and periods were thoroughly studied, through which their pore-forming mechanism was elucidated. The understanding of the pore-forming mechanism may lead to the flexible adjustment of their pore size distribution. In addition, the activated MWCNTs provide a good platform to investigate the effect of absorbent's pore structures on its CO₂ capture behavior. The relationship between CO₂ uptake and the pore structure of activated MWCNTs was further studied in this paper.

2.2 Experimental

The as-purchased MWCNTs (NanoLab Co., produced via CVD method, outer diameter: 15 ± 5 nm, tube length: 5-20 μ m) [27] was washed by 1 M HCl and de-ionized water at room

temperature thoroughly prior to use. XPS results gave 99.58 wt.% C and 0.42 wt.% O with no detection of other elements (Table 2.1). Elemental analysis using ICP-MS (Nu PlasmaTM inductively coupled plasma mass spectrometer) indicated major detections of Fe (2.00 wt%) and Ni (0.96 wt%) (Table 2.2). This may be due to the fact that small amount of Fe/Ni catalyst particles are buried inside MWCNTs and difficult to be dissolved by acid. In total, the after-washed MWCNTs have a purity of > 95% and were used without further purification.

Table 2.1 XPS elemental analysis of as-received MWCNTs.

	C	O	Other elements
Amount (wt. %)	99.58	0.42	—

Table 2.2 ICP-MS analysis of metal composition of as-received MWCNTs.

	Fe	Mo	Other metals
Amount (wt. %)	2.00	0.96	<0.01

Activating agent KOH was purchased from Fisher Scientific Canada. MWCNTs and KOH were physically mixed at a weight ratio of 1:6, and the mixture was then put in an alumina boat and quickly placed into a quartz tube. The tube was vacuumed to a pressure below 30 Pa before Argon was introduced at a steady flow rate of 100 cm³/min. After purging for 1h, the furnace was heated up to 150 °C and held at the temperature for 2 h. This was followed by heating the furnace to various activation temperatures at a rate of 10 °C/min. Samples

with different activation condition were labelled as ACNT-x-y, x representing activation temperature and y representing activation time. After activation, the mixture was washed with 1 M hydrochloric acid followed by copious deionized water.

The porous structure was analyzed by N₂ adsorption/desorption at 77 K by using an Autosorb-1 system (Quantachrome). All the samples were outgassed at 150 °C for over 15 hours before they were tested. Pore size distribution was calculated by Non-local density functional theory (NLDFT, slit/cylindrical pore model for carbon). Brunauer, Emmett and Teller (BET) surface area (S_{BET}) was calculated by using N₂ adsorption data in relative pressure range from 0.1 to 0.3. Micropore surface area (S_{micro}), micropore volume (V_{micro}), pore <1 nm volume ($V_{<1\text{nm}}$) were calculated from NLDFT method. Mesopore surface area (S_{meso}) was the difference of BET surface area and micropore surface area.

Scanning electron microscopy (SEM) was done by EVO MA 15 (Zeiss), equipped with Silicon Drift Detector for Energy Dispersive X-Ray (EDX) analysis/ mapping (Bruker). High resolution SEM images were taken by a JAMP-9500F (JEOL, Tokyo, Japan) operated at 15 kV. The microstructures of MWCNTs before and after activation were investigated by a JOEL 2010 transmission electron microscope (TEM) operated at 200 kV (JEOL, Tokyo, Japan). X-ray photoelectron spectroscopy (XPS) was done with an AXIS 165 system (Kratos Analytical Ltd., UK). X-ray diffraction (XRD) was applied with a Rigaku Geigerflex 2173 diffractometer (Rigaku Corp., Tokyo, Japan) operating with a source of Cu $K\alpha$, $\lambda=0.154$ nm.

CO₂ adsorption was tested by thermalgravimetric analysis (TGA). Usually a ~5 mg sample was placed in a platinum crucible in a TGA machine (SDT Q600, TA Instrument). The

sample was first heated to 105 °C for 30 min to be fully desorbed, and then equilibrated at 25 °C, after which pure N₂ environment will be changed to 95% CO₂ with 5% N₂. The sample was then kept at this condition for 1 h for adsorption. The weight change profile measured was determined to be the amount of CO₂ adsorption.

2.3 Results and discussion

2.3.1 Influence of temperature

MWCNTs samples were activated at temperatures from 400 °C to 900 °C for 2 hours. Nitrogen adsorption/desorption isotherms are shown in Figure 2.1. The curves can be categorized into two groups. The first one (Group I) includes pristine CNTs and those activated at 400 °C and 500 °C, which exhibits type II isotherm and indicates non-porous structures according to IUPAC [28]. The other group (Group II) includes CNTs after activation at temperatures from 600 °C to 900 °C. This group of isotherms shows a smaller adsorption amount at high relative pressures and obvious hysteresis. These are features of type IV classification, indicating the presence of mesopores (2-50 nm). In addition, the knees of the curves (indicated by the arrow in Figure 2.1) in Group 2 are higher than those in Group 1, revealing the increased amount of micropores (<2 nm).

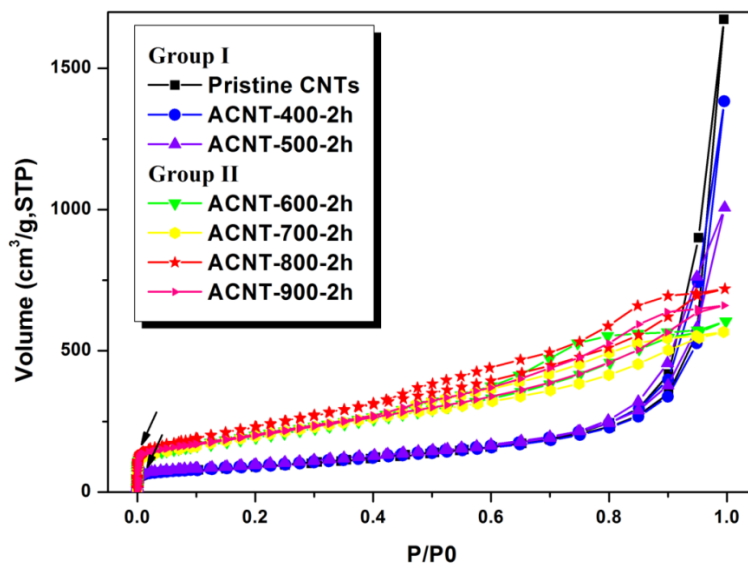


Figure 2.1 N_2 adsorption isotherms of pristine CNTs and activated CNTs obtained at different temperatures

Statistical pore structural information in Table 2.3 also shows major differences between these two groups. The BET surface area for the samples from Group I demonstrates little change at around $325 \text{ m}^2/\text{g}$; while the ones from Group II show much improved BET surface areas with an increasing trend up to $856 \text{ m}^2/\text{g}$ at $800 \text{ }^\circ\text{C}$. Data involving different sized pores (S_{micro} , S_{meso}) also show the similar trend. For pore volume, however, V_T values from Group II are much smaller than those from Group I, even with significantly increased micropore volume (V_{micro}), suggesting the disappearance of large mesopores for the samples in Group II.

Table 2.3 Statistical pore structure information and CO₂ uptake of activated CNTs under different temperature.

	$S_{\text{BET}}^{\text{a}}$	$S_{\text{micro}}^{\text{b}}$	$S_{\text{meso}}^{\text{c}}$	V_{T}^{d}	$V_{\text{micro}}^{\text{e}}$	$V_{<1\text{nm}}^{\text{f}}$	$W_{\text{CO}_2}^{\text{g}}$	
	(m ² /g)	(m ² /g)	(m ² /g)	(cm ³ /g)	(cm ³ /g)	(cm ³ /g)	(mg/g)	
Group I	Pristine CNTs	324	254	70	1.52	0.14	0.012	-
	ACNT- 400 -2h	325	230	95	1.28	0.11	0.017	18.1
	ACNT- 500 -2h	351	246	105	1.23	0.12	0.021	19.8
Group II	ACNT- 600 -2h	707	489	218	0.94	0.24	0.065	25.2
	ACNT- 700 -2h	729	477	252	0.88	0.23	0.067	27.6
	ACNT- 800 -2h	856	532	324	1.12	0.27	0.061	27.5
	ACNT- 900 -2h	730	498	232	1.03	0.25	0.057	-

^aBET surface area; ^bmicropore surface area; ^ctotal pore volume; ^dtotal pore volume; ^emicropore(<2nm) volume; ^fpore(<1nm) volume; ^gCO₂ adsorption amount.

In order to further analyze the pore structure, pore size distributions (PSDs) were calculated from isotherm data using a slit/cylindrical pore NLDFT model. PSDs of micropore range and mesopore range are shown in Figure 2.2a and Figure 2.2b, respectively. In the micropore range in Figure 2.2a, a strong peak between 1.0 nm and 1.2 nm is shown for pristine CNTs and all activated CNTs. The peak keeps the same position while the peak intensity differs for different activation temperatures. Hence, the peak at 1.0-1.2 nm is suggested to be originated from CNT fabrication processes; and the activation process may

change the volume of these intrinsic pores. After activation, however, a new peak at 0.8 nm appears. Interestingly, the intensity of this new peak is small when the temperature is lower than 500 °C; and it increases dramatically when the temperature goes higher than 600 °C. This trend correlates well with those of S_{BET} and S_{micro} shown in Table 2.3, implying the important role of this new peak to the surface area. Therefore, the micropores at 0.8 nm is the characteristic pores for the activated CNT samples that were developed during the activation process. Note that the pore volume (< 1 nm), $V_{<1\text{nm}}$, in Table 2.3 is the calculated micropore volume up to the end of the new peak at 0.8 nm.

In the mesopore range in Figure 2.2b, samples from Group I present very small mesopore volume, with broad peaks showing at the pore size larger than 15 nm. The formation of these broad pores (>15 nm) is due to the inter-tube space caused by entanglement/aggregation of long nanotubes [29, 30]. On the contrary, samples from Group II show much improved mesopore volume, with a large number of pores present in a narrow range between 2 and 10 nm. The highest peak sits at 5.3 nm. This PSD curve is different from the curves obtained from other activated carbons that generally have small mesopore volumes with the sizes smaller than 4 nm [5, 18, 25]. It is noted that the broad peaks at the pore size larger than 15 nm disappear in Group II, which explains the decrease of V_{T} for Group II in Table 2.3.

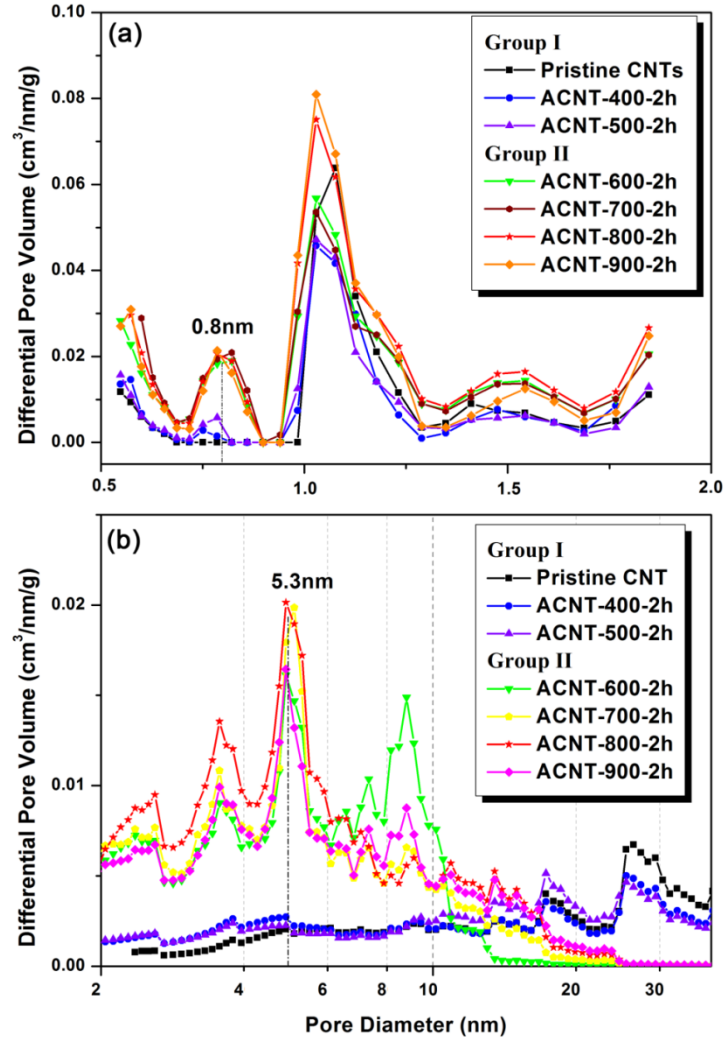


Figure 2.2 Pore size distribution of pristine and activated CNTs at different temperature. (a) micropore size distribution; (b) mesopore size distribution.

2.3.2 Influence of time

Figure 2.3 and Table 2.4 show graphic and statistical pore characteristics after activation at 600 °C for various periods. Figure 2.3a and Figure 2.3b shows similar isotherm shapes and no obvious changes in micropore size distribution. However, from Figure 2.3c, it is observed that, as activation time increases up to 10 hours, the intensity of the strongest peak

(at 5.3 nm) increases continuously while another small peak at 8.8 nm decreases accordingly. Similar behavior can also be observed in Figure 2.2b for Group II when the activation temperature increases, indicating a similar influence on the pore structure for the activation factors of temperature and time. Another resemblance is that both the sample with the highest temperature and the one with the longest time show decreased pore volume and BET surface area, as can be seen in Table 2.3 and Table 2.4. This is the phenomenon of over-activation. The detailed analysis of the pore-forming mechanisms and over-activation will be discussed in Section 2.3.3.

Table 2.4 Statistical pore structure information and CO₂ uptake of activated CNTs with different time.

	$S_{\text{BET}}^{\text{a}}$	$S_{\text{micro}}^{\text{b}}$	$S_{\text{meso}}^{\text{c}}$	V_{T}^{d}	$V_{\text{micro}}^{\text{e}}$	$V_{<1\text{nm}}^{\text{f}}$	$W_{\text{CO}_2}^{\text{g}}$
	(m ² /g)	(m ² /g)	(m ² /g)	(cm ³ /g)	(cm ³ /g)	(cm ³ /g)	(mg/g)
ACNT-600-2h	707	489	218	0.94	0.24	0.065	25.2
ACNT-600-5h	741	509	232	0.76	0.25	0.072	26.1
ACNT-600-10h	800	556	244	0.76	0.27	0.081	31.4
ACNT-600-15h	732	513	219	0.69	0.24	0.074	29.7

^aBET surface area; ^bmicropore surface area; ^ctotal pore volume; ^dtotal pore volume; ^emicropore(<2nm) volume; ^fpore(<1nm) volume; ^gCO₂ adsorption amount.

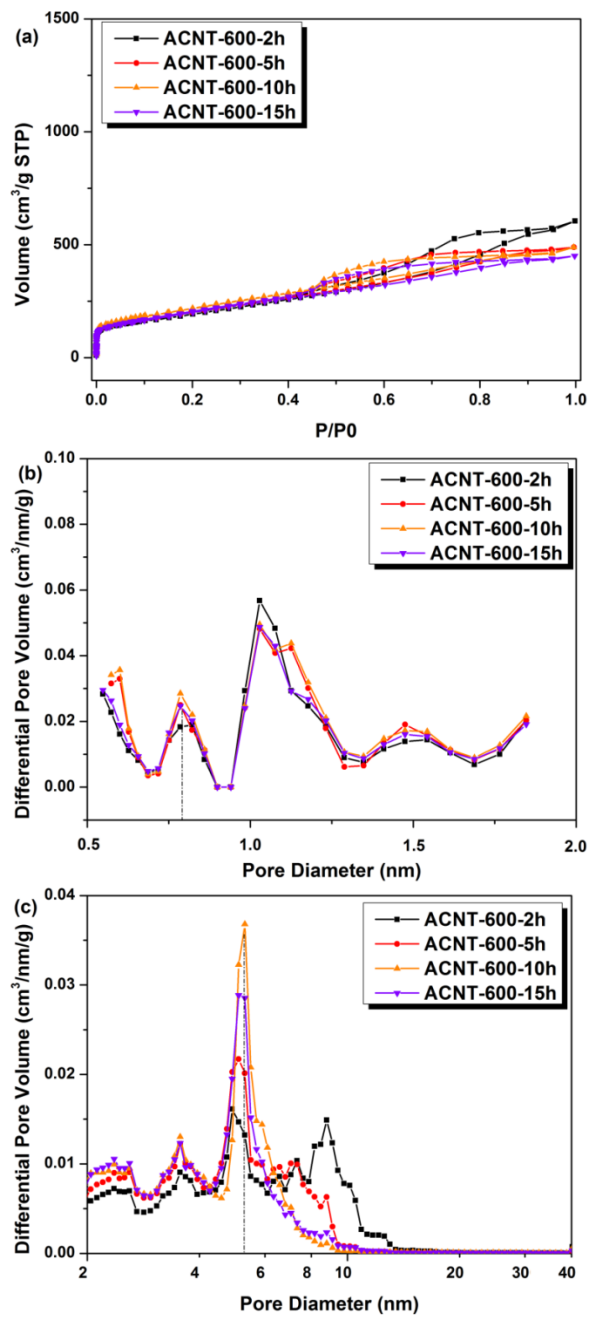


Figure 2.3 Pore structure of activated MWCNTs with different activation time. (a) isotherm; (b) micropore size distribution; (c) mesopore size distribution.

2.3.3 Pore-forming mechanism

2.3.3.1 Micropores

High-resolution TEM images are presented in Figure 2.4 to compare different surface morphologies on CNTs before and after activation, respectively. In Figure 2.4a, pristine CNTs have intact, parallel graphene layers; while in Figure 2.4b, graphene layers decorated with defects can be found on the MWCNT walls. It is also observed that distorted graphene layers appear, which is suggested to be the origin of increased micropores during the activation process [31]. Table 2.5 also gives XPS elemental analysis for activated CNTs and shows insignificant increase of oxygen amounts. Therefore, it can be concluded from Figure 2.4 and Table 2.5 that the micropores formed are mainly due to the KOH-C redox reaction occurring along CNT walls, that is, the etching of carbon framework followed by potassium intercalation. Also note that it is the KOH-C redox reaction that causes the formation of the characteristic peak at 0.8 nm in Figure 2.2 Pore size distribution of pristine and activated CNTs at different temperature. (a) micropore size distribution; (b) mesopore size distribution. Figure 2.2b during activation.

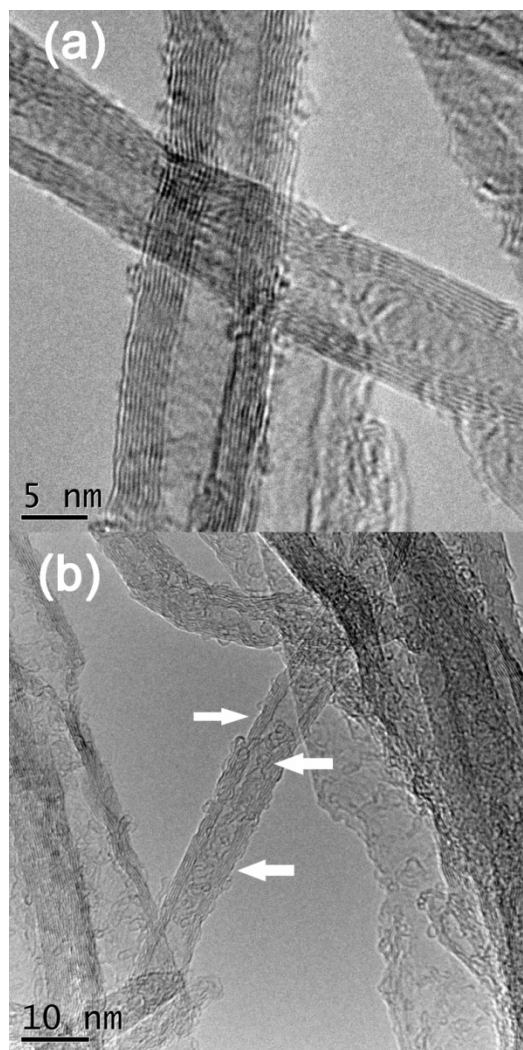


Figure 2.4 High resolution TEM images. (a) Pristine MWCNTs; (b) activated MWCNTs (sample: ACNT-800-2h, with white arrows pointing to developed micropores)

Table 2.5 XPS elemental analysis of activated CNTs.

At. %	C	O
Pristine CNTs	99.58	0.42

ACNT- 400 -2h	98.86	1.14
ACNT- 500 -2h	98.15	1.85
ACNT- 600 -2h	97.96	2.04
ACNT- 700 -2h	98.34	1.66
ACNT- 800 -2h	98.26	1.74
ACNT- 900 -2h	98.09	1.91

2.3.3.2 Mesopores

Coalescence of micropores was used to explain the formation of mesopores [25]. However, in the case of CNTs, more interesting results were found. Figure 2.5 shows that the inner diameter distribution of pristine CNTs correlates well with the PSD of sample ACNT-600-2h, the critical condition at which mesoporous features were developed. The data of MWCNTs inner diameter were obtained from inspection of over 200 high-resolution TEM images (taken at the same resolution) with aid of graphic editing software. This strong correlation suggests that the appearance of mesopores during activation is due to the opening of inner space of the pristine CNTs. Figure 2.6 presents high-resolution SEM images, showing different morphologies of CNTs before and after activation. Apparently, the length of nanotubes has been shortened after activation, implying that single nanotubes were transversely sectioned into shorter ones as the carbon framework was etched further. This transverse sectioning leads to the opening of inner space of MWCNTs. Therefore, it is concluded that coalescence of micropores sections MWCNTs, and thus exposes their inner space as the mesopores detected. The size of mesopores is strictly controlled by the inner

diameter of MWCNTs, which explains a wide range of mesopore sizes of activated CNTs compared with other activated carbons [5, 18, 25]. This result may project a new way to manipulate the size of mesopores in carbon materials.

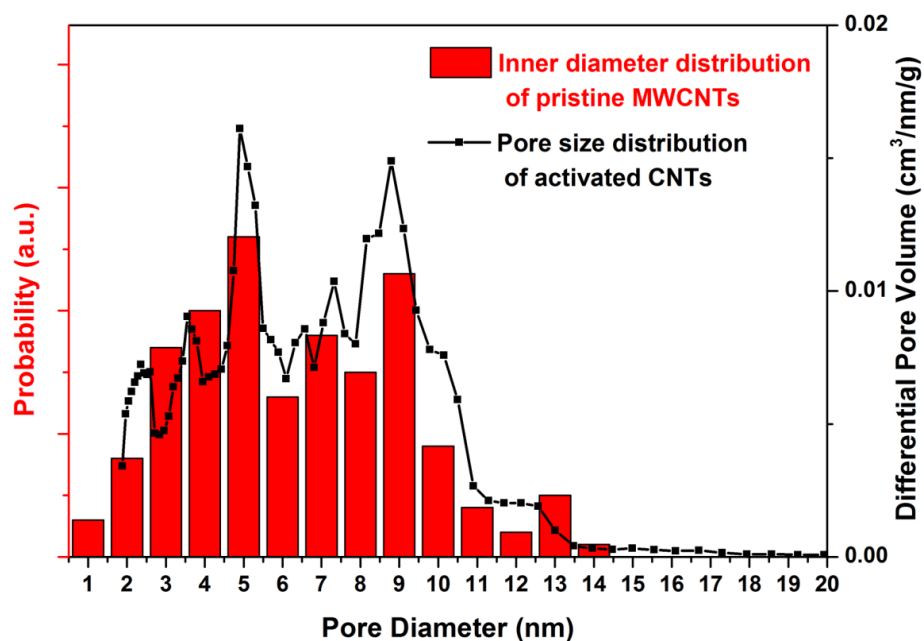


Figure 2.5 Frequency histogram of pristine CNTs inner diameter distribution.
(Overlay: PSD of ACNT-600-2h)

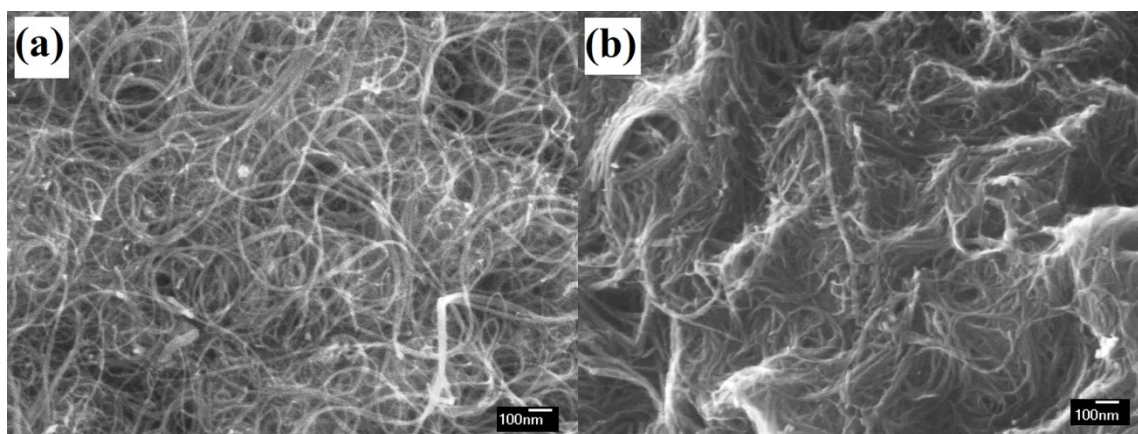


Figure 2.6 High resolution SEM images of MWCNTs. a) pristine CNTs; b) activated CNTs (ACNT-600-2h).

Figure 2.7a shows XRD spectra and SEM images of samples activated at different temperatures. The opening of inner space of MWCNTs is consistent with the identification of catalyst particles in Figure 2.7a. In the XRD spectra, all samples show broad peaks at 26° and 44° , representing the graphitic carbon peaks of C (002) and C (101), respectively. However, only samples activated at 600°C or higher demonstrate very sharp Fe peaks. The absence of Fe peaks in XRD results for the samples activated below 600°C should be caused by the entrapment of nanosize catalyst particles within CNTs [32], which results in the broadening and weakening of Fe peaks that are hidden by strong carbon peaks. Hence, the appearance of Fe peaks activated at 600°C or higher suggests that Fe catalyst particles were released from within MWCNTs and aggregated to larger sizes as a result of coarsening at high temperatures. EDX mappings of Fe in Figure 2.7a also support this finding. Fe mapping for the low-resolution SEM image shows a clear difference between the two samples (Pristine CNTs and 600°C). For pristine CNTs, Fe particles are small and evenly distributed. For the 600°C -activated sample, in contrast, only a few particles can be detected but with increased sizes. It reveals the occurrence of aggregation of catalyst particles that released from MWCNT walls during activation. In terms of time influence, Figure 2.7b shows only carbon peaks for the samples after activation at 500°C for 2 h and 15 h. With the extending activation period to 30 h, the catalyst particle peaks appear, indicating a similar mechanism as temperature influence in Figure 2.7a. Therefore, Figure 2.7 further proves that the coalescence of micropores transversely sectioned nanotubes and released catalyst particles, leaving the inner space of MWCNTs open to be mesopores. Additionally, as discussed in Figure 2.2b, the formation of the pores with the size larger than 15 nm is attributed to entanglement/aggregation of long nanotubes [29, 30]. The

disappearance of these pores in Group II of Figure 2.2b was therefore caused by the shortening of the nanotubes, as discussed in Figure 2.6 and Figure 2.7.

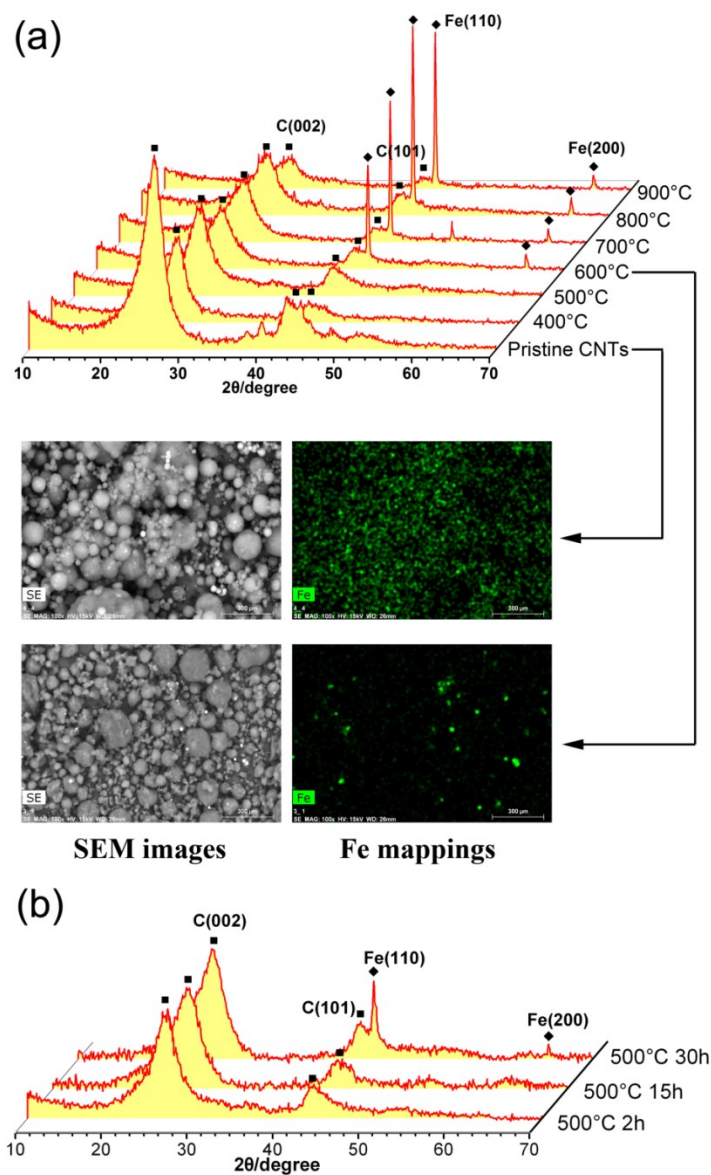


Figure 2.7 a) XRD analysis of activated MWCNTs at different temperature, with corresponding SEM images and EDX Mappings; b) XRD analysis of activated MWCNTs at 500°C with different activation time.

2.3.3.3 Over-activation

It is also noted in Table 2.3 that the volume of mesopores starts to decrease at the activation temperature of 900 °C. A similar observation can also be seen in Figure 2.2b and Figure 2.3c. These phenomena can be described as over-activation. However, the proposed formation mechanism of mesopores discussed above cannot explain the decreasing trend of the mesopore volume. Interestingly, the TEM image of the over-activated samples in Figure 2.8 shows that the tubular structure of MWCNTs starts to change substantially at 900 °C, by forming large pieces of graphene sheets with small carbon particles (as indicated by the white arrows) decorated on the surface. The breakdown of tubular structures shown in Figure 2.8 destroys the inner space of MWCNTs, and therefore, decreases the volume of mesopores. This observation, in turn, supports the formation mechanism of mesopores proposed in Figure 2.5. In addition, the characteristic micropore at 0.8 nm, as shown in Figure 2.2a, has not been influenced by the destruction of tubular structures.

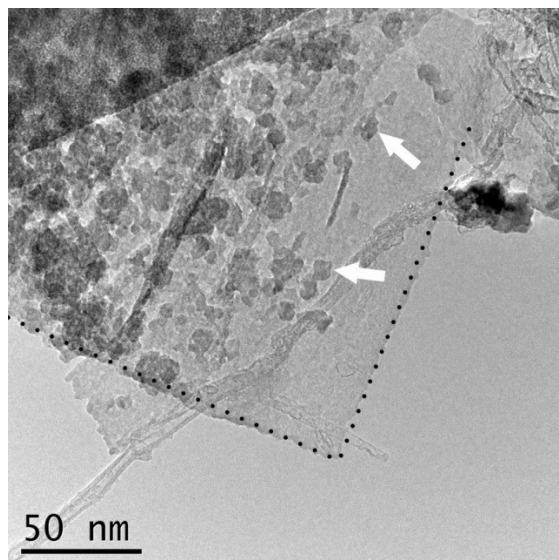


Figure 2.8 High resolution TEM image of ACNT-900-2h. (Black dashes denote the edges of graphene layers; white arrows denote carbon particles.)

A summarized schematic diagram is drawn in Figure 2.9 to illustrate the pore forming mechanisms of KOH-activated MWCNTs.

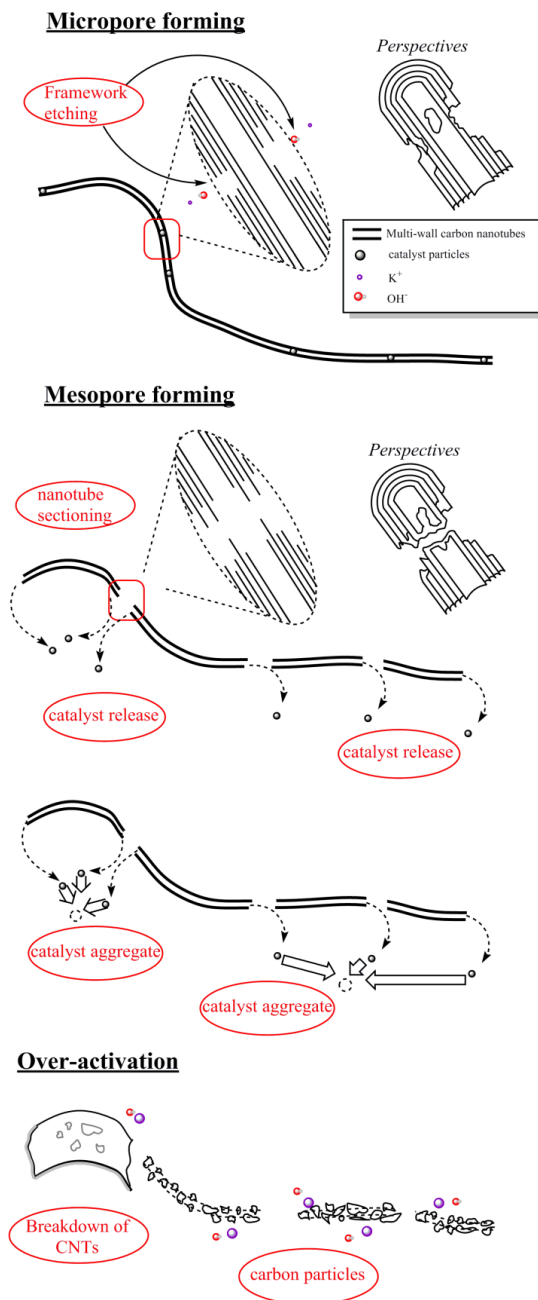


Figure 2.9 Schematic diagram of pore forming mechanisms for KOH activated MWCNTs.

2.3.4 CO₂ adsorption

The understanding of the pore-forming mechanism during the activation of MWCNTs, as discussed above, may lead to the flexible adjustment of their pore size distribution. In addition to the adjustable porous structures, the activated CNTs are decorated with few nitrogen-free functional groups (XPS analysis in Table 2.5), which also provides a good platform to investigate the CO₂ capture behavior solely resulted from the pore structure of adsorbents. As shown in Figure 2.5, the sizes of pores developed during activation are mostly below 15 nm. In Figure 2.10a, however, no clear relationship was found between pore (<15 nm) volume and CO₂ uptake. Instead, when plotting the volume of micropore (<1 nm) versus CO₂ uptake, as shown in Figure 2.10b, all data points including the samples obtained at different activation temperatures and periods can be fitted well to a linear line with a good coefficient of determination ($R^2=0.91$). This results indicate that micropores with sizes <1 nm play a significant role in the physic-sorption of CO₂ molecules, which is consistent with the previous work [33]. The significant influence of micropores on the adsorption of CO₂ molecules was attributed to stronger interactions between CO₂ molecules and multiple surfaces in micropores, when comparing with layer-by-layer CO₂ adsorption on a single surface [34, 35]. More importantly, in the current MWCNT system, there is no doping of heteroatoms (such as N, S) that influences CO₂ capture. Therefore, the linear relationship between micropores with sizes <1 nm and CO₂ adsorption clearly show that increasing <1 nm micropore volume is an efficient method to improve CO₂ adsorption performance.

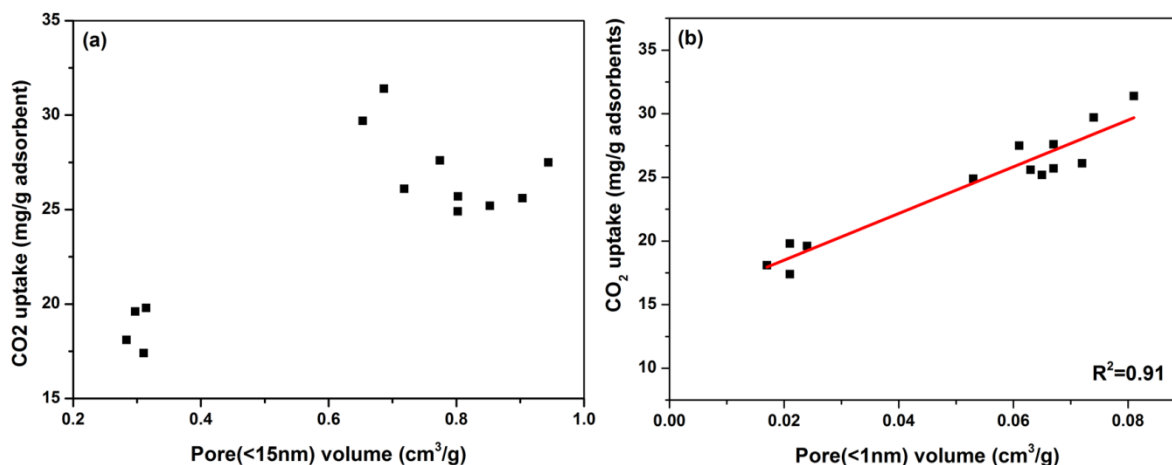


Figure 2.10 (a) CO₂ uptake vs. pore (<15nm) volume; (b) CO₂ uptake vs. pore (<1nm) volume.

2.4 Conclusions

The porous structures of KOH-activated multi-wall carbon nanotubes (MWCNTs) under different activation temperatures and periods were studied, through which the pore-forming mechanisms of the activated MWCNTs were elucidated. It was found that micropores (<2 nm) were developed by KOH-C redox reaction occurring along the walls of MWCNTs, causing the formation of a characteristic peak of micropores at 0.8 nm. More importantly, the in-depth activation was found to transversely section the nanotubes, release the catalyst particles, and expose the inner space of MWCNTs to be mesopores. The understanding of the pore-forming mechanism may lead to the flexible adjustment of their pore size distribution. In addition, the activated CNTs provide a good platform to investigate the effect of adsorbent's pore structures on its CO₂ capture behavior. It was further demonstrated that the amount of CO₂ uptake increased linearly with increasing volume of micropores with the pore sizes <1 nm, implying that the micropores when <1nm played a significant role in the physic-sorption of CO₂ molecules.

2.5 References

- [1] Zhu Y., Murali S., Stoller M.D., Ganesh K.J., Cai W., Ferreira P.J., et al. Carbon-based supercapacitors produced by activation of graphene. *Science*. 2011;**332**(6037):1537-1541.
- [2] Ahmadpour A., Do D.D. The preparation of activated carbon from macadamia nutshell by chemical activation. *Carbon*. 1997;**35**(12):1723-1732.
- [3] Lozano-Castello D., Lillo-Rodenas M.A., Cazorla-Amoros D., Linares-Solano A. Preparation of activated carbons from Spanish anthracite I. Activation by KOH. *Carbon*. 2001;**39**(5):741-749.
- [4] Jiang Q., Qu M.Z., Zhang B.L., Yu Z.L. Preparation of activated carbon nanotubes. *Carbon*. 2002;**40**(14):2743-2745.
- [5] Kubota M., Hata A., Matsuda H. Preparation of activated carbon from phenolic resin by KOH chemical activation under microwave heating. *Carbon*. 2009;**47**(12):2805-2811.
- [6] Vilaplana-Ortego E., Lillo-Rodenas M.A., Alcaniz-Monge J., Cazorla-Amoros D., Linares-Solano A. Isotropic petroleum pitch as a carbon precursor for the preparation of activated carbons by KOH activation. *Carbon*. 2009;**47**(8):2141-2142.
- [7] Raymundo-Piñero E., Azaïs P., Cacciaguerra T., Cazorla-Amorós D., Linares-Solano A., Béguin F. KOH and NaOH activation mechanisms of multiwalled carbon nanotubes with different structural organisation. *Carbon*. 2005;**43**(4):786-795.
- [8] Otowa T., Tanibata R., Itoh M. Production and adsorption characteristics of MAXSORB: high-surface-area active carbon. *Gas Separation & Purification*. 1993;**7**(4):241-245

- [9] Oh G.H., Park C.R. Preparation and characteristics of rice-straw-based porous carbons with high adsorption capacity. *Fuel*. 2002;**81**(3):327-336
- [10] Guo J., Lua A.C. Textural and chemical characterizations of adsorbent prepared from palm shell by potassium hydroxide impregnation at different stages. *Journal of Colloid and Interface Science*. 2002;**254**(2):227-233
- [11] Díaz-Terán J., Nevskaja D.M., Fierro J.L.G., López-Peinado A.J., Jerez A. Study of chemical activation process of a lignocellulosic material with KOH by XPS and XRD. *Microporous and Mesoporous Materials*. 2003;**60**(1):173-181.
- [12] Lillo-Rodenas M.A., Cazorla-Amoros D., Linares-Solano A. Understanding chemical reactions between carbons and NaOH and KOH - An insight into the chemical activation mechanism. *Carbon*. 2003;**41**(2):267-275.
- [13] Xue R., Shen Z. Formation of graphite-potassium intercalation compounds during activation of MCMB with KOH. *Carbon*. 2003;**41**(9):1862-1864.
- [14] Lillo-Ródenas M.A., Juan-Juan J., Cazorla-Amorós D., Linares-Solano A. About reactions occurring during chemical activation with hydroxides. *Carbon*. 2004;**42**(7):1371-1375.
- [15] Murali S., Potts J.R., Stoller S., Park J., Stoller M.D., Zhang L.L., et al. Preparation of activated graphene and effect of activation parameters on electrochemical capacitance. *Carbon*. 2012;**50**(10):3482-3485.
- [16] Wang J.C., Kaskel S. KOH activation of carbon-based materials for energy storage. *Journal of Materials Chemistry*. 2012;**22**(45):23710-23725.

- [17] Lozano-Castello D., Calo J.M., Cazorla-Amoros D., Linares-Solano A. Carbon activation with KOH as explored by temperature programmed techniques, and the effects of hydrogen. *Carbon*. 2007;**45**(13):2529-2536.
- [18] Chunlan L., Shaoping X., Yixiong G., Shuqin L., Changhou L. Effect of pre-carbonization of petroleum cokes on chemical activation process with KOH. *Carbon*. 2005;**43**(11):2295-2301.
- [19] Kawano T., Kubota M., Onyango M.S., Watanabe F., Matsuda H. Preparation of activated carbon from petroleum coke by KOH chemical activation for adsorption heat pump. *Applied Thermal Engineering*. 2008;**28**(8):865-871
- [20] Yamashita Y., Ouchi K. Influence of Alkali on the Carbonization Process .1. Carbonization of 3,5-Dimethylphenol-Formaldehyde Resin with Naoh. *Carbon*. 1982;**20**(1):41-45.
- [21] Niu J.J., Wang J.N. Effect of temperature on chemical activation of carbon nanotubes. *Solid State Sciences*. 2008;**10**(9):1189-1193.
- [22] Li C., Wang D., Liang T., Wang X., Ji L. A study of activated carbon nanotubes as double-layer capacitors electrode materials. *Materials Letters*. 2004;**58**(29):3774-3777.
- [23] Smith M.R., Bittner E.W., Shi W., Johnson J.K., Bockrath B.C. Chemical activation of single-walled carbon nanotubes for hydrogen adsorption. *Journal of Physical Chemistry B*. 2003;**107**(16):3752-3760.
- [24] Cinke M., Li J., Bauschlicher Jr C.W., Ricca A., Meyyappan M. CO₂ adsorption in single-walled carbon nanotubes. *Chemical Physics Letters*. 2003;**376**(5):761-766

- [25] Romanos J., Beckner M., Rash T., Firlej L., Kuchta B., Yu P., et al. Nanospace engineering of KOH activated carbon. *Nanotechnology*. 2012, Doi 10.1088/0957-4484/23/1/015401.
- [26] Raymundo-Pinero E., Cazorla-Amoros A., Delpoux S., Frackowiak E., Szostak K., Beguin F. High surface area carbon nanotubes prepared by chemical activation. *Carbon*. 2002;**40**(9):1614-1617.
- [27] Available from: <http://www.nano-lab.com/nanotubes-research-grade.html>
- [28] K. S. W. Sing D.H.E., R. A. W. Haul, L. Moscou, R. A. Pierotti, J. Rouquerol, T. Siemieniowska. Reporting physisorption data for gassolid systems with special reference to the determination of surface area and porosity. *Pure & Appl Chem*. 1985;**57**(4):603-619.
- [29] Yang Q.H., Hou P.X., Bai S., Wang M.Z., Cheng H.M. Adsorption and capillarity of nitrogen in aggregated multi-walled carbon nanotubes. *Chemical Physics Letters*. 2001;**345**(1):18-24.
- [30] Hou P.X., Xu S.T., Ying Z., Yang Q.H., Liu C., Cheng H.M. Hydrogen adsorption/desorption behavior of multi-walled carbon nanotubes with different diameters. *Carbon*. 2003;**41**(13):2471-2476.
- [31] Huttepain M., Oberlin A. Microtexture of Nongraphitizing Carbons and Tem Studies of Some Activated Samples. *Carbon*. 1990;**28**(1):103-111.
- [32] Cui X.W., Wei W.F., Harrower C., Chen W.X. Effect of catalyst particle interspacing on the growth of millimeter-scale carbon nanotube arrays by catalytic chemical vapor deposition. *Carbon*. 2009;**47**(15):3441-3451.

- [33] Presser V., McDonough J., Yeon S.H., Gogotsi Y. Effect of pore size on carbon dioxide sorption by carbide derived carbon. *Energy & Environmental Science*. 2011;**4**(8):3059-3066.
- [34] Dubinin M. Generalization of the theory of volume filling of micropores to nonhomogeneous microporous structures. *Carbon*. 1985;**23**(4):373-380.
- [35] Yang R.T. Adsorbents: fundamentals and applications. Hoboken, New Jersey, U.S.: John Wiley & Sons; 2003.

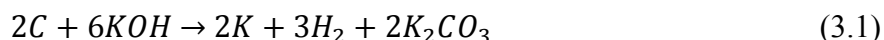
Chapter 3 A Comprehensive Study of Polyaniline-derived Porous Carbons via KOH Activation¹

In this chapter, we are focusing on KOH activation of polyaniline. This study contributes to the understanding of pore forming mechanism of KOH activated carbons.

3.1 Introduction

Activated carbons (ACs) possess large specific surface area (SSA), well-developed porous structure and good thermal/chemical stability [1-3]. They are widely used in various applications such as gas adsorption [4, 5], water treatment [6, 7] and energy storage [8, 9]. When comparing two main activation methods (physical and chemical activation), chemical activation is usually preferred due to its lower activation temperature and higher yields, less activation time and higher SSA and pore volume [10]. In particular, activation by KOH is of increasing interest recently as most of the ultrahigh-SSA (3100~3500 m² g⁻¹) AC materials [11-14] are produced by this method.

KOH activation is a well-known method to produce carbon materials made up of micropores and some small mesopores. However, considering a large number of experimental variables and precursor selections, the activation mechanisms have not been well understood albeit with intensive studies [12, 15-18]. A generally accepted theory for KOH activation is KOH etching carbon framework by the global reaction:



¹ Reproduced from X. Zhang, X. Cui, W. Chen, *RSC adv.*, 2015, **5**, 77629-77636, with permission from the Royal Society of Chemistry.

which was proposed by Linares-Solano's group [19] based on experimental results and theoretical calculations. Additionally, at temperatures higher than 700 °C, the decomposition of K_2CO_3 into K_2O and CO_2 brings up physical activation effect of CO_2 [20]. The produced K in the global reaction also could intercalate into the carbon lattice and cause irreversible expansion. After washing off the potassium compound, these expansions cannot return to their non-porous structure [17, 21]. In most occasions the ultrahigh SSA and the well-developed microporosity are resulted from the synergetic contributions of the chemical activation, the physical activation and the potassium intercalation [22].

Experimentally, the porous structure and chemical composition of the resulting ACs depend on activation conditions (activation temperature and KOH ratio), carbon precursor and preheating temperature. Most studies show that by controlling the activation temperature and KOH ratio, a maximum Brunauer Emmett Teller (BET) surface area value and optimized microporous structure can be obtained [23-26]. In 2011 Sevilla *et al.* [27] synthesized a high SSA porous carbon with activation temperature of 700 °C and KOH ratio = 4. The resulting carbon possessed a BET surface area of $3480 \text{ m}^2 \text{ g}^{-1}$ and a micropore volume of $1.18 \text{ cm}^3 \text{ g}^{-1}$. However, further increasing temperature and KOH dosage leads to pore widening effect and consequently decrease of BET surface area and micropore volume [22, 23, 28, 29]. Use of different precursors leads to ACs with various unique porous structures [3, 30]. Recently, many synthesized polymers (such as polyacrylonitrile [29, 31], polypyrrole [11], polyaniline [32]) were employed as carbon precursors due to their controllable structures and composition. The preheating temperature has been considered to be another important parameter for the activation process and could

be critical to pore development [33, 34], but the mechanisms behind this influence have not been discussed before.

In this work polyaniline (PANI) was selected as the carbon precursor. PANI is a low-cost, environmentally stable, conductive polymer [35] and has thus been studied extensively. The well-studied synthesis process of PANI [36, 37] enables a better control of chemical composition and pore morphology, which provides a promising opportunity to understand the structures of subsequent ACs from microscopic level. A comprehensive study was carried out in this investigation to determine how the properties of PANI-derived porous carbon are affected by activation temperature, KOH ratio and preheating temperature. By tuning these factors, the BET surface area of the obtained ACs could achieve $\sim 3800 \text{ m}^2 \text{ g}^{-1}$. Particularly, the influence of preheating temperature was thoroughly investigated. By examining samples after preheating stage, a new mechanism was proposed to elucidate the formation of porous structure. It is believed that this mechanism could be applied to the activation of other carbon precursors achieving improved SSA and micropore volume. This high SSA porous carbon could be applied as potential electrode materials for such energy devices as supercapacitors.

3.2 Experimental

The method of synthesizing PANI can be found from our previous work [38]. Briefly, aniline (0.23 M, 350 mL) acid solution was slowly dropped into an ammonium persulfate (0.54 M, 150 mL) acid solution under ice bath (0~1 °C) and then the mixture was further magnetically stirred for 12 h. The resulting mixture was vacuum-filtrated and washed by copious deionized water until the pH was ~ 7 , which was followed by oven drying. The final PANI yield was around 100%. For the KOH activation of PANI, KOH (pellet, Fisher

Scientific) and PANI were ground separately before being physically mixed with a weight ratio of KOH:PANI = 1~3:1, and put into a round alumina crucible. The crucible was placed into a horizontal quartz tube and purged with Ar flow (100 mL min^{-1}) for 1h before the thermal treatment. The temperature-time program of activation process is illustrated in Figure 3.1. A hold at 150/200/250 °C for 1 h was made before it was ramped to the activation temperature at a rate of $3 \text{ }^\circ\text{C min}^{-1}$. The activation process took 1 h and the samples were allowed to cool in the furnace under argon protection. The resulting samples were washed first with 1M HCl and then deionized water until near-neutral pH (~ 7) was reached before being dried in an oven at 80 °C for at least 24 h. The after-dry activated carbon yield was 5%~20%. It was found that the higher the activation temperature/KOH ratio, the lower the yield. This is consistent with previous work [39-41]. These carbon samples were denoted as C-x-y-z, where x represents KOH to PANI ratio, y represents the preheating temperature (in °C) and z is the activation temperature (in °C). In addition, samples after preheating stage were taken out and washed with deionized water until near-neutral pH (~ 7) was reached. The samples were then oven dried at 80 °C for at least 24 h. The dried samples were denoted as P-150/200/250, corresponding to different preheating temperature (150 °C/200 °C/250 °C). The KOH to PANI ratio of these samples was kept at 2.

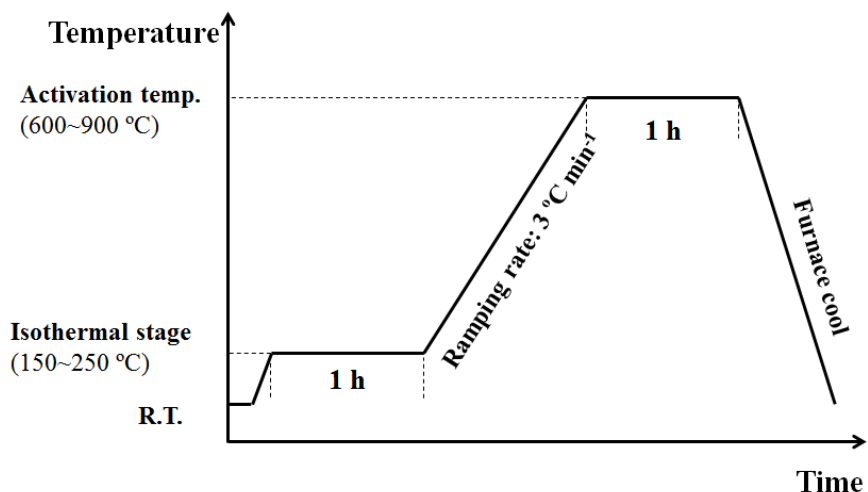


Figure 3.1 Schematic of temperature program for KOH activation process.

The morphologies of the samples were examined by scanning electron microscopy (SEM) using a JAMP-9500F system (JEOL, Tokyo, Japan) under 15 kV and by transmission electron microscopy (TEM) using a JEOL-2010 system (JEOL, Tokyo, Japan) with an operating voltage of 200 kV. Low-temperature nitrogen adsorption test was performed at 77 K with Autosorb 1MP (Quantachrome). All the samples (20~30 mg) were outgassed under high vacuum at 130 °C for 4 h before the adsorption tests. The BET surface area data were calculated using data points at a relative pressure of 0.05~0.2. The total pore volume was obtained based on adsorption data at $P/P_0 = 0.995$. Pore size distributions (PSDs) were determined using quenched solid density functional theory (QSDFT) model, assuming a slit pore shape. For PANI/P-150/P-200/P250, PSDs were determined using Barrett-Joyner-Halenda (BJH) desorption model due to the sample's absence of micropores. In order to characterize chemical properties, infrared spectrum was recorded with a Nicolet 8700 Fourier transformation infrared (FTIR) spectrometer (Thermal Scientific), the scanning range was between 500 and 4000 cm^{-1} , with a resolution of 1.93 cm^{-1} and 64 scans per test. Differential scanning calorimetry (DSC) was applied using Q1000 (TA Instrument). The

sample (~5 mg) was sealed in an aluminum pan with pinhole, and then placed in the machine and purged with 50 mL min⁻¹ N₂ (99.999% pure). The sample was first cooled to 0 °C and then ramped to 400 °C at a rate of 5 °C min⁻¹. Thermal gravimetric analysis (TGA) was carried out using SDT Q600 (TA Instrument), where the samples (5~10 mg) were placed in a platinum crucible pans under nitrogen atmosphere (99.999% pure, flow rate: 100 mL min⁻¹). The temperature was then ramped from room temperature to 600 °C at a rate of 10 °C min⁻¹.

3.3 Results and discussion

3.3.1 Study of pore structure

Figure 3.2 shows microscopic morphologies of as-synthesized PANI and PANI-derived activated carbon (C-2-200-800). The SEM image of PANI (Figure 3.2a) exhibits a sponge-like texture with fibrous structures embedded inside. The TEM image shown in Figure 3.2b indicates that PANI nanofibers were formed and surrounded by polymer aggregates. This typical structure is caused by intrinsic morphology of PANI (fibrous structure) and its heterogeneous nucleation (aggregates) [37, 42]. After activation, the carbon sample (Figure 3.2c) presents a smooth surface with some large cavities under low magnification. However, a high-resolution TEM image (Figure 3.2d) displays a representative microporous structure with worm-like graphitic layers.

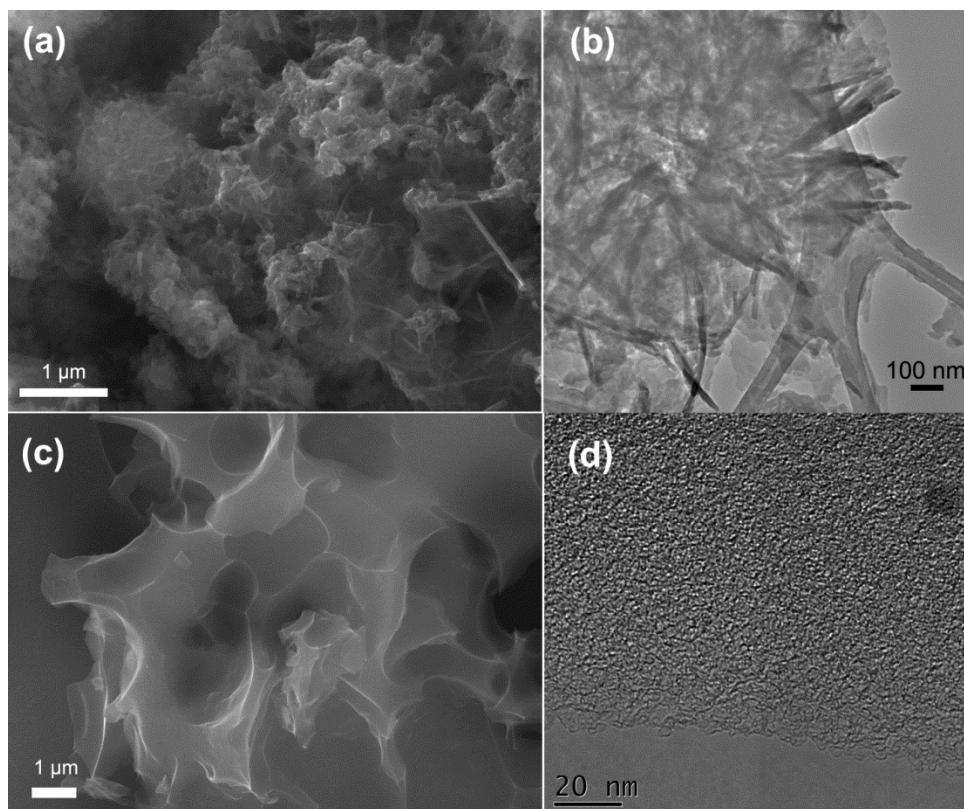


Figure 3.2 Morphologies of PANI and PANI-derived carbons (C-2-200-800): (a) SEM image of PANI; (b) TEM image of PANI; (c) SEM image of C-2-200-800; (d) High-resolution TEM image of C-2-200-800.

The porous structure was further characterized by N₂ adsorption/desorption analysis and the results obtained are shown in Figure 3.3, with statistic pore characteristics listed in Table 3.1. From the isotherms of different carbon samples (Figure 3.3a, c, e), it could be observed that all these curves present significant amount of adsorption at relatively low pressure ($P/P_0 < 0.1$), followed by a relatively flat plateau characteristics (except C-2-200-900 and C-3-200-800). This means that most activated carbons are microporous and lacks of mesopores (except C-2-200-900 and C-3-200-800). C-2-200-900 and C-3-200-800 were obtained at high activation temperature/KOH ratio, and their isotherms display an obvious

increase of adsorption at high pressure and hysteresis, implying the existence of considerable mesopores.

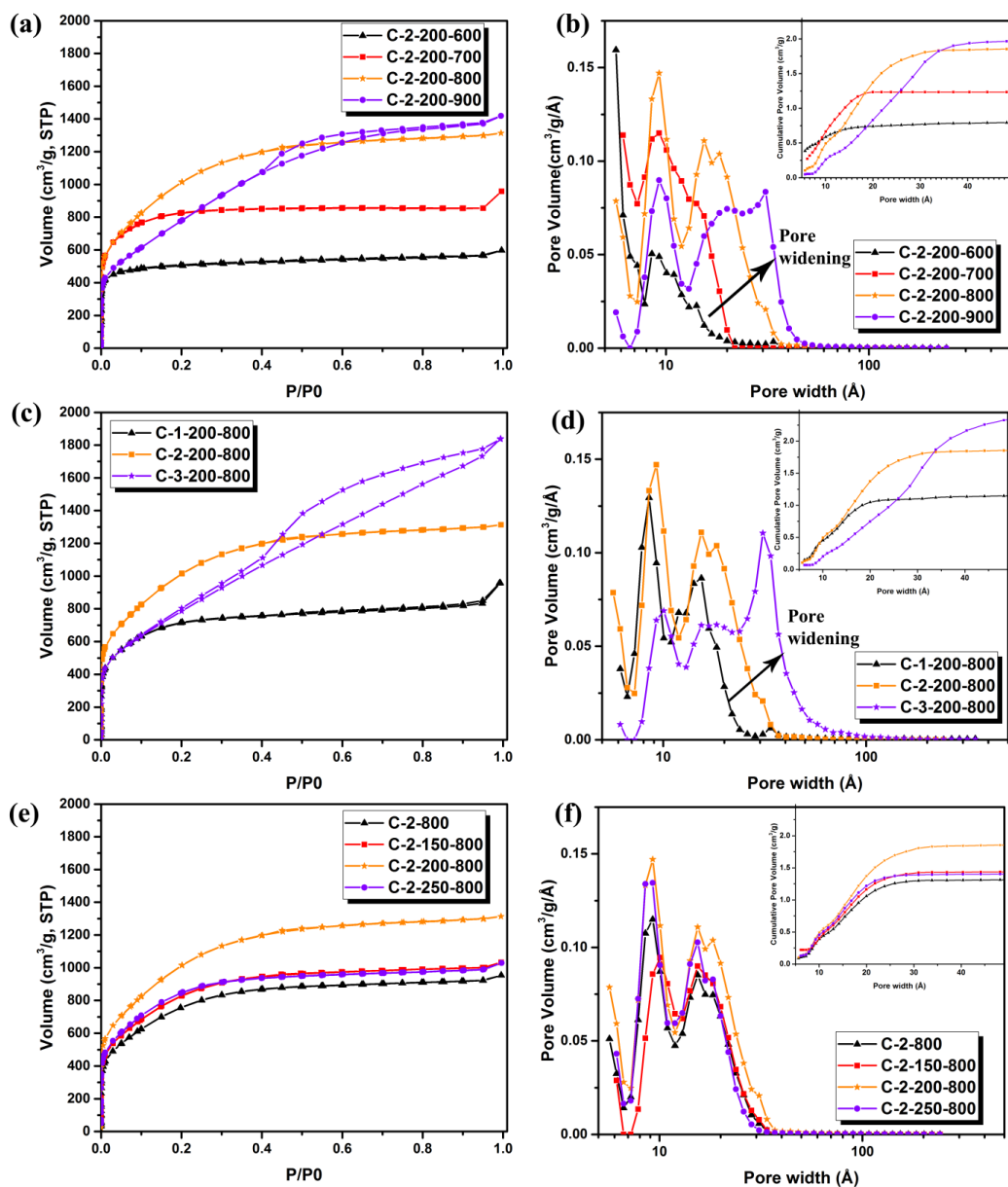


Figure 3.3 Isotherms (a, c, e) and pore size distributions (b, d, f) of PANI-derived carbons under various activation conditions. (a) (b): different activation temperature; (c) (d): different KOH ratio; (e) (f): different preheating temperature. (C-2-800 represents the sample without preheating stage)

Table 3.1 Porous structure data of PANI-derived carbons under various activation conditions.

Sample	BET surface area ^a (m ² /g)	Total pore volume ^b (cm ³ g ⁻¹)	Micropore volume ^c (cm ³ g ⁻¹)	<1 nm pore volume ^c (cm ³ g ⁻¹)	<0.7 nm pore volume ^c (cm ³ g ⁻¹)
C-2-200-600	1711	0.92	0.74	0.59	0.47
C-2-200-700	2889	1.48	1.23	0.67	0.36
C-2-200-800	3768	2.03	1.37	0.49	0.16
C-2-200-900	2914	2.19	0.83	0.26	0.06
C-1-200-800	2575	1.48	1.05	0.45	0.19
C-3-200-800	2901	2.85	0.75	0.20	0.07
C-2-800 ^d	2800	1.47	1.06	0.39	0.12
C-2-150-800	3059	1.60	1.16	0.40	0.22
C-2-250-800	3115	1.59	1.22	0.46	0.15

^aBET surface area obtained using BET method at P/P₀=0.05-0.2.

^bTotal pore volume calculated at P/P₀=0.995.

^cMicropore, <1 nm pore volume and <0.7 nm pore volume obtained from QSDFT slit pore model.

^dC-2-800 represents the activated sample without preheating stage.

A more direct observation could be made from PSDs in Figure 3.3b, d and f. Figure 3.3b and d show influences of activation temperature and KOH ratio on the pore development of the prepared carbons, respectively. It could be seen that at the activation temperature of 600 °C, the sample presents mainly micropores with pore sizes smaller than 0.7 nm. As the temperature increases, the amount of narrow micropores (<0.7 nm) decreases while large micropores (~1 nm) and small mesopores are formed. At 800 °C, the major peaks are at ~1 nm and ~2 nm. At 900 °C, the pore size is even larger. This is evidently caused by

micropore coalescence to form larger pores (such as mesopores) due to severe KOH-C reaction (over-activation). At the same time, new micropores fail to emerge at a satisfactory rate, resulting in a gradual decrease of narrow micropore (<1 nm and <0.7 nm) volume with the increase of activation temperature, as could be observed in Table 3.1. As a consequence, the BET surface area increases from C-2-200-600 (1711 m² g⁻¹) to C-2-200-800 (3768 m² g⁻¹), and then decreases for C-2-200-900 (2914 m² g⁻¹). Similar pore widening effect occurs when the KOH ratio increases. As could be seen in Figure 3.3d, from C-1-200-800 to C-3-200-800, the largest pore size increases from ~1.5 nm to ~3 nm and the number of pores with sizes <1 nm decreases substantially. In Table 3.1, the BET values first increase from C-1-200-800 (2575 m² g⁻¹) to C-2-200-800 (3768 m² g⁻¹) and then decrease for C-3-200-800 (2901 m² g⁻¹). This is similar with the effect of temperature. These observations are also consistent with previous study [22]. Particularly, at activation temperature of 800 °C and KOH ratio of 2, the activated carbon achieves an optimum micropore volume of 1.37 cm³ g⁻¹ and the highest BET surface area of 3768 m² g⁻¹. In Figure 3.3f, however, preheating temperature has not caused pore widening as samples with different preheating temperature have similar pore size distributions, although the pore volume and SSA are different. This indicates that the preheating temperature influenced the pore structures of PANI-derived carbons through mechanisms other than KOH-C reaction.

3.3.2 Study of the preheating stage

In order to understand how the preheating temperature influences porous structure of the PANI-derived carbons, PANI/KOH mixtures were taken out after the preheating stage and KOH was washed off carefully to study the remaining materials (P150, P200 and P250). As could be observed in TEM images from Figure 3.4, different preheating temperatures have

resulted in different morphologies of the resulting materials. P-150 demonstrates a nanofiber/agglomerate structure similar to the original PANI (Figure 3.2b), which means that no obvious morphological change occurred during preheating at 150 °C. However, P-200 shows a network-like nanostructure. Considering the fact that the width of the nanofibers in P-150 is similar to that of the network structures in P-200, it is suggested that the network of PANI was formed by nanofiber fragmentation, possibly through melting and cross-linking with each other. The size of the cavities in the PANI network is several tens of nanometers. For P-250, the TEM image shows that no network-like structure but some disordered agglomerates is present.

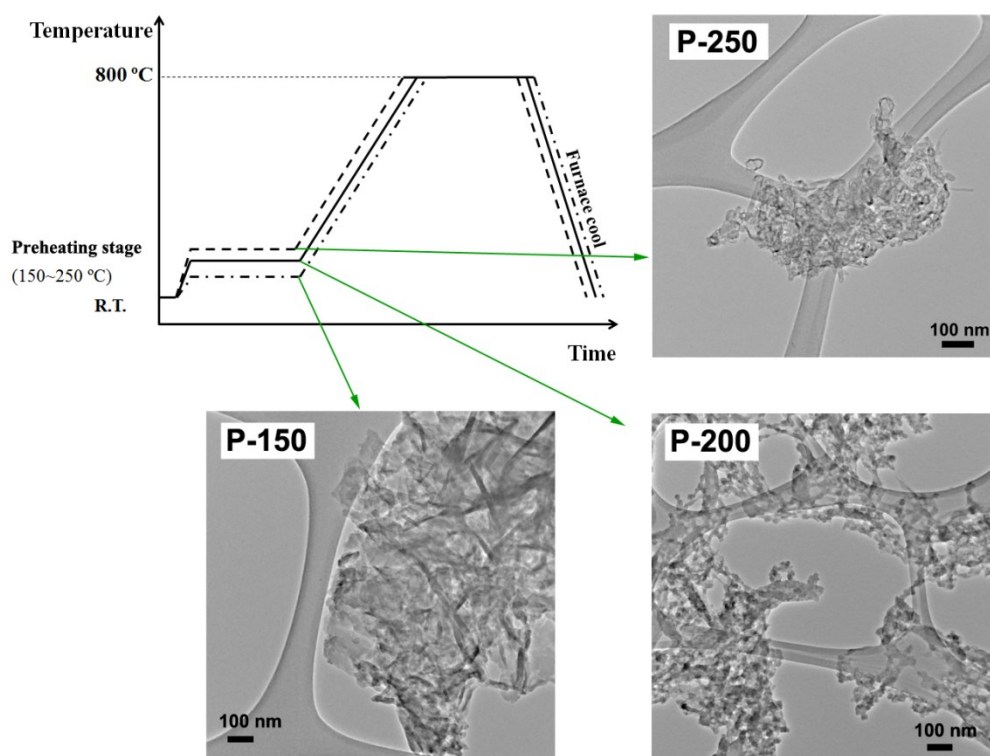


Figure 3.4 Morphologies of PANI after preheating stage of different temperatures.

Figure 3.5 and Table 3.2 further display the N₂ adsorption/desorption analysis of the PANIs after preheating at different temperatures. As can be seen in Figure 3.5, isotherms of all

samples are type II (according to IUPAC), revealing non-porous nature of the materials. PSDs (Figure 3.5b) at small pore range (<10 nm) are rather random. However, it could be found in Table 3.2 that at pore sizes ranging between 10 nm and 100 nm, the pore volume increases slightly from $0.20 \text{ cm}^3 \text{ g}^{-1}$ (PANI) to $0.22 \text{ cm}^3 \text{ g}^{-1}$ (P-200). This range of pore sizes (10~100 nm) is very comparable to the range of cavity sizes observed in Figure 3.4, and an increase of the BET surface area with increasing preheating temperature, from $27 \text{ m}^2 \text{ g}^{-1}$ (original PANI) to $34 \text{ m}^2 \text{ g}^{-1}$ (200 °C) as listed in Table 3.2, is observed. In contrast, the BET surface area was decreased to $18 \text{ m}^2 \text{ g}^{-1}$ at the preheating temperature of 250 °C, which should be related to the non-network-type structure of the PANI-derived carbons, as evidenced in Figure 3.4. These observations also imply that the formation of network nanostructure increased the surface area, and the network morphology may offer a large interfacial area for the polymer to react with KOH, which is essentially important to achieve a homogeneous reaction and well-developed porosity. This also explains the reason that the trend of the PANI-derived carbons' BET values in Table 3.1 correlates well with the trend of the PANIs' listed in Table 3.2. Furthermore, the low BET surface areas and the absence of micropores after pre-heating also reveal that KOH-C reaction does not occur at temperatures below 250 °C. This further confirms that the different pore structure of PANI-derived carbons under different preheating temperature was not caused by KOH-C reaction. Instead, it is suggested that the morphologies of PANIs resulting from a non-activation process during preheating stage may play an important role.

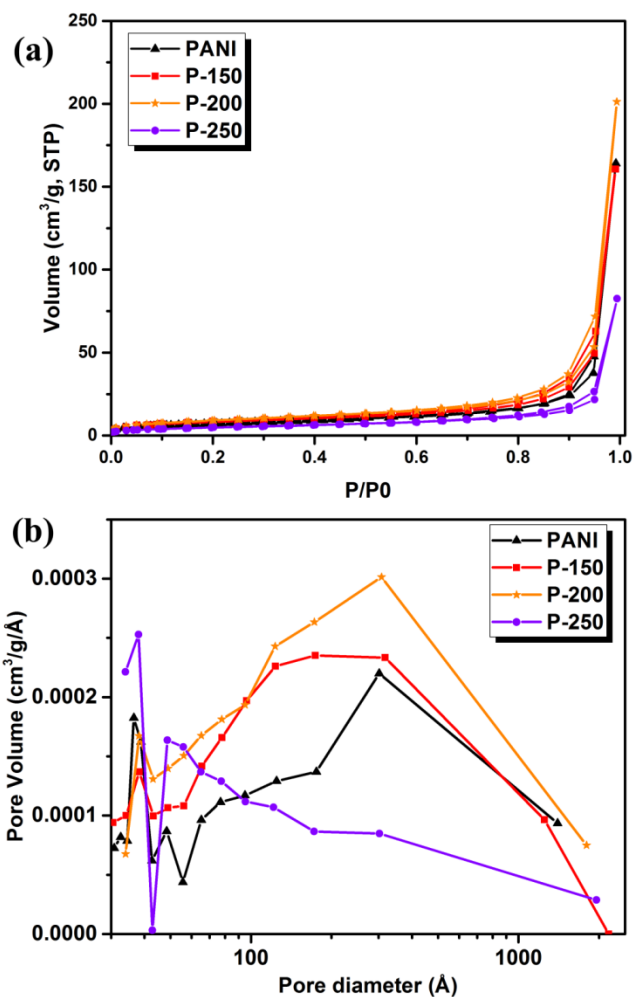


Figure 3.5 (a) Isotherms and (b) pore size distributions (based on BJH desorption model) of samples after preheating stage of different temperatures.

Table 3.2 Porous structure data of PANI after different preheating condition.

Sample	BET surface area ^a (m ² /g)	Total pore volume ^b (cm ³ g ⁻¹)	10~100 nm pore volume ^c
PANI	27	2.54	0.20
P-150	30	2.48	0.21
P-200	34	3.11	0.22

P-250	18	1.28	0.08
-------	----	------	------

^aBET surface area obtained using BET method at $P/P_0=0.05-0.2$.

^bTotal pore volume calculated at $P/P_0=0.995$.

^c10~100 nm pore volume obtained from BJH desorption model.

In order to reveal the causes of the morphology change in the preheating stage, FTIR was conducted after different preheating processes and the results obtained are shown in Figure 3.6. Compared with the original PANI sample, the samples after preheating show intensity changes at 1585 cm^{-1} , 1504 cm^{-1} and 1160 cm^{-1} (peaks with arrows). Specifically, the decreased peak intensity at 1585 cm^{-1} represents the C=C stretching vibration of quinoid rings, the increased peak intensity at 1504 cm^{-1} represents the C=C stretching of benzenoid rings and the intensity of the 1160 cm^{-1} peak representing N=Q=N (Q means quinoid rings) also decreases. [43, 44] These changes indicate that at preheating stage a crosslinking reaction occurs among PANI nanofibers. As proposed in Figure 3.6b, the crosslinking is established through a link of the imine nitrogen with its neighboring quinoid rings [45], which is consistent with the decrease of N=Q=N and quinoid rings peaks in Figure 3.6a. It is also proposed that the crosslinking reaction was triggered by thermal treatment [43, 46, 47] (in this case the preheating stage). Furthermore, P-200 presents the strongest intensity change, implying the most intense crosslinking activity. It is suggested that the PANI network morphology of P-200 in Figure 3.4 is resulted from the crosslinking. This is consistent with the study of Huang. *et al.* [43], who melted and merged PANI nanofibres via crosslinking induced by high-power camera flash. Figure 3.6a shows that P-150 exhibits changes similar to those of P-200, but the intensities of the 3 representative peaks (indicated with arrows) are weaker than P-200, implying the degree of cross-linking of PANI at $150\text{ }^\circ\text{C}$ is less than at $200\text{ }^\circ\text{C}$. Indeed, previous study [48] showed that the

crosslinking time required at 150 °C is 4 times more than that at 200 °C for the same conversion rate. Therefore, the fact that the morphology of P-150 (from Figure 3.4) is not the same as that of P-200 is mainly caused by incomplete crosslinking at 150 °C. Thus it can be concluded that the network morphology of PANI at preheating stage was caused by more complete crosslinking reaction, and this in turn resulted in higher SSA and well-developed pore structure of PANI-derived carbon. Additionally, P-250 displays a decrease of all peak intensity compared with P-200 because of its non-cross-linked structure. Since the non-cross-linked structure led to a smaller SSA and undesirable structure of PANI-derived carbon, it is necessary to further study the behavior of PANIs at this preheating temperature (250 °C).

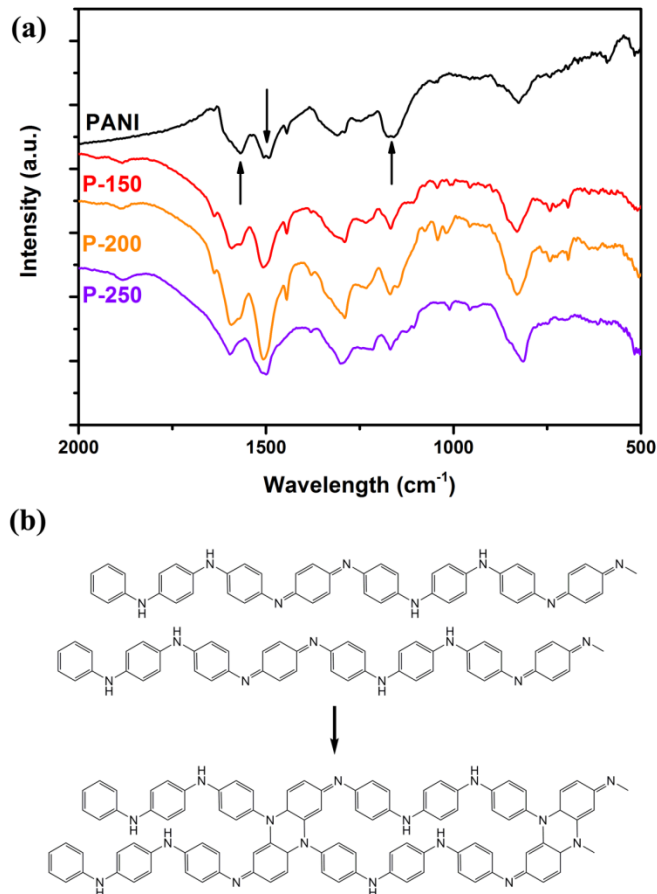


Figure 3.6 (a) FTIR spectra of PANI and samples after preheating stage of different temperatures; (b) schematic for thermal crosslinking of PANI.(remake from [36])

DSC and TGA were conducted to further characterize the effect of preheating at 250 °C and the results obtained are shown in Figure 3.7a and Figure 3.7b, respectively. In Figure 3.7a, the endothermic peak at ~100 °C was attributed to the evaporation of water. The following two broad exothermic peaks between ~155 °C and ~220 °C were assigned to crosslinking reaction [45, 49], which confirms the crosslinking effect found from the FTIR analysis shown in Figure 3.6. Another strong endothermic peak appears at 240~350 °C. In the TGA curve of Figure 3.7b it could be observed that a slow weight loss occurred at a low

temperature (<250 °C). This is followed by a major weight loss at ~300 °C. In the derivative weight curve in Figure 3.7b, three peaks can be identified. The first two small peaks are located at 160~220 °C, in accord with the crosslinking peaks in Figure 3.7a. The next broad but strong peak is located at 250~320 °C. Based on the obvious weight loss observed from the weight profile, this peak should be resulted from evolution of volatile species, which proves to be the degradation of PANI [50], and explains the appearance of the peak at 240~350 °C in Figure 3.7a. It is suggested that the degradation may have destroyed the favorable network structure if formed initially, and consequently produced PANI-derived carbons with lower SSA and decreased porosity. Since the degradation involves in decomposition of functional groups [51, 52], it should be the degradation of PANI at 250 °C that causes the decrease of peak intensities for P-250 in FTIR spectrum in Figure 3.6a.

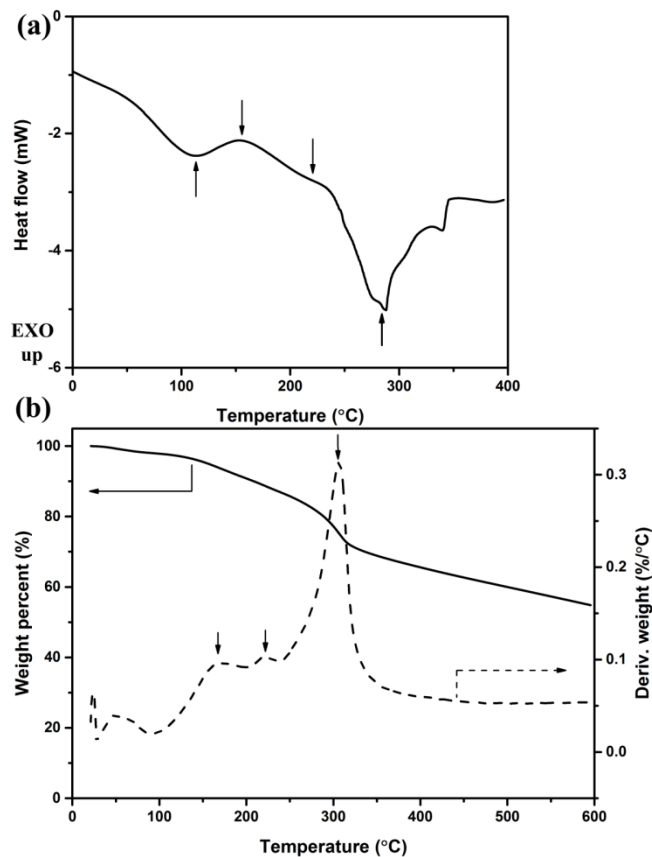


Figure 3.7 (a) DSC curves of original PANI and (b) TGA and its derivative curves of the original PANI.

Figure 3.4 to Figure 3.7 illustrate how the preheating stage influences PANI and PANI-derived carbons. Briefly, at low preheating temperatures (150~200 °C), crosslinking reaction occurs and the degree of crosslinking increases as the preheating temperature. A complete crosslinked PANI will result in a network-like nanostructure. This structure increases the surface area of PANI and leads to a more homogeneous activation and a higher SSA/better developed porosity of the PANI-derived carbon. At high preheating temperature (>250 °C), degradation of PANI is triggered, which destroys the favorable structure of PANI, and thus decreases the surface area of PANI. In this case, the pore

development of the PANI-derived carbon is restricted. Therefore, a well-tuned preheating stage is beneficial for obtaining high surface area and highly porous ACs.

3.4 Conclusion

In conclusion, a comprehensive study on KOH activation of PANI has been carried out.

1) The PANI-derived carbons have BET surface area of 1711~3768 m² g⁻¹ and micropore volume of 0.74~1.37 cm³ g⁻¹. Specifically, C-2-200-800 has the highest BET surface area of 3768 m² g⁻¹ and the largest micropore volume of 1.37 cm³ g⁻¹.

2) It has been found that the BET surface area and micropore volume increase as the activation temperature/KOH ratio increases, but start to decrease at 900 °C or at KOH:PANI ratios higher than 3:1. This is caused by widening of narrow micropores because of intensive reactions during activation.

3) Varying preheating temperature does not widen the pore size. Characterizations of the after-preheating samples show that thermal crosslinking is maximized at ~200 °C, which leads to the formation of network-like nanostructures. These nanostructures are beneficial to the pore development during subsequent activation at high temperatures and can lead to ACs with high BET surface area and microporosity.

3.5 References

- [1] Zhang L.L., Zhao X.S. Carbon-based materials as supercapacitor electrodes. *Chemical Society Reviews*. 2009;**38**(9):2520-2531.
- [2] Lee J., Kim J., Hyeon T. Recent progress in the synthesis of porous carbon materials. *Advanced Materials*. 2006;**18**(16):2073-2094.

- [3] Wang S.P., Zhang J.N., Shang P., Li Y.Y., Chen Z.M., Xu Q. N-doped carbon spheres with hierarchical micropore-nanosheet networks for high performance supercapacitors. *Chemical Communications*. 2014;**50**(81):12091-12094.
- [4] Morris R.E., Wheatley P.S. Gas storage in nanoporous materials. *Angewandte Chemie-International Edition*. 2008;**47**(27):4966-4981.
- [5] Li Y.Q., Ben T., Zhang B.Y., Fu Y., Qiu S.L. Ultrahigh Gas Storage both at Low and High Pressures in KOH-Activated Carbonized Porous Aromatic Frameworks. *Scientific Reports*. 2013;**3**.
- [6] Rivera-Utrilla J., Sanchez-Polo M., Gomez-Serrano V., Alvarez P.M., Alvim-Ferraz M.C.M., Dias J.M. Activated carbon modifications to enhance its water treatment applications. An overview. *Journal of Hazardous Materials*. 2011;**187**(1-3):1-23.
- [7] Otowa T., Nojima Y., Miyazaki T. Development of KOH activated high surface area carbon and its application to drinking water purification. *Carbon*. 1997;**35**(9):1315-1319.
- [8] Li M.J., Liu C.M., Cao H.B., Zhao H., Zhang Y., Fan Z.J. KOH self-templating synthesis of three-dimensional hierarchical porous carbon materials for high performance supercapacitors. *Journal of Materials Chemistry A*. 2014;**2**(36):14844-14851.
- [9] Zhu Y.W., Murali S., Stoller M.D., Ganesh K.J., Cai W.W., Ferreira P.J., et al. Carbon-Based Supercapacitors Produced by Activation of Graphene. *Science*. 2011;**332**(6037):1537-1541.
- [10] Wang J.C., Kaskel S. KOH activation of carbon-based materials for energy storage. *Journal of Materials Chemistry*. 2012;**22**(45):23710-23725.

- [11] Sevilla M., Valle-Vigon P., Fuertes A.B. N-Doped Polypyrrole-Based Porous Carbons for CO₂ Capture. *Advanced Functional Materials*. 2011;**21**(14):2781-2787.
- [12] Wang H.L., Gao Q.M., Hu J. High Hydrogen Storage Capacity of Porous Carbons Prepared by Using Activated Carbon. *Journal of the American Chemical Society*. 2009;**131**(20):7016-7022.
- [13] Zhang L., Zhang F., Yang X., Long G.K., Wu Y.P., Zhang T.F., et al. Porous 3D graphene-based bulk materials with exceptional high surface area and excellent conductivity for supercapacitors. *Scientific Reports*. 2013, Doi 10.1038/Srep01408.
- [14] Almasoudi A., Mokaya R. Preparation and hydrogen storage capacity of templated and activated carbons nanocast from commercially available zeolitic imidazolate framework. *Journal of Materials Chemistry*. 2012;**22**(1):146-152.
- [15] Otowa T., Tanibata R., Itoh M. Production and adsorption characteristics of MAXSORB: high-surface-area active carbon. *Gas Separation & Purification*. 1993;**7**(4):241-245
- [16] Lozano-Castello D., Calo J.M., Cazorla-Amoros D., Linares-Solano A. Carbon activation with KOH as explored by temperature programmed techniques, and the effects of hydrogen. *Carbon*. 2007;**45**(13):2529-2536.
- [17] Raymundo-Piñero E., Azais P., Cacciaguerra T., Cazorla-Amorós D., Linares-Solano A., Béguin F. KOH and NaOH activation mechanisms of multiwalled carbon nanotubes with different structural organisation. *Carbon*. 2005;**43**(4):786-795.
- [18] Qiao W.M., Yoon S.H., Mochida I. KOH activation of needle coke to develop activated carbons for high-performance EDLC. *Energy & Fuels*. 2006;**20**(4):1680-1684.

- [19] Lillo-Rodenas M.A., Cazorla-Amoros D., Linares-Solano A. Understanding chemical reactions between carbons and NaOH and KOH - An insight into the chemical activation mechanism. *Carbon*. 2003;**41**(2):267-275.
- [20] Swiatkowski A. *Studies in Surface Science and Catalysis*: Elsevier; 1999.
- [21] Xue R.S., Shen Z.M. Formation of graphite-potassium intercalation compounds during activation of MCMB with KOH. *Carbon*. 2003;**41**(9):1862-1864.
- [22] Wang J.C., Senkovska I., Kaskel S., Liu Q. Chemically activated fungi-based porous carbons for hydrogen storage. *Carbon*. 2014;**75**:372-380.
- [23] Wang J.C., Heerwig A., Lohe M.R., Oschatz M., Borchardt L., Kaskel S. Fungi-based porous carbons for CO₂ adsorption and separation. *Journal of Materials Chemistry*. 2012;**22**(28):13911-13913.
- [24] Zhang Z.J., Cui P., Chen X.Y., Liu J.W. The production of activated carbon from cation exchange resin for high-performance supercapacitor. *Journal of Solid State Electrochemistry*. 2013;**17**(6):1749-1758.
- [25] Cong H., Zhang M., Chen Y., Chen K., Hao Y., Zhao Y., et al. Highly Selective CO₂ Capture by Nitrogen Enriched Porous Carbons. *Carbon*. 2015;**92**:297-304.
- [26] Romanos J., Beckner M., Rash T., Firlej L., Kuchta B., Yu P., et al. Nanospace engineering of KOH activated carbon. *Nanotechnology*. 2012, Doi 10.1088/0957-4484/23/1/015401.
- [27] Sevilla M., Mokaya R., Fuertes A.B. Ultrahigh surface area polypyrrole-based carbons with superior performance for hydrogen storage. *Energy & Environmental Science*. 2011;**4**(8):2930-2936.

- [28] Wu M.B., Zha Q.F., Qiu J.S., Guo Y.S., Shang H.Y., Yuan A.J. Preparation and characterization of porous carbons from PAN-based preoxidized cloth by KOH activation. *Carbon*. 2004;**42**(1):205-210.
- [29] Lee Y.J., Kim J.H., Kim J., Lee D.B., Lee J.C., Chung Y.J., et al. Fabrication of activated carbon fibers from stabilized PAN-based fibers by KOH. *Designing, Processing and Properties of Advanced Engineering Materials, Pts 1 and 2*. 2004;**449-452**:217-220.
- [30] Lv Y.Y., Zhang F., Dou Y.Q., Zhai Y.P., Wang J.X., Liu H.J., et al. A comprehensive study on KOH activation of ordered mesoporous carbons and their supercapacitor application. *Journal of Materials Chemistry*. 2012;**22**(1):93-99.
- [31] Shen W.Z., Zhang S.C., He Y., Li J.F., Fan W.B. Hierarchical porous polyacrylonitrile-based activated carbon fibers for CO₂ capture. *Journal of Materials Chemistry*. 2011;**21**(36):14036-14040.
- [32] Zhang Z.S., Zhou J., Xing W., Xue Q.Z., Yan Z.F., Zhuo S.P., et al. Critical role of small micropores in high CO₂ uptake. *Physical Chemistry Chemical Physics*. 2013;**15**(7):2523-2529.
- [33] Zhu X.P., Fu Y., Hu G.S., Shen Y., Dai W., Hu X. CO₂ Capture with Activated Carbons Prepared by Petroleum Coke and KOH at Low Pressure. *Water Air and Soil Pollution*. 2013, Doi: 10.1007/S11270-012-1387-Y.
- [34] Hu Z.H., Srinivasan M.P. Preparation of high-surface-area activated carbons from coconut shell. *Microporous and Mesoporous Materials*. 1999;**27**(1):11-18.
- [35] Weng S.H., Lin Z.H., Zhang Y., Chen L.X., Zhou J.Z. Facile synthesis of SBA-15/polyaniline nanocomposites with high electrochemical activity under neutral and acidic conditions. *Reactive & Functional Polymers*. 2009;**69**(2):130-136.

- [36] Huang J.X., Kaner R.B. The intrinsic nanofibrillar morphology of polyaniline. *Chemical Communications*. 2006;**10**(4):367-376.
- [37] Li D., Huang J.X., Kaner R.B. Polyaniline Nanofibers: A Unique Polymer Nanostructure for Versatile Applications. *Accounts of chemical research*. 2009;**42**(1):135-145.
- [38] Lin D.H., Zhang X.T., Cui X.W., Chen W.X. Highly porous carbons with superior performance for CO₂ capture through hydrogen-bonding interactions. *Rsc Advances*. 2014;**4**(52):27414-27421.
- [39] Yoshizawa N., Maruyama K., Yamada Y., Ishikawa E., Kobayashi M., Toda Y., et al. XRD evaluation of KOH activation process and influence of coal rank. *Fuel*. 2002;**81**(13):1717-1722.
- [40] Wu F.C., Tseng R.L., Juang R.S. Preparation of highly microporous carbons from fir wood by KOH activation for adsorption of dyes and phenols from water. *Separation and Purification Technology*. 2005;**47**(1-2):10-19.
- [41] Tay T., Ucar S., Karagoz S. Preparation and characterization of activated carbon from waste biomass. *Journal of Hazardous Materials*. 2009;**165**(1-3):481-485.
- [42] Li D., Kaner R.B. How nucleation affects the aggregation of nanoparticles. *Journal of Materials Chemistry*. 2007;**17**(22):2279-2282.
- [43] Huang J.X., Kaner R.B. Flash welding of conducting polymer nanofibres. *Nature Materials*. 2004;**3**(11):783-786.
- [44] Ding L.L., Wang X.W., Gregory R.V. Thermal properties of chemically synthesized polyaniline (EB) powder. *Synthetic Metals*. 1999;**104**(2):73-78.

- [45] Mathew R., Mattes B.R., Espe M.P. A solid state NMR characterization of cross-linked polyaniline powder. *Synthetic Metals*. 2002;**131**(1-3):141-147.
- [46] Sedenkova I., Trchova M., Stejskal J. Thermal degradation of polyaniline films prepared in solutions of strong and weak acids and in water - FTIR and Raman spectroscopic studies. *Polymer Degradation and Stability*. 2008;**93**(12):2147-2157.
- [47] Chen C.H. Thermal and morphological studies of chemically prepared emeraldine-base-form polyaniline powder. *Journal of Applied Polymer Science*. 2003;**89**(8):2142-2148.
- [48] Pandey S.S., Gerard M., Sharma A.L., Malhotra B.D. Thermal analysis of chemically synthesized polyemeraldine base. *Journal of Applied Polymer Science*. 2000;**75**(1):149-155
- [49] Conklin J.A., Huang S.C., Huang S.M., Wen T.L., Kaner R.B. Thermal-Properties of Polyaniline and Poly(Aniline-Co-O-Ethylaniline). *Macromolecules*. 1995;**28**(19):6522-6527.
- [50] Kieffel Y., Travers J.P., Ermolieff A., Rouchon D. Thermal aging of undoped polyaniline: Effect of chemical degradation on electrical properties. *Journal of Applied Polymer Science*. 2002;**86**(2):395-404.
- [51] Patil S.F., Bedekar A.G., Agashe C. Effect of Electrode Conductivity on Electrochemically Deposited Polyaniline Films. *Materials Letters*. 1992;**14**(5-6):307-312.
- [52] Sreedhar B., Sairam M., Chattopadhyay D.K., Mitra P.P., Rao D.V.M. Thermal and XPS studies on polyaniline salts prepared by inverted emulsion polymerization. *Journal of Applied Polymer Science*. 2006;**101**(1):499-508.

Chapter 4 Nitrogen-doped porous carbon prepared from liquid carbon precursor for CO₂ adsorption¹

In this chapter, we are focusing on designing a new kind of activated carbon via KOH activation of polyethylenimine. This study contributes to the knowledge of employing new N-containing carbon precursors for KOH activation and examining the CO₂ adsorption performances of the resulting carbons.

4.1 Introduction

Concerns about excessive CO₂ emission (such as global warming) have led to research on many promising solutions to the problem [1, 2]. The current technology used to reduce CO₂ emission in power plants, a major source of CO₂ emission, is liquid amine-based absorption [3]. However, disadvantages such as limited absorption capacity and high-energy consumption urged us to look for more cost-effective methods. Recently, materials based on zeolites [4-6], mesoporous silica [7-9], metal-organic frameworks (MOFs) [10-12], covalent-organic frameworks (COFs) [13] and porous carbons [14, 15], especially N-enriched porous carbons [16-21] have been reported for CO₂ adsorption and storage. Among them, zeolites are very sensitive to moisture, impregnated mesoporous materials suffer instability during cyclic tests, and MOFs/COFs are expensive and complex upon synthesis. Carbon-based adsorbents, however, possess high thermal/chemical stability, high surface area, large adsorption capacity and reasonable cost. Therefore they are one of the most promising materials for CO₂ capture.

¹ Reproduced from X. Zhang, D.H. Lin, W. Chen, *RSC Adv.*, 2015, **5**, 45136-45143, with permission from the Royal Society of Chemistry.

For N-enriched porous carbons, CO₂ adsorption could be facilitated by the presence of microporous structure and strong interaction between the CO₂ molecules with the framework (especially N-containing groups) through H-bonding or dipole–quadrupole interactions [2]. As for pore development, KOH activation is highly desirable because it develops large amount of micropores with high surface area [22, 23]. In 2011 Sevilla *et al.* [24] further demonstrated how severe (KOH four times the precursor) and mild activation conditions (KOH two times the precursor) at various temperatures affect the texture of the porous carbons and their CO₂ adsorption ability. Whereas the mildly-activated carbons showed small surface area (1300 m²/g) and narrow micropores (<1 nm), the severely-activated ones showed greater surface area (>2000 m²/g) and larger pore sizes (1–3 nm). However, the former condition exhibited a better CO₂ uptake primarily due to the presence of narrow micropores (<1 nm), while the surface area is playing a less significant role. Moreover, the porous structure and required KOH amount are closely related to carbon precursors, since many activated carbons [24-26] required different KOH/C ratio for optimized CO₂ adsorption. Therefore it is possible to prepare activated carbons using low KOH/C ratio from carefully selected carbon precursors.

Branched polyethyleneimine (PEI, Figure 4.1) is inexpensive, non-toxic and widely used for DNA transfection in cell studies [27]. PEI also has abundant amino groups, as a result it was employed as an impregnating agent for mesoporous silica, such as MCM-41 [28], SBA-15 [29] and MCF [30, 31] for the sake of CO₂ adsorption. However, considerable leaching of the amines may be a major drawback for the use of PEI-impregnated mesoporous silica sorbents for CO₂ [5]. For example, it has been reported that the performance of a typical PEI/silica material dropped ~30% after only 6 cycles [32].

Therefore in this paper, we explored a one-step KOH activation method using PEI as carbon precursor. To our best knowledge, this is the first time that PEI is employed to produce activated carbon material and a liquid carbon precursor has been used. The synthesis process is facile. Owing to its liquid property, PEI could be completely mixed with KOH at the early stage, which results in well-developed porous structure as well as rich nitrogen content at very low KOH/C ratio. Considering the corrosive nature and comparably high price of KOH, this material is much more cost-saving in terms of synthesis and facility. In this study, PEI-derived carbons were carefully examined in terms of pore structures and N-containing functionalities. The contributions of microporosity and N-containing groups to CO₂ adsorption capacity were discussed.

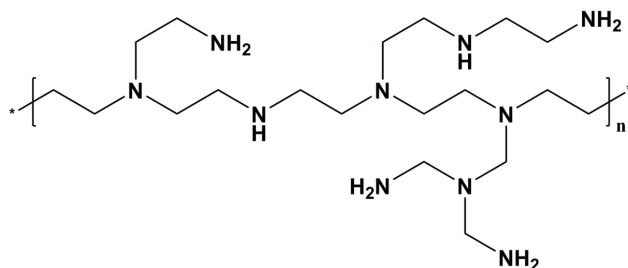


Figure 4.1 Schematic diagram for branched Polyethylenimine (PEI).

4.2 Experimental

4.2.1 Preparation of PEI-derived carbon

The PEI-derived carbon was synthesized via a carbonization-activation process by using KOH as an activation agent. Commercialized PEI, purchased from MP Biomedicals, was used as carbon precursor without any further purification. KOH (pellet) was purchased from Fisher Scientific Canada. In a typical synthesis, 4 g viscous PEI was first dissolved in 50 ml ethanol and magnetically stirred for 15 min until a clear solution was obtained. Then

2 g KOH was added to the solution followed by 6 hours of magnetic stirring with a speed of 300 rpm. After fully mixed, the mixture was transferred into a rectangular alumina boat and dried in an oven at 80 °C for 12 hours. The after-dry mixture returned to a viscous state due to evaporation of solvent. The boat was allowed to cool down to room temperature and placed into a horizontal quartz tube. The tube was initially vacuumed to a pressure below 30 Pa before N₂ (purity > 99.998%) was introduced at a steady flow rate of 100 cm³/min. After purging for 1h, the furnace was ramped up to activation temperature with a heating rate of 3 °C/min and held for 3 hours. After activation, the furnace was allowed to cool down naturally. Then the samples were taken out and washed with copious Milli-Q water several times until the pH was ~7. The washed carbons were dried again at 90 °C for over 24 hours. The samples after synthesizing were denoted as C-x, where x is the activation temperature. The dried samples were ~490 mg for C-500, ~210 mg for C-600 and ~130 mg for C-700.

For acid neutralization process, samples were first treated with excess amount of 37 wt% concentrated HCl solution for 24 hours, followed by copious Milli-Q water wash until the pH was ~7. The HCl-treated carbons were sent in oven and dried at 90 °C for 24 hours.

4.2.2 Characterization

The morphologies of the samples were examined by scanning electron microscopy (SEM) using a JAMP-9500F system (JEOL, Tokyo, Japan) under 15 kV. Transmission electron microscopy (TEM) images were received from a JOEL 2010 system with an operating voltage of 200 kV. N₂ adsorption/desorption results were obtained at 77 K by an Autosorb-1 system (Quantachrome). Every sample (~30 mg) was outgassed under high vacuum at 150 °C for over 4 h before test. The specific surface area was calculated by Brunauer-

Emmett-Teller (B.E.T.) method based on data points in the partial pressure range of 0.03-0.1, within which the linear correction coefficient was > 0.9999 . This range is lower than the usual range ($P/P_0 = 0.1\sim 0.3$) because their microporous properties render capillary condensation at lower relative pressure [33]. The pore size distribution was determined using quenched-solid density functional theory (QSDFT) method assuming a slit/cylindrical pore model. For characterization of chemical properties, infrared spectrum was recorded with a Nicolet 8700 Fourier transformation infrared (FTIR) spectrometer (Thermal Scientific), the scanning range was between 500 and 4000 cm^{-1} , with a resolution of 1.93 cm^{-1} and 128 scans per test. X-ray photoelectron spectroscopy (XPS) was carried with an AXIS 165 system (Kratos Analytical Ltd., UK) using a monochromated Al Ka excitation source.

4.2.3 CO₂ adsorption

CO₂ adsorption capacity at different temperatures was collected by Autosorb iQ (Quantachrome). Before adsorption every sample (~ 50 mg) was outgassed under high vacuum at $150\text{ }^\circ\text{C}$ for over 4 h before test. The temperature control was performed by a tube furnace. Adsorption-desorption multi-cycle stability was tested by thermalgravimetric analysis (TGA). A sample of ~ 5 mg was placed in a platinum crucible in a TGA machine (SDT Q600, TA Instrument). The sample was first heated to $105\text{ }^\circ\text{C}$ under N₂ environment for 30 min to be fully desorbed, and then equilibrated at $25\text{ }^\circ\text{C}$. During adsorption, the sample was exposed to a desired mixed gas (100 mL/min, 95% CO₂ with balance of N₂, CO₂ concentration cannot reach 100% due to facility limitation). The sample was then kept at this condition for 1h for adsorption. Once the adsorption is completed, the gas was switched from mixed gas to pure N₂ (100 mL/min), and the sample was heated to $105\text{ }^\circ\text{C}$

for thorough desorption. The weight change profile measured was determined to be the amount of CO₂ adsorption. This process then was repeated for 30 times.

4.3 Results and Discussion

4.3.1 Porous structure

Figure 4.2 shows microscopic images of a typical sample (C-600). As could be seen in Figure 4.2a, the activated carbon demonstrates a generally smooth surface decorated with macropores. However, a sponge-like structure was revealed in the cross-sectional morphology of Figure 4.2b. The TEM image of PEI-derived carbon in Figure 4.2c shows typical amorphous structure of activated carbon. Worm-like micropores composed of deformed graphitic layers can be observed in HR-TEM image of Figure 4.2d.

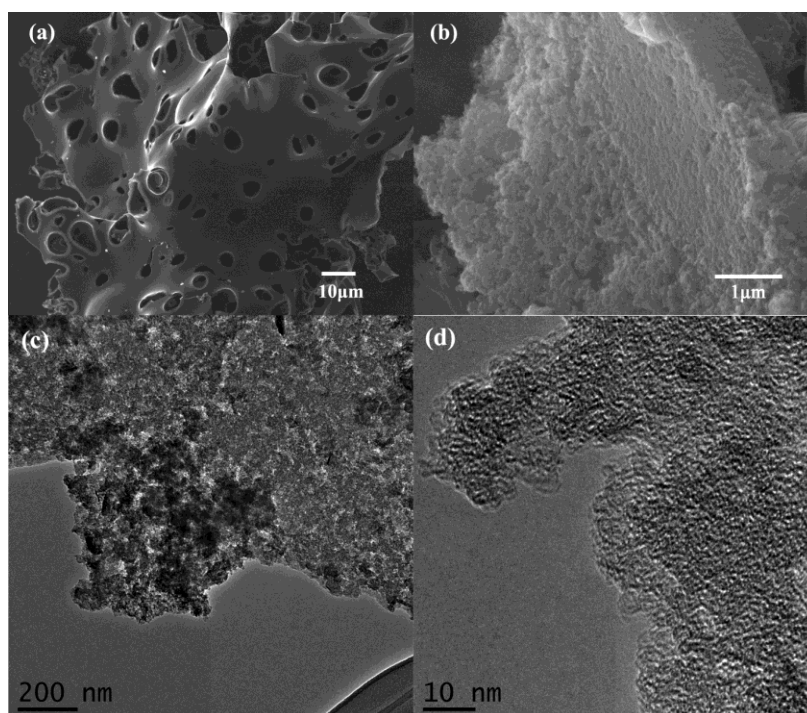


Figure 4.2 SEM and TEM images of PEI-derived carbon (C-600): a) surface; b) cross-section; c) TEM image; d) HR-TEM image.

Nitrogen adsorption/desorption analysis was also performed to characterize the porous structure of the PEI-derived carbon. Figure 4.3 shows isotherms of PEI-derived carbons activated at different temperatures. According to the IUPAC [34], all three isotherms in Figure 4.3a are type I. The significant amount of adsorption at low pressures indicated the existence of large amount of micropores. The uptrend at high pressures is consistent with the macropores observed in microscopic images. In terms of the effect of the activation temperature, the main difference lies at the positions of knee points, which indicates different amount of micropores. A closer look is presented by portraying pore size distributions of different samples in Figure 4.3b. Obviously, most of pores are micropores with major peaks centered at $\sim 10 \text{ \AA}$, which are best pore sizes for CO_2 adsorption according to literature [35, 36]. Additionally, the number of mesopores ($20\sim 50 \text{ \AA}$) keeps increasing from C-500 to C-700. Statistic pore characteristics of different samples are listed in Table 4.1. From the results, the total volume increases with increasing activation temperature. However, micropore volume, micropore volume percentage and $<1 \text{ nm}$ pore volume peak at $600 \text{ }^\circ\text{C}$ (sample C-600) have the best developed microporosity, with BET surface area of $1540 \text{ m}^2/\text{g}$, total pore volume of $0.75 \text{ cm}^3/\text{g}$ and micropore volume of $0.52 \text{ cm}^3/\text{g}$.

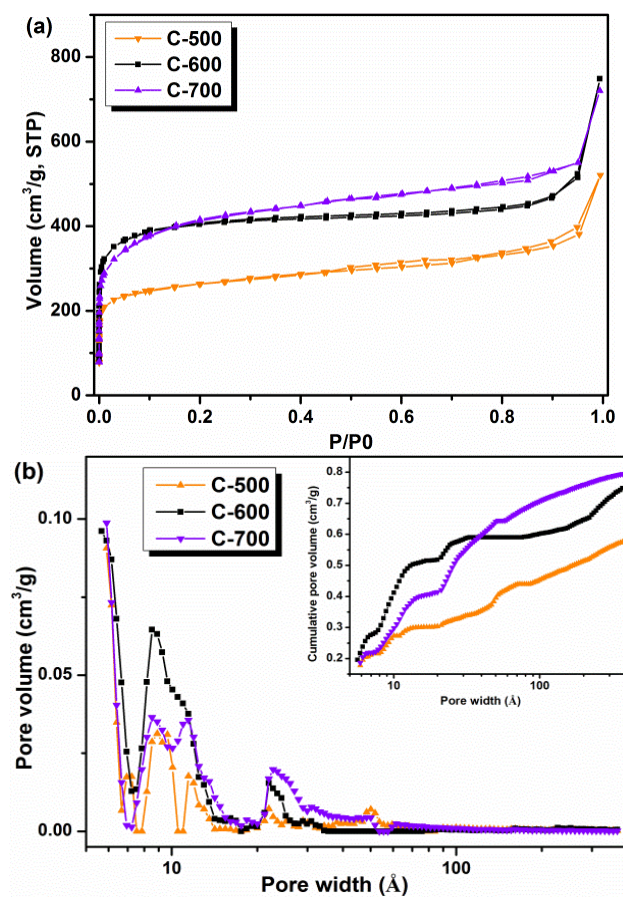


Figure 4.3 Nitrogen adsorption/desorption isotherms (a) and pore size distribution (b) of PEI-derived carbon samples under different temperature.

Table 4.1 Porous structure of PEI-derived carbon and their CO₂ capture performance

Sample	BET surface area ^a (m ² /g)	Total pore volume ^b (cc/g)	Micropore volume ^c (cc/g)	Micropore volume percentage ^d	<1nm pore volume ^c (cc/g)
C-500	978	0.58	0.30	52%	0.27
C-600	1540	0.75	0.52	69%	0.41
C-700	1538	0.79	0.41	52%	0.30

^aBET surface area obtained using BET method at P/P₀=0.03-0.1.

^bTotal pore volume at P/P₀=0.995.

^cMicropore and <1nm pore volume obtained from QSDFT slit/cylindrical pore model.

^dMicropore volume percentage was obtained as micropore volume/total pore volume.

4.3.2 Chemical characterization

Surface functional groups and chemical composition of the PEI-derived carbons were analyzed by FTIR in Figure 4.4a and XPS in Figure 4.5, respectively. As presented in Figure 4.4a, most peaks in the spectra could be clearly resolved. The two top spectra are similar: The weak band at 3450 cm^{-1} is assigned to O-H (from absorbed water and/or hydroxyl groups) [37]. The broad band at 3200 cm^{-1} is due to N-H symmetric stretching vibration [38, 39]. A doublet at 2898 cm^{-1} and 2830 cm^{-1} is attributed to CH stretching vibration of $-\text{CH}_2-$ [40]. As is shown in Figure 4.1, these groups come from the original structure of PEI. The next two weak but distinct bands at 2351 cm^{-1} and 2200 cm^{-1} are reported to result from absorbed CO_2 [41]. The range from 1800 cm^{-1} to 600 cm^{-1} is often called the fingerprint region and difficult to analyze in detail. However, several obvious bands could still be identified. Two strong bands at 1585 cm^{-1} and $\sim 1300\text{ cm}^{-1}$ are attributed to C=C/C-N stretching and C-H bending [42], respectively. A weak band of frequency slightly higher than 1585 cm^{-1} is referred to be C=O bond (1660 cm^{-1}). The broad band at 780 cm^{-1} can be assigned to N-H wagging of the secondary amines [43]. The bottom signal (C-700) is different. Generally, the signal is weaker, indicating a smaller amount of functional groups. This implies that a lot of thermally-unstable functional groups were eliminated at $700\text{ }^\circ\text{C}$. In addition, instead of 1300 cm^{-1} , C-700 has a band at 1136 cm^{-1} , which is attributed to C-N bonds. The disappearance of C-H peak may result from strong carbonization process at higher temperature. The carbonization mechanism of PEI was hypothesized in Figure 4.4b, which is similar to carbonization of polyacrylonitrile (PAN) [18, 44]. At low temperature, the polymers undergo a dehydrogenation process, which leads

to cyclization inside the polymer framework. This cyclization step helps preserve the volatile species. As the temperature increases, the framework gradually aromatizes and further crosslinks to form the carbon monolith embedded with nitrogen atoms.

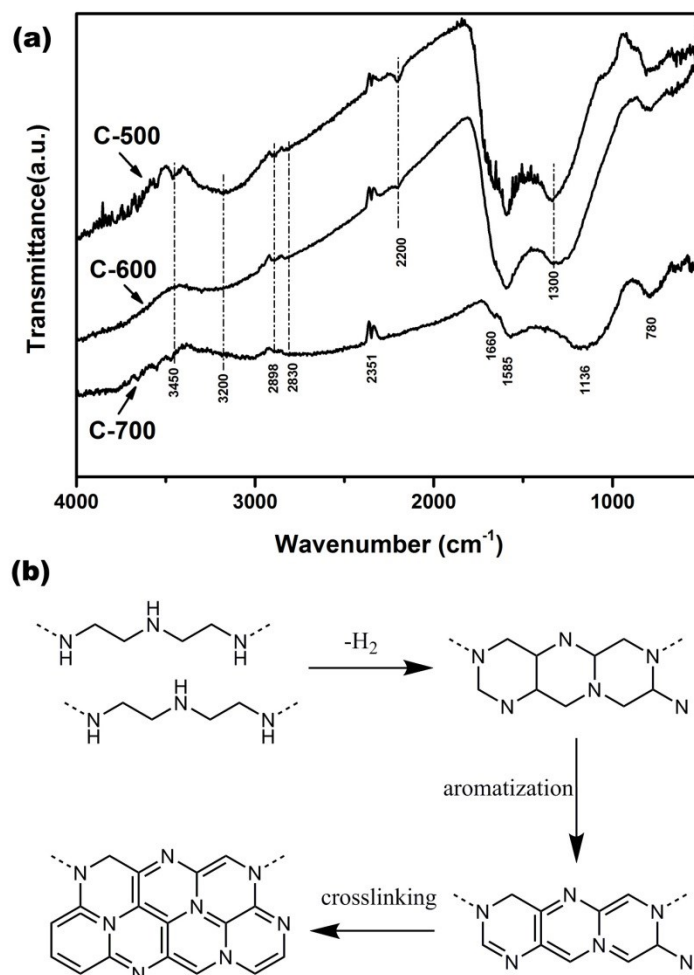


Figure 4.4 (a) FT-IR spectrums of PEI-derived carbons at different activation temperatures (Curves were displaced vertically in order to be differentiated.) ; (b) hypothesized carbonization of PEI.

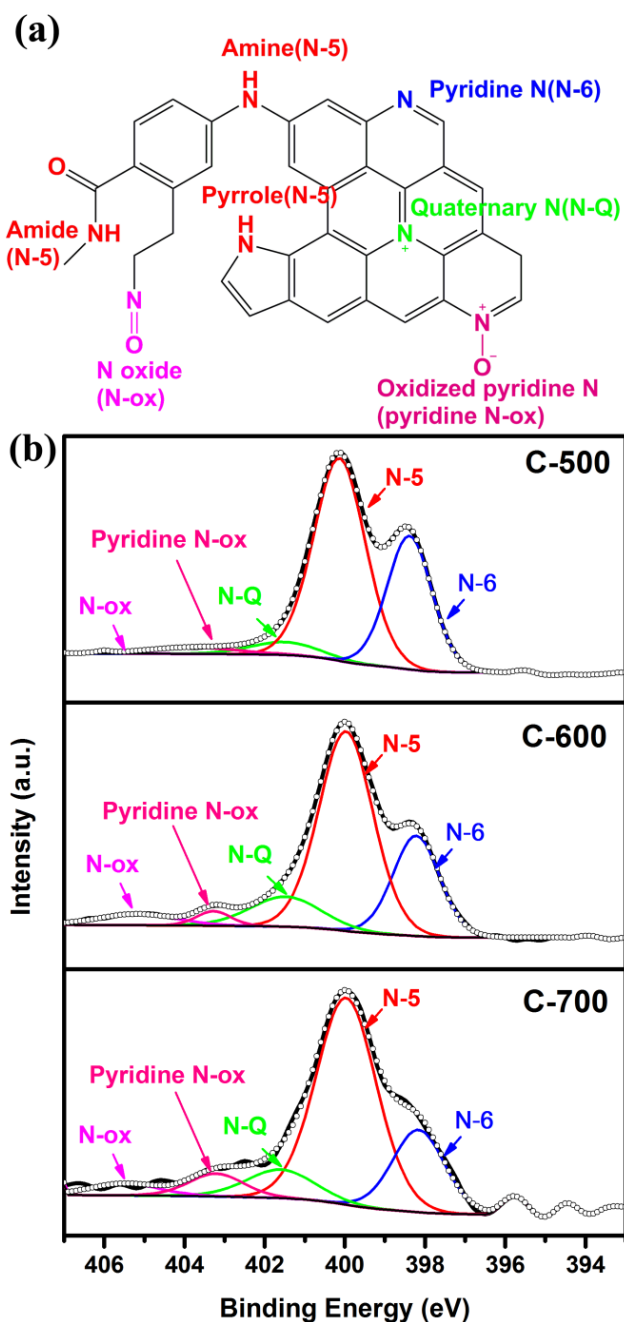


Figure 4.5 XPS N 1s spectra of PEI-derived carbons. (a) Schematics of different nitrogen groups on PEI-derived carbons; (b) resolved peaks XPS N 1s spectra of PEI-derived carbons with different conditions.

Elemental analysis and quantitative determination of nitrogen-related functional groups is shown in Table 4.2 and Figure 4.5. Sample C-500 has the highest N content, which is 11.1%. At 600 °C this value dropped about half, to 6.9%. These two samples could be considered nitrogen-rich. For C-700, the N content is only 2.7%. The N content decreases quickly with increasing activation temperature. As for specific nitrogen functionality, N 1s spectra with resolved peaks are given in Figure 4.5b. It is obvious that three main peaks could be found in all samples. The signal at 398.0 eV is assigned to pyridine N (N-6), the one at 400.0 eV to pyrrole and imine, amine, imide (N-5), and the one at 401.5 eV to quaternary N (N-Q). The two small peaks at higher binding energy (403.3 eV, 405.1 eV) are attributed to oxidized pyridine N oxide (pyridine N-ox) and N oxide (N-ox) [45]. N-5 is the dominant nitrogen species for all samples, which is mostly resulted from pristine PEI structure (Figure 4.1). N-6 contribution decreases as activation temperature increases, which was also observed in reference [23]. On the other hand, N-Q and oxidized N contributions increase, implying better stability of these species. The existence of oxidized N was previous observed in similar condition from another study [46]. Since there was no oxygen content in PEI, the oxidized nitrogen groups are presumably caused by the addition of KOH. Many research [47, 48] proposed that with existence of KOH, oxygen is able to link to carbon/sulfur atom in the framework. It is also possible that oxygen could be incorporated into the framework through nitrogen. To conclude, PEI-derived carbons contain various nitrogen functional groups with a majority of N-5. This could be beneficial to CO₂ adsorption, for that many previous studies [22, 38, 49] claim positive influence of N-containing groups.

Table 4.2 XPS element content and the contribution of nitrogen species.

Sample	XPS element (atomic %)			Nitrogen species contribution (%)				
	C	O	N	N-5	N-6	N-Q	Pyridine -N-ox	N-ox
C-500	77.0	11.8	11.1	58.4	33.3	4.9	3.2	0.2
C-600	82.8	10.3	6.9	57.1	24.7	11.1	2.6	4.5
C-700	83.9	13.4	2.7	60.2	20.6	9.3	6.0	3.9

4.3.3 CO₂ adsorption performance

In Table 4.3, CO₂ adsorption performance of PEI-derived carbons was shown at 0 °C and 25 °C under ambient and sub-ambient pressure (1 bar and 0.15 bar). All the examined samples show good adsorption capacity at 0 °C. C-600 has the highest CO₂ uptake value among the samples, 5.7 mmol/g at 0 °C 1bar and 3.6 mmol/g at 25 °C 1 bar, which are competitive values to some of the N-doped porous carbons recently reported [22, 23, 38, 50, 51]. In contrast, C-700 has a similar BET surface area, but achieves less CO₂ uptake (5.0 mmol/g), which is reasonable because C-700 has less fine microporosity (<1 nm sized pores) and less nitrogen content. Additionally, although C-500 (4.8 mmol/g) has much smaller BET value than C-700, it has similar CO₂ adsorption results at 1 bar, possibly due to the compensation of rich nitrogen content in C-500. In order to demarcate the contribution of microporosity with N-containing groups, PEI-derived carbons were treated with concentrated HCl (37%) solution in order to neutralize the effect of nitrogen groups. The reduction of CO₂ uptake after acid neutralization is 0.5~0.6 mmol/g at 1 bar, as shown in Table 4.3. Based on this, the contribution of N-containing groups is about 9% ~13%. At 0.15 bar, the reduction of CO₂ uptake after acid neutralization is 0.2~0.5 mmol/g, taking 13%

~23% of the total capacity. An increase of the contribution at lower pressure shows a more significant role of N-containing groups for low-pressure CO₂ adsorption.

Isotherms at various temperatures were also presented in Figure 4.6. It is observed that as expected, when temperature increases the adsorption capacity drops quickly for all three samples, implying the physisorption nature of the materials. At 0 °C, the capacity at 1 bar is 4.9~5.7 mmol/g. At 25 °C, it is 2.9~3.7 mmol/g. When the temperature increases to 75 °C, the uptake is only 1.1~1.5 mmol/g. What is notable in Figure 4.6 is that C-500 has competitive adsorption capacity with C-600 at low pressures (<0.15 bar), but fails to be comparable at near-atmospheric pressure.

Table 4.3 CO₂ adsorption capacity of PEI-derived carbons at different temperatures.

Sample	CO ₂ uptake (mmol/g)			
	0 °C, 1 bar(After HCl neutralization)	0 °C, 0.15 bar(After HCl neutralization)	25 °C, 1 bar	25° C, 0.15 bar
C-500	4.8(4.2)	2.3(1.8)	2.8	0.9
C-600	5.7(5.2)	2.3(1.9)	3.6	1.0
C-700	5.0(4.5)	1.6(1.4)	2.8	0.6

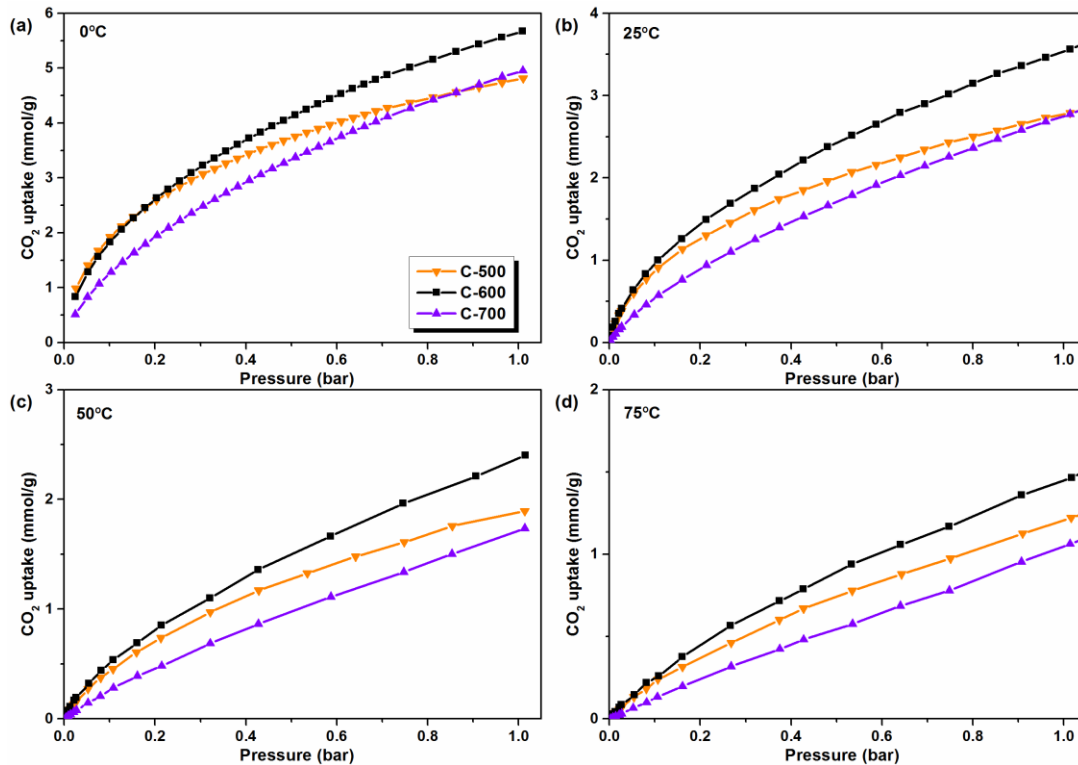


Figure 4.6 CO₂ adsorption isotherms of PEI-derived carbons at different temperatures. (a) 0 °C; (b) 25 °C; (c) 50 °C; (d) 75 °C.

In Figure 4.7 the isosteric heat of adsorption (Q_{st}) was calculated by applying Clausius—Clayperon equation on isotherms at 0 °C, 25 °C, 50 °C and 75 °C. It could be seen that the initial value of adsorption heat is high, in the range of 39~43 kJ/mol. This Q_{st} is higher than those of many previously reported nitrogen-rich carbons (30.4~36 kJ/mol as referred in literatures [22, 49]), indicating strong interaction between CO₂ with the sorbent surface. The Q_{st} decreases with increased adsorption amount, revealing that CO₂ adsorption is heterogeneous. This fact emphasizes the important role of N-containing groups in the high initial Q_{st} . Interestingly, C-500 has higher N content than C-600 while they present similar Q_{st} value. This is probably due to a limited access of gas molecule to some of the N-containing groups on C-500 sample, induced by not-well-developed microporosity.

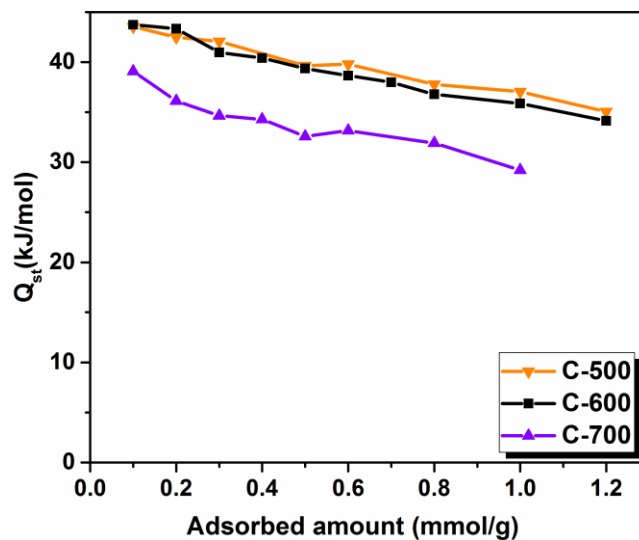


Figure 4.7 Isosteric heat of adsorption for PEI-derived carbons.

For a cost-efficient adsorbent, the material should also present satisfactory stability during cyclic adsorption-desorption processes. The stability test in Figure 4.8 was measured at 25 °C. It shows less than 1% drop (from 2nd cycle, 3.35 mmol/g to 30th cycle, 3.32 mmol) for C-600 after ~30 cycles, demonstrating a very good stability. This means that the material could be used for long-term purpose and further lowers the cost. Additionally, the selectivity of C-600 at 25 °C was demonstrated in Figure 4.9. Figure 4.9a shows CO₂ and N₂ isotherms while in Figure 4.9b the initial slopes of CO₂ and N₂ isotherms were determined. The selectivity of CO₂ over N₂ was calculated using Henry's Law through the initial slopes of the isotherms. Therefore the selectivity of C-600 is 33 at 25 °C, which is also a competitively high value compared to previous report [22, 49, 52].

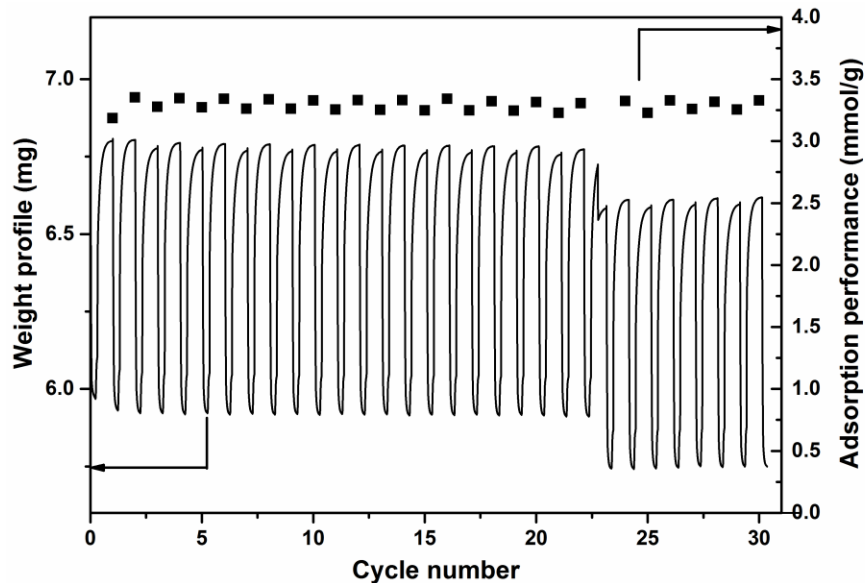


Figure 4.8 Stability test (30 cycles) for PEI-derived carbon (C-600) at 25 °C. 1st cycle: 3.18 mmol/g, 2nd cycle: 3.35 mmol/g; 30th cycle: 3.32 mmol/g.

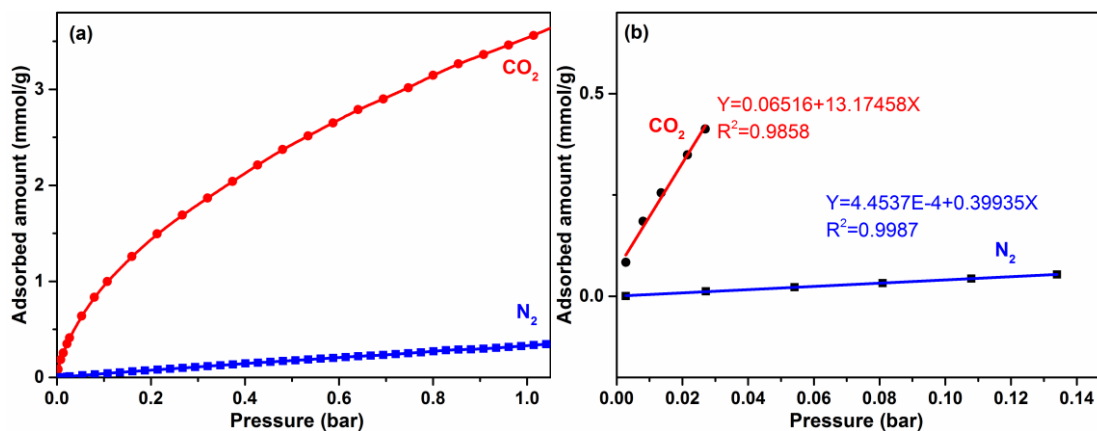


Figure 4.9 (a) CO₂ and N₂ isotherms of PEI-derived carbon (C-600) at 25 °C and (b) initial slope for CO₂/N₂ selectivity calculation.

4.4 Conclusion

A new kind of porous carbon has been successfully synthesized by using a liquid precursor—PEI. The synthesizing process is facile and the resulting carbon possesses well-developed microporosity and rich nitrogen content (up to 11%). These PEI-derived carbons

present good CO₂ adsorption capacity at ambient pressure, up to 5.7 mmol/g at 0 °C and up to 3.7 mmol/g at 25 °C. By applying concentrated HCl solution, the contribution of N-containing groups was determined to be 9% ~13% at 1bar and increases at lower pressure. The initial value of heat of adsorption was measured to be 39~43 kJ/mol, indicating strong interaction between CO₂ and the sorbent surface. Additionally, the optimized PEI-derived carbons exhibit high multi-cycle adsorption/desorption stability and highly selective adsorption of CO₂ over N₂ at 25 °C demonstrates a very good potential for industrial scale-up application.

4.5 References

- [1] Spigarelli B.P., Kawatra S.K. Opportunities and challenges in carbon dioxide capture. *Journal of CO2 Utilization*. 2013;**1**:69-87.
- [2] Nandi M., Uyama H. Exceptional CO₂ Adsorbing Materials under Different Conditions. *Chemical Record*. 2014;**14**(6):1134-1148.
- [3] Vaidya P.D., Kenig E.Y. CO₂-alkanolamine reaction kinetics: A review of recent studies. *Chemical Engineering & Technology*. 2007;**30**(11):1467-1474.
- [4] Banerjee R., Phan A., Wang B., Knobler C., Furukawa H., O'Keeffe M., et al. High-throughput synthesis of zeolitic imidazolate frameworks and application to CO₂ capture. *Science*. 2008;**319**(5865):939-943.
- [5] Samanta A., Zhao A., Shimizu G.K.H., Sarkar P., Gupta R. Post-Combustion CO₂ Capture Using Solid Sorbents: A Review. *Industrial & Engineering Chemistry Research*. 2012;**51**(4):1438-1463.

- [6] Kim E., Lee T., Kim H., Jung W.J., Han D.Y., Baik H., et al. Chemical Vapor Deposition on Chabazite (CHA) Zeolite Membranes for Effective Post-Combustion CO₂ Capture. *Environmental Science & Technology*. 2014;**48**(24):14828-14836.
- [7] Wang D.X., Wang X.X., Ma X.L., Fillerup E., Song C.S. Three-dimensional molecular basket sorbents for CO₂ capture: Effects of pore structure of supports and loading level of polyethylenimine. *Catalysis Today*. 2014;**233**:100-107.
- [8] Patil U., Fihri A., Emwas A.H., Polshettiwar V. Silicon oxynitrides of KCC-1, SBA-15 and MCM-41 for CO₂ capture with excellent stability and regenerability. *Chemical Science*. 2012;**3**(7):2224-2229.
- [9] Wang L., Yao M.L., Hu X., Hu G.S., Lu J.Q., Luo M.F., et al. Amine-modified ordered mesoporous silica: The effect of pore size on CO₂ capture performance. *Applied Surface Science*. 2015;**324**:286-292.
- [10] Zhang Z.J., Yao Z.Z., Xiang S.C., Chen B.L. Perspective of microporous metal-organic frameworks for CO₂ capture and separation. *Energy & Environmental Science*. 2015;**7**(9):2868-2899.
- [11] Srinivas G., Krungleviciute V., Guo Z.X., Yildirim T. Exceptional CO₂ capture in a hierarchically porous carbon with simultaneous high surface area and pore volume. *Energy & Environmental Science*. 2014;**7**(1):335-342.
- [12] Yu J.M., Balbuena P.B. How Impurities Affect CO₂ Capture in Metal-Organic Frameworks Modified with Different Functional Groups. *Acs Sustainable Chemistry & Engineering*. 2015;**3**(1):117-124.

- [13] Furukawa H., Yaghi O.M. Storage of Hydrogen, Methane, and Carbon Dioxide in Highly Porous Covalent Organic Frameworks for Clean Energy Applications. *Journal of the American Chemical Society*. 2009;**131**(25):8875-8883.
- [14] Vaidhyanathan R., Iremonger S.S., Shimizu G.K.H., Boyd P.G., Alavi S., Woo T.K. Direct Observation and Quantification of CO₂ Binding Within an Amine-Functionalized Nanoporous Solid. *Science*. 2010;**330**(6004):650-653.
- [15] Lin D.H., Zhang X.T., Cui X.W., Chen W.X. Highly porous carbons with superior performance for CO₂ capture through hydrogen-bonding interactions. *Rsc Advances*. 2014;**4**(52):27414-27421.
- [16] Luo Z.Q., Lim S.H., Tian Z.Q., Shang J.Z., Lai L.F., MacDonald B., et al. Pyridinic N doped graphene: synthesis, electronic structure, and electrocatalytic property. *Journal of Materials Chemistry*. 2011;**21**(22):8038-8044.
- [17] Wang L.F., Yang R.T. Significantly Increased CO₂ Adsorption Performance of Nanostructured Templated Carbon by Tuning Surface Area and Nitrogen Doping. *Journal of Physical Chemistry C*. 2012;**116**(1):1099-1106.
- [18] Nandi M., Okada K., Dutta A., Bhaumik A., Maruyama J., Derks D., et al. Unprecedented CO₂ uptake over highly porous N-doped activated carbon monoliths prepared by physical activation. *Chemical Communications*. 2012;**48**(83):10283-10285.
- [19] Lin D.H., Jiang Y.X., Chen S.R., Chen S.P., Sun S.G. Preparation of Pt nanoparticles supported on ordered mesoporous carbon FDU-15 for electrocatalytic oxidation of CO and methanol. *Electrochimica Acta*. 2012;**67**:127-132.

- [20] Zhong M.J., Natesakhawat S., Baltrus J.P., Luebke D., Nulwala H., Matyjaszewski K., et al. Copolymer-templated nitrogen-enriched porous nanocarbons for CO₂ capture. *Chemical Communications*. 2012;**48**(94):11516-11518.
- [21] Zhong M., Kim E.K., McGann J.P., Chun S.E., Whitacre J.F., Jaroniec M., et al. Electrochemically Active Nitrogen-Enriched Nanocarbons with Well-Defined Morphology Synthesized by Pyrolysis of Self-Assembled Block Copolymer. *Journal of the American Chemical Society*. 2012;**134**(36):14846-14857.
- [22] Fan X.Q., Zhang L.X., Zhang G.B., Shu Z., Shi J.L. Chitosan derived nitrogen-doped microporous carbons for high performance CO₂ capture. *Carbon*. 2013;**61**:423-430.
- [23] Sevilla M., Valle-Vigon P., Fuertes A.B. N-Doped Polypyrrole-Based Porous Carbons for CO₂ Capture. *Advanced Functional Materials*. 2011;**21**(14):2781-2787.
- [24] Sevilla M., Fuertes A.B. Sustainable porous carbons with a superior performance for CO₂ capture. *Energy & Environmental Science*. 2011;**4**(5):1765-1771.
- [25] Wahby A., Ramos-Fernandez J.M., Martinez-Escandell M., Sepulveda-Escribano A., Silvestre-Albero J., Rodriguez-Reinoso F. High-Surface-Area Carbon Molecular Sieves for Selective CO₂ Adsorption. *Chemsuschem*. 2010;**3**(8):974-981.
- [26] Wang R.T., Wang P.Y., Yan X.B., Lang J.W., Peng C., Xue Q.J. Promising Porous Carbon Derived from Celtuce Leaves with Outstanding Supercapacitance and CO₂ Capture Performance. *Acs Applied Materials & Interfaces*. 2012;**4**(11):5800-5806.
- [27] Liu Y., Wu D.C., Zhang W.D., Jiang X., He C.B., Chung T.S., et al. Polyethylenimine-grafted multiwalled carbon nanotubes for secure noncovalent immobilization and efficient delivery of DNA. *Angewandte Chemie-International Edition*. 2005;**44**(30):4782-4785.

- [28] Le M.U.T., Lee S.Y., Park S.J. Preparation and characterization of PEI-loaded MCM-41 for CO₂ capture. *International Journal of Hydrogen Energy*. 2014;**39**(23):12340-12346.
- [29] Wang X.X., Ma X.L., Song C.S., Locke D.R., Siefert S., Winans R.E., et al. Molecular basket sorbents polyethylenimine-SBA-15 for CO₂ capture from flue gas: Characterization and sorption properties. *Microporous and Mesoporous Materials*. 2013;**169**:103-111.
- [30] Zhao J.Q., Simeon F., Wang Y.J., Luo G.S., Hatton T.A. Polyethylenimine-impregnated siliceous mesocellular foam particles as high capacity CO₂ adsorbents. *Rsc Advances*. 2012;**2**(16):6509-6519.
- [31] Yan W., Tang J., Bian Z.J., Hu J., Liu H.L. Carbon Dioxide Capture by Amine-Impregnated Mesocellular-Foam-Containing Template. *Industrial & Engineering Chemistry Research*. 2012;**51**(9):3653-3662.
- [32] Yang S.B., Zhan L., Xu X.Y., Wang Y.L., Ling L.C., Feng X.L. Graphene-Based Porous Silica Sheets Impregnated with Polyethyleneimine for Superior CO₂ Capture. *Advanced Materials*. 2013;**25**(15):2130-2134.
- [33] Kruk M., Jaroniec M., Ryoo R., Joo S.H. Characterization of ordered mesoporous carbons synthesized using MCM-48 silicas as templates. *Journal of Physical Chemistry B*. 2000;**104**(33):7960-7968.
- [34] Sing K.S.W., Everett D.H., Haul R.A.W., Moscou L., Pierotti R.A., Rouquerol J., et al. Reporting Physisorption Data for Gas Solid Systems with Special Reference to the Determination of Surface-Area and Porosity (Recommendations 1984). *Pure and Applied Chemistry*. 1985;**57**(4):603-619.

- [35] Hu X., Radosz M., Cychosz K.A., Thommes M. CO₂-Filling Capacity and Selectivity of Carbon Nanopores: Synthesis, Texture, and Pore-Size Distribution from Quenched-Solid Density Functional Theory (QSDFT). *Environmental Science & Technology*. 2011;**45**(16):7068-7074.
- [36] Wickramaratne N.P., Jaroniec M. Tailoring microporosity and nitrogen content in carbons for achieving high uptake of CO₂ at ambient conditions. *Adsorption-Journal of the International Adsorption Society*. 2014;**20**(2-3):287-293.
- [37] Wang J.T., Chen H.C., Zhou H.H., Liu X.J., Qiao W.M., Long D.H., et al. Carbon dioxide capture using polyethylenimine-loaded mesoporous carbons. *Journal of Environmental Sciences-China*. 2013;**25**(1):124-132.
- [38] Hao G.P., Li W.C., Qian D., Lu A.H. Rapid Synthesis of Nitrogen-Doped Porous Carbon Monolith for CO₂ Capture. *Advanced Materials*. 2010;**22**(7):853-857.
- [39] Zhang X.T., Zhang J., Song W.H., Liu Z.F. Controllable synthesis of conducting polypyrrole nanostructures. *Journal of Physical Chemistry B*. 2006;**110**(3):1158-1165.
- [40] Lin D.H., Jiang Y.X., Wang Y., Sun S.G. Silver nanoparticles confined in SBA-15 mesoporous silica and the application as a sensor for detecting hydrogen peroxide. *Journal of Nanomaterials*. 2008, Doi: 10.1155/2008/473791.
- [41] Wang X.X., Schwartz V., Clark J.C., Ma X.L., Overbury S.H., Xu X.C., et al. Infrared Study of CO₂ Sorption over "Molecular Basket" Sorbent Consisting of Polyethylenimine-Modified Mesoporous Molecular Sieve. *Journal of Physical Chemistry C*. 2009;**113**(17):7260-7268.
- [42] Larkin P.J. Infrared and Raman Spectroscopy: Principles and Spectral Interpretation. *Infrared and Raman Spectroscopy: Principles and Spectral Interpretation*. 2011:1-228.

- [43] Spell H.L. Determination of Piperazine Rings in Ethyleneamines Poly(Ethyleneamine) and Polyethylenimine by Infrared Spectrometry. *Analytical Chemistry*. 1969;**41**(7):902-905.
- [44] Weidenthaler C., Lu A.H., Schmidt W., Schuth F. X-ray photoelectron spectroscopic studies of PAN-based ordered mesoporous carbons (OMC). *Microporous and Mesoporous Materials*. 2006;**88**(1-3):238-243.
- [45] Pietrzak R. XPS study and physico-chemical properties of nitrogen-enriched microporous activated carbon from high volatile bituminous coal. *Fuel*. 2009;**88**(10):1871-1877.
- [46] Kumar B., Asadi M., Pisasale D., Sinha-Ray S., Rosen B.A., Haasch R., et al. Renewable and metal-free carbon nanofibre catalysts for carbon dioxide reduction. *Nature Communications*. 2013, Doi 10.1038/Ncomms3819.
- [47] Lee S.H., Choi C.S. Chemical activation of high sulfur petroleum cokes by alkali metal compounds. *Fuel Processing Technology*. 2000;**64**(1-3):141-153.
- [48] Yoshizawa N., Maruyama K., Yamada Y., Ishikawa E., Kobayashi M., Toda Y., et al. XRD evaluation of KOH activation process and influence of coal rank. *Fuel*. 2002;**81**(13):1717-1722.
- [49] Xia Y.D., Mokaya R., Walker G.S., Zhu Y.Q. Superior CO₂ Adsorption Capacity on N-doped, High-Surface-Area, Microporous Carbons Templated from Zeolite. *Advanced Energy Materials*. 2011;**1**(4):678-683.
- [50] Pevida C., Drage T.C., Snape C.E. Silica-templated melamine-formaldehyde resin derived adsorbents for CO₂ capture. *Carbon*. 2008;**46**(11):1464-1474.

- [51] Liu L., Deng Q.F., Ma T.Y., Lin X.Z., Hou X.X., Liu Y.P., et al. Ordered mesoporous carbons: citric acid-catalyzed synthesis, nitrogen doping and CO₂ capture. *Journal of Materials Chemistry*. 2011;**21**(40):16001-16009.
- [52] Chen C., Kim J., Ahn W.S. Efficient carbon dioxide capture over a nitrogen-rich carbon having a hierarchical micro-mesopore structure. *Fuel*. 2012;**95**(1):360-364.

Chapter 5 Preparation of LiCl-incorporated Activated carbons for CO₂ adsorption

In this chapter, we are focusing on incorporating LiCl into activated carbons and their CO₂ adsorption performance. This study contributes to the knowledge of surface modification of activated carbons with emerging CO₂-philic chemicals for CO₂ adsorption.

5.1 Introduction

The rapidly increasing level of carbon dioxide in atmosphere is one of the greatest challenges today, which requires immediate attention and measures for CO₂ emission reduction. One of the most promising approaches is carbon capture and sequestration (CCS) [1]. It involves in CO₂ capture from large point sources (such as power plants), CO₂ transportation to assigned spots, and CO₂ injection into geologic formations for sequestration. Under current technological condition, it is estimated that the capture stage accounts for 70~90% of the total cost of CCS system [2]. The state-of-art technology for CO₂ capture, i.e. liquid amine-based absorption suffers great energy penalty and chemical cost issues [3]. Recently, adsorption by solid sorbents [4-8] has become attractive, mainly due to its advantages in lower energy cost during regeneration and competitive CO₂ adsorption capacity.

Activated carbon (AC), with its high specific surface area (SSA), highly developed micro/mesoporous structure and low cost, has been widely used as a versatile adsorbent for different gas separation/storage as well as waste water treatment [9-11]. It has been reported that at high pressure (300 psi), the CO₂ adsorption capacity could reach ~9 mmol/g

[12], much better than that of materials like zeolites at the same condition. However, the relative uniform electric potential on the surfaces of ACs leads to a low enthalpy of adsorption for CO₂, and hence moderate performance for CO₂ adsorption at low pressure [13]. In order to increase the binding forces between CO₂ molecules and the AC surfaces, surface modification by CO₂-philic polymers is often required. Specifically, amines [14-16] could interact with CO₂ via chemisorption and lead to good adsorption capacity. However, most amines are not stable at elevated temperature, which causes degradation problems during regeneration [17].

Recently, it has been reported that dispersion of metal ions on the surface of porous materials could improve gas adsorption capacity. Mg/Ni [18], Cu [19], Li [20-22] *etc.* modified metal organic frameworks (MOFs)/ porous organic frameworks (POFs) exhibited improved CO₂ adsorption performance and excellent selectivity at ambient/ sub-ambient pressures. Especially, Konstas *et al.* [21] synthesized a lithiated porous aromatic framework, to deliver a low-pressure CO₂ storage increase of 320%. De Lange *et al.* [23] also demonstrated that Li compounds (LiCl, LiF, LiH) presented strong interactions with CO₂ molecule via theoretical calculation. Therefore, it is promising to incorporate Li compounds into porous materials for improvement of CO₂ adsorption ability. However, most of the attempts were focus on modification of MOFs. What's more, some of the Li-doped MOFs or POFs have limited success or even negative effect in terms of gas storage due to the instability of modified porous structure or blocking of the pores [22, 24, 25]. To the best of our knowledge, there has been little study of Li-doped ACs for the application of CO₂ adsorption.

In this paper, we successfully synthesized LiCl-incorporated ACs via both melting-diffusion method and freeze-drying method. The chemical composition and porous structures of ACs before and after LiCl incorporation were carefully characterized. Both incorporation methods were successful. Additionally, the CO₂ adsorption performances of these samples were examined. The heat of adsorption value was calculated via isotherms at different temperatures. The effects of micropores and LiCl were attentively discussed.

5.2 Experimental

5.2.1 Synthesis of porous ACs

The porous ACs were produced by KOH activation of polyaniline (PANI). All the chemicals were purchased from Sigma-Aldrich. In brief, aniline (0.23 M, 350 mL) acidic solution was dropped into an ammonium persulfate (0.54 M, 150 mL) acidic solution under ice-water bath (0 °C), followed by a continuous magnetic stirring of 6 h. The resulting mixture was then vacuum-filtrated and washed with copious de-ionized water to obtain dark-green PANI. The after-dry PANI was weighed and the yield was ~100%. 2 g PANI and 4 g KOH were physically mixed in a mortar. The mixture was then transferred into an alumina boat and sent into a horizontal quartz tube. The tube was first preheated at 200 °C for 1 h under 100 cm³ min⁻¹ Ar flow, and then the temperature was ramped to the desired temperature (3 °C min⁻¹, to 600 °C/800 °C) for 1 h activation. The activated materials were subsequently washed with de-ionized water until the pH was ~7. The washed ACs were then sent in an oven and dried at 80 °C for at least 12 h.

5.2.2 Synthesis of LiCl-incorporated ACs

In order to produce LiCl-incorporated ACs, two approaches were applied. For melting-diffusion method, ~100 mg AC was first dispersed in 50 ml LiCl solution, with a weight ratio of AC:LiCl = 10:1. Prior to oven drying at 80 °C, the solution was sonicated for 15 min. The dried mixture was further treated at 300 °C for 24 h in an Ar environment with a steady flow rate of 100 cm³ min⁻¹. Taking into account that the Tammann temperature (the significant temperature at which the metal salt starts to diffuse into a solid lattice, usually half of the melting point) of LiCl is relatively low, it is sufficient for LiCl diffusion. For the freeze-drying method, ~100 mg AC was dispersed in 50 ml LiCl solution. The weight ratio of AC and LiCl is also 10:1, which means ~1.5 wt% Li loading. After 15 min sonication, the solution was snap-frozen in liquid nitrogen (LN) until all the liquid froze. Then the sample was kept in the LN environment for additional 15 min. After this, the solid sample was placed in a freeze dryer (Savant SuperModulyo) and dried for over 20 h. The freeze-dried LiCl-incorporated AC was denoted as C-x-drying, the LiCl-incorporated AC obtained by melting-diffusion was denoted as C-x-melting, while x means the activation temperature (600 or 800 in °C).

5.2.3 Characterization

The morphology of the LiCl-incorporated ACs was characterized by scanning electron microscopy (SEM) using a JAMP-9500F system (JEOL, Tokyo Japan) under 15 kV. N₂ adsorption/desorption analysis was obtained at 77 K by an Autosorb iQ (Quantachrome). All samples (~50 mg) were outgassed under high vacuum at 130 °C for over 4 h prior to the adsorption/desorption tests. The specific surface area of the samples was determined by Brunauer-Emmett-Teller (B.E.T.) method using data points in the pressure range of P/P₀=

0.1~0.3. The pore size distribution (PSD) was calculated with quenched-solid density functional theory (QSDFT) method assuming a slit pore model. In terms of elemental analysis and high-resolution Li 1s spectra, X-ray photoelectron spectroscopy (XPS) was carried out by AXIS 165 system (Kratos Analytical Ltd., UK) using a monochromated Al K_α excitation source.

5.2.4 CO₂ adsorption

CO₂ adsorption isotherms at 0 °C and various elevated temperatures were obtained by an Autosorb iQ (Quantachrome). All samples (~50 mg) were outgassed under high vacuum at 130 °C for over 4 h. The 0 °C isotherms were achieved by using a thermal-stated bath, while the isotherms at elevated temperatures were achieved by using a tube furnace. The heat of adsorption value (Q_{st}) was calculated from CO₂ isotherms measured at elevated temperatures (25/30 °C, 50 °C and 75 °C) based on Clausius-Clapeyron equation. A virial expression (Eq. 5.1) was used to fit the isotherms. In Eq. 5.1, P is the pressure, N is the adsorbed CO₂ amount, T is temperature, and m and n are the numbers of coefficients required to sufficiently describe the isotherms.

$$\ln P = \ln N + \frac{1}{T} \sum_{i=0}^m a_i N^i + \sum_{i=0}^n b_i N^i \quad (5.1)$$

Then Eq. 5.2 was applied to estimate Q_{st}, where R is the universal gas constant.

$$Q_{st} = -R \sum_{i=0}^m a_i N^i \quad (5.2)$$

5.3 Results and discussion

5.3.1 Chemical properties

Table 5.1 shows the chemical composition of the ACs before and after LiCl incorporation. As could be seen in Table 5.1, the ACs activated at 600 °C (C-600 series) contain lower C, higher O and N content than those activated at 800 °C, which is because that higher activation temperature favors the carbonization process and eliminates more oxygen & nitrogen groups. Furthermore, all the LiCl-incorporated samples show existence of Cl, which is an indication of LiCl. Although missing in the elemental analysis from XPS wide-scan spectra (Table 5.1), Li peaks of all LiCl-incorporated ACs have been obviously shown in high-resolution Li 1s analysis from Figure 5.1. This implies that LiCl was successfully incorporated into the ACs after the modifications. Additionally, based on the percentage of Cl (1.7% ~ 4.8%) and the fact that there is no Cl source other than LiCl, it could be estimated that the weight percentage of LiCl is 2.0% ~ 5.7%. From the data in Table 5.1, it could also be noticed that the Cl content of C-600-drying is higher than that of C-600-melting, C-800-drying higher than C-800-melting. Therefore it is inferred that the drying method has a higher efficiency than the melting method in terms of LiCl incorporation.

Table 5.1 XPS elemental analysis of original and modified ACs.

Samples	C (wt. %)	O (wt. %)	N (wt. %)	Cl (wt. %)
C-600	80.2	16.1	3.7	-
C-600 series	C-600-melting	78.0	17.6	2.6
	C-600-drying	76.5	15.5	3.8

	C-800	92.2	7.8	-	-
C-800 series	C-800-melting	89.0	8.8	-	2.2
	C-800-drying	88.2	7.0	-	4.8

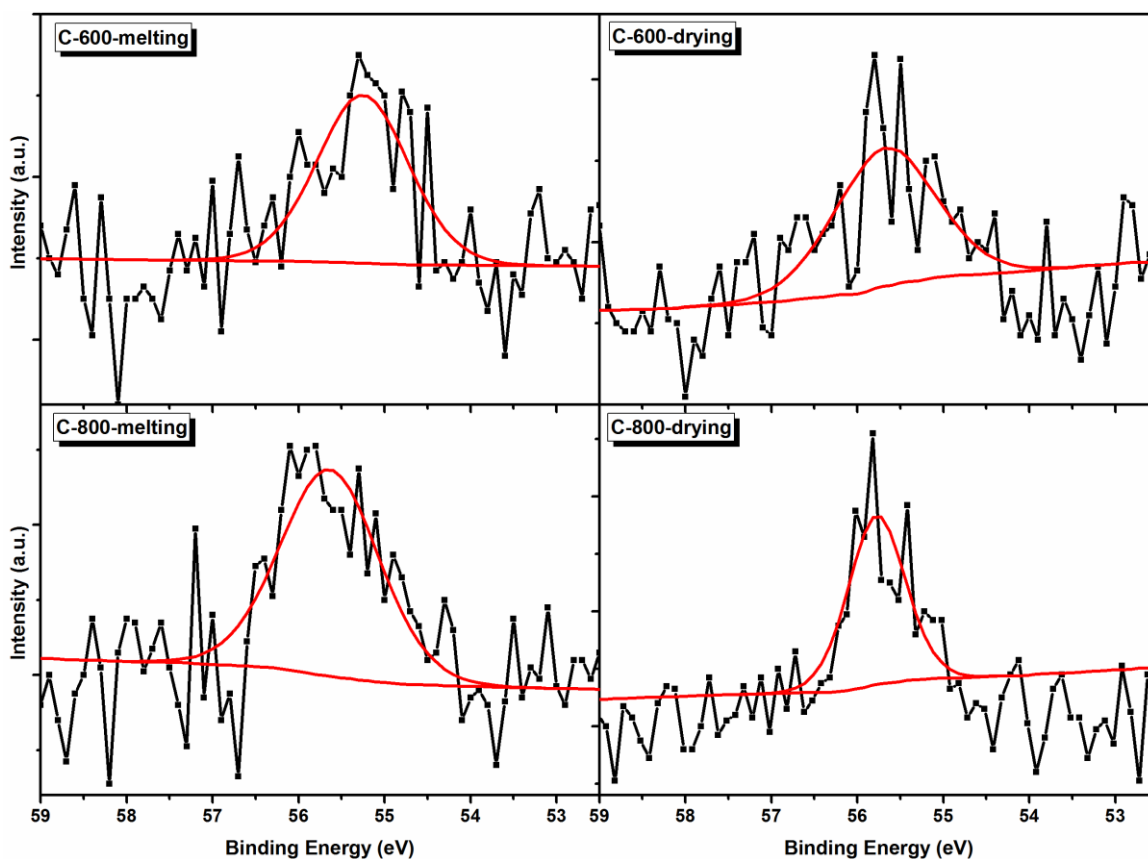


Figure 5.1 Li 1s XPS spectra of LiCl-incorporated ACs.

5.3.2 Porous structure

The morphologies of the ACs before and after LiCl incorporation were characterized by SEM and shown in Figure 5.2. ACs before incorporation (C-600 and C-800) show smooth, clean surfaces decorated with micro-sized pores. After LiCl incorporation, small pieces on the surface of ACs could be observed (as indicated in Figure 5.2). It is suggested that these small pieces are LiCl aggregates.

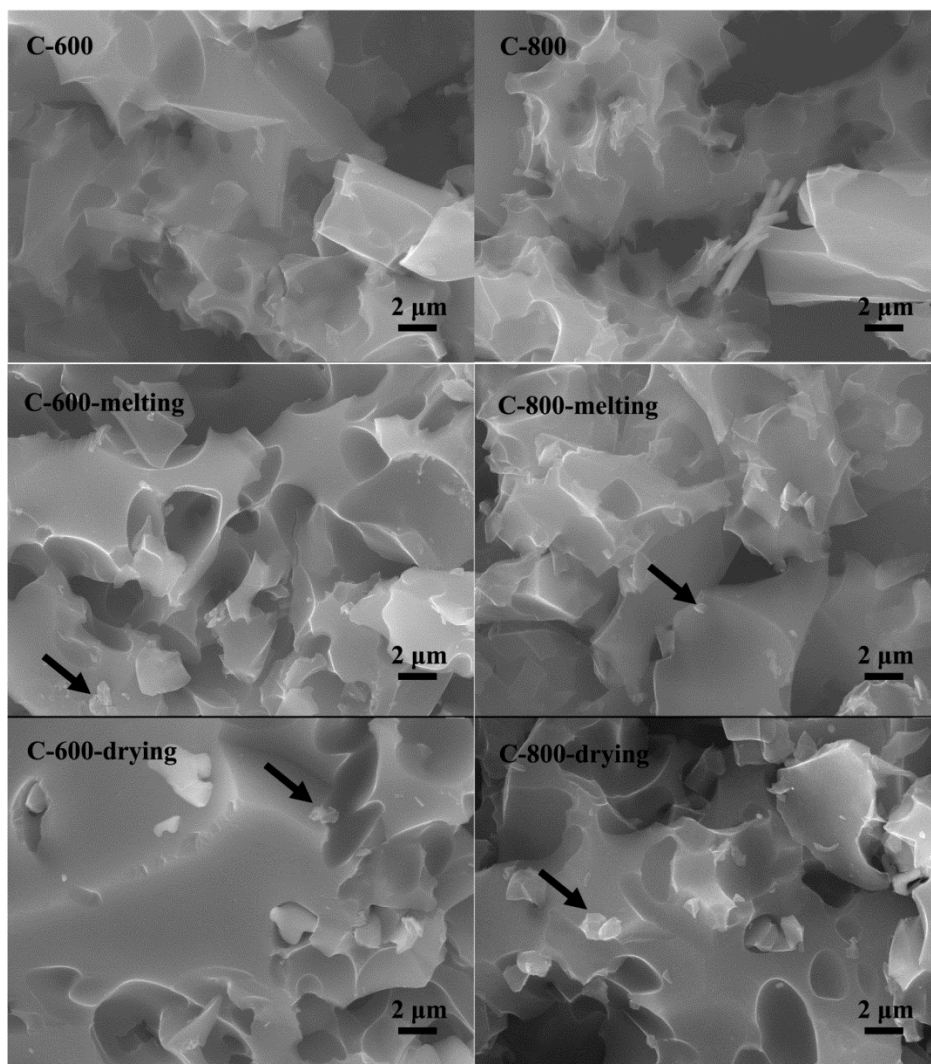


Figure 5.2 SEM images of ACs and LiCl-incorporated ACs (black arrows indicate small pieces of LiCl).

In order to study the microporous structures of the LiCl-incorporated ACs, N_2 adsorption/desorption analysis was applied. Figure 5.3 portrays the isotherms and PSDs of the ACs before and after LiCl incorporation. It could be observed in Figure 5.3a that C-600 series display type I isotherms, which indicate a characteristic of mainly microporous structure. The PSDs in Figure 5.3c also show that all the developed pores are under 1 nm (half pore width), which is well-defined in micropore range. Furthermore, the ACs show

decreased micropore volume after LiCl incorporation(C-600-melting and C-600-drying), which may be due to the pore blocking effect of the incorporated LiCl. This is another evidence of successful LiCl incorporation except for the XPS results. When comparing the two incorporation methods, C-600-drying shows bigger pore volume decrease than C-600-melting, meaning that more LiCl was loaded. This is consistent with the XPS result that the drying method has a higher efficiency for LiCl incorporation. On the other hand, the isotherms of C-800 series (Figure 5.3b) have features of both type I and type IV (according to IUPAC), expressed by significant amount of adsorption at low relative pressure ($P/P_0 < 0.1$) and pronounced plateau at intermediate pressure with hysteresis. A more direct observation could be made from Figure 5.3d, which exhibits bimodal pore size distributions of ACs prepared at 800 °C. Specifically, all PSD curves have a microporous peak at half pore width of ~ 0.5 nm (pore diameter of 1 nm) and a mesoporous peak at half pore width of ~ 1.1 nm (pore diameter of 2.2 nm). Although the pore volume is decreased after LiCl modification (both melting and drying methods), the bimodal PSD has shown no change. This implies that the LiCl incorporation has little effect on the porous structure of C-800 series samples, probably because that the pores of these samples are large and difficult to be blocked. Various porous structure parameters of all prepared ACs are listed in Table 5.2. As could be seen, C-600 has a SSA of $1120 \text{ m}^2 \text{ g}^{-1}$ and a total pore volume of $0.67 \text{ cm}^3 \text{ g}^{-1}$, while after LiCl modification the SSA has decreased to $695 \text{ m}^2 \text{ g}^{-1}$ for C-600-melting and $429 \text{ m}^2 \text{ g}^{-1}$ for C-600-drying. After LiCl incorporation, the micropore volume (V_{micro}), and < 1 nm pore volume also decrease significantly. This is consistent with the observation from PSDs in Figure 5.3c. C-800 has an ultra-high SSA of $3643 \text{ m}^2 \text{ g}^{-1}$ and a total pore volume of $2.7 \text{ cm}^3 \text{ g}^{-1}$. However, C-800 has fewer < 1 nm pores than C-600. After LiCl

modification, both the SSA and the total pore volume of C-800-melting and C-800-drying decrease. What's worth noting is that similar to C-600 series, C-800-drying has lower SSA and total pore volume than C-800-melting. Combined with the results from C-600 series, this proves that whatever the porous structure is, drying method is better than melting method in terms of incorporation efficiency.

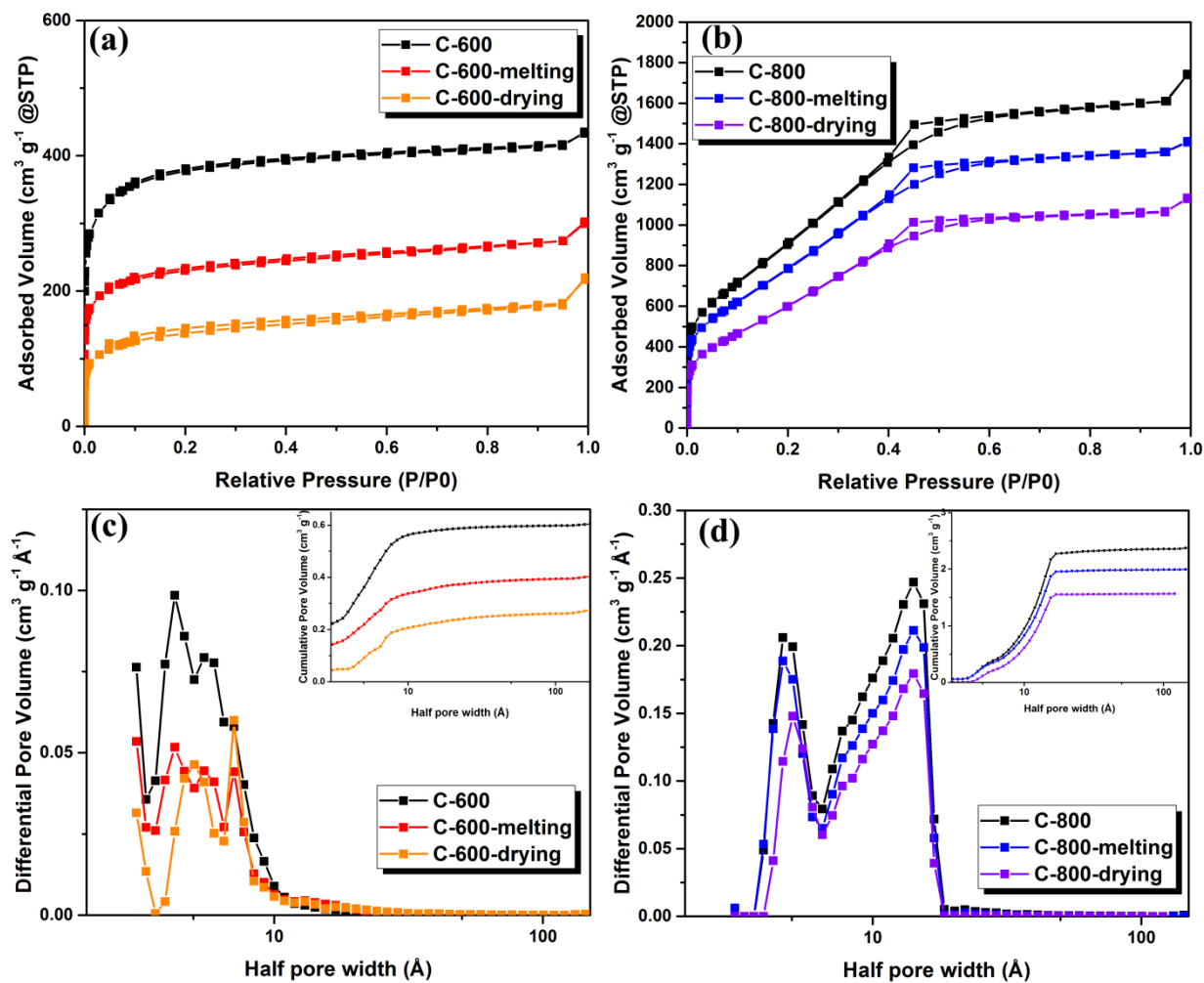


Figure 5.3 N₂ adsorption/desorption isotherms of ACs and LiCl-incorporated ACs.

Table 5.2 Porous structure parameters and CO₂ adsorption capacity of all prepared ACs.

	S_{BET} ($\text{m}^2 \text{g}^{-1}$)	V_{T} ($\text{cm}^3 \text{g}^{-1}$)	V_{micro} ($\text{cm}^3 \text{g}^{-1}$)	$V_{<1\text{nm}}$ ($\text{cm}^3 \text{g}^{-1}$)	$V_{<0.85\text{nm}}$ ($\text{cm}^3 \text{g}^{-1}$)	CO ₂ adsorption capacity at 0 °C, 1 bar (mmol g^{-1})
C-600	1127	0.67	0.56	0.36	0.30	5.3
C-600-melting	695	0.47	0.34	0.22	0.19	3.7
C-600-drying	429	0.34	0.21	0.09	0.06	2.0
C-800	3643	2.70	0.95	0.28	0.12	3.8
C-800-melting	3132	2.18	0.83	0.26	0.19	3.4
C-800-drying	2488	1.75	0.61	0.11	0.06	2.0

5.3.3 CO₂ adsorption

0 °C CO₂ isotherms of the ACs before and after LiCl modifications are drawn in Figure 5.4. In Figure 5.4a, C-600 achieved a CO₂ adsorption capacity of > 5 mmol g⁻¹ at 1atm. However, after LiCl modification, the adsorption value decreased to ~4 mmol g⁻¹ for C-600-melting and ~2 mmol g⁻¹ for C-600-drying. The decreased capacity was probably due to the blocking of small micropores by LiCl. The strong influence of micropores on CO₂ adsorption is consistent with many investigations previously reported.[26-28] Combined with data from Table 5.2, it is also suggested that the higher LiCl loading is, the more small micropores are blocked, the lower the CO₂ adsorption capacity is. In this case, the micropore is the predominant factor for CO₂ adsorption and it is suggested that the influence of micropore is so strong that the influence of the incorporated LiCl could hardly

be noticed. For C-800 series, C-800 achieves $\sim 4 \text{ mmol g}^{-1}$ at 1 atm. This result is lower than that of C-600 mainly owing to the lack of micropores, in spite that C-800 has a much higher SSA and larger total pore volume (Table 5.2). C-800-melting presents similar CO_2 adsorption performance with C-800, while C-800-drying has a much lower adsorption capacity of $\sim 2 \text{ mmol g}^{-1}$. Based on the porous structure parameters from Table 5.2, C-800-melting does have a lower S_{BET} value and a smaller total pore volume, in spite of its comparable CO_2 capacity with C-800. This suggests a positive role of LiCl in terms of CO_2 adsorption. Recalling the results of C-600 series, the fact that influence of LiCl is revealed only in C-800 series is because of a reduced influence of micropores. C-800-drying, however, does not show good CO_2 adsorption performance in spite of its higher LiCl loading. This suggests that LiCl in C-800-drying might be overdosed and could adversely affect the CO_2 adsorption.

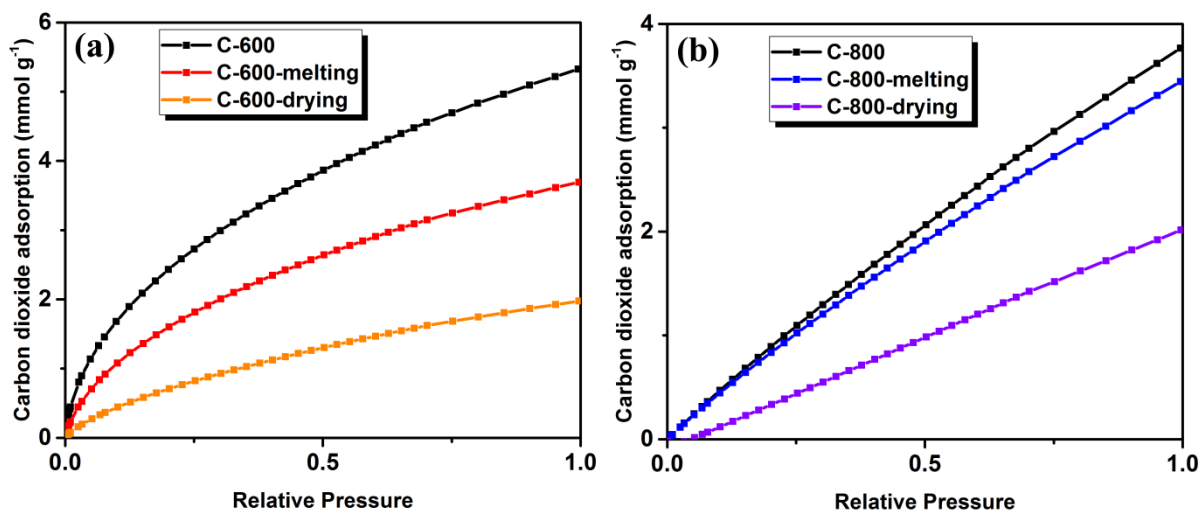


Figure 5.4 CO_2 adsorption isotherms of ACs and LiCl-incorporated ACs at 0°C .

Figure 5.5 presents CO_2 adsorption isotherms of different prepared ACs under various elevated temperatures. It is obvious that the adsorption amount of all prepared ACs

decreases with increasing temperature, indicating the adsorption is mainly physisorption. Based on the isotherms in Figure 5.5, heat of adsorption (Q_{st}) of these prepared ACs are calculated and presented in Figure 5.6. In general, the initial Q_{st} values of C-600 series samples are in the range of 28~42 kJ mol^{-1} , much higher than those of C-800 series samples (18~23 kJ mol^{-1}). This strong interaction between CO_2 and the sorbent surface is ascribed to the strong adsorption potential of small micropores [27] and rich N content [29]. Compared with C-600, C-600-melting has a lower initial value of Q_{st} and C-600-drying is even lower. Obviously the decreased Q_{st} was due to the blocking of small micropores by loaded LiCl. As C-600-drying has a high loading of LiCl than C-600-melting, the Q_{st} of C-600-drying is lower than C-600-melting. Additionally, Q_{st} gradually decreases with increasing adsorbed CO_2 amount. This implies that the CO_2 adsorption on C-600 series samples is heterogeneous and further proves the positive effect of N content on CO_2 binding. For the C-800 series, the situation is different. Lack of micropores and N content lead to reduced binding forces between CO_2 molecule and sorbent surfaces, which result in much lower initial values of Q_{st} . Furthermore, it could be observed that the initial Q_{st} values of C-800-melting and C-800-drying are slightly higher than that of C-800, proving the positive effect of incorporated LiCl. As the CO_2 adsorbed amount increases, the Q_{st} values of all the C-800 series samples show little decrease. This is also consistent with the N free composition of the C-800 series samples.

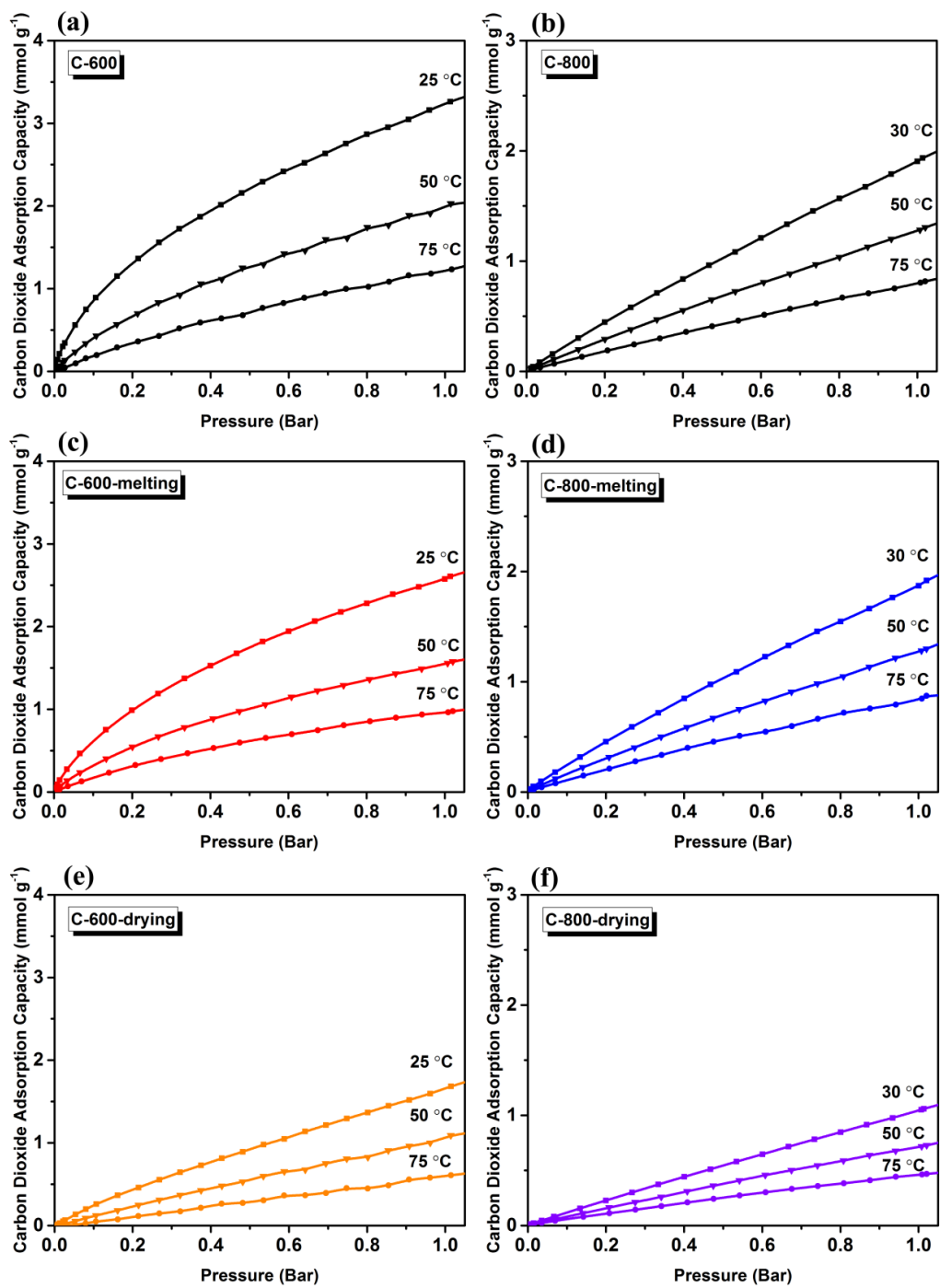


Figure 5.5 CO₂ adsorption isotherms of ACs and LiCl-incorporated ACs at various elevated temperatures (25/30 °C, 50 °C, and 75 °C).

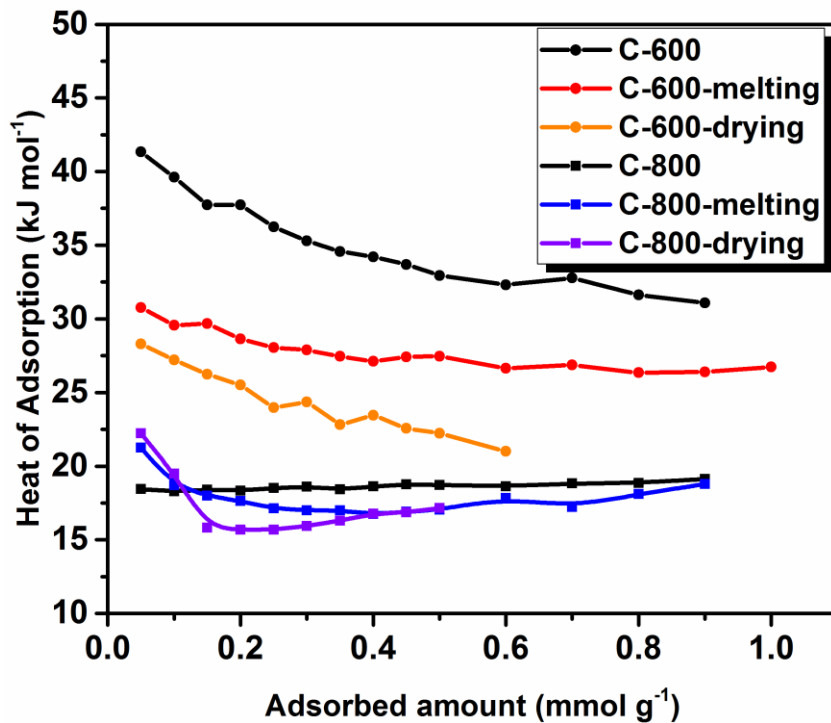


Figure 5.6 Heat of adsorption (Q_{st}) of ACs and LiCl-incorporated ACs.

5.4 Conclusions

In summary, LiCl was successfully incorporated into the PANI-derived activated carbons via two different methods, elevated temperature melting method and freeze drying method. It is determined that the drying method has a higher efficiency of LiCl incorporation than the melting method. However, the porous structures were affected by the LiCl incorporation for C-600 series ACs because of the pore blocking effect. The porous structures of C-800 series ACs were less affected by LiCl incorporation than those of C-600 series. For CO₂ adsorption capacity, C-600 showed the best CO₂ adsorption performance of 5.3 mmol g⁻¹. After LiCl incorporation the CO₂ adsorption amount decreased for both methods, indicating a predominant role of small micropore. On the other hand, C-800 has a CO₂ adsorption performance of 3.8 mmol g⁻¹, while C-800-melting present comparable performance due to the positive effect of LiCl. C-800-drying showed decreased CO₂

adsorption capacity, probably because of LiCl overdose. The calculated initial Q_{st} value for the C-800 series samples also confirms the positive roles of LiCl in terms of CO_2 interaction with sorbent surfaces.

5.5 References

- [1] Rackley S. Carbon Capture and Storage Cambridge: Butterworth-Heinemann; 2009.
- [2] Herzog H., Golomb D. Carbon capture and storage from fossil fuel use. *Encyclopedia of energy*. 2004;**1**:1-11.
- [3] Vaidya P.D., Kenig E.Y. CO_2 -alkanolamine reaction kinetics: A review of recent studies. *Chemical Engineering & Technology*. 2007;**30**(11):1467-1474.
- [4] Wang J.T., Chen H.C., Zhou H.H., Liu X.J., Qiao W.M., Long D.H., et al. Carbon dioxide capture using polyethylenimine-loaded mesoporous carbons. *Journal of Environmental Sciences-China*. 2013;**25**(1):124-132.
- [5] Boonpoke A., Chiarakorn S., Laosiripojana N., Towprayoon S., Chidthaisong A. Investigation of CO_2 adsorption by bagasse-based activated carbon. *Korean Journal of Chemical Engineering*. 2012;**29**(1):89-94.
- [6] Qi G.G., Wang Y.B., Estevez L., Duan X.N., Anako N., Park A.H.A., et al. High efficiency nanocomposite sorbents for CO_2 capture based on amine-functionalized mesoporous capsules. *Energy & Environmental Science*. 2011;**4**(2):444-452.
- [7] Srinivas G., Krungleviciute V., Guo Z.X., Yildirim T. Exceptional CO_2 capture in a hierarchically porous carbon with simultaneous high surface area and pore volume. *Energy & Environmental Science*. 2014;**7**(1):335-342.

- [8] Zhang Z.J., Yao Z.Z., Xiang S.C., Chen B.L. Perspective of microporous metal-organic frameworks for CO₂ capture and separation. *Energy & Environmental Science*. 2015;**7**(9):2868-2899.
- [9] Himeno S., Komatsu T., Fujita S. High-pressure adsorption equilibria of methane and carbon dioxide on several activated carbons. *Journal of Chemical and Engineering Data*. 2005;**50**(2):369-376.
- [10] Mukherjee S., Kumar S., Misra A.K., Acharya P.C. Removal of aqueous nickel (II) using laterite as a low-cost adsorbent. *Water Environment Research*. 2006;**78**(11):2268-2275.
- [11] Dias J.M., Alvim-Ferraz M.C.M., Almeida M.F., Rivera-Utrilla J., Sanchez-Polo M. Waste materials for activated carbon preparation and its use in aqueous-phase treatment: A review. *Journal of Environmental Management*. 2007;**85**(4):833-846.
- [12] Siriwardane R.V., Shen M.S., Fisher E.P., Poston J.A. Adsorption of CO₂ on molecular sieves and activated carbon. *Energy & Fuels*. 2001;**15**(2):279-284.
- [13] Sumida K., Rogow D.L., Mason J.A., McDonald T.M., Bloch E.D., Herm Z.R., et al. Carbon Dioxide Capture in Metal-Organic Frameworks. *Chemical Reviews*. 2012;**112**(2):724-781.
- [14] Lee C.S., Ong Y.L., Aroua M.K., Daud W.M.A.W. Impregnation of palm shell-based activated carbon with sterically hindered amines for CO₂ adsorption. *Chemical Engineering Journal*. 2013;**219**:558-564.
- [15] Chen Z.H., Deng S.B., Wei H.R., Wang B., Huang J., Yu G. Activated carbons and amine-modified materials for carbon dioxide capture - a review. *Frontiers of Environmental Science & Engineering*. 2013;**7**(3):326-340.

- [16] Shafeeyan M.S., Daud W.M.A.W., Houshmand A., Arami-Niya A. Ammonia modification of activated carbon to enhance carbon dioxide adsorption: Effect of pre-oxidation. *Applied Surface Science*. 2011;**257**(9):3936-3942.
- [17] Drage T.C., Arenillas A., Smith K.M., Snape C.E. Thermal stability of polyethylenimine based carbon dioxide adsorbents and its influence on selection of regeneration strategies. *Microporous and Mesoporous Materials*. 2008;**116**(1-3):504-512.
- [18] Yazaydin A.O., Snurr R.Q., Park T.H., Koh K., Liu J., LeVan M.D., et al. Screening of Metal-Organic Frameworks for Carbon Dioxide Capture from Flue Gas Using a Combined Experimental and Modeling Approach. *Journal of the American Chemical Society*. 2009;**131**(51):18198-18199.
- [19] Aprea P., Caputo D., Gargiulo N., Iucolano F., Pepe F. Modeling Carbon Dioxide Adsorption on Microporous Substrates: Comparison between Cu-BTC Metal-Organic Framework and 13X Zeolitic Molecular Sieve. *Journal of Chemical and Engineering Data*. 2010;**55**(9):3655-3661.
- [20] Bae Y.S., Hauser B.G., Farha O.K., Hupp J.T., Snurr R.Q. Enhancement of CO₂/CH₄ selectivity in metal-organic frameworks containing lithium cations. *Microporous and Mesoporous Materials*. 2011;**141**(1-3):231-235.
- [21] Konstas K., Taylor J.W., Thornton A.W., Doherty C.M., Lim W.X., Bastow T.J., et al. Lithiated Porous Aromatic Frameworks with Exceptional Gas Storage Capacity. *Angewandte Chemie-International Edition*. 2012;**51**(27):6639-6642.
- [22] Ma H.P., Ren H., Zou X.Q., Sun F.X., Yan Z.J., Cai K., et al. Novel lithium-loaded porous aromatic framework for efficient CO₂ and H₂ uptake. *Journal of Materials Chemistry A*. 2013;**1**(3):752-758.

- [23] de Lange K.M., Lane J.R. Quantifying cooperative intermolecular interactions for improved carbon dioxide capture materials. *Journal of Chemical Physics*. 2011, Doi 10.1063/1.3624363(6).
- [24] Li A., Lu R.F., Wang Y., Wang X., Han K.L., Deng W.Q. Lithium-Doped Conjugated Microporous Polymers for Reversible Hydrogen Storage. *Angewandte Chemie-International Edition*. 2010;**49**(19):3330-3333.
- [25] Mulfort K.L., Wilson T.M., Wasielewski M.R., Hupp J.T. Framework Reduction and Alkali-Metal Doping of a Triply Catenating Metal-Organic Framework Enhances and Then Diminishes H₂ Uptake. *Langmuir*. 2009;**25**(1):503-508.
- [26] Presser V., McDonough J., Yeon S.H., Gogotsi Y. Effect of pore size on carbon dioxide sorption by carbide derived carbon. *Energy & Environmental Science*. 2011;**4**(8):3059-3066.
- [27] Zhang Z.S., Zhou J., Xing W., Xue Q.Z., Yan Z.F., Zhuo S.P., et al. Critical role of small micropores in high CO₂ uptake. *Physical Chemistry Chemical Physics*. 2013;**15**(7):2523-2529.
- [28] Casco M.E., Martinez-Escandell M., Silvestre-Albero J., Rodriguez-Reinoso F. Effect of the porous structure in carbon materials for CO₂ capture at atmospheric and high-pressure. *Carbon*. 2014;**67**:230-235.
- [29] Bai R.Z., Yang M.L., Hu G.S., Xu L.Q., Hu X., Li Z.M., et al. A new nanoporous nitrogen-doped highly-efficient carbonaceous CO₂ sorbent synthesized with inexpensive urea and petroleum coke. *Carbon*. 2015;**81**:465-473.

Chapter 6 Conclusions and Recommendations

6.1 Summarized conclusions

In order to provide helpful and practical information to KOH activated carbons in aspects including synthesis, characterization and application in CO₂ capture, several materials were studied in Chapter 2-5. In Chapter 2, multi-wall carbon nanotubes were activated by KOH and the obtained materials were examined to reveal the pore forming mechanism. Chapter 3 studied a polyaniline-derived porous carbon by KOH activation. This kind of PANI-derived carbon possesses very high specific surface area (3768 m² g⁻¹). Several activation parameters such as activation temperature, KOH ratio and preheating temperature were comprehensively studied. The high specific surface area was attributed to the nanostructure formation during the preheating stage. In Chapter 4 a new kind of N-doped porous carbon was synthesized from a liquid carbon precursor via KOH activation and its CO₂ adsorption performance were carefully examined. Chapter 5 presented LiCl modification of PANI-derived activated carbon and its application in CO₂ adsorption. In the following, detailed conclusions from these studies are summarized.

6.1.1 Mechanism of pore formation on multi-wall carbon nanotubes by KOH activation

(1) It was found that micropores (<2 nm) were developed by KOH-C redox reaction occurring along the walls of MWCNTs, causing the formation of a characteristic peak of micropores at 0.8 nm.

(2) The in-depth activation could transversely section the nanotubes, release the catalyst particles, and expose the inner space of MWCNTs to be mesopores.

(3) It was further demonstrated that the amount of CO₂ uptake increased linearly with increasing volume of micropores with the pore sizes <1 nm, implying that the micropores when <1 nm played a significant role in the physic-sorption of CO₂ molecules.

6.1.2 A comprehensive study of polyaniline-derived porous carbons via KOH activation

(1) The PANI-derived carbons have BET surface area of 1711~3768 m² g⁻¹ and micropore volume of 0.74~1.37 cm³ g⁻¹. Specifically, C-2-200-800 has the highest BET surface area of 3768 m² g⁻¹ and the largest micropore volume of 1.37 cm³ g⁻¹.

(2) The BET surface area and micropore volume increase as the activation temperature/KOH ratio increases, but start to decrease at 900 °C or at KOH:PANI ratios higher than 3:1. This is caused by widening of narrow micropores because of intensive reactions during activation.

(3) Varying preheating temperature does not widen the pore size. At ~200 °C thermal crosslinking is maximized, which leads to the formation of network-like nanostructures. These nanostructures are beneficial to the pore development during subsequent activation at high temperatures and can lead to ACs with high BET surface area and microporosity.

6.1.3 Nitrogen-doped porous carbon prepared from a liquid carbon precursor for CO₂ adsorption

(1) A new kind of porous carbon has been successfully synthesized by using a liquid precursor—PEI. The synthesizing process is facile and the resulting carbon possesses well-developed microporosity and rich nitrogen content (up to 11%).

(2) These PEI-derived carbons present good CO₂ adsorption capacity at ambient pressure, up to 5.7 mmol/g at 0 °C and up to 3.7 mmol/g at 25 °C.

(3) By applying concentrated HCl solution, the contribution of N-containing groups was determined to be 9% ~13% at 1bar and increases at lower pressure.

(4) The initial value of heat of adsorption was measured to be 39~43 kJ mol⁻¹, indicating strong interaction between CO₂ and the sorbent surface.

(5) The PEI-derived carbons exhibit high multi-cycle adsorption/desorption stability and highly selective adsorption of CO₂ over N₂ at 25 °C, demonstrating a very good potential for industrial scale-up application.

6.1.4 Preparation of LiCl-incorporated Activated carbons for CO₂ adsorption

(1) LiCl was successfully incorporated into the PANI-derived activated carbons via two different methods, elevated temperature melting method and freeze drying method. The drying method has a higher efficiency of LiCl incorporation than the melting method.

(2) The porous structures were affected by the LiCl incorporation for C-600 series ACs because of the pore blocking effect. The porous structures of C-800 series ACs were less affected by LiCl incorporation than those of C-600 series.

(3) For CO₂ adsorption capacity, C-600 showed the best CO₂ adsorption performance of 5.3 mmol g⁻¹. After LiCl incorporation the CO₂ adsorption amount decreased for both methods, indicating a predominant role of small micropore. On the other hand, C-800 has a CO₂ adsorption performance of 3.8 mmol g⁻¹, while C-800-melting present comparable performance due to the positive effect of LiCl. C-800-drying showed decreased CO₂ adsorption capacity, probably because of LiCl overdose. The calculated initial Q_{st} value for the C-800 series samples also confirms the positive roles of LiCl in terms of CO₂ interaction with sorbent surfaces.

6.2 Research contributions

(1) The pore forming mechanism of KOH activation of multi-wall carbon nanotubes were proposed in detail.

(2) Influence of the preheating temperature was illuminated through KOH activation of polyaniline. The pore forming mechanism through varying preheating temperature was proposed in detail.

(3) A new kind of activated carbon was synthesized by KOH activation of polyethylenimine.

6.3 Recommendations for future work

(1) Although the KOH-C reaction has been considered the main activation mechanism, a unique problem faced is the very large number of precursors available. Therefore, it is still necessary to continue examining the activated carbons derived from different novel materials (such as polymers, MOFs, COFs, *etc.*).

(2) High BET surface area is advantageous for pre-combustion CO₂ capture. It is reported that some MOFs-derived carbons could reach an SSA of over 5000 m² g⁻¹ [1]. To compete with these carbons, multiple pore forming mechanisms (except for chemical activation) need to be considered in order to develop high SSA porous carbon materials.

(3) Recent efforts for improving CO₂ adsorption of carbon adsorbents have been focused on investigating (i) quantitative influence of the particle shape, size and pore structure, (ii) surface modification via doping of such elements as nitrogen, sulfur etc [2]. It is still debatable for the influence of the most commonly studied element (nitrogen), letting alone other recently explored elements. It is interesting to further revealing their effects.

(4) Carbon-based hybrid composites possess advantages from several materials. It is interesting to explore their performances of CO₂ capture.

6.4 References

[1] Hu M., Reboul J., Furukawa S., Torad N.L., Ji Q.M., Srinivasu P., et al. Direct Carbonization of Al-Based Porous Coordination Polymer for Synthesis of Nanoporous Carbon. *Journal of the American Chemical Society*. 2012;**134**(6):2864-2867.

[2] Wang J.Y., Huang L., Yang R.Y., Zhang Z., Wu J.W., Gao Y.S., et al. Recent advances in solid sorbents for CO₂ capture and new development trends. *Energy & Environmental Science*. 2014;**7**(11):3478-3518.

References

- [1] Available from: http://cdiac.ornl.gov/trends/emis/meth_reg.html
- [2] Available from: <http://www.globalccsinstitute.com/projects/large-scale-ccs-projects>
- [3] Available from: <http://www.thelocal.se/20140507/vattenfall-abandons-research-on-co2-storage>
- [4] Available from: <http://www.nano-lab.com/nanotubes-research-grade.html>
- [5] Available from: http://data.giss.nasa.gov/gistemp/taledata_v3/GLB.Ts+dSST.txt
- [6] Available from: <http://www.zeroco2.no/projects/countries/the-netherlands>
- [7] Available from: <http://www.esrl.noaa.gov/gmd/ccgg/trends/index.html>
- [8] Bertsch L., Habgood H.W. An infrared spectroscopic study of the adsorption of water and carbon dioxide by Linde molecular sieve X1. *The Journal of Physical Chemistry*. 1963;**67**(8):1621-1628.
- [9] Ross S., Olivier J.P., de Boer J.H. On physical adsorption. New York: Interscience; 1964.
- [10] Ward J.W., Habgood H.W. The infrared spectra of carbon dioxide adsorbed on zeolite X. *The Journal of Physical Chemistry*. 1966;**70**(4):1178-1182.
- [11] Spell H.L. Determination of Piperazine Rings in Ethyleneamines Poly(Ethyleneamine) and Polyethylenimine by Infrared Spectrometry. *Analytical Chemistry*. 1969;**41**(7):902-905.
- [12] Gallei E., Stumpf G. Infrared spectroscopic studies of the adsorption of carbon dioxide and the coadsorption of carbon dioxide and water on CaY and NiY zeolites. *Journal of Colloid and Interface Science*. 1976;**55**(2):415-420

- [13] Barrer R.M. Zeolites and clay minerals as sorbents and molecular sieves. London - New York: Academic Press; 1978.
- [14] Andrieu J., Smith J.M. Rate Parameters for Adsorption of CO₂ in Beds of Carbon Particles. *Aiche Journal*. 1980;**26**(6):944-948.
- [15] Yucel H., Ruthven D.M. Diffusion of CO₂ in 4A and 5A Zeolite Crystals. *Journal of Colloid and Interface Science*. 1980;**74**(1):186-195.
- [16] Yamashita Y., Ouchi K. Influence of Alkali on the Carbonization Process .1. Carbonization of 3,5-Dimethylphenol-Formaldehyde Resin with Naoh. *Carbon*. 1982;**20**(1):41-45.
- [17] Horvath G., Kawazoe K. Method for the calculation of effective pore size distribution in molecular sieve carbon. *Journal of Chemical Engineering of Japan*. 1983;**16**(6):470-475
- [18] Dubinin M. Generalization of the theory of volume filling of micropores to nonhomogeneous microporous structures. *Carbon*. 1985;**23**(4):373-380.
- [19] K. S. W. Sing D.H.E., R. A. W. Haul, L. Moscou, R. A. Pierotti, J. Rouquerol, T. Siemieniowska. Reporting physisorption data for gassolid systems with special reference to the determination of surface area and porosity. *Pure & Appl Chem*. 1985;**57**(4):603-619.
- [20] Sing K.S.W., Everett D.H., Haul R.A.W., Moscou L., Pierotti R.A., Rouquerol J., et al. Reporting Physisorption Data for Gas Solid Systems with Special Reference to the Determination of Surface-Area and Porosity (Recommendations 1984). *Pure and Applied Chemistry*. 1985;**57**(4):603-619.

- [21] Doong S.J., Yang R.T. Bulk Separation of Multicomponent Gas-Mixtures by Pressure Swing Adsorption - Pore Surface-Diffusion and Equilibrium-Models. *Aiche Journal*. 1986;**32**(3):397-410.
- [22] Adams L.B., Hall C.R., Holmes R.J., Newton R.A. An Examination of How Exposure to Humid Air Can Result in Changes in the Adsorption Properties of Activated Carbons. *Carbon*. 1988;**26**(4):451-459.
- [23] Mazumdar B.K., Banerjee D.D., Ghosh G. Coal Zinc-Chloride Reaction - an Interpretation. *Energy & Fuels*. 1988;**2**(2):224-230.
- [24] Huttepain M., Oberlin A. Microtexture of Nongraphitizing Carbons and Tem Studies of Some Activated Samples. *Carbon*. 1990;**28**(1):103-111.
- [25] Caturla F., Molinasabio M., Rodriguezreinoso F. Preparation of Activated Carbon by Chemical Activation with ZnCl₂. *Carbon*. 1991;**29**(7):999-1007.
- [26] Iijima S. Helical Microtubules of Graphitic Carbon. *Nature*. 1991;**354**(6348):56-58.
- [27] Patil S.F., Bedekar A.G., Agashe C. Effect of Electrode Conductivity on Electrochemically Deposited Polyaniline Films. *Materials Letters*. 1992;**14**(5-6):307-312.
- [28] Jagtoyen M., Derbyshire F. Some Considerations of the Origins of Porosity in Carbons from Chemically Activated Wood. *Carbon*. 1993;**31**(7):1185-1192.
- [29] Kikkinides E.S., Yang R.T., Cho S.H. Concentration and Recovery of CO₂ from Flue-Gas by Pressure Swing Adsorption. *Industrial & Engineering Chemistry Research*. 1993;**32**(11):2714-2720.
- [30] Otowa T., Tanibata R., Itoh M. Production and adsorption characteristics of MAXSORB: high-surface-area active carbon. *Gas Separation & Purification*. 1993;**7**(4):241-245

- [31] Choudhary V.R., Mayadevi S., Singh A.P. Sorption Isotherms of Methane, Ethane, Ethene and Carbon-Dioxide on NaX, NaY and Na-Mordenite Zeolites. *Journal of the Chemical Society-Faraday Transactions*. 1995;**91**(17):2935-2944.
- [32] Chue K.T., Kim J.N., Yoo Y.J., Cho S.H., Yang R.T. Comparison of Activated Carbon and Zeolite 13X for CO₂ Recovery from Flue-Gas by Pressure Swing Adsorption. *Industrial & Engineering Chemistry Research*. 1995;**34**(2):591-598.
- [33] Conklin J.A., Huang S.C., Huang S.M., Wen T.L., Kaner R.B. Thermal-Properties of Polyaniline and Poly(Aniline-Co-O-Ethylaniline). *Macromolecules*. 1995;**28**(19):6522-6527.
- [34] Cracknell R.F., Gubbins K.E., Maddox M., Nicholson D. Modeling fluid behavior in well-characterized porous materials. *Accounts of chemical research*. 1995;**28**(7):281-288
- [35] Foley H.C. Carbogenic Molecular-Sieves - Synthesis, Properties and Applications. *Microporous Materials*. 1995;**4**(6):407-433.
- [36] Khodakov A.Y., Rees L.V.C. Effect of Propane on the Kinetics of Carbon-Dioxide Adsorption in NaA Zeolites. *Gas Separation & Purification*. 1995;**9**(4):253-257.
- [37] Solum M.S., Pugmire R.J., Jagtoyen M., Derbyshire F. Evolution of Carbon Structure in Chemically Activated Wood. *Carbon*. 1995;**33**(9):1247-1254.
- [38] Ahmadpour A., Do D.D. The preparation of activated carbon from macadamia nutshell by chemical activation. *Carbon*. 1997;**35**(12):1723-1732.
- [39] Change U.N.F.C.o.C. Kyoto Protocol. 1997.
- [40] Otowa T., Nojima Y., Miyazaki T. Development of KOH activated high surface area carbon and its application to drinking water purification. *Carbon*. 1997;**35**(9):1315-1319.

- [41] Ding L.L., Wang X.W., Gregory R.V. Thermal properties of chemically synthesized polyaniline (EB) powder. *Synthetic Metals*. 1999;**104**(2):73-78.
- [42] Dreisbach F., Staudt R., Keller J.U. High pressure adsorption data of methane, nitrogen, carbon dioxide and their binary and ternary mixtures on activated carbon. *Adsorption-Journal of the International Adsorption Society*. 1999;**5**(3):215-227.
- [43] Hu Z.H., Srinivasan M.P. Preparation of high-surface-area activated carbons from coconut shell. *Microporous and Mesoporous Materials*. 1999;**27**(1):11-18.
- [44] Swiatkowski A. *Studies in Surface Science and Catalysis*: Elsevier; 1999.
- [45] Coriani S., Halkier A., Rizzo A., Ruud K. On the molecular electric quadrupole moment and the electric-field-gradient-induced birefringence of CO₂ and CS₂. *Chemical Physics Letters*. 2000;**326**(3-4):269-276.
- [46] Kruk M., Jaroniec M., Ryoo R., Joo S.H. Characterization of ordered mesoporous carbons synthesized using MCM-48 silicas as templates. *Journal of Physical Chemistry B*. 2000;**104**(33):7960-7968.
- [47] Lee S.H., Choi C.S. Chemical activation of high sulfur petroleum cokes by alkali metal compounds. *Fuel Processing Technology*. 2000;**64**(1-3):141-153.
- [48] Pandey S.S., Gerard M., Sharma A.L., Malhotra B.D. Thermal analysis of chemically synthesized polyemeraldine base. *Journal of Applied Polymer Science*. 2000;**75**(1):149-155
- [49] Van der Vaart R., Huiskes C., Bosch H., Reith T. Single and mixed gas adsorption equilibria of carbon dioxide/methane on activated carbon. *Adsorption-Journal of the International Adsorption Society*. 2000;**6**(4):311-323.

- [50] Illing G., Hellgardt K., Wakeman R.J., Jungbauer A. Preparation and characterisation of polyaniline based membranes for gas separation. *Journal of Membrane Science*. 2001;**184**(1):69-78.
- [51] Lozano-Castello D., Lillo-Rodenas M.A., Cazorla-Amoros D., Linares-Solano A. Preparation of activated carbons from Spanish anthracite I. Activation by KOH. *Carbon*. 2001;**39**(5):741-749.
- [52] Na B.K., Koo K.K., Eum H.M., Lee H., Song H.K. CO₂ recovery from flue gas by PSA process using activated carbon. *Korean Journal of Chemical Engineering*. 2001;**18**(2):220-227.
- [53] R. V. Siriwardane M.S.S., E. P. Fisher, J. A. Poston, A. Shamsi. Adsorption and Desorption of CO₂ on Solid Sorbents. *Journal of Energy Environment Research*. 2001;**1**:19-31.
- [54] Siriwardane R.V., Shen M.S., Fisher E.P., Poston J.A. Adsorption of CO₂ on molecular sieves and activated carbon. *Energy & Fuels*. 2001;**15**(2):279-284.
- [55] Yang Q.H., Hou P.X., Bai S., Wang M.Z., Cheng H.M. Adsorption and capillarity of nitrogen in aggregated multi-walled carbon nanotubes. *Chemical Physics Letters*. 2001;**345**(1):18-24.
- [56] El-Sayed Y., Bandosz T.J. Acetaldehyde adsorption on nitrogen-containing activated carbons. *Langmuir*. 2002;**18**(8):3213-3218.
- [57] Guo J., Lua A.C. Textural and chemical characterizations of adsorbent prepared from palm shell by potassium hydroxide impregnation at different stages. *Journal of Colloid and Interface Science*. 2002;**254**(2):227-233

- [58] Jia Y.F., Xiao B., Thomas K.M. Adsorption of metal ions on nitrogen surface functional groups in activated carbons. *Langmuir*. 2002;**18**(2):470-478.
- [59] Jiang Q., Qu M.Z., Zhang B.L., Yu Z.L. Preparation of activated carbon nanotubes. *Carbon*. 2002;**40**(14):2743-2745.
- [60] Kieffel Y., Travers J.P., Ermolieff A., Rouchon D. Thermal aging of undoped polyaniline: Effect of chemical degradation on electrical properties. *Journal of Applied Polymer Science*. 2002;**86**(2):395-404.
- [61] Mathew R., Mattes B.R., Espe M.P. A solid state NMR characterization of cross-linked polyaniline powder. *Synthetic Metals*. 2002;**131**(1-3):141-147.
- [62] Oh G.H., Park C.R. Preparation and characteristics of rice-straw-based porous carbons with high adsorption capacity. *Fuel*. 2002;**81**(3):327-336
- [63] Raymundo-Pinero E., Cazorla-Amoros A., Delpeux S., Frackowiak E., Szostak K., Beguin F. High surface area carbon nanotubes prepared by chemical activation. *Carbon*. 2002;**40**(9):1614-1617.
- [64] Wang Q.M., Shen D.M., Bulow M., Lau M.L., Deng S.G., Fitch F.R., et al. Metallo-organic molecular sieve for gas separation and purification. *Microporous and Mesoporous Materials*. 2002;**55**(2):217-230.
- [65] Xu X.C., Song C.S., Andresen J.M., Miller B.G., Scaroni A.W. Novel polyethylenimine-modified mesoporous molecular sieve of MCM-41 type as high-capacity adsorbent for CO₂ capture. *Energy & Fuels*. 2002;**16**(6):1463-1469.
- [66] Xu Z.K., Dannenberg C., Springer J., Banerjee S., Maier G. Novel poly(arylene ether) as membranes for gas separation. *Journal of Membrane Science*. 2002;**205**(1-2):23-31.

- [67] Yoshizawa N., Maruyama K., Yamada Y., Ishikawa E., Kobayashi M., Toda Y., et al. XRD evaluation of KOH activation process and influence of coal rank. *Fuel*. 2002;**81**(13):1717-1722.
- [68] Akten E.D., Siriwardane R., Sholl D.S. Monte Carlo simulation of single- and binary-component adsorption of CO₂, N₂, and H₂ in zeolite Na-4A. *Energy & Fuels*. 2003;**17**(4):977-983.
- [69] Chang A.C.C., Chuang S.S.C., Gray M., Soong Y. In-situ infrared study of CO₂ adsorption on SBA-15 grafted with gamma-(aminopropyl)triethoxysilane. *Energy & Fuels*. 2003;**17**(2):468-473.
- [70] Chen C.H. Thermal and morphological studies of chemically prepared emeraldine-base-form polyaniline powder. *Journal of Applied Polymer Science*. 2003;**89**(8):2142-2148.
- [71] Cinke M., Li J., Bauschlicher Jr C.W., Ricca A., Meyyappan M. CO₂ adsorption in single-walled carbon nanotubes. *Chemical Physics Letters*. 2003;**376**(5):761-766
- [72] Díaz-Terán J., Nevskaia D.M., Fierro J.L.G., López-Peinado A.J., Jerez A. Study of chemical activation process of a lignocellulosic material with KOH by XPS and XRD. *Microporous and Mesoporous Materials*. 2003;**60**(1):173-181.
- [73] Harlick P.J.E., Tezel F.H. Adsorption of carbon dioxide, methane and nitrogen: pure and binary mixture adsorption for ZSM-5 with SiO₂/Al₂O₃ ratio of 280. *Separation and Purification Technology*. 2003;**33**(2):199-210.
- [74] Hou P.X., Xu S.T., Ying Z., Yang Q.H., Liu C., Cheng H.M. Hydrogen adsorption/desorption behavior of multi-walled carbon nanotubes with different diameters. *Carbon*. 2003;**41**(13):2471-2476.

- [75] Huang H.Y., Yang R.T., Chinn D., Munson C.L. Amine-grafted MCM-48 and silica xerogel as superior sorbents for acidic gas removal from natural gas. *Industrial & Engineering Chemistry Research*. 2003;**42**(12):2427-2433.
- [76] Klara S.M., Srivastava R.D., McIlvried H.G. Integrated collaborative technology development program for CO₂ sequestration in geologic formations—United States Department of Energy R&D. *Energy Conversion and Management*. 2003;**44**(17):2699-2712
- [77] Ko D., Siriwardane R., Biegler L.T. Optimization of a pressure-swing adsorption process using zeolite 13X for CO₂ sequestration. *Industrial & Engineering Chemistry Research*. 2003;**42**(2):339-348.
- [78] Lillo-Rodenas M.A., Cazorla-Amoros D., Linares-Solano A. Understanding chemical reactions between carbons and NaOH and KOH - An insight into the chemical activation mechanism. *Carbon*. 2003;**41**(2):267-275.
- [79] Pan L., Adams K.M., Hernandez H.E., Wang X.T., Zheng C., Hattori Y., et al. Porous lanthanide-organic frameworks: Synthesis, characterization, and unprecedented gas adsorption properties. *Journal of the American Chemical Society*. 2003;**125**(10):3062-3067.
- [80] Pereira M.F.R., Soares S.F., Orfao J.J.M., Figueiredo J.L. Adsorption of dyes on activated carbons: influence of surface chemical groups. *Carbon*. 2003;**41**(4):811-821.
- [81] Siriwardane R.V., Shen M.S., Fisher E.P. Adsorption of CO₂, N₂, and O₂ on natural zeolites. *Energy & Fuels*. 2003;**17**(3):571-576.
- [82] Smith M.R., Bittner E.W., Shi W., Johnson J.K., Bockrath B.C. Chemical activation of single-walled carbon nanotubes for hydrogen adsorption. *Journal of Physical Chemistry B*. 2003;**107**(16):3752-3760.

- [83] Tan Y.Q., Thambimuthu K.V., Douglas M.A., Mortazavi R. Oxy-fuel combustion research at the CANMET Energy Technology Centre. *Coal Combustion Facing the 21st Century*. 2003:550-554.
- [84] Xu X.C., Song C.S., Andresen J.M., Miller B.G., Scaroni A.W. Preparation and characterization of novel CO₂ "molecular basket" adsorbents based on polymer-modified mesoporous molecular sieve MCM-41. *Microporous and Mesoporous Materials*. 2003;**62**(1-2):29-45.
- [85] Xue R.S., Shen Z.M. Formation of graphite-potassium intercalation compounds during activation of MCMB with KOH. *Carbon*. 2003;**41**(9):1862-1864.
- [86] Yang K.S., Edie D.D., Lim D.Y., Kim Y.M., Choi Y.O. Preparation of carbon fiber web from electrostatic spinning of PMDA-ODA poly(amic acid) solution. *Carbon*. 2003;**41**(11):2039-2046.
- [87] Yang R.T. Adsorbents: fundamentals and applications. Hoboken, New Jersey, U.S.: John Wiley & Sons; 2003.
- [88] Brandani F., Ruthven D.M. The effect of water on the adsorption of CO₂ and C₃H₈ on type X zeolites. *Industrial & Engineering Chemistry Research*. 2004;**43**(26):8339-8344.
- [89] Cavenati S., Grande C.A., Rodrigues A.E. Adsorption equilibrium of methane, carbon dioxide, and nitrogen on zeolite 13X at high pressures. *Journal of Chemical and Engineering Data*. 2004;**49**(4):1095-1101.
- [90] Ferey G., Serre C., Mellot-Draznieks C., Millange F., Surble S., Dutour J., et al. A hybrid solid with giant pores prepared by a combination of targeted chemistry, simulation, and powder diffraction. *Angewandte Chemie-International Edition*. 2004;**43**(46):6296-6301.

- [91] Harlick P.J.E., Tezel F.H. An experimental adsorbent screening study for CO₂ removal from N₂. *Microporous and Mesoporous Materials*. 2004;**76**(1-3):71-79.
- [92] Herzog H., Golomb D. Carbon capture and storage from fossil fuel use. *Encyclopedia of energy*. 2004;**1**:1-11.
- [93] Hiyoshi N., Yogo K., Yashima T. Adsorption of carbon dioxide on amine modified SBA-15 in the presence of water vapor. *Chemistry Letters*. 2004;**33**(5):510-511.
- [94] Huang J.X., Kaner R.B. Flash welding of conducting polymer nanofibres. *Nature Materials*. 2004;**3**(11):783-786.
- [95] Lee Y.J., Kim J.H., Kim J., Lee D.B., Lee J.C., Chung Y.J., et al. Fabrication of activated carbon fibers from stabilized PAN-based fibers by KOH. *Designing, Processing and Properties of Advanced Engineering Materials, Pts 1 and 2*. 2004;**449-452**:217-220.
- [96] Li C., Wang D., Liang T., Wang X., Ji L. A study of activated carbon nanotubes as double-layer capacitors electrode materials. *Materials Letters*. 2004;**58**(29):3774-3777.
- [97] Lillo-Ródenas M.A., Juan-Juan J., Cazorla-Amorós D., Linares-Solano A. About reactions occurring during chemical activation with hydroxides. *Carbon*. 2004;**42**(7):1371-1375.
- [98] Lin H., Freeman B.D. Gas solubility, diffusivity and permeability in poly(ethylene oxide). *Journal of Membrane Science*. 2004;**239**(1):105-117.
- [99] Przepiorski J., Skrodzewicz M., Morawski A.W. High temperature ammonia treatment of activated carbon for enhancement of CO₂ adsorption. *Applied Surface Science*. 2004;**225**(1-4):235-242.

- [100] Wu M.B., Zha Q.F., Qiu J.S., Guo Y.S., Shang H.Y., Yuan A.J. Preparation and characterization of porous carbons from PAN-based preoxidized cloth by KOH activation. *Carbon*. 2004;**42**(1):205-210.
- [101] Xu X., Song C., Andresen J.M., Miller B.G. Adsorption separation of CO₂ from simulated flue gas mixtures by novel CO₂ molecular basket adsorbents. *International journal of environmental technology and management*. 2004;**4**(1):32-52.
- [102] Zheng F., Tran D.N., Busche B., Fryxell G.E., Addleman R.S., Zemanian T.S., et al. Ethylenediamine-modified SBA-15 as regenerable CO₂ sorbents. *Abstracts of Papers of the American Chemical Society*. 2004;**227**:1086-1087.
- [103] Bert Metz O.D., Heleen de Coninck, Manuela Loos, Leo Meyer. The IPCC special report on carbon dioxide capture and storage. United Kingdom and New York, NY, USA; 2005.
- [104] Chunlan L., Shaoping X., Yixiong G., Shuqin L., Changhou L. Effect of pre-carbonization of petroleum cokes on chemical activation process with KOH. *Carbon*. 2005;**43**(11):2295-2301.
- [105] Ferey G., Mellot-Draznieks C., Serre C., Millange F., Dutour J., Surble S., et al. A chromium terephthalate-based solid with unusually large pore volumes and surface area. *Science*. 2005;**309**(5743):2040-2042.
- [106] Himeno S., Komatsu T., Fujita S. High-pressure adsorption equilibria of methane and carbon dioxide on several activated carbons. *Journal of Chemical and Engineering Data*. 2005;**50**(2):369-376.

- [107] Hiyoshi N., Yogo K., Yashima T. Adsorption characteristics of carbon dioxide on organically functionalized SBA-15. *Microporous and Mesoporous Materials*. 2005;**84**(1-3):357-365.
- [108] Knowles G.P., Graham J.V., Delaney S.W., Chaffee A.L. Aminopropyl-functionalized mesoporous silicas as CO₂ adsorbents. *Fuel Processing Technology*. 2005;**86**(14-15):1435-1448.
- [109] Liu Y., Wu D.C., Zhang W.D., Jiang X., He C.B., Chung T.S., et al. Polyethylenimine-grafted multiwalled carbon nanotubes for secure noncovalent immobilization and efficient delivery of DNA. *Angewandte Chemie-International Edition*. 2005;**44**(30):4782-4785.
- [110] Maroto-Valer M.M., Tang Z., Zhang Y.Z. CO₂ capture by activated and impregnated anthracites. *Fuel Processing Technology*. 2005;**86**(14-15):1487-1502.
- [111] Matsuoka K., Yamagishi Y., Yamazaki T., Setoyama N., Tomita A., Kyotani T. Extremely high microporosity and sharp pore size distribution of a large surface area carbon prepared in the nanochannels of zeolite Y. *Carbon*. 2005;**43**(4):876-879.
- [112] Maurin G., Llewellyn P.L., Bell R.G. Adsorption mechanism of carbon dioxide in faujasites: Grand canonical Monte Carlo simulations and microcalorimetry measurements. *Journal of Physical Chemistry B*. 2005;**109**(33):16084-16091.
- [113] McCool B.A., DeSisto W.J. Amino-functionalized silica membranes for enhanced carbon dioxide permeation. *Advanced Functional Materials*. 2005;**15**(10):1635-1640.
- [114] Millward A.R., Yaghi O.M. Metal-organic frameworks with exceptionally high capacity for storage of carbon dioxide at room temperature. *Journal of the American Chemical Society*. 2005;**127**(51):17998-17999.

- [115] Raymundo-Piñero E., Azañs P., Cacciaguerra T., Cazorla-Amorós D., Linares-Solano A., Béguin F. KOH and NaOH activation mechanisms of multiwalled carbon nanotubes with different structural organisation. *Carbon*. 2005;**43**(4):786-795.
- [116] Siriwardane R.V., Shen M.S., Fisher E.P. Adsorption of CO₂ on zeolites at moderate temperatures. *Energy & Fuels*. 2005;**19**(3):1153-1159.
- [117] Wu F.C., Tseng R.L., Juang R.S. Preparation of highly microporous carbons from fir wood by KOH activation for adsorption of dyes and phenols from water. *Separation and Purification Technology*. 2005;**47**(1-2):10-19.
- [118] Xomeritakis G., Tsai C.Y., Brinker C.J. Microporous sol-gel derived aminosilicate membrane for enhanced carbon dioxide separation. *Separation and Purification Technology*. 2005;**42**(3):249-257.
- [119] Xu X.C., Song C.S., Miller B.G., Scaroni A.W. Influence of moisture on CO₂ separation from gas mixture by a nanoporous adsorbent based on polyethylenimine-modified molecular sieve MCM-41. *Industrial & Engineering Chemistry Research*. 2005;**44**(21):8113-8119.
- [120] Bandosz T.J. Activated Carbon Surfaces in Environmental Remediation. *Activated Carbon Surfaces in Environmental Remediation*. 2006;**7**:1-571.
- [121] Huang J.X., Kaner R.B. The intrinsic nanofibrillar morphology of polyaniline. *Chemical Communications*. 2006;**10**(4):367-376.
- [122] Idem R., Wilson M., Tontiwachwuthikul P., Chakma A., Veawab A., Aroonwilas A., et al. Pilot plant studies of the CO₂ capture performance of aqueous MEA and mixed MEA/MDEA solvents at the University of Regina CO₂ capture technology development

plant and the Boundary Dam CO₂ capture demonstration. *Industrial & Engineering Chemistry Research*. 2006;**45**(8):2414-2420.

[123] Khatri R.A., Chuang S.S.C., Soong Y., Gray M. Thermal and chemical stability of regenerable solid amine sorbent for CO₂ capture. *Energy & Fuels*. 2006;**20**(4):1514-1520.

[124] Lee J., Kim J., Hyeon T. Recent progress in the synthesis of porous carbon materials. *Advanced Materials*. 2006;**18**(16):2073-2094.

[125] Mukherjee S., Kumar S., Misra A.K., Acharya P.C. Removal of aqueous nickel (II) using laterite as a low-cost adsorbent. *Water Environment Research*. 2006;**78**(11):2268-2275.

[126] Powell C.E., Qiao G.G. Polymeric CO₂/N₂ gas separation membranes for the capture of carbon dioxide from power plant flue gases. *Journal of Membrane Science*. 2006;**279**(1-2):1-49.

[127] Qiao W.M., Yoon S.H., Mochida I. KOH activation of needle coke to develop activated carbons for high-performance EDLC. *Energy & Fuels*. 2006;**20**(4):1680-1684.

[128] Sreedhar B., Sairam M., Chattopadhyay D.K., Mitra P.P., Rao D.V.M. Thermal and XPS studies on polyaniline salts prepared by inverted emulsion polymerization. *Journal of Applied Polymer Science*. 2006;**101**(1):499-508.

[129] Walton K.S., Abney M.B., LeVan M.D. CO₂ adsorption in Y and X zeolites modified by alkali metal cation exchange. *Microporous and Mesoporous Materials*. 2006;**91**(1-3):78-84.

[130] Weidenthaler C., Lu A.H., Schmidt W., Schuth F. X-ray photoelectron spectroscopic studies of PAN-based ordered mesoporous carbons (OMC). *Microporous and Mesoporous Materials*. 2006;**88**(1-3):238-243.

- [131] Zhang X.T., Zhang J., Song W.H., Liu Z.F. Controllable synthesis of conducting polypyrrole nanostructures. *Journal of Physical Chemistry B*. 2006;**110**(3):1158-1165.
- [132] Dias J.M., Alvim-Ferraz M.C.M., Almeida M.F., Rivera-Utrilla J., Sanchez-Polo M. Waste materials for activated carbon preparation and its use in aqueous-phase treatment: A review. *Journal of Environmental Management*. 2007;**85**(4):833-846.
- [133] Forster P., Ramaswamy V. Changes in Atmospheric Constituents and in Radiative Forcing. *Climate Change 2007: The Physical Science Basis*. 2007:129-234.
- [134] Konduru N., Lindner P., Assaf-Anad N.M. Curbing the greenhouse effect by carbon dioxide adsorption with zeolite 13X. *Aiche Journal*. 2007;**53**(12):3137-3143.
- [135] Li D., Kaner R.B. How nucleation affects the aggregation of nanoparticles. *Journal of Materials Chemistry*. 2007;**17**(22):2279-2282.
- [136] Lozano-Castello D., Calo J.M., Cazorla-Amoros D., Linares-Solano A. Carbon activation with KOH as explored by temperature programmed techniques, and the effects of hydrogen. *Carbon*. 2007;**45**(13):2529-2536.
- [137] Metz B., Davidson O.R., Bosch P.R., Dave R., Meyer L.A. Contribution of working group III to the fourth assessment report of the intergovernmental panel on climate change. Cambridge, United Kingdom and New York, NY, USA: Cambridge University Press 2007.
- [138] Oyenekan B.A., Rochelle G.T. Alternative stripper configurations for CO₂ capture by aqueous amines. *Aiche Journal*. 2007;**53**(12):3144-3154.
- [139] Plaza M.G., Pevida C., Arenillas A., Rubiera F., Pis J.J. CO₂ capture by adsorption with nitrogen enriched carbons. *Fuel*. 2007;**86**(14):2204-2212.

- [140] Rubin E.S., Yeh S., Antes M., Berkenpas M., Davison J. Use of experience curves to estimate the future cost of power plants with CO₂ capture. *International Journal of Greenhouse Gas Control*. 2007;**1**(2):188-197.
- [141] Vaidya P.D., Kenig E.Y. CO₂-alkanolamine reaction kinetics: A review of recent studies. *Chemical Engineering & Technology*. 2007;**30**(11):1467-1474.
- [142] Volkringer C., Popov D., Loiseau T., Guillou N., Ferey G., Haouas M., et al. A microdiffraction set-up for nanoporous metal-organic-framework-type solids. *Nature Materials*. 2007;**6**(10):760-764.
- [143] Bae Y.S., Farha O.K., Spokoyny A.M., Mirkin C.A., Hupp J.T., Snurr R.Q. Carborane-based metal-organic frameworks as highly selective sorbents for CO₂ over methane. *Chemical Communications*. 2008;**13**(35):4135-4137.
- [144] Banerjee R., Phan A., Wang B., Knobler C., Furukawa H., O'Keeffe M., et al. High-throughput synthesis of zeolitic imidazolate frameworks and application to CO₂ capture. *Science*. 2008;**319**(5865):939-943.
- [145] Cavka J.H., Jakobsen S., Olsbye U., Guillou N., Lamberti C., Bordiga S., et al. A new zirconium inorganic building brick forming metal organic frameworks with exceptional stability. *Journal of the American Chemical Society*. 2008;**130**(42):13850-13851.
- [146] Choi J.S., Son W.J., Kim J., Ahn W.S. Metal-organic framework MOF-5 prepared by microwave heating: Factors to be considered. *Microporous and Mesoporous Materials*. 2008;**116**(1-3):727-731.

- [147] Diaz E., Munoz E., Vega A., Ordonez S. Enhancement of the CO₂ retention capacity of Y zeolites by Na and Cs treatments: Effect of adsorption temperature and water treatment. *Industrial & Engineering Chemistry Research*. 2008;**47**(2):412-418.
- [148] Drage T.C., Arenillas A., Smith K.M., Snape C.E. Thermal stability of polyethylenimine based carbon dioxide adsorbents and its influence on selection of regeneration strategies. *Microporous and Mesoporous Materials*. 2008;**116**(1-3):504-512.
- [149] Figueroa J.D., Fout T., Plasynski S., McIlvried H., Srivastava R.D. Advances in CO₂ capture technology—The US Department of Energy's Carbon Sequestration Program. *International Journal of Greenhouse Gas Control*. 2008;**2**(1):9-20
- [150] Ghosh A., Subrahmanyam K.S., Krishna K.S., Datta S., Govindaraj A., Pati S.K., et al. Uptake of H₂ and CO₂ by graphene. *The Journal of Physical Chemistry C*. 2008;**112**(40):15704-15707.
- [151] Ho M.T., Allinson G.W., Wiley D.E. Reducing the cost of CO₂ capture from flue gases using pressure swing adsorption. *Industrial & Engineering Chemistry Research*. 2008;**47**(14):4883-4890.
- [152] Kawano T., Kubota M., Onyango M.S., Watanabe F., Matsuda H. Preparation of activated carbon from petroleum coke by KOH chemical activation for adsorption heat pump. *Applied Thermal Engineering*. 2008;**28**(8):865-871
- [153] Kim S.N., Son W.J., Choi J.S., Ahn W.S. CO₂ adsorption using amine-functionalized mesoporous silica prepared via anionic surfactant-mediated synthesis. *Microporous and Mesoporous Materials*. 2008;**115**(3):497-503.

- [154] Krishna R., van Baten J.M. Segregation effects in adsorption of CO₂-containing mixtures and their consequences for separation selectivities in cage-type zeolites. *Separation and Purification Technology*. 2008;**61**(3):414-423.
- [155] Lee S., Filburn T.P., Gray M., Park J.W., Song H.J. Screening test of solid amine sorbents for CO₂ capture. *Industrial & Engineering Chemistry Research*. 2008;**47**(19):7419-7423.
- [156] Liang C.D., Li Z.J., Dai S. Mesoporous carbon materials: Synthesis and modification. *Angewandte Chemie-International Edition*. 2008;**47**(20):3696-3717.
- [157] Lin D.H., Jiang Y.X., Wang Y., Sun S.G. Silver nanoparticles confined in SBA-15 mesoporous silica and the application as a sensor for detecting hydrogen peroxide. *Journal of Nanomaterials*. 2008, Doi: 10.1155/2008/473791.
- [158] Llewellyn P.L., Bourrelly S., Serre C., Vimont A., Daturi M., Hamon L., et al. High uptakes of CO₂ and CH₄ in mesoporous metal-organic frameworks MIL-100 and MIL-101. *Langmuir*. 2008;**24**(14):7245-7250.
- [159] Maroto-Valer M.M., Lu Z., Zhang Y.Z., Tang Z. Sorbents for CO₂ capture from high carbon fly ashes. *Waste Management*. 2008;**28**(11):2320-2328.
- [160] Morris R.E., Wheatley P.S. Gas storage in nanoporous materials. *Angewandte Chemie-International Edition*. 2008;**47**(27):4966-4981.
- [161] Niu J.J., Wang J.N. Effect of temperature on chemical activation of carbon nanotubes. *Solid State Sciences*. 2008;**10**(9):1189-1193.
- [162] Pevida C., Drage T.C., Snape C.E. Silica-templated melamine-formaldehyde resin derived adsorbents for CO₂ capture. *Carbon*. 2008;**46**(11):1464-1474.

- [163] Pevida C., Plaza M.G., Arias B., Feroso J., Rubiera F., Pis J.J. Surface modification of activated carbons for CO₂ capture. *Applied Surface Science*. 2008;**254**(22):7165-7172.
- [164] Radosz M., Hu X.D., Krutkramelis K., Shen Y.Q. Flue-gas carbon capture on carbonaceous sorbents: Toward a low-cost multifunctional Carbon Filter for "Green" energy producers. *Industrial & Engineering Chemistry Research*. 2008;**47**(10):3783-3794.
- [165] Available from: <http://edgar.jrc.ec.europa.eu/overview.php?v=42>
- [166] Sedenkova I., Trchova M., Stejskal J. Thermal degradation of polyaniline films prepared in solutions of strong and weak acids and in water - FTIR and Raman spectroscopic studies. *Polymer Degradation and Stability*. 2008;**93**(12):2147-2157.
- [167] Son W.J., Choi J.S., Ahn W.S. Adsorptive removal of carbon dioxide using polyethyleneimine-loaded mesoporous silica materials. *Microporous and Mesoporous Materials*. 2008;**113**(1-3):31-40.
- [168] Wang Y.X., Zhou Y.P., Liu C.M., Zhou L. Comparative studies of CO₂ and CH₄ sorption on activated carbon in presence of water. *Colloids and Surfaces a-Physicochemical and Engineering Aspects*. 2008;**322**(1-3):14-18.
- [169] Yang H.Q., Xu Z.H., Fan M.H., Gupta R., Slimane R.B., Bland A.E., et al. Progress in carbon dioxide separation and capture: A review. *Journal of Environmental Sciences-China*. 2008;**20**(1):14-27.
- [170] Yue M.B., Sun L.B., Cao Y., Wang Y., Wang Z.J., Zhu J.H. Efficient CO₂ capturer derived from as-synthesized MCM-41 modified with amine. *Chemistry-a European Journal*. 2008;**14**(11):3442-3451.

- [171] Zelenak V., Badanicova M., Halamova D., Cejka J., Zukal A., Murafa N., et al. Amine-modified ordered mesoporous silica: Effect of pore size on carbon dioxide capture. *Chemical Engineering Journal*. 2008;**144**(2):336-342.
- [172] Zhang J., Webley P.A. Cycle development and design for CO₂ capture from flue gas by vacuum swing adsorption. *Environmental Science & Technology*. 2008;**42**(2):563-569.
- [173] Babarao R., Jiang J.W., Sandler S.I. Molecular Simulations for Adsorptive Separation of CO₂/CH₄ Mixture in Metal-Exposed, Catenated, and Charged Metal-Organic Frameworks. *Langmuir*. 2009;**25**(9):5239-5247.
- [174] Bara J.E., Carlisle T.K., Gabriel C.J., Camper D., Finotello A., Gin D.L., et al. Guide to CO₂ Separations in Imidazolium-Based Room-Temperature Ionic Liquids. *Industrial & Engineering Chemistry Research*. 2009;**48**(6):2739-2751.
- [175] Blomen E., Hendriks C., Neele F. Capture technologies: Improvements and Promising Developments. *Greenhouse Gas Control Technologies-9*. 2009;**1**(1):1505-1512.
- [176] Choi S., Drese J.H., Jones C.W. Adsorbent Materials for Carbon Dioxide Capture from Large Anthropogenic Point Sources. *Chemsuschem*. 2009;**2**(9):796-854.
- [177] Couck S., Denayer J.F.M., Baron G.V., Remy T., Gascon J., Kapteijn F. An Amine-Functionalized MIL-53 Metal-Organic Framework with Large Separation Power for CO₂ and CH₄. *Journal of the American Chemical Society*. 2009;**131**(18):6326-6327.
- [178] Cui X.W., Wei W.F., Harrower C., Chen W.X. Effect of catalyst particle interspacing on the growth of millimeter-scale carbon nanotube arrays by catalytic chemical vapor deposition. *Carbon*. 2009;**47**(15):3441-3451.

- [179] Dasgupta S., Nanoti A., Gupta P., Jena D., Goswami A.N., Garg M.O. Carbon Dioxide Removal with Mesoporous Adsorbents in a Single Column Pressure Swing Adsorber. *Separation Science and Technology*. 2009;**44**(16):3973-3983.
- [180] Dietzel P.D.C., Besikiotis V., Blom R. Application of metal-organic frameworks with coordinatively unsaturated metal sites in storage and separation of methane and carbon dioxide. *Journal of Materials Chemistry*. 2009;**19**(39):7362-7370.
- [181] Drese J.H., Choi S., Lively R.P., Koros W.J., Fauth D.J., Gray M.L., et al. Synthesis-Structure-Property Relationships for Hyperbranched Aminosilica CO₂ Adsorbents. *Advanced Functional Materials*. 2009;**19**(23):3821-3832.
- [182] Furukawa H., Yaghi O.M. Storage of Hydrogen, Methane, and Carbon Dioxide in Highly Porous Covalent Organic Frameworks for Clean Energy Applications. *Journal of the American Chemical Society*. 2009;**131**(25):8875-8883.
- [183] Ghoufi A., Gaberova L., Rouquerol J., Vincent D., Llewellyn P.L., Maurin G. Adsorption of CO₂, CH₄ and their binary mixture in Faujasite NaY: A combination of molecular simulations with gravimetry-manometry and microcalorimetry measurements. *Microporous and Mesoporous Materials*. 2009;**119**(1-3):117-128.
- [184] Haszeldine R.S. Carbon Capture and Storage: How Green Can Black Be? *Science*. 2009;**325**(5948):1647-1652.
- [185] Kaufman D.S., Schneider D.P., McKay N.P., Ammann C.M., Bradley R.S., Briffa K.R., et al. Recent Warming Reverses Long-Term Arctic Cooling. *Science*. 2009;**325**(5945):1236-1239.

- [186] Kubota M., Hata A., Matsuda H. Preparation of activated carbon from phenolic resin by KOH chemical activation under microwave heating. *Carbon*. 2009;**47**(12):2805-2811.
- [187] Li D., Huang J.X., Kaner R.B. Polyaniline Nanofibers: A Unique Polymer Nanostructure for Versatile Applications. *Accounts of chemical research*. 2009;**42**(1):135-145.
- [188] Liang Z.J., Marshall M., Chaffee A.L. Comparison of Cu-BTC and zeolite 13X for adsorbent based CO₂ separation. *Greenhouse Gas Control Technologies* 2009;**1**(1):1265-1271.
- [189] Liang Z.J., Marshall M., Chaffee A.L. CO₂ Adsorption-Based Separation by Metal Organic Framework (Cu-BTC) versus Zeolite (13X). *Energy & Fuels*. 2009;**23**:2785-2789.
- [190] Low J.J., Benin A.I., Jakubczak P., Abrahamian J.F., Faheem S.A., Willis R.R. Virtual High Throughput Screening Confirmed Experimentally: Porous Coordination Polymer Hydration. *Journal of the American Chemical Society*. 2009;**131**(43):15834-15842.
- [191] Ma X.L., Wang X.X., Song C.S. "Molecular Basket" Sorbents for Separation of CO₂ and H₂S from Various Gas Streams. *Journal of the American Chemical Society*. 2009;**131**(16):5777-5783.
- [192] Mulfort K.L., Wilson T.M., Wasielewski M.R., Hupp J.T. Framework Reduction and Alkali-Metal Doping of a Triply Catenating Metal-Organic Framework Enhances and Then Diminishes H₂ Uptake. *Langmuir*. 2009;**25**(1):503-508.
- [193] Pietrzak R. XPS study and physico-chemical properties of nitrogen-enriched microporous activated carbon from high volatile bituminous coal. *Fuel*. 2009;**88**(10):1871-1877.

- [194] Plaza M.G., Pevida C., Arias B., Feroso J., Casal M.D., Martin C.F., et al. Development of low-cost biomass-based adsorbents for postcombustion CO₂ capture. *Fuel*. 2009;**88**(12):2442-2447.
- [195] Rackley S. Carbon Capture and Storage Cambridge: Butterworth-Heinemann; 2009.
- [196] Su F.S., Lu C.S., Cnen W.F., Bai H.L., Hwang J.F. Capture of CO₂ from flue gas via multiwalled carbon nanotubes. *Science of the Total Environment*. 2009;**407**(8):3017-3023.
- [197] Tay T., Ucar S., Karagoz S. Preparation and characterization of activated carbon from waste biomass. *Journal of Hazardous Materials*. 2009;**165**(1-3):481-485.
- [198] Vilaplana-Ortego E., Lillo-Rodenas M.A., Alcaniz-Monge J., Cazorla-Amoros D., Linares-Solano A. Isotropic petroleum pitch as a carbon precursor for the preparation of activated carbons by KOH activation. *Carbon*. 2009;**47**(8):2141-2142.
- [199] Wang H.L., Gao Q.M., Hu J. High Hydrogen Storage Capacity of Porous Carbons Prepared by Using Activated Carbon. *Journal of the American Chemical Society*. 2009;**131**(20):7016-7022.
- [200] Wang X.X., Schwartz V., Clark J.C., Ma X.L., Overbury S.H., Xu X.C., et al. Infrared Study of CO₂ Sorption over "Molecular Basket" Sorbent Consisting of Polyethylenimine-Modified Mesoporous Molecular Sieve. *Journal of Physical Chemistry C*. 2009;**113**(17):7260-7268.
- [201] Weng S.H., Lin Z.H., Zhang Y., Chen L.X., Zhou J.Z. Facile synthesis of SBA-15/polyaniline nanocomposites with high electrochemical activity under neutral and acidic conditions. *Reactive & Functional Polymers*. 2009;**69**(2):130-136.

- [202] Yazaydin A.O., Snurr R.Q., Park T.H., Koh K., Liu J., LeVan M.D., et al. Screening of Metal-Organic Frameworks for Carbon Dioxide Capture from Flue Gas Using a Combined Experimental and Modeling Approach. *Journal of the American Chemical Society*. 2009;**131**(51):18198-18199.
- [203] Zhang L.L., Zhao X.S. Carbon-based materials as supercapacitor electrodes. *Chemical Society Reviews*. 2009;**38**(9):2520-2531.
- [204] Zhao Z.X., Li Z., Lin Y.S. Adsorption and Diffusion of Carbon Dioxide on Metal-Organic Framework (MOF-5). *Industrial & Engineering Chemistry Research*. 2009;**48**(22):10015-10020.
- [205] Aprea P., Caputo D., Gargiulo N., Iucolano F., Pepe F. Modeling Carbon Dioxide Adsorption on Microporous Substrates: Comparison between Cu-BTC Metal-Organic Framework and 13X Zeolitic Molecular Sieve. *Journal of Chemical and Engineering Data*. 2010;**55**(9):3655-3661.
- [206] Chidambareswarapattar C., Larimore Z., Sotiriou-Leventis C., Mang J.T., Leventis N. One-step room-temperature synthesis of fibrous polyimide aerogels from anhydrides and isocyanates and conversion to isomorphic carbons. *Journal of Materials Chemistry*. 2010;**20**(43):9666-9678.
- [207] D'Alessandro D.M., Smit B., Long J.R. Carbon dioxide capture: prospects for new materials. *Angewandte Chemie International Edition*. 2010;**49**(35):6058-6082.
- [208] Furukawa H., Ko N., Go Y.B., Aratani N., Choi S.B., Choi E., et al. Ultrahigh Porosity in Metal-Organic Frameworks. *Science*. 2010;**329**(5990):424-428.
- [209] Hao G.P., Li W.C., Qian D., Lu A.H. Rapid Synthesis of Nitrogen-Doped Porous Carbon Monolith for CO₂ Capture. *Advanced Materials*. 2010;**22**(7):853-857.

- [210] Hsu S.C., Lu C., Su F., Zeng W., Chen W. Thermodynamics and regeneration studies of CO₂ adsorption on multiwalled carbon nanotubes. *Chemical Engineering Science*. 2010;**65**(4):1354-1361
- [211] Karadas F., Atilhan M., Aparicio S. Review on the Use of Ionic Liquids (ILs) as Alternative Fluids for CO₂ Capture and Natural Gas Sweetening. *Energy & Fuels*. 2010;**24**:5817-5828.
- [212] Leventis N., Sotiriou-Leventis C., Chandrasekaran N., Mulik S., Larimore Z.J., Lu H.B., et al. Multifunctional Polyurea Aerogels from Isocyanates and Water. A Structure-Property Case Study. *Chemistry of Materials*. 2010;**22**(24):6692-6710.
- [213] Li A., Lu R.F., Wang Y., Wang X., Han K.L., Deng W.Q. Lithium-Doped Conjugated Microporous Polymers for Reversible Hydrogen Storage. *Angewandte Chemie-International Edition*. 2010;**49**(19):3330-3333.
- [214] Liu J., Wang Y., Benin A.I., Jakubczak P., Willis R.R., LeVan M.D. CO₂/H₂O Adsorption Equilibrium and Rates on Metal-Organic Frameworks: HKUST-1 and Ni/DOBDC. *Langmuir*. 2010;**26**(17):14301-14307.
- [215] Liu N.N., Yin L.W., Wang C.X., Zhang L.Y., Lun N., Xiang D., et al. Adjusting the texture and nitrogen content of ordered mesoporous nitrogen-doped carbon materials prepared using SBA-15 silica as a template. *Carbon*. 2010;**48**(12):3579-3591.
- [216] Liu Q.L., Mace A., Bacsik Z., Sun J.L., Laaksonen A., Hedin N. NaKA sorbents with high CO₂-over-N₂ selectivity and high capacity to adsorb CO₂. *Chemical Communications*. 2010;**46**(25):4502-4504.
- [217] Pei S.P., Qu S., Zhang Y.M. Direct Electrochemistry and Electrocatalysis of Hemoglobin at Mesoporous Carbon Modified Electrode. *Sensors*. 2010;**10**(2):1279-1290.

- [218] Sayari A., Belmabkhout Y. Stabilization of Amine-Containing CO₂ Adsorbents: Dramatic Effect of Water Vapor. *Journal of the American Chemical Society*. 2010;**132**(18):6312-6314.
- [219] Su F.S., Lu C.Y., Kuo S.C., Zeng W.T. Adsorption of CO₂ on Amine-Functionalized Y-Type Zeolites. *Energy & Fuels*. 2010;**24**:1441-1448.
- [220] Thote J.A., Iyer K.S., Chatti R., Labhsetwar N.K., Biniwale R.B., Rayalu S.S. In situ nitrogen enriched carbon for carbon dioxide capture. *Carbon*. 2010;**48**(2):396-402.
- [221] Vaidhyanathan R., Iremonger S.S., Shimizu G.K.H., Boyd P.G., Alavi S., Woo T.K. Direct Observation and Quantification of CO₂ Binding Within an Amine-Functionalized Nanoporous Solid. *Science*. 2010;**330**(6004):650-653.
- [222] Wahby A., Ramos-Fernandez J.M., Martinez-Escandell M., Sepulveda-Escribano A., Silvestre-Albero J., Rodriguez-Reinoso F. High-Surface-Area Carbon Molecular Sieves for Selective CO₂ Adsorption. *Chemsuschem*. 2010;**3**(8):974-981.
- [223] Wappel D., Gronald G., Kalb R., Draxler J. Ionic liquids for post-combustion CO₂ absorption. *International Journal of Greenhouse Gas Control*. 2010;**4**(3):486-494.
- [224] Available from: http://www.spc.jst.go.jp/hottopics/1003biomass/r1003_danxing.html
- [225] Bae Y.S., Hauser B.G., Farha O.K., Hupp J.T., Snurr R.Q. Enhancement of CO₂/CH₄ selectivity in metal-organic frameworks containing lithium cations. *Microporous and Mesoporous Materials*. 2011;**141**(1-3):231-235.
- [226] Bao Z.B., Yu L.A., Ren Q.L., Lu X.Y., Deng S.G. Adsorption of CO₂ and CH₄ on a magnesium-based metal organic framework. *Journal of Colloid and Interface Science*. 2011;**353**(2):549-556.

- [227] de Lange K.M., Lane J.R. Quantifying cooperative intermolecular interactions for improved carbon dioxide capture materials. *Journal of Chemical Physics*. 2011, Doi 10.1063/1.3624363(6).
- [228] Hu X., Radosz M., Cychosz K.A., Thommes M. CO₂-Filling Capacity and Selectivity of Carbon Nanopores: Synthesis, Texture, and Pore-Size Distribution from Quenched-Solid Density Functional Theory (QSDFT). *Environmental Science & Technology*. 2011;**45**(16):7068-7074.
- [229] Israelachvili J.N. Intermolecular and surface forces. 3rd ed. University of California Santa Barbara, California, U.S.: Elsevier; 2011.
- [230] Larkin P.J. Infrared and Raman Spectroscopy: Principles and Spectral Interpretation. *Infrared and Raman Spectroscopy: Principles and Spectral Interpretation*. 2011:1-228.
- [231] Liu L., Deng Q.F., Ma T.Y., Lin X.Z., Hou X.X., Liu Y.P., et al. Ordered mesoporous carbons: citric acid-catalyzed synthesis, nitrogen doping and CO₂ capture. *Journal of Materials Chemistry*. 2011;**21**(40):16001-16009.
- [232] Luo Z.Q., Lim S.H., Tian Z.Q., Shang J.Z., Lai L.F., MacDonald B., et al. Pyridinic N doped graphene: synthesis, electronic structure, and electrocatalytic property. *Journal of Materials Chemistry*. 2011;**21**(22):8038-8044.
- [233] Mason J.A., Sumida K., Herm Z.R., Krishna R., Long J.R. Evaluating metal-organic frameworks for post-combustion carbon dioxide capture via temperature swing adsorption. *Energy & Environmental Science*. 2011;**4**(8):3030-3040.
- [234] McDonald T.M., D'Alessandro D.M., Krishna R., Long J.R. Enhanced carbon dioxide capture upon incorporation of N,N'-dimethylethylenediamine in the metal-organic framework CuBTTri. *Chemical Science*. 2011;**2**(10):2022-2028.

- [235] Olah G.A., Prakash G.K.S., Goepfert A. Anthropogenic Chemical Carbon Cycle for a Sustainable Future. *Journal of the American Chemical Society*. 2011;**133**(33):12881-12898.
- [236] Presser V., McDonough J., Yeon S.H., Gogotsi Y. Effect of pore size on carbon dioxide sorption by carbide derived carbon. *Energy & Environmental Science*. 2011;**4**(8):3059-3066.
- [237] Qi G.G., Wang Y.B., Estevez L., Duan X.N., Anako N., Park A.H.A., et al. High efficiency nanocomposite sorbents for CO₂ capture based on amine-functionalized mesoporous capsules. *Energy & Environmental Science*. 2011;**4**(2):444-452.
- [238] Rivera-Utrilla J., Sanchez-Polo M., Gomez-Serrano V., Alvarez P.M., Alvim-Ferraz M.C.M., Dias J.M. Activated carbon modifications to enhance its water treatment applications. An overview. *Journal of Hazardous Materials*. 2011;**187**(1-3):1-23.
- [239] Rochelle G., Chen E., Freeman S., Van Wagener D., Xu Q., Voice A. Aqueous piperazine as the new standard for CO₂ capture technology. *Chemical Engineering Journal*. 2011;**171**(3):725-733.
- [240] Sevilla M., Fuertes A.B. Sustainable porous carbons with a superior performance for CO₂ capture. *Energy & Environmental Science*. 2011;**4**(5):1765-1771.
- [241] Sevilla M., Mokaya R., Fuertes A.B. Ultrahigh surface area polypyrrole-based carbons with superior performance for hydrogen storage. *Energy & Environmental Science*. 2011;**4**(8):2930-2936.
- [242] Sevilla M., Valle-Vigon P., Fuertes A.B. N-Doped Polypyrrole-Based Porous Carbons for CO₂ Capture. *Advanced Functional Materials*. 2011;**21**(14):2781-2787.

- [243] Shafeeyan M.S., Daud W.M.A.W., Houshmand A., Arami-Niya A. Ammonia modification of activated carbon to enhance carbon dioxide adsorption: Effect of pre-oxidation. *Applied Surface Science*. 2011;**257**(9):3936-3942.
- [244] Shen W.Z., Zhang S.C., He Y., Li J.F., Fan W.B. Hierarchical porous polyacrylonitrile-based activated carbon fibers for CO₂ capture. *Journal of Materials Chemistry*. 2011;**21**(36):14036-14040.
- [245] Xia Y.D., Mokaya R., Walker G.S., Zhu Y.Q. Superior CO₂ Adsorption Capacity on N-doped, High-Surface-Area, Microporous Carbons Templated from Zeolite. *Advanced Energy Materials*. 2011;**1**(4):678-683.
- [246] Zhu Y.W., Murali S., Stoller M.D., Ganesh K.J., Cai W.W., Ferreira P.J., et al. Carbon-Based Supercapacitors Produced by Activation of Graphene. *Science*. 2011;**332**(6037):1537-1541.
- [247] Almasoudi A., Mokaya R. Preparation and hydrogen storage capacity of templated and activated carbons nanocast from commercially available zeolitic imidazolate framework. *Journal of Materials Chemistry*. 2012;**22**(1):146-152.
- [248] Boonpoke A., Chiarakorn S., Laosiripojana N., Towprayoon S., Chidthaisong A. Investigation of CO₂ adsorption by bagasse-based activated carbon. *Korean Journal of Chemical Engineering*. 2012;**29**(1):89-94.
- [249] Chandra V., Yu S.U., Kim S.H., Yoon Y.S., Kim D.Y., Kwon A.H., et al. Highly selective CO₂ capture on N-doped carbon produced by chemical activation of polypyrrole functionalized graphene sheets. *Chemical Communications*. 2012;**48**(5):735-737.
- [250] Chen C., Kim J., Ahn W.S. Efficient carbon dioxide capture over a nitrogen-rich carbon having a hierarchical micro-mesopore structure. *Fuel*. 2012;**95**(1):360-364.

- [251] Dasgupta S., Biswas N., Aarti, Gode N.G., Divekar S., Nanoti A., et al. CO₂ recovery from mixtures with nitrogen in a vacuum swing adsorber using metal organic framework adsorbent: A comparative study. *International Journal of Greenhouse Gas Control*. 2012;**7**:225-229.
- [252] Hu M., Reboul J., Furukawa S., Torad N.L., Ji Q.M., Srinivasu P., et al. Direct Carbonization of Al-Based Porous Coordination Polymer for Synthesis of Nanoporous Carbon. *Journal of the American Chemical Society*. 2012;**134**(6):2864-2867.
- [253] Konstas K., Taylor J.W., Thornton A.W., Doherty C.M., Lim W.X., Bastow T.J., et al. Lithiated Porous Aromatic Frameworks with Exceptional Gas Storage Capacity. *Angewandte Chemie-International Edition*. 2012;**51**(27):6639-6642.
- [254] Lee S.Y., Park S.J. Comprehensive review on synthesis and adsorption behaviors of graphene-based materials. *Carbon Letters*. 2012;**13**(2):73-87.
- [255] Lin D.H., Jiang Y.X., Chen S.R., Chen S.P., Sun S.G. Preparation of Pt nanoparticles supported on ordered mesoporous carbon FDU-15 for electrocatalytic oxidation of CO and methanol. *Electrochimica Acta*. 2012;**67**:127-132.
- [256] Lv Y.Y., Zhang F., Dou Y.Q., Zhai Y.P., Wang J.X., Liu H.J., et al. A comprehensive study on KOH activation of ordered mesoporous carbons and their supercapacitor application. *Journal of Materials Chemistry*. 2012;**22**(1):93-99.
- [257] Murali S., Potts J.R., Stoller S., Park J., Stoller M.D., Zhang L.L., et al. Preparation of activated graphene and effect of activation parameters on electrochemical capacitance. *Carbon*. 2012;**50**(10):3482-3485.

- [258] Nandi M., Okada K., Dutta A., Bhaumik A., Maruyama J., Derks D., et al. Unprecedented CO₂ uptake over highly porous N-doped activated carbon monoliths prepared by physical activation. *Chemical Communications*. 2012;**48**(83):10283-10285.
- [259] Patil U., Fihri A., Emwas A.H., Polshettiwar V. Silicon oxynitrides of KCC-1, SBA-15 and MCM-41 for CO₂ capture with excellent stability and regenerability. *Chemical Science*. 2012;**3**(7):2224-2229.
- [260] Ramdin M., de Loos T.W., Vlucht T.J.H. State-of-the-Art of CO₂ Capture with Ionic Liquids. *Industrial & Engineering Chemistry Research*. 2012;**51**(24):8149-8177.
- [261] Romanos J., Beckner M., Rash T., Firlej L., Kuchta B., Yu P., et al. Nanospace engineering of KOH activated carbon. *Nanotechnology*. 2012, Doi 10.1088/0957-4484/23/1/015401.
- [262] Samanta A., Zhao A., Shimizu G.K.H., Sarkar P., Gupta R. Post-Combustion CO₂ Capture Using Solid Sorbents: A Review. *Industrial & Engineering Chemistry Research*. 2012;**51**(4):1438-1463.
- [263] Shan M.X., Xue Q.Z., Jing N.N., Ling C.C., Zhang T., Yan Z.F., et al. Influence of chemical functionalization on the CO₂/N₂ separation performance of porous graphene membranes. *Nanoscale*. 2012;**4**(17):5477-5482.
- [264] Shen W.Z., He Y., Zhang S.C., Li J.F., Fan W.B. Yeast-Based Microporous Carbon Materials for Carbon Dioxide Capture. *Chemosuschem*. 2012;**5**(7):1274-1279.
- [265] Srinivas G., Burrell J., Yildirim T. Graphene oxide derived carbons (GODCs): synthesis and gas adsorption properties. *Energy & Environmental Science*. 2012;**5**(4):6453-6459.

- [266] Sumida K., Rogow D.L., Mason J.A., McDonald T.M., Bloch E.D., Herm Z.R., et al. Carbon Dioxide Capture in Metal-Organic Frameworks. *Chemical Reviews*. 2012;**112**(2):724-781.
- [267] Titirici M.M., White R.J., Falco C., Sevilla M. Black perspectives for a green future: hydrothermal carbons for environment protection and energy storage. *Energy & Environmental Science*. 2012;**5**(5):6796-6822.
- [268] Wang J.C., Heerwig A., Lohe M.R., Oschatz M., Borchardt L., Kaskel S. Fungi-based porous carbons for CO₂ adsorption and separation. *Journal of Materials Chemistry*. 2012;**22**(28):13911-13913.
- [269] Wang J.C., Kaskel S. KOH activation of carbon-based materials for energy storage. *Journal of Materials Chemistry*. 2012;**22**(45):23710-23725.
- [270] Wang L.F., Yang R.T. Significantly Increased CO₂ Adsorption Performance of Nanostructured Templated Carbon by Tuning Surface Area and Nitrogen Doping. *Journal of Physical Chemistry C*. 2012;**116**(1):1099-1106.
- [271] Wang R.T., Wang P.Y., Yan X.B., Lang J.W., Peng C., Xue Q.J. Promising Porous Carbon Derived from Celtuce Leaves with Outstanding Supercapacitance and CO₂ Capture Performance. *Acs Applied Materials & Interfaces*. 2012;**4**(11):5800-5806.
- [272] Wei H.R., Deng S.B., Hu B.Y., Chen Z.H., Wang B., Huang J., et al. Granular Bamboo-Derived Activated Carbon for High CO₂ Adsorption: The Dominant Role of Narrow Micropores. *Chemsuschem*. 2012;**5**(12):2354-2360.
- [273] Xing W., Liu C., Zhou Z.Y., Zhang L., Zhou J., Zhuo S.P., et al. Superior CO₂ uptake of N-doped activated carbon through hydrogen-bonding interaction. *Energy & Environmental Science*. 2012;**5**(6):7323-7327.

- [274] Yan W., Tang J., Bian Z.J., Hu J., Liu H.L. Carbon Dioxide Capture by Amine-Impregnated Mesocellular-Foam-Containing Template. *Industrial & Engineering Chemistry Research*. 2012;**51**(9):3653-3662.
- [275] Zhang X.P., Zhang X.C., Dong H.F., Zhao Z.J., Zhang S.J., Huang Y. Carbon capture with ionic liquids: overview and progress. *Energy & Environmental Science*. 2012;**5**(5):6668-6681.
- [276] Zhao J.Q., Simeon F., Wang Y.J., Luo G.S., Hatton T.A. Polyethylenimine-impregnated siliceous mesocellular foam particles as high capacity CO₂ adsorbents. *Rsc Advances*. 2012;**2**(16):6509-6519.
- [277] Zhong M., Kim E.K., McGann J.P., Chun S.E., Whitacre J.F., Jaroniec M., et al. Electrochemically Active Nitrogen-Enriched Nanocarbons with Well-Defined Morphology Synthesized by Pyrolysis of Self-Assembled Block Copolymer. *Journal of the American Chemical Society*. 2012;**134**(36):14846-14857.
- [278] Zhong M.J., Natesakhawat S., Baltrus J.P., Luebke D., Nulwala H., Matyjaszewski K., et al. Copolymer-templated nitrogen-enriched porous nanocarbons for CO₂ capture. *Chemical Communications*. 2012;**48**(94):11516-11518.
- [279] Alslaibi T.M., Abustan I., Ahmad M.A., Abu Foul A. A review: production of activated carbon from agricultural byproducts via conventional and microwave heating. *Journal of Chemical Technology and Biotechnology*. 2013;**88**(7):1183-1190.
- [280] Chen Z.H., Deng S.B., Wei H.R., Wang B., Huang J., Yu G. Activated carbons and amine-modified materials for carbon dioxide capture - a review. *Frontiers of Environmental Science & Engineering*. 2013;**7**(3):326-340.

- [281] Fan X.Q., Zhang L.X., Zhang G.B., Shu Z., Shi J.L. Chitosan derived nitrogen-doped microporous carbons for high performance CO₂ capture. *Carbon*. 2013;**61**:423-430.
- [282] Frailie P.T., Madan T., Sherman B.J., Rochelle G.T. Energy performance of advanced stripper configurations. *Greenhouse Gas Control Technology-11*. 2013;**37**:1696-1705.
- [283] Kumar B., Asadi M., Pisasale D., Sinha-Ray S., Rosen B.A., Haasch R., et al. Renewable and metal-free carbon nanofibre catalysts for carbon dioxide reduction. *Nature Communications*. 2013, Doi 10.1038/Ncomms3819.
- [284] Lee C.S., Ong Y.L., Aroua M.K., Daud W.M.A.W. Impregnation of palm shell-based activated carbon with sterically hindered amines for CO₂ adsorption. *Chemical Engineering Journal*. 2013;**219**:558-564.
- [285] Lee S.Y., Park S.J. Determination of the optimal pore size for improved CO₂ adsorption in activated carbon fibers. *Journal of Colloid and Interface Science*. 2013;**389**:230-235.
- [286] Li L., Zhao N., Wei W., Sun Y.H. A review of research progress on CO₂ capture, storage, and utilization in Chinese Academy of Sciences. *Fuel*. 2013;**108**:112-130.
- [287] Li Y.Q., Ben T., Zhang B.Y., Fu Y., Qiu S.L. Ultrahigh Gas Storage both at Low and High Pressures in KOH-Activated Carbonized Porous Aromatic Frameworks. *Scientific Reports*. 2013, Doi 10.1038/Srep02420.
- [288] Ma H.P., Ren H., Zou X.Q., Sun F.X., Yan Z.J., Cai K., et al. Novel lithium-loaded porous aromatic framework for efficient CO₂ and H₂ uptake. *Journal of Materials Chemistry A*. 2013;**1**(3):752-758.

- [289] Plaza M.G., Thurecht K.J., Pevida C., Rubiera F., Pis J.J., Snape C.E., et al. Influence of oxidation upon the CO₂ capture performance of a phenolic-resin-derived carbon. *Fuel Processing Technology*. 2013;**110**:53-60.
- [290] Spigarelli B.P., Kawatra S.K. Opportunities and challenges in carbon dioxide capture. *Journal of CO₂ Utilization*. 2013;**1**:69-87.
- [291] Voice A.K., Cloosmann F., Rochelle G.T. Oxidative degradation of amines with high-temperature cycling. *Greenhouse Gas Control Technology-11*. 2013;**37**:2118-2132.
- [292] Wang J.C., Senkovska I., Oschatz M., Lohe M.R., Borchardt L., Heerwig A., et al. Highly porous nitrogen-doped polyimine-based carbons with adjustable microstructures for CO₂ capture. *Journal of Materials Chemistry A*. 2013;**1**(36):10951-10961.
- [293] Wang J.T., Chen H.C., Zhou H.H., Liu X.J., Qiao W.M., Long D.H., et al. Carbon dioxide capture using polyethylenimine-loaded mesoporous carbons. *Journal of Environmental Sciences-China*. 2013;**25**(1):124-132.
- [294] Wang X.X., Ma X.L., Song C.S., Locke D.R., Siefert S., Winans R.E., et al. Molecular basket sorbents polyethylenimine-SBA-15 for CO₂ capture from flue gas: Characterization and sorption properties. *Microporous and Mesoporous Materials*. 2013;**169**:103-111.
- [295] Wickramaratne N.P., Jaroniec M. Importance of small micropores in CO₂ capture by phenolic resin-based activated carbon spheres. *Journal of Materials Chemistry A*. 2013;**1**(1):112-116.
- [296] Yang S.B., Zhan L., Xu X.Y., Wang Y.L., Ling L.C., Feng X.L. Graphene-Based Porous Silica Sheets Impregnated with Polyethyleneimine for Superior CO₂ Capture. *Advanced Materials*. 2013;**25**(15):2130-2134.

- [297] Zhang L., Zhang F., Yang X., Long G.K., Wu Y.P., Zhang T.F., et al. Porous 3D graphene-based bulk materials with exceptional high surface area and excellent conductivity for supercapacitors. *Scientific Reports*. 2013, Doi 10.1038/Srep01408.
- [298] Zhang Z., Zhou J., Xing W., Xue Q., Yan Z., Zhuo S., et al. Critical role of small micropores in high CO₂ uptake. *Physical Chemistry Chemical Physics*. 2013;**15**(7):2523-2529.
- [299] Zhang Z.J., Cui P., Chen X.Y., Liu J.W. The production of activated carbon from cation exchange resin for high-performance supercapacitor. *Journal of Solid State Electrochemistry*. 2013;**17**(6):1749-1758.
- [300] Zhu X.P., Fu Y., Hu G.S., Shen Y., Dai W., Hu X. CO₂ Capture with Activated Carbons Prepared by Petroleum Coke and KOH at Low Pressure. *Water Air and Soil Pollution*. 2013, Doi: 10.1007/S11270-012-1387-Y.
- [301] Boot-Handford M.E., Abanades J.C., Anthony E.J., Blunt M.J., Brandani S., Mac Dowell N., et al. Carbon capture and storage update. *Energy & Environmental Science*. 2014;**7**(1):130-189.
- [302] Casco M.E., Martínez-Escandell M., Silvestre-Albero J., Rodríguez-Reinoso F. Effect of the porous structure in carbon materials for CO₂ capture at atmospheric and high-pressure. *Carbon*. 2014;**67**:230-235.
- [303] E.I.A. U.S. Annual energy outlook 2014; 2014.
- [304] Kim E., Lee T., Kim H., Jung W.J., Han D.Y., Baik H., et al. Chemical Vapor Deposition on Chabazite (CHA) Zeolite Membranes for Effective Post-Combustion CO₂ Capture. *Environmental Science & Technology*. 2014;**48**(24):14828-14836.

- [305] Le M.U.T., Lee S.Y., Park S.J. Preparation and characterization of PEI-loaded MCM-41 for CO₂ capture. *International Journal of Hydrogen Energy*. 2014;**39**(23):12340-12346.
- [306] Le Quéré C., Moriarty R., Andrew R.M., Peters G.P., Ciais P., Friedlingstein P., et al. Global carbon budget 2014. *Earth System Science Data Discussions*. 2014;**7**(2):521-610.
- [307] Li M.J., Liu C.M., Cao H.B., Zhao H., Zhang Y., Fan Z.J. KOH self-templating synthesis of three-dimensional hierarchical porous carbon materials for high performance supercapacitors. *Journal of Materials Chemistry A*. 2014;**2**(36):14844-14851.
- [308] Lin D.H., Zhang X.T., Cui X.W., Chen W.X. Highly porous carbons with superior performance for CO₂ capture through hydrogen-bonding interactions. *Rsc Advances*. 2014;**4**(52):27414-27421.
- [309] Lu A.-H.D., Sheng. Porous Materials for Carbon Dioxide Capture. Springer, 2014.
- [310] Marco-Lozar J.P., Kunowsky M., Suarez-Garcia F., Linares-Solano A. Sorbent design for CO₂ capture under different flue gas conditions. *Carbon*. 2014;**72**:125-134.
- [311] Nandi M., Uyama H. Exceptional CO₂ Adsorbing Materials under Different Conditions. *Chemical Record*. 2014;**14**(6):1134-1148.
- [312] Seema H., Kemp K.C., Le N.H., Park S.W., Chandra V., Lee J.W., et al. Highly selective CO₂ capture by S-doped microporous carbon materials. *Carbon*. 2014;**66**:320-326.
- [313] Song C.W., Wu S.H., Cheng M.R., Tao P., Shao M.H., Gao G.R. Adsorption Studies of Coconut Shell Carbons Prepared by KOH Activation for Removal of Lead(II) From Aqueous Solutions. *Sustainability*. 2014;**6**(1):86-98.

- [314] Srinivas G., Krungleviciute V., Guo Z.X., Yildirim T. Exceptional CO₂ capture in a hierarchically porous carbon with simultaneous high surface area and pore volume. *Energy & Environmental Science*. 2014;**7**(1):335-342.
- [315] Wang D.X., Wang X.X., Ma X.L., Fillerup E., Song C.S. Three-dimensional molecular basket sorbents for CO₂ capture: Effects of pore structure of supports and loading level of polyethylenimine. *Catalysis Today*. 2014;**233**:100-107.
- [316] Wang J.C., Senkovska I., Kaskel S., Liu Q. Chemically activated fungi-based porous carbons for hydrogen storage. *Carbon*. 2014;**75**:372-380.
- [317] Wang J.Y., Huang L., Yang R.Y., Zhang Z., Wu J.W., Gao Y.S., et al. Recent advances in solid sorbents for CO₂ capture and new development trends. *Energy & Environmental Science*. 2014;**7**(11):3478-3518.
- [318] Wang S.P., Zhang J.N., Shang P., Li Y.Y., Chen Z.M., Xu Q. N-doped carbon spheres with hierarchical micropore-nanosheet networks for high performance supercapacitors. *Chemical Communications*. 2014;**50**(81):12091-12094.
- [319] Wickramaratne N.P., Jaroniec M. Tailoring microporosity and nitrogen content in carbons for achieving high uptake of CO₂ at ambient conditions. *Adsorption-Journal of the International Adsorption Society*. 2014;**20**(2-3):287-293.
- [320] Yu J.Y., Guo M.Y., Muhammad F., Wang A.F., Zhang F., Li Q., et al. One-pot synthesis of highly ordered nitrogen-containing mesoporous carbon with resorcinol-urea-formaldehyde resin for CO₂ capture. *Carbon*. 2014;**69**:502-514.
- [321] Yu Q.F., Li M., Ning P., Yi H.H., Tang X.L. Preparation and Phosphine Adsorption of Activated Carbon Prepared from Walnut Shells by KOH Chemical Activation. *Separation Science and Technology*. 2014;**49**(15):2366-2375.

- [322] Bai R.Z., Yang M.L., Hu G.S., Xu L.Q., Hu X., Li Z.M., et al. A new nanoporous nitrogen-doped highly-efficient carbonaceous CO₂ sorbent synthesized with inexpensive urea and petroleum coke. *Carbon*. 2015;**81**:465-473.
- [323] Cong H., Zhang M., Chen Y., Chen K., Hao Y., Zhao Y., et al. Highly Selective CO₂ Capture by Nitrogen Enriched Porous Carbons. *Carbon*. 2015;**92**:297-304.
- [324] Available from: <http://www.wwdmag.com/activated-carbon/global-demand-activated-carbon-rise-report-says>
- [325] Wang L., Yao M.L., Hu X., Hu G.S., Lu J.Q., Luo M.F., et al. Amine-modified ordered mesoporous silica: The effect of pore size on CO₂ capture performance. *Applied Surface Science*. 2015;**324**:286-292.
- [326] Yu J.M., Balbuena P.B. How Impurities Affect CO₂ Capture in Metal-Organic Frameworks Modified with Different Functional Groups. *Acs Sustainable Chemistry & Engineering*. 2015;**3**(1):117-124.
- [327] Zhang X.T., Chen W.X. Mechanisms of pore formation on multi-wall carbon nanotubes by KOH activation. *Microporous and Mesoporous Materials*. 2015;**206**:194-201.
- [328] Zhang Z.J., Yao Z.Z., Xiang S.C., Chen B.L. Perspective of microporous metal-organic frameworks for CO₂ capture and separation. *Energy & Environmental Science*. 2015;**7**(9):2868-2899.